UNIVERSITY OF NOTTINGHAM

Impedance Based Fault Location in Power Distribution Systems

Ke Jia

A thesis submitted in partial fulfilment for the degree of Doctor of Philosophy

in the

Faculty of engineering

Department of Electrical and Electronic Engineering

August 2011

Abstract

This thesis presents an investigation into impedance based fault location methods which directly use the fault transient as an excitation source to provide fast and accurate fault locations in small distribution systems such as the modern marine and aircraft power systems which have Integrated Power System (IPS) configuration. Fast and accurate fault location on un-exposed power distribution lines is of vital importance to expedite service restoration and improving the reliability of the power system.

Two fault location algorithms are developed: the single-ended method and the double-ended method. The singled-ended algorithm which captures current and voltage waveforms from one end of the distribution cable estimates the fault locations using an iteration calculation. The double-ended method has a simple algorithm and is robust to different fault situations but requires additional data measured from the remote end of the cable. Both simulation and experimental tests have been done and the results are good enough to validate that the developed methods can locate fault positions using a 12ms window and offer an accuracy of within 1m in the proposed distribution system.

The advantages and disadvantages of the proposed fault location methods are investigated under different fault situations. The possibility of employing the two methods in protection of faults in a marine power system is demonstrated. Due to the special characteristics of the marine power system, an active method which simply involves adding an IGBT switch is proposed for the earth fault protection.

The work in this thesis has been published in several publications as:

1. Ke Jia, David Thomas and Mark Sumner, "Fault location in power distribution systems," Patent applied in British Intellectual Property Office. Application Number: GB 1104567.1. (Until 18/01/2012, it is in the process for a full patent and the current status is "patent application number").

2. Ke Jia, David Thomas and Mark Sumner, "A Novel Fault Location Algorithm Utilized in Marine System with CWT," International Conference on Advanced Power System Automation and Protection, China, October, 2011.

3. Ke Jia, David Thomas and Mark Sumner, "Single-ended Fault Location Scheme for Utilization in Integrated Power System" Submitted to the IEEE Journal of on Power Delivery, May, 2011.

4. Ke Jia, David Thomas and Mark Sumner, "Double-ended Fault Location Scheme for Utilization in Integrated Power System" Submitted to the IEEE Journal of on Power Delivery, April, 2011.

Acknowledgement

I would like to thank all those who have helped me through the past three years.

In particular, I would like to express my gratitude to my supervisors: Dr. Dave Thomas and Prof. Mark Sumner for their guidance, support and inspiration in every stage of my PhD work.

I would like to also give thanks to Dr. Jing Wang, Dr. Xiaohui Wand, Dr. Dave Coggins, Dr. Edward Christopher and Dr. Qian Zhou for their technical support.

Finally, thanks to my parents, my girlfriend and her parents for their trust, encouragements and considerations.

Content

List of figures

List of tables

List of Acronyms

AC—Alternating Current

ABT—Automatic Bus Transfer

ADC—Analog to Digital Converter

ASF—Active Shunt Filter

AIE—Active Impedance Estimation

ANN—Artificial Neural Network

AUB —Athens Utilities Board

BDB—Backup Distribution Board

BIU—Bus Interface Unit

CWT—Continuous Wavelet Transform

CPS—Combined Power System

CB—Circuit Breaker

DAC—Digital to Analog Converter

DC—Direct Current

DF—Distribution Factor

DFT—Discrete Fourier Transform

EMPT—Electromagnetic Transients Program

EHV—Extreme High Voltage

FFT—Fast Fourier Transform

FPGA—Field Programmable Gate Array

GPS—Global Positioning System

HVAC—High voltage AC

HVDC—High voltage DC

IPS—Integrated Power System

IAI—Impedance Analysis Interface

JTAG—Joint Test Action Group

MBT—Manual Bus Transfer

MDB—Main Distribution Board

MEM—More Electric Marine

MEA—More Electric Vehicles

MEA—More Electric Aircraft

POM—Point of Measurement

POI—Point of Injection

PIE—Passive Impedance Estimation

PSD—Power Spectral Density

PROM—Programmable Read Only Memory

PWM—Pulse Width Modulation

PV—Photovoltaic

QDR— Quad Data Rate

SNR—Signal to Noise Ratio

SPS— Segregated Power System

TFE—Transfer Function Estimation

THD—Total Harmonic Distortion

STATCOM— Static Synchronous Compensator

Chapter 1

Introduction

1.1 More electric vehicles and integrated power system

The concept of More Electric Vehicles (MEV) system, as one type of power distribution systems, emphasizes the utilization of electrical power system instead of non-electrical power transfer systems [1]. Morden MEV systems are commonly utilized in aircrafts, land and sea vehicles for the advantages as high efficiency and survivability. Compared with traditional vehicle systems, the concept of MEV emphasizes the utilization of electrical systems instead of mechanical, hydraulic, and pneumatic system to optimize the vehicle economy, emissions, performance and reliability [1]. Therefore electric power distribution systems with larger capacities and more complex configurations are required to facilitate increasing electrical demands in an MEV power system [2].

Power converters are involved in MEV for power generation, distribution and utilization of the power supply sources, power distribution lines and loads as shown in Figure 1.1

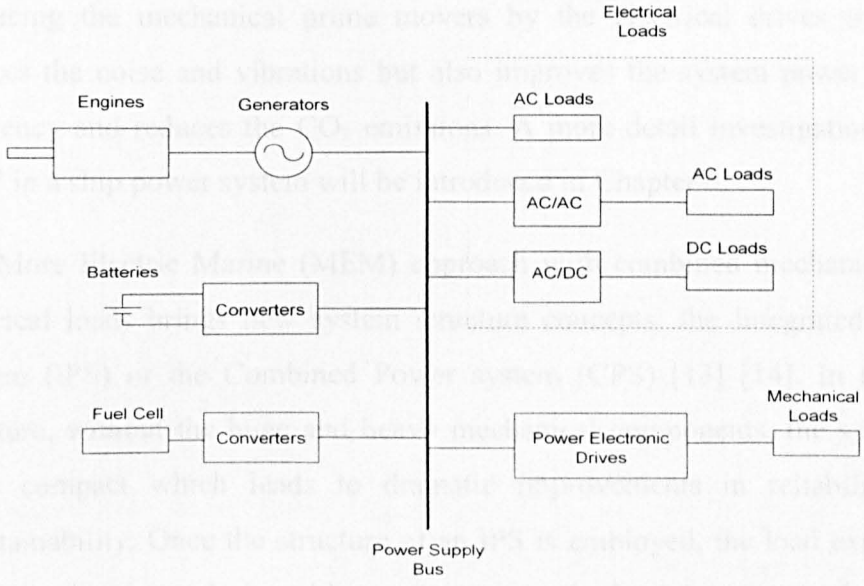

Figure 1.1 Typical power distribution system configuration of a MEV

A typical power marine distribution system configuration of MEV is shown in Figure 1.1. The electrical power generated by generators, energy storage units (batteries) and fuel cells provides the electric power through the power distribution buses to both electrical loads and mechanical loads. Thanks to the development of the power electronic converters and drives, different loads and power supplies can be connected together simply by distribution cables. For example, in the marine system, based on the concept of MEV, the traditional mechanical propulsion system is replaced by the electric proposition [11] [12] as shown in Figure 1.2. This gives the concept of More Electrical Marines (MEMs).

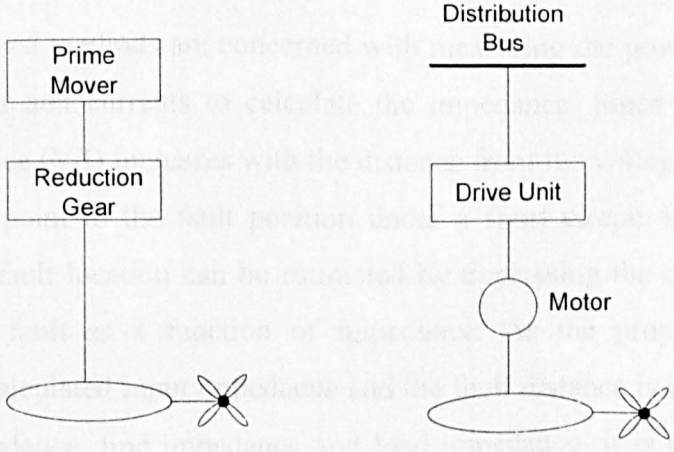

Figure 1.2 Propulsion systems in conventional marine and MEM

Replacing the mechanical prime movers by the electrical drives not only reduces the noise and vibrations but also improves the system power supply efficiency and reduces the CO_2 emissions. A more detail investigation about MEV in a ship power system will be introduced in Chapter 6.

The More Electric Marine (MEM) approach with combined mechanical and electrical loads brings new system structure concepts: the Integrated Power System (IPS) or the Combined Power system (CPS) [13] [14]. In the IPS structure, without the huge and heavy mechanical components, the system is more compact which leads to dramatic improvements in reliability and maintainability. Once the structure of an IPS is employed, the load expansion can be realized simply by adding or removing the load accompanied with its drive unit to the IPS. With the "plug in and plug out" function, the system flexibility is enhanced according to load development and technology requirement. However, for a vehicular system which relies mainly on the electric power supply, the system survivability in case of electrical faults is more important than ever. A fast and accurate fault location method which is designed to realize a quick system recovery is required in the protection scheme of a vehicular IPS.

1.2 Traditional distance protection schemes

1.2.1 Impedance based protection

Impedance based methods are concerned with measuring the power frequency phase voltages and currents to calculate the impedance. Since the value of input impedance (V/I) increases with the distance from the voltage and current measurement point to the fault position under a short circuit fault situation [15][16], the fault location can be estimated by expressing the distance from substation to fault as a function of impedance. As the proportion factor between the calculated input impedance and the fault distance is influenced by the fault impedance, line impedance and load impedance, it is impossible to determine if the fault is inside or outside the line section by using single zone protection (at least two zones are required)[115].

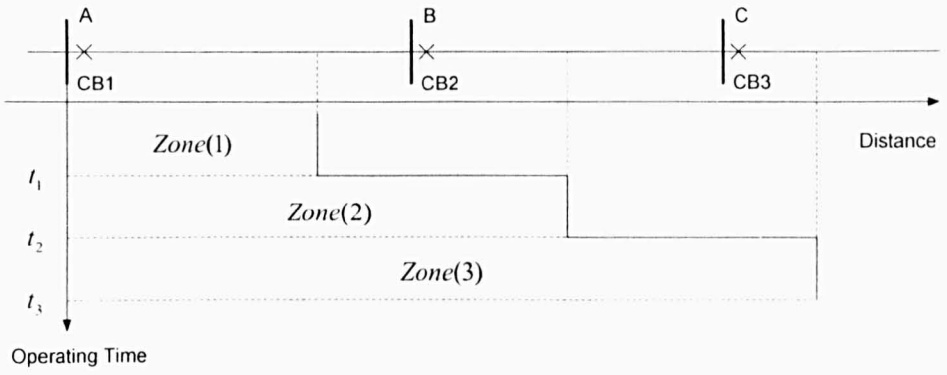

Figure 1.3 Three zones impedance based distance protection strategy

A Typical three zones impedance based scheme shown in Figure 1.3, for circuit breaker 1 (CB1), *Zone(1)* covers 90% of the line impedance of line section (A-B) within time setting t_1, *Zone(2)* approximately covers 50% into the next adjacent line section and *Zone(3)* covers 25% into the adjacent line section beyond at operating time t_2 and t_3 respectively. Each circuit breaker (CB) has three zone impedance settings, and these settings co-operate. *Zone(2)* for CB1 act as backup for *Zone(1)* of CB2. *Zone(3)* of CB1 and *Zone(2)* of CB2 act as backup of for *Zone(1)* of CB3.

1.2.2 Travelling wave based protection

The travelling wave based protection scheme is well known for its fast and accurate fault location on transmission lines [17-20]. Short circuit faults on the transmission line create a sudden collapse in voltage at the fault location. The abrupt changes in the voltage causes high frequency travelling waves at the fault point, superimposed on the power frequency signals, to propagate away along the transmission line in both directions from the fault at a speed close to the speed of light as shown in Figure 1.4.

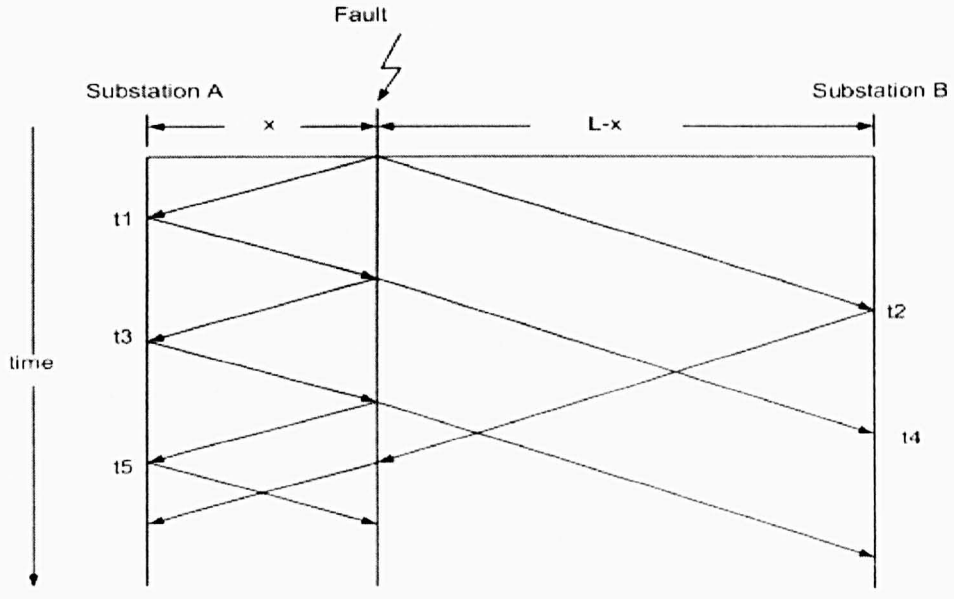

Figure 1.4 A Bewley Lattice diagram depicting a fault

The Bewley Lattice diagram [36] given in Figure 1.4 shows that a fault occurs at a distance x to the substation A on the transmission line which connects substation A and B over a distance L. Travelling waves generated by the fault propagate in both directions towards substation A and B and reflect once they reach the substations.

For a single-ended method which measures the fault transients at one location only and relies on identifying the second or third incident pulse reflected from the fault location, fault distance can be decided by:

$$x = \frac{(t_3 - t_1)u}{2} \tag{1.1}$$

where u is the wave propagation speed on transmission lines

For a double-ended method which requires synchronised measurements from both ends of the line, the fault location is calculated using the absolute arrival times of the initial wave fronts at each end of the line.

$$x = \frac{(t_1 - t_2)u + L}{2} \tag{1.2}$$

The accuracy of travelling wave scheme relies highly on the performance of the data acquisition units and this limits its utilization in small distribution system such as the vehicular IPS.

1.2.3 Knowledge based protection

The knowledge based distance protection schemes such as expert systems [21] and Artificial Neural Networks [22]-[24] use a heuristic way to solve the problem which cannot be solved by algorithmic formulating. Instead of covering a single line section, the knowledge based scheme is normally utilized in a distribution system with a complex structure and covers the whole or a large portion of the system.

Expert systems are intelligent interactive computer systems which act as human experts (sometimes a human is involved) and make decisions based on a pre-set database of the system configuration, geographical information, experiential cases and rules. In [21], parts of the rules of the expert system are the combination of the conventional protection schemes such as: distance protection, differential protection, over current protection and over load protection. It requires the communication and interaction of all the relays within the covered area to decide the protection action in case of fault.

The Artificial Neural Network (ANN) [22] is a computational network which has a lot of nodes, connections and layers based on the brain neural network. The ANN model has to be pre-trained according to different fault situations and modified to achieve the predicted results. Similar to the expert system, an ANN model contains details of the system information, but the ANN is able to self learn after training without fixed rules. For example, a system contains N layer of nodes and connections with input from first layer and output from the last layer. The training procedure chooses nodes and connections to form different paths from first layer to last layer according to different fault situations then the self learning process can form its own paths. It does not have to be told a specific set of rules like expert systems but instead establishes its own set of rules based on the data it is trained with. Once sufficient training has been performed, the neural networks can make accurate (but not with 100% accuracy) fault predictions of fault locations under a variety of fault conditions and fault resistances [23][24].

The knowledge based protection scheme requires very accurate input information and once the conclusion is made, it is very difficult to re-evaluate the accuracy of the results (such as the results derived by self learning of ANN). The protected system has to be studied in detail to obtain the system information required for learning.

1.3 Research objectives

1.3.1 Project challenges

Faults on power system transmission lines and distribution lines can be classified into two classes: open circuit fault and short circuit fault. The open circuit fault causes load power supply interruption while the short circuit fault is considered to be more dangerous due to the fact that the larger short circuit current may cause overheating or damage system equipment. Therefore short circuit faults should be discovered and located as fast and accurately as possible for fault removal and system recovery.

Conventional protection schemes have more focus on the system fault detection and isolation than accurate location. As in an integrated power system (IPS) in a More Electric Marine (MEM), faults can easily be detected by monitoring the system current variations (the over current scheme and current differential scheme). Once the faults are detected and the fault sections are isolated, it is more helpful to know the precise position of the faults for a fast system repair. Unlike overhead transmission lines which are exposed to faults [4], for the protection of an IPS within modern trains, more electric ships [5]-[10]which have no exposed power transmission cables, it is difficult to remove or restore the faulted line sections without accurately knowing the fault position. Also a fast system recovery in these power systems not only brings benefits in economy but also to the safety of the passengers.

The discussed travelling wave method in Section1.3.3 is fast and accurate when applied into transmission line fault protection. Compared with the travelling wave method, the impedance method is cheaper and more suitable

for small distribution system such as IPS. The Traditional distance protection is based on impedance measurement at the power frequency (50 or 60 Hz), but for typical cable parameters this only has an accuracy of a few km and so is not suitable for distribution systems [3]. A new protection scheme which provides a short fault location time and at the same time achieving high accuracy is required.

1.3.2 Project objectives

The research described in the thesis investigates general fault impedance based fault location techniques and develops a new fault algorithm which can be used in small power distribution systems such as an IPS. Compared with the traditional passive impedance estimation (PIE) based methods [78] [79] which analyse the pre-fault and post fault system impedance at supply power frequencies the proposed method directly uses the fault transients and the fault location time is greatly reduced and the accuracy is greatly increased as well. Unlike the Active impedance estimation (AIE) method [91] which involves an extra controlled power electronic device for current or voltage distortion injection, the proposed passive methods (single-ended method and double-ended method) only requires voltage and current acquisition units from single (or both) ends of the protection cables.

Considering online impedance estimation, the AIE methods normally generate bigger and controllable disturbances which have higher signal to noise ratio and produce more accurate results than the PIE methods. However, from the point of fault location, the fault transients are big enough for an accurate fault locating calculation and this is especially true for systems with a high voltage level and low fault impedances. Also the passive methods do not have to deal with the noise generated by the injection unit for AIE.

The main objectives of the Thesis are therefore summarised as:

1. Develop a fast and accurate single-ended fault location method based on system impedance estimation using fault transients.

2. Develop a fast and accurate double-end fault location method based on system impedance estimation using fault transients as an alternative option for applications according to different fault conditions.

3. Evaluate the proposed single-ended and double-ended algorithms according to different system conditions and fault conditions.

4. Apply the proposed fault location schemes into the protection of a zonal marine power system and also solve the earth fault location problem when the generator is high impedance earth connected.

1.4 Thesis structure

Chapter 2 investigate the previous work relating to online impedance measurement and the fault location algorithms based on impedance estimation. Both passive and active impedance estimation methods are discussed and, compared with the passive method, active methods offer controllable excitation and high signal to noise ratio. Three commonly adopted analysing techniques: Fast Fourier Transform (FFT), Continuous Wavelet Transform (CWT) and Power Spectral Density (PSD) are demonstrated and the CWT is shown to produce smooth results in noisy situation but the curves are not suitable for curve fitting. The strong and weak points of the previous impedance based fault location method (both active and passive) are discussed.

Chapter 3 proposes a single-ended fault location method which directly uses the voltage and current fault transients measured from the power supply point. The idea is demonstrated by simulation and then proved by experimental results from a 20m length cable system which has similar parameters as the cable used in aircrafts. Systems with both linear and non-linear loads, both AC and DC supply situation are investigated and the advantages of the proposed algorithm are then demonstrated by comparing with other single-ended fault location methods which use the power frequency system voltage and current information.

Chapter 4 proposes a double-ended fault location method which directly uses the voltage and current fault transients measured from both the power supply side and the load side. Both a hard fault (step fault) and a restriking fault (bouncing fault) with different fault impedances are investigated. The advantages of the proposed algorithm are then demonstrated by comparing with other double-ended fault location methods which use the power frequency system voltage and current information.

Chapter 5 further examines the experimental results by using a Matlab simulation model which has the same parameters as the experimental system. Then, with the confidence that the simulation can produce similar results under the same fault situations, conditions that the proposed method cannot be demonstrated by the experimental equipments are investigated. The possibilities of 'dead zones' in which the proposed methods may not work are discussed and demonstrated.

Chapter 6 applies the proposed fault location method in the protection of a 50Hz AC 440Vrms line voltage zonal marine system which is considered as a future IPS vessel. The single-end method works alone in each zone without requiring any communication equipment. The double-ended method can cover two zones and provide more accurate results and is more robust to different fault situations. The potential danger caused by earth faults in a high impedance grounded marine power system is discussed and a method using a simple switch unit is proposed to eliminate the potential harm.

Chapter 7 concludes the thesis by summarising the research work investigated and developed, knowledge gained and the contributions made to this research field. The employment of the fault location method into bigger and more detail distribution systems and transmission systems, and also the possibility of arc faults are considered and future work are discussed.

Chapter 2

Impedance estimation and fault location

2.1 Introduction

System impedance estimation techniques have been investigated and developed in the past 80 years [27]-[57]. The commonly adopted methods can be classified into different groups with respect to:

- **Measurement frequency**
  - Sub-synchronous frequency [27]
  - Synchronous frequency [45][46]
  - Super-synchronous frequency [47]-[56]
- **Excitation sources**
  - Active methods [39]-[56]
  - Passive methods [50]
- **System power supply states**
  - Online measurement [27]-[30]

Offline measurement

- **Data processing techniques**

  Fourier Transform [30]-[32]

  Wavelet Transform [56][57]

  Power Spectral Density [51][52]

Effective and accurate estimation of the source, line and load impedance at a certain frequency range from a particular point of inception is an important and challenging task. The basic principle of the impedance measurement is to apply Ohm's law to the measured current and the measured voltage data from the point of common coupling (PCC) at each required frequency as in equation (2.1)

$$Z_f = \frac{V_f}{I_f} \tag{2.1}$$

Compared with the impedance measurement at sub-synchronous and synchronous frequencies, the super-synchronous frequency estimations require a shorter data segment but need to deal with the noise and distortions which already exist in the system or are caused by the extra injection and measurement equipment. Also, due to the attenuation of the excitation sources in the high frequency range, it is more challenging to maintain a good signal to noise ratio (SNR). Online impedance measurement (impedance measured during normal system operation when system is energized) draws more attention than the off line measurement (the impedance is measured when system is de-energized) because it does not interrupt the healthy power system operation and the results can easily by used by other system online monitoring devices. It also, brings more challenges as energized systems are more noisy and un-predictable than de-energized systems. Considering the excitation sources (or the system disturbances), the impedance measurement can be classified into invasive (active) methods [39]-[57] which involve using the switching or injection from extra equipment to deliberately inject distortions into the system as an excitation source and the non-invasive (passive) methods [28]-[38] which use the existing system distortions (most commonly from a

non-linear load or capacitor banks) as the excitation sources. A general review of both methods is present in [63].

Power system fault location algorithms based on on-line impedance estimation can be categorized as active methods [91]-[97] and passive methods [78]-[90]. Active methods use additional injection unit to predict the fault positions by comparing the system impedance changes after fault occurs. Passive methods calculate the line impedances between the observation point and fault location by using the power frequency system voltage and current information in pre-fault, post-fault or during fault situation. This chapter introduces the previous work on the impedance estimation methods and discusses the three commonly adopted data processing algorithms, and then demonstrates the developed fault location methods based on impedance estimations.

2.2 Online impedance measurement

The techniques of online impedance measurement have been developed because they create only a small disturbance to the healthy operation of the system and bring benefit to the electrical system study, passive and active filter design and system protection schemes will benefit from the accurate knowledge of system impedance. Online impedance measurement techniques usually involve the measurement of the voltage and current disturbances (or transients) from which the impedance can be evaluated by using signal processing techniques based on time to frequency domain transformation algorithms such as FFT, CWT and PSD.

Typical online impedance measurement including: the excitation source (transient source) creates voltage and current disturbance to the system (which can include the supply impedance, the line impedance and the load impedance or a combination of these impedances) through the coupling impedance as shown in Figure 2.1.

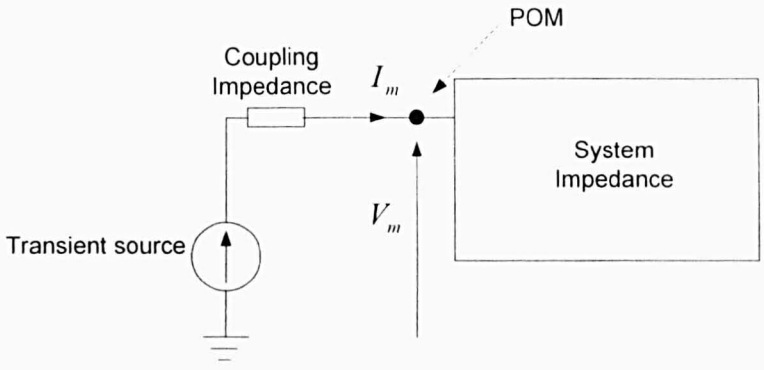

Figure 2.1 Circuit for online impedance measurement

From the view of the excitation source, the online impedance measurement can be classified into passive and active methods.

2.2.1 Passive online impedance measurement

Passive online impedance measurement is realized by monitoring the transients generated by system components such as electronic converters, load switching, capacitor bank switching, tap changing of the transformers and sometimes even the faults.

Passive system impedance measurement using fault transients is not common and difficult to realize in the field test due to the fact that a large fault current may damage the system components. In 1984, Hughes presented a system impedance measurement technique by temporarily imposing a phase to phase fault into a 500kV hydro power system [27]. The field test results were compared with the simulation results derived by using the Electromagnetic Transients Program (EMPT) [27]. The impedance was derived by analysing the fault current and the phase-to-phase voltage obtained from a staged phase-to-phase fault applied to the transmission network and no external source of excitation is required. This work involved measuring the sub-synchronous positive sequence impedance so that the fault duration had to be kept small and equal to an odd number of half-cycles to get more information in the sub-synchronous frequency range. The main advantages of this method are that it does not require any extra device to create the excitation and the transient generated by a short circuit fault is big enough to produce a good signal to

noise ratio (SNR) in the frequency range of interest. The disadvantage is that the fault may create un-expected large disturbance and possible damage to equipment.

The switching of capacitor banks which are commonly used on transmission lines for reactive power compensation (power factor correction) has been used as an excitation source for system impedance estimation [28]-[36]. In 1978, Crevier and Mercier processed an impedance estimation test on a 12kV substation by means of the switching of a 10MVA capacitor bank [28]. The current and voltage was recorded digitally and the phase and amplitude of the harmonic impedance were estimated at harmonic frequencies up to the 19^{th} order. Because of the relatively low SNR which is especially true in the high frequency range, this method has to deal with the issue of precision.

The method of using the transients generated by capacitor switching has be developed and widely used due to the fact that the auto-capacitor bank switching is commonly adopted for power factor control in distribution power systems. D. T. Rizy presented a paper which studied the system voltage harmonics due to the switching of different capacitor configurations on the Athens Utilities Board (AUB) in Athens in 1987[29]. Both harmonics and transients were analyzed by using total harmonic distortion (THD) and a transient network analyzer to detect the contribution of the switch component to both the harmonic overvoltage and the transient overvoltage. In the same year, A. S. Morched and P. Kundur performed an experimental test on a distribution system using the capacitor bank switching to calculate the load feeder impedance (12.58MVA and 14.9MVA) in a frequency range up to 5kHz [30]. The transients generated by the 27.6kV capacitor banks were captured by a potential transformer and a feeder current transformer and the data was recorded with a 200kHz sampling rate to ensure good frequency resolution with a short time domain data segment (0.04s). This load impedance measurement configuration, as shown in Figure 2.2, has been commonly used [32].

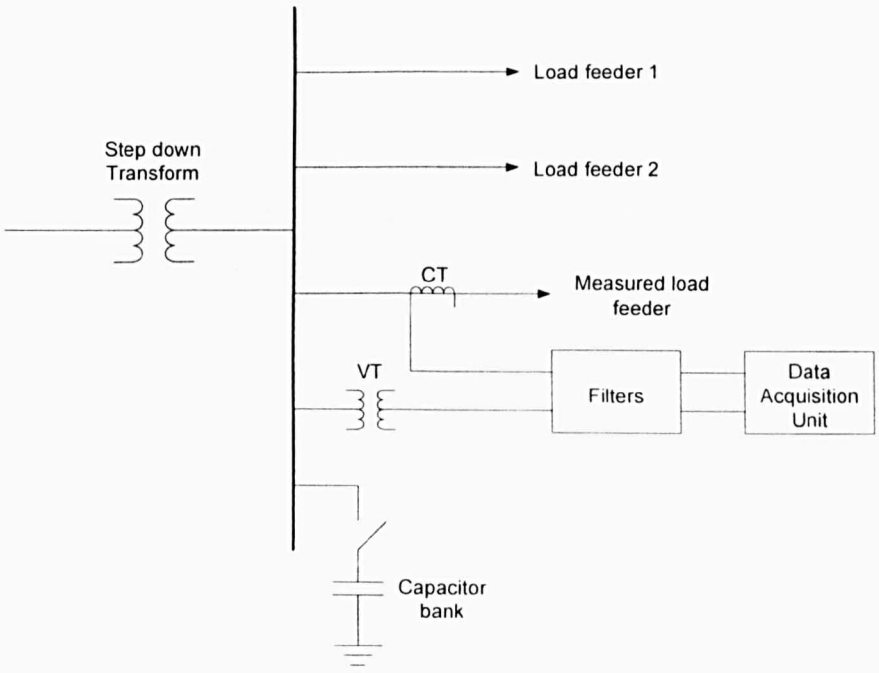

Figure 2.2 Configuration of load impedance estimation

Girgis and McManis used the same measurement configuration in their paper [31], and the power spectral density was applied in the frequency domain transformation. By using the index of the correlation of the input and the output (current and voltage), the results with high noise level (low index value) can be rejected. Compared with the FFT, the power spectral density method involves correlation filtering and offers more smooth results in a low SNR situation. However this method suffers from spurious cross correlations between the voltage and current. Papers [33] and [34] showed the advantages of the Clark transform (α, β, 0) during transient calculations compared with the synchronous component method during the three-phase system impedance estimation.

Transients generated by transformer tap changing were used in Palmer's paper [36] and this method acts as an alternative excitation source for three phase impedance measurement. Test results of both capacitor bank switching and transformer tap changing were presented and although the capacitor switching offers higher spectral energy, the author suggested that the viability of the using the tap changing operation should be investigated further because it makes the harmonic measurement easier given the wider availability of on-

load tap changing transformers compared with the availability of capacitor banks.

In Oliveira's paper [37], the author presented three approaches based on using a known switchable shunt impedance and/or nonlinear load. This method can be explained by using a simplified system model as shown in Figure 2.3.

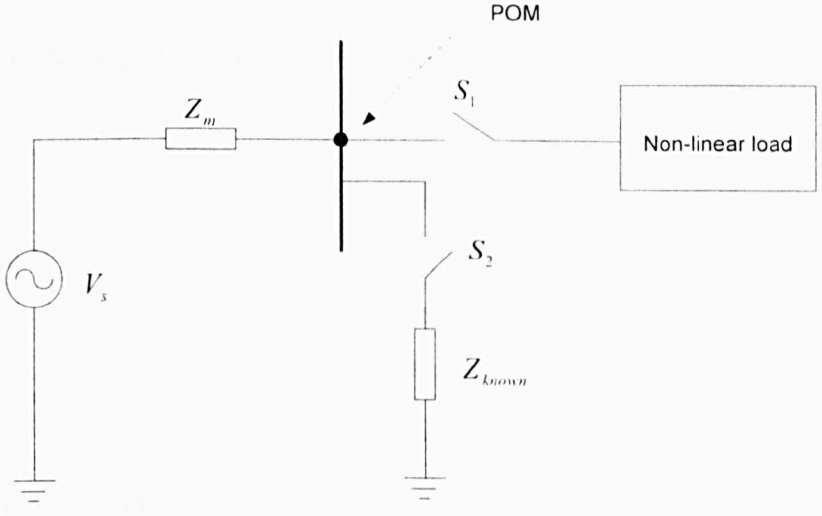

Figure 2.3 Oliveira's circuit for impedance measurement

The system in Figure 2.3 contains the system supply voltage (V_s), the measured impedance (Z_m), the known impedance (Z_{known}) and the non-linear load. The first approach assumes that the load is not connected to the system ($S_1$is open) and the supply voltage contains harmonic distortion and it can be measured when both S_1 and S_2 are open. So that after S_2 closed, the measured current (I_m) at POM can be used to calculated the Z_m:

$$Z_m = \frac{V_s - I_m \cdot Z_{known}}{I_m} \tag{2.2}$$

The second approach assumes that V_s is purely sinusoidal and after closing S_1 the distortion of the non-linear load can be used for the estimation of Z_m and at harmonic frequencies V_s is short circuited. The third approach considers harmonics that exist in V_s and the switch transient of S_1 can be seen as another harmonic source and, beside the current measurement, adds another voltage measurement unit at the POM, then the Z_m can be calculated.

$$Z_m = \frac{V_s - V_m}{I_m} \tag{2.3}$$

This paper simply discussed the possibility of using the load distortion for impedance estimation and this was developed in Xiao's paper [38] which investigated the error caused by asynchronous measurement with a 100kVA 6-pulse AD/DC rectifier bridge load.

2.2.2 Active online impedance measurement

The active online impedance measurement techniques involve the use of controlled electronic devices to introduce a current or voltage transient distortion to the system through coupling impedances at variable locations of the system and measuring the corresponding voltage and current response. Although extra equipment is normally needed, this method has been developed because of its controllable operation and high flexibility.

Between 1994 and 1996 Harris and Rhode developed an online active impedance measurement technique by injecting a small current with known frequency into the system [39]-[41]. The device, called a Digital Implemented Network Analyzer, can be used to measure any part of the system impedance without disturbing the healthy operation of the power system.

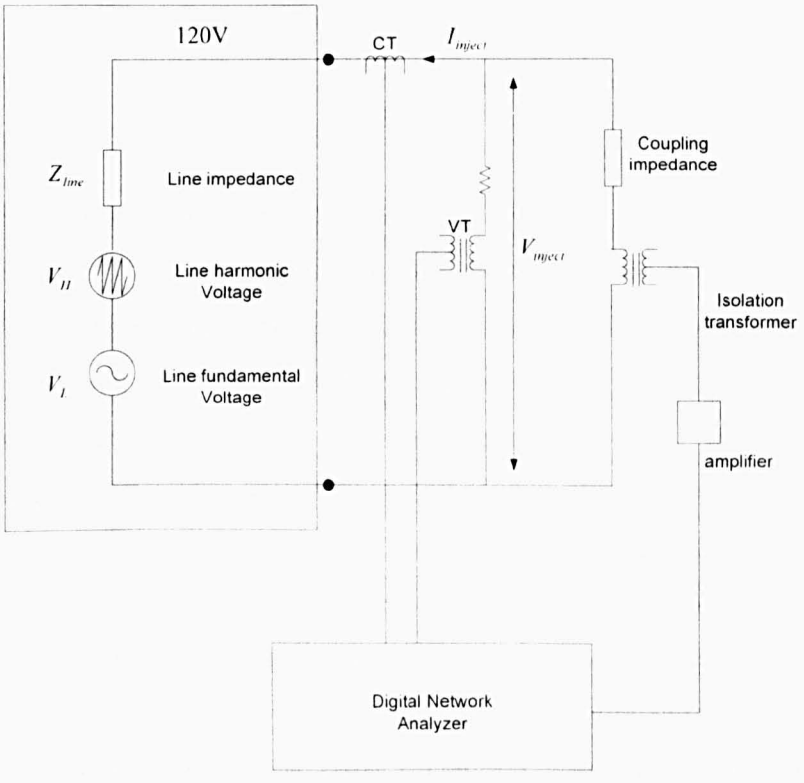

Figure 2.4 Circuit of active impedance measurement unit

As in Figure2.4, the line impedance circuit was modelled as impedance, line harmonic voltage and line fundamental voltage. A sinusoidal current was injected into the 120V line model circuit through the coupling impedance and by choosing the frequency of injected signal the influence of voltage harmonic inside the line model can be reduced.

A similar injection method was used by Czarmecki and Staroszczyk [42] [43], and the injected current was not a sinusoidal signal but a current transient. The authors designed a harmonic generating device connect to the load side as a current injecting source. It was found that the transients injected by additional device have larger SNR than the disturbance created by capacitor bank switching. A four parameter method was employed: using the system supply harmonic, load harmonic, supply impedance and load impedance, two equations can be formed and by repeat measurement the four parameters can be derived. Moreover the noise influence coming from both system and the injection unit was investigated on the measurement and calculation errors during the impedance estimation process. The author found out that the estimation accuracy can be improved by increasing the disturbance level, but

the disturbance level has to be a compromise value which enables accurate impedance estimation and at the same time does not interrupt the system operation.

In 2000, Tsukamoto proposed an advanced measurement technology to clarify interaction between a harmonic current source and the utility power system [44]. The author's impedance measurement was based on inter-harmonic current injection. A device which generated inter-harmonic current was used and due to the fact that little inter-harmonics exist in the power system, by measuring the inter-harmonic voltage and current, the harmonic impedance can be achieved by interpolation of the adjacent inter-harmonic impedance. This process was investigated to measure the supply side and the load side impedance individually and to classify the harmonic current flow into and out of the load. Field tests were processed and the results showed this technique can greatly increase the measurement accuracy and eliminate the influence of system harmonics.

Active online impedance measurement without using additional device has been investigated with the development and wide utilization of power electronic converters in power systems. By modifying the existing converters, a harmonic current can be generated and used to estimate the system impedance. Asiminoaei et al. develop an active on line grid impedance estimation method by using the current transient generated by Photovoltaic (PV) inverter [45]-[48]. The author injected a non-characteristic harmonic current at POM by using the control logic and the frequency of the injected signal was chosen to be close to the fundamental frequency to eliminate the influence of a parallel capacitor. A 75 Hz, 1.5A current was injected in to the system and in order to calculate the system fundamental frequency impedance, a correction factor based on grid characteristic is implemented for error correction. The proposed method is suitable for systems with high inductance, because in the low frequency range the calculated system reactance is much smaller than the resistance in a normal grid.

Corzine et al [49] suggested an AC impedance measurement technique based on d-q reference frame instead of the normal a-b-c reference frame. The author

investigated three different situations of current injection for the AC impedance measurement: by using power converters, chopper circuits and induction machines. Comparing with the advantages and disadvantages of each current injection unit and its switching frequency characteristic, the author suggested that power converters should be used in low voltage and low power systems, chopper circuits are suitable for medium voltage systems and the induction machine can be used in different voltage levels but the wound rotor needs a custom design for current injection.

Authors from the University of Nottingham carried out development of a fully controlled injection technique for online impedance measurement between 2000 and 2006[50]-[57]. [50] proposed an online active harmonic impedance measurement technique by using the injected current from a controlled converter. This converter could be a stand alone device, or embedded into the existing power quality components in the system such as active shunt filter (ASF) or in the power-electronic interfaces for embedded generation.

The test system is shown in Figure 2.5 in which both the value of supply impedance and value of system impedance (the supply impedance in parallel with the load impedance) were estimated.

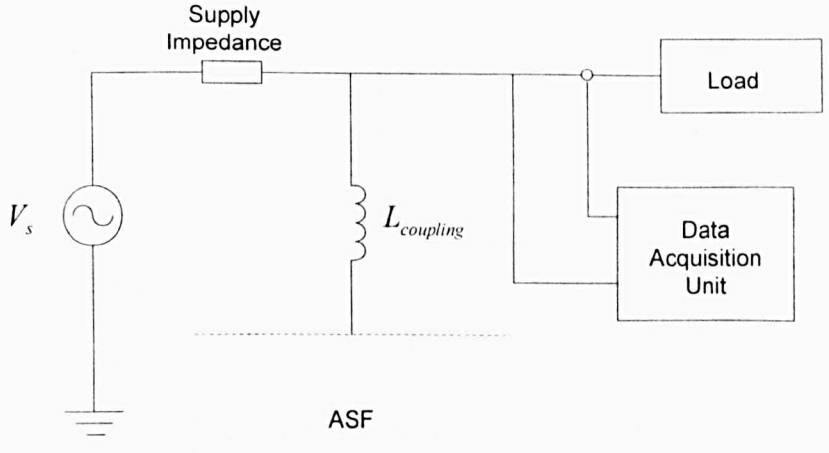

Figure 2.5 Impedance measurement involving ASF

As the technique employs controlled power electronic devices it may either be used as a stand alone piece of measurement equipment, or it has the possibility of be embedded into the functions of an Active Shunt Filter for improved harmonic control (Although the ASF is not included in Zanchetta's paper). Using a similar injection method, [51] and [52] investigated an impedance estimation test by injecting a step voltage disturbance into different load models as in Figure 2.6.

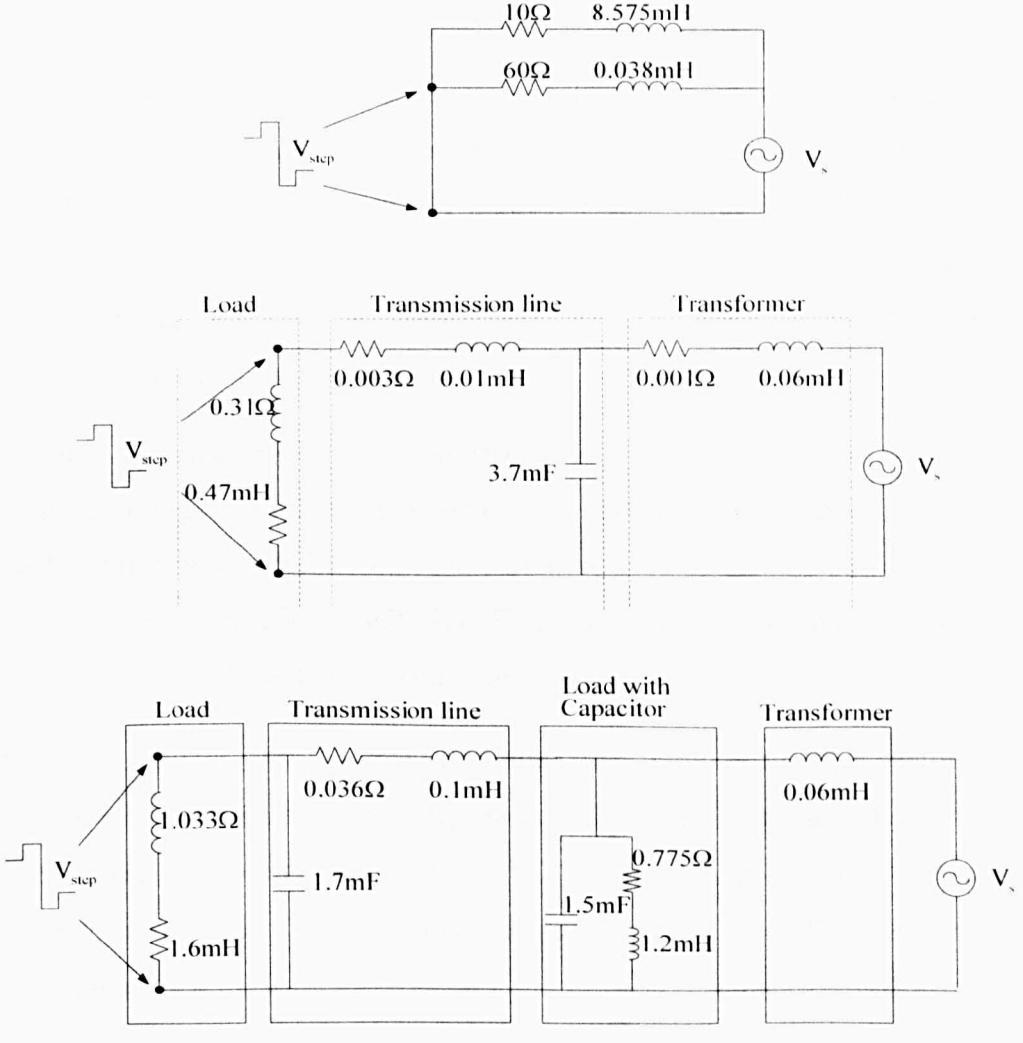

Figure 2.6 Load models for impedance estimation [52]

Both simulation and experimental tests were performed and the acquired measurement data was analyzed using both Discrete Fourier Transform (DFT) and the Power Spectral Density (PSD) transformation packages embedded in the Transfer Function Estimation (TFE) function of MATLAB. The TFE function estimates the transfer function of a system with measured input and

output quantities using *Welch's Averaged Periodogram* Method [58]. The TFE method divides the measured voltage and current into overlapping sections. For example 8192 recorded samples are split into 8 sections (1024 points each). Each section of data is treated individually for initial processing. PSD of each section is calculated and overall PSD of the entire data is found by averaging the individual sections. Then a Hanning window was used to smooth the edges of the data sections and then the data was zero-padded to the required length to improve the output frequency resolution. The transfer function of the system can be derived by dividing the PSD of P_{xx} and P_{xy} (which are the DFT of the input auto-correlation and the cross correlation between the input and the output). The correlation process before the DFT improves the SNR by filtering out the uncorrelated noise and in particular case reduces the large absolute errors in the impedance estimate at the frequencies where the voltage and current signal strengths are low. Very good accuracy of the impedance estimation results was achieved.

Besides injecting the voltage disturbance to the system, several approaches (supply voltage modification, voltage feed forward control and current feed back control) were tried to limit the current to 10A so that the current will not damage the system components and the accuracy of the impedance estimation is significantly affected at the same time [51].

In 2001 Sumner and Thomas continued the work of voltage disturbance injection by using three-phase fully controlled power electronic converters [53]. The voltage transients were extended to 160ms to give a good frequency resolution (6.25Hz). The experiment tests were carried out in the system model as in Figure 2.7.

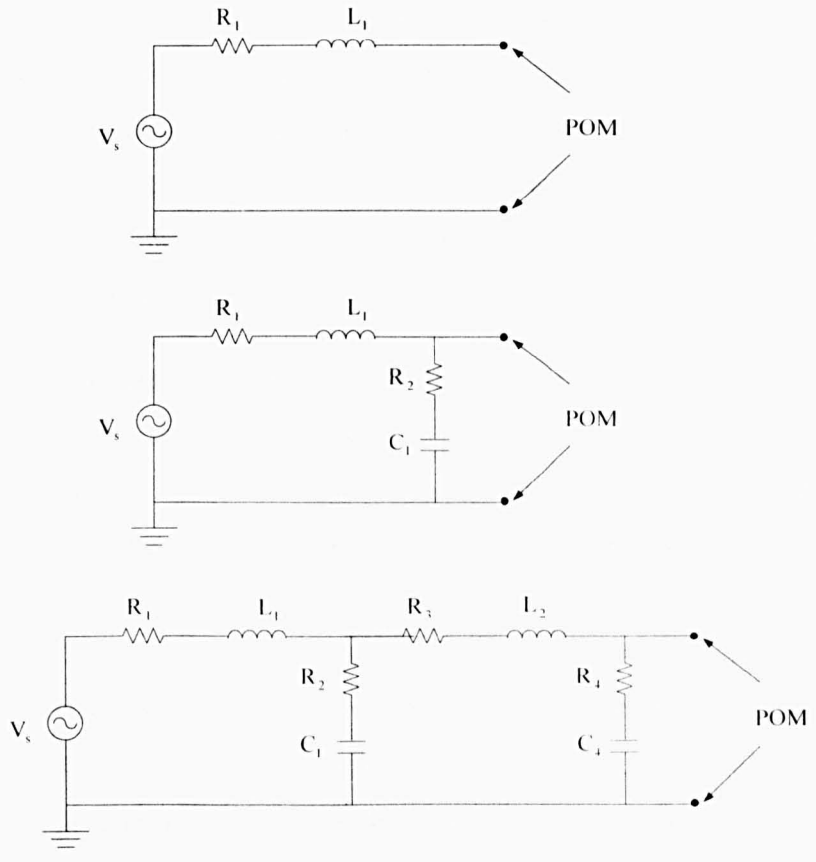

Figure 2.7 Experiment setup for impedance estimation [53]

The three experimental setups, as shown in Figure 2.7, involving different complexity were tested. The first model demonstrated the system supply impedance (transformer), the second model added a parallel capacitance with series resistance based on the first model to include the resonances and the third model consists of transformer, parallel capacitor, line inductor and further parallel capacitor.

This method involved a steady state compensation which cancels the harmonic contribution from the power supply. The voltage and current were recorded for eight cycles just before the injection of the transients (160ms) and then subtracting this from the recorded transient data. This procedure will only eliminate the influence of the existing harmonic in the system before injection and also remove the edges of the steady state waveforms so that no further edges smoothing window (Hanning window or Harming window) is needed. Both the DFT and TFE were used to estimate the system impedance and the results showed that the TFE is more suitable to work in a noisy situation than

DFT for all the three tested models. Although the system impedance and the resonant peaks can be identified accurately, this technique has the limitation that the supply voltage discontinuities due to the switching power electronic equipment will result in inaccuracy in the results and also the 160ms voltage disturbance injection may cause significant influence in the healthy operation of the tested network.

Therefore, an alternative current injection method was investigated in [54] and [55]. Due to the fact that the system is assumed to be stationary during the injection and the transient should decay completely before impedance estimation, it is more practical to derive an accurate impedance estimation results by using transients with short duration. The short term current injection was utilized in [54]. Compared with the voltage disturbance injection which lasts for 160ms in [53], the short term injection was operated by modifying the voltage applied to the coupling inductors in the existing ASF to generate a 550μs triangular current pulse into the system. A time-domain extended Prony method [59][60] was used to analyze the transient data with very few data points and this method works in both linear and non-linear load system. This short term injection method can be widely utilized in power systems because it is able to fully control the amplitude and the duration of the injected current spikes. The injection unit can also be embedded into existing power system components (ASF or controlled induction motor) to regularly update the system impedance information.

Further improvements were made in [56] and [57] which involve Continuous Wavelet Transform (CWT) simulation work. Compared with DFT and TFE which required 160ms (60Hz steady state) data to give a frequency resolution of 6.25Hz. High frequency resolution is required for curve fitting and future data processing. However, the CWT required much less data (5ms). Rather than having a fixed time sinusoidal window in DFT and TFE, the window type of the CWT could be chosen by varying its mother wavelet and the length of the window could be adjusted according to the frequency range of interest (900Hz to 1200Hz).

2.3 Impedance analyzing techniques

2.3.1 Fast Fourier Transform

The Fourier Transform is one of the most frequently adopted signal processing tools for frequency response calculation and on-line impedance estimation. For a series of digital recorded sampling signals, with N samples (x(n)), the DFT can be realized by equation (2.4)

$$X(K) = \sum_{n=0}^{N-1} x(n) e^{-\frac{2\pi i}{N} Kn} \qquad K = 0, 1, \ldots\ldots, N-1 \qquad (2.4)$$

If the N sample series DFT is performed by a computer programme, it requires N^2 complex multiplications and additions [61]. Due to the symmetrical characteristic of $e^{-\frac{2\Omega i}{N} Kn}$, using the 'butterfly representation' of the numerical process [99], the DFT procedure can be simplified and the number of multiplications can be reduce to $N\log_2^N$. This modified calculation is called the Fast Fourier Transform (FFT) which produces the same results as a DFT but is able to greatly speed up the calculations and this is especially true for a data series with a large amount samples.

The FFT is one of the common options because of its fast calculating speed and easy operating logic. In Matlab, the FFT can be realized by a simple code or a function model. The impedance frequency response of a sinusoidal input at its frequency can be estimated accurately with an integer number of cycles of the measured data. However, for a transient input, in order to perform accurate impedance calculation, the FFT needs to include a time domain window to prevent frequency leakage and most importantly to eliminate the influence of the edges of the measured finite signals. This can be demonstrated by measuring the impedance of an RLC circuit with a step current excitation.

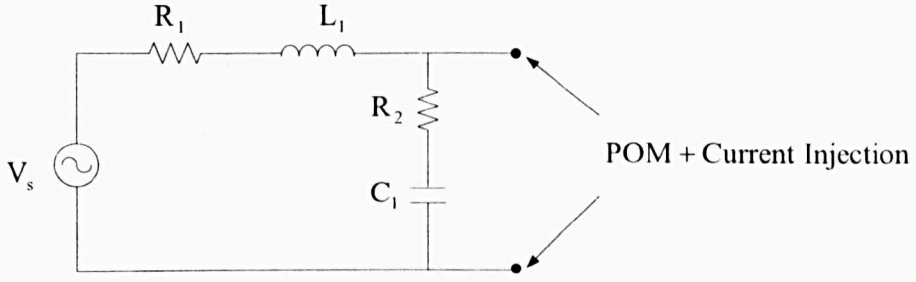

Figure 2.8 Test circuit for impedance measurement techniques: R_1=0.4Ω, L_1=1.15mH, R_2=0.4Ω, C_1=100μF and Vs=10V (peak).

As shown in Figure 2.8, a step current is injected into a 10V(peak), 50Hz AC system. The step current and the system voltage transient response at the Point of Measurement (POM) are recorded as shown in Figure 2.9.

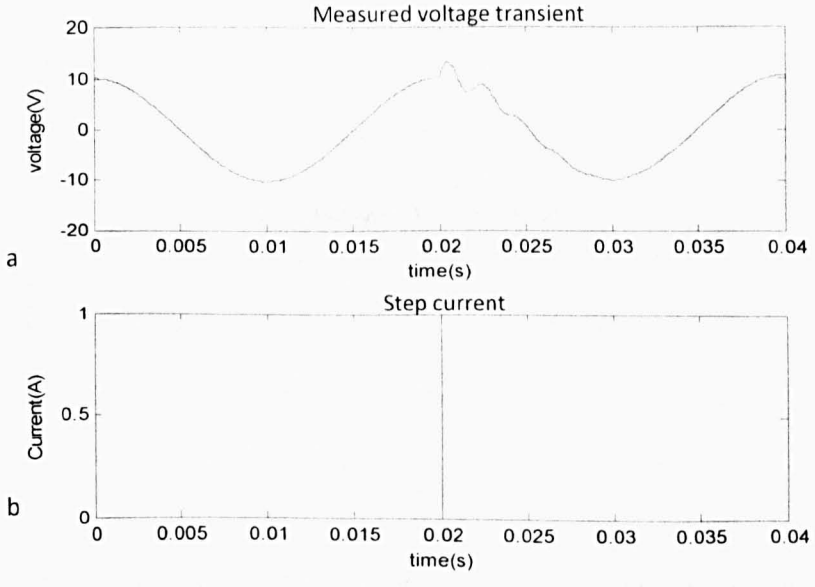

Figure 2.9 Measured step current and voltage transients from POM
a)Measured system voltage response b) Injected step current

As shown in Figure 2.9, two cycles (0.04s) of voltage and current transient data including steady state waveforms were recorded and the current has a step change at 0.02s. The captured data was then transformed into the frequency domain for the system impedance frequency response estimation. However, unlike impedance estimation at the fixed system frequency (50Hz in this system), for a transient impedance estimation which normally involves calculating the impedance at a range of frequencies, more possibilities of influences which may bring errors to the results have to be considered. For the

steady state impedance estimation at a certain frequency, the spectral leakage can be cancelled with integer cycles of data measurement, the transients or noise within the captured data are considered influences only existing in the high frequency results. So that the accurate results can be provided by directly applying a FFT to measured time data after a low pass filter. However, for the transient impedance estimation, the influence introduced by the edges of the steady state waveform is far more serious.

Figure 2.10 shows the FFT results of amplitudes and phase of the impedance versus frequency by directly using the measured data as shown in Figure 2.9.

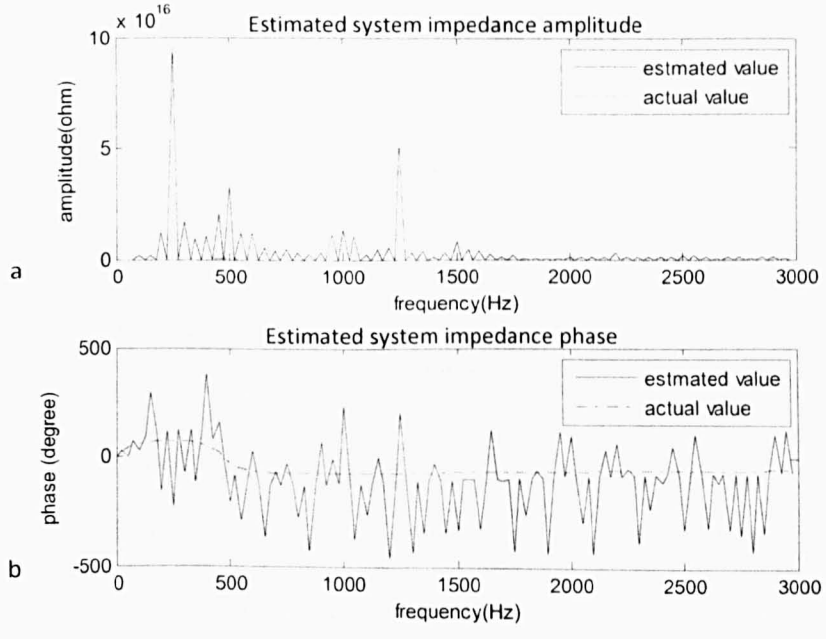

Figure 2.10 Impedance results calculated using FFT without Blackman window

a) Amplitude of the system impedance b) Phase of the system impedance

Compared with the actual value (dashed lines), the estimated results (solid lines) are extremely inaccurate. For this situation, there is no noise added in the system so that all the errors (except the value at 50Hz) are contributed by the edges of the measured signal. As proposed in [53][54], the influence caused by the edges of the measured waveforms can be eliminated by a procedure called steady state compensation which removes the edges and other harmonic distortion already existing in the system signal waveforms before current injection by subtracting an integer number of cycles of the data measured just after the current injection with the same amount of data recorded before the

injection. This procedure could completely remove the information at the system frequency, the edges and most of the system harmonic distortions, but it also adds complexity to the algorithms. The alternative option is to add a window to the measured data. A Blackman window [98] has been added to the data of Figure 2.9 and is shown in figure 2.11.

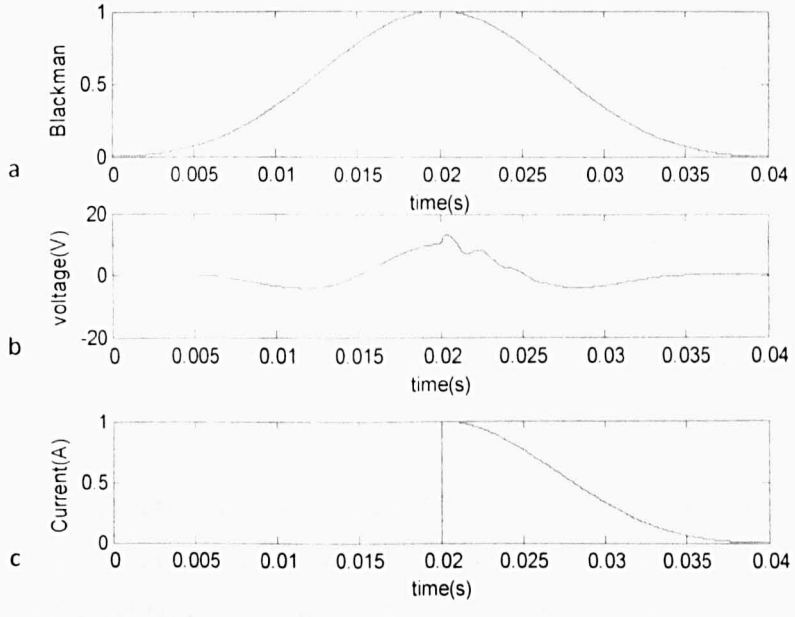

Figure 2.11The captured data after processed with a Blackman window

a) Blackman window b) Windowed voltage c) windowed current

After the application of a Blackman window, as seen in Figure 2.11, the edges of the measured data are smoothed to zero and according to the time domain characteristic of the edge filtering windows, normally the useful transient waveforms are located in the centre of the window where the values of the window are close to 1 to keep the useful transients less influenced by the window. Once the edges of the transient data is removed, the impedance estimating results improve as shown in Figure 2.12,.

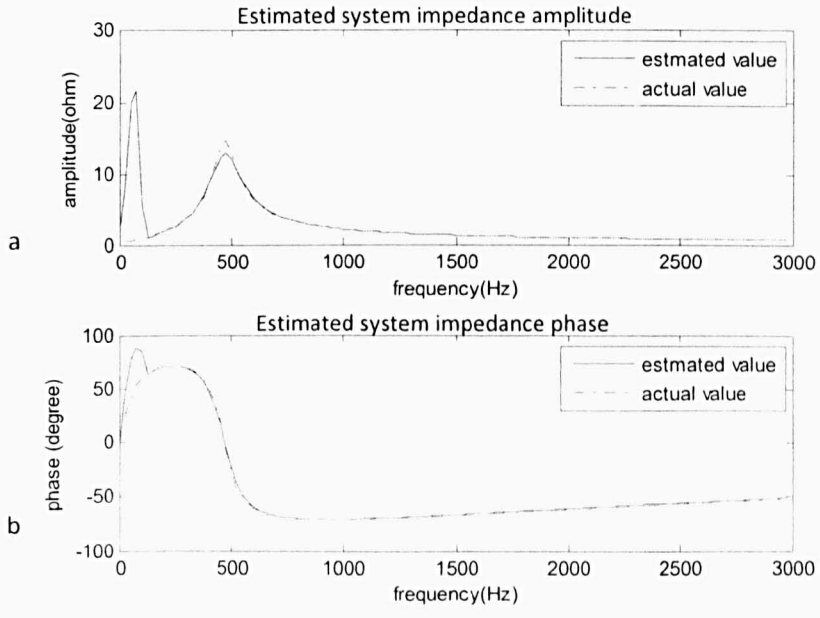

Figure 2.12 The FFT results after processed with a Blackman window

a) Amplitude of the system impedance b) Phase of the system impedance

The largest estimation errors exist at 50Hz due to the steady state influence of the supply. The inaccurate result of the peak value of the amplitude at low frequency (at 480Hz), in Figure 2.12, is caused by the short data segment (two cycles) in which the voltage transient is not fully captured and the low frequency transient oscillations close to the edges of the data segment are removed by the Blackman windowing. The accuracy at this point can be improved by using a longer data segment. However, it is not necessary because the results in the high frequency range show good accuracy.

In order to test the behaviour of the windowed FFT method under a random noise situation, wide band white noise was added to the measured data (both voltage and current information) with 3% (according to rms value of the each recorded data) amplitude. The estimated impedance results are shown in Figure 2.13

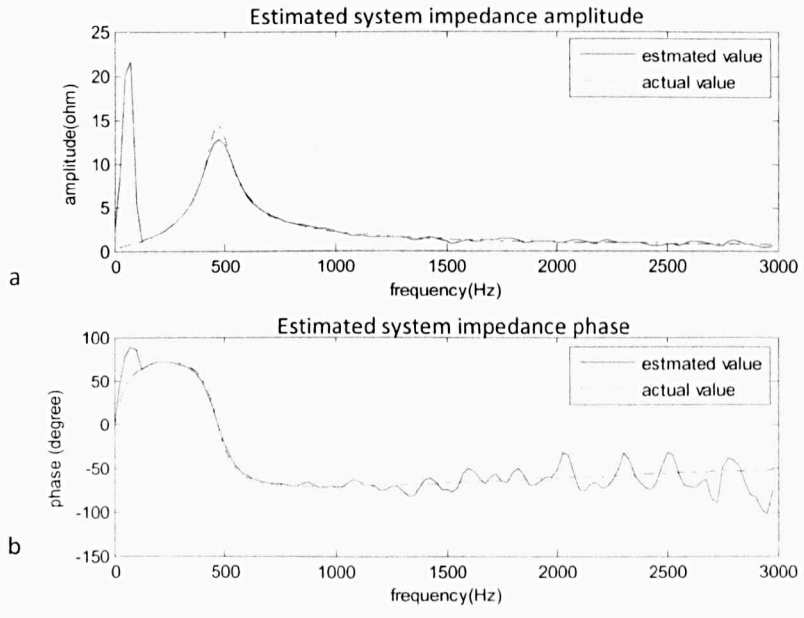

Figure 2.13 Windowed FFT results with a 3% noise

a) Amplitude of the system impedance b) Phase of the system impedance

The noise causes inaccurate estimated results in the high frequency range due to the low SNR of the voltage and current components in this frequency range. The waveform oscillations produced random noise which in practice is due to the data recording A/D quantization errors, transducer errors and the system noise. A curve fitting processes can be applied if the order of the system transfer function is known. This will be demonstrated in Chapter 3 and Chapter 4 with the experimental test results.

2.3.2 Power Spectral Density

The system transfer function can be estimated using several different techniques. The basic method involves dividing the output voltage by the input current in the frequency domain after the raw data has been processed with a FFT. The Power Spectral Density (PSD) is an alternative impedance estimation technique which uses the power spectral analysis of the voltage and current transient to derive the system transfer function [31]. Due to the fact that a correlation which eliminates the un-correlated information is involved during

the PSD calculation, this method is considered to be more effective in dealing with noise than the FFT.

The power spectrum of a signal is the Fourier transform of the auto-correlation and similarly the power spectrum of two signals is the Fourier transform of the cross-correlation of the two signals. The auto-correlation function of a random signal is the expectation value of the product of two samples at time t and time lag τ as in equation (2.5)

$$R_{xx}(t) = E\big(x(t)x(t+\tau)\big) \tag{2.5}$$

where $x(t)$ is the random signal and $R_{xx}(t)$ is the auto-correlation result. The cross-correlation function of two signal $x(t)$ and $y(t)$ is:

$$R_{xy}(t) = E\big(x(t)y(t+\tau)\big) \tag{2.6}$$

According to Jenkins and Watts [62], the discrete biased auto-correlation and cross-correlation are presented in equation (2.7)-(2.8)

$$R_{xx}(m) = \frac{1}{N}\sum_{n=0}^{N-m-1} x(n)x(n+m) \tag{2.7}$$

$$R_{xy}(m) = \frac{1}{N}\sum_{n=0}^{N-m-1} x(n)y(n+m) \tag{2.8}$$

The auto-PSD and cross-PSD can then be calculated by directly applying a Fourier transform to the auto-correlation and the cross-correlation.

The system transfer function calculation using the PSD can be demonstrated using a single input and single output (SISO) system with input $x(t)$ and output $y(t)$:

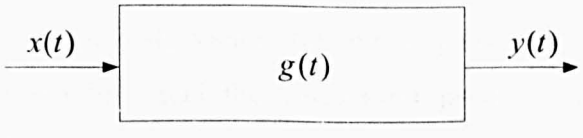

Figure 2.14 SISO system

The direct relation between input, output and the impulse response in the time domain is:

$$y(t) = g(t)x(t) \tag{2.9}$$

The system impulse response $g(t)$ relates to the auto-correlation of the input and the cross-correlation of the output and is shown in (2.10). This equation represents the convolution of the system impulse response and the auto-correlation of the input:

$$R_{xy}(\tau) = \int_0^{\infty} g(t)R_{xx}(t-\tau)\,dt \tag{2.10}$$

and after Fourier transform

$$F[R_{xy}(\tau)] = G(f)F[R_{xx}(\tau)] \tag{2.11}$$

so that

$$P_{xy}(f) = G(f)P_{xx}(f) \tag{2.12}$$

and the frequency response of the system can be derived:

$$G(f) = \frac{P_{xy}(f)}{P_{xx}(f)} \tag{2.13}$$

Considering the system impedance estimation, the input is the system current and the output is the system voltage. The system impedance frequency response can be written as:

$$Z(f) = \frac{P_{iv}(f)}{P_{ii}(f)} \tag{2.14}$$

For the same noisy situation as discussed in Section 2.3.1, compared with the results in Figure 2.12, the PSD results shown in Figure 2.15 provides a slightly better result than the FFT and the correlation process can provide better frequency resolution for the same data length. For this test, the PSD dose not provide much better results than a FFT and it also requires windowing to filter out the edges of the measured waveforms.

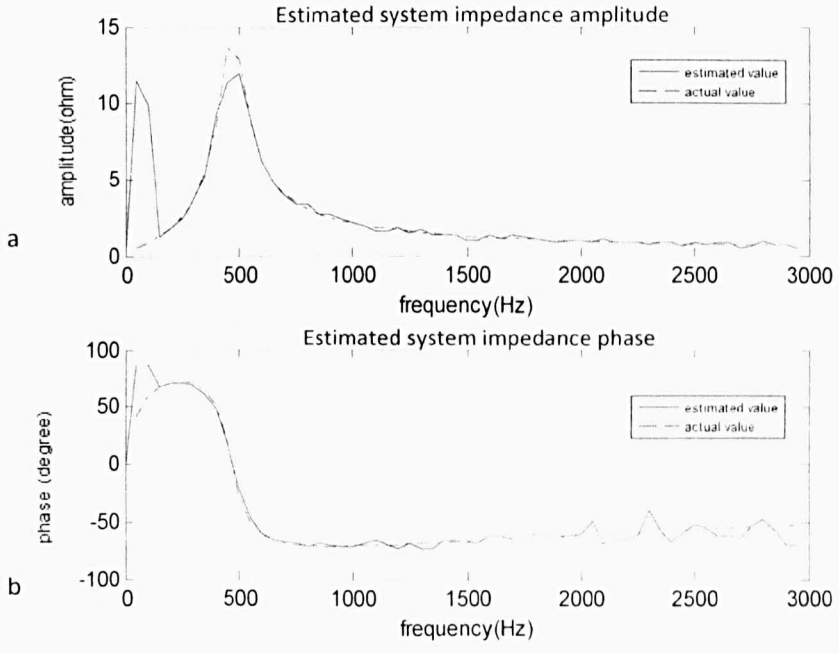

Figure 2.15 Results derived by PSD in noisy situation with Blackman window

a) Amplitude of the system impedance b) Phase of the system impedance

The PSD method which uses the periodogram technique [141][142] involves the squared magnitude of the Fourier transform and should have the same results as FFT. The TFE (transfer function estimation) in Matlab which calculated the PSD uses Welch's averaged periodogram can provide much better results than a direct FFT. It has a default Hanning window to filter out the edges of the measured waveforms. By using the average periodogram, it divides the measured data into several equal length sections and computes the PSD for each section and then derives the average value. This process involves less noise in each calculation by using small lengths of data segments.

2.3.3 Continuous Wavelet Transform

The Continuous Wavelet Transform (CWT) is known as a more effective data processing tool when dealing with non-periodic signals than the PSD and FFT due to the fact that it uses special series of non-sinusoidal wavelets.

The PSD is considered as an improved noise filtering data analysis method based on the Fourier Transform which consists of sinusoidal waveforms. (2.4) can be written as

$$X(K) = \sum_{n=0}^{N-1} x(n)(cos\frac{2\pi i}{N}Kn - sin\frac{2\pi i}{N}Kn) \quad K = 0, 1, \ldots\ldots, N-1 \qquad (2.16)$$

The Continuous Wavelet Transform [64][65] is based on a set of 'mother wavelets' which is not necessarily in the sinusoidal form. By scaling and shifting the mother wavelet function, the coefficient of the frequency of interest at a certain time can be estimated. Compared with the DFT which gives the signal a frequency domain transform, the CWT produces a coefficient with reference to both time and frequency. The CWT calculation of $f(t)$ can be defined by equation (2.17).

$$C(scale, position) = \int_{-\infty}^{+\infty} f(t)\varphi(scale, position, t)dt \qquad (2.17)$$

As shown in (2.17), the CWT is defined as the sum over time of the signal multiplied by scaled, shifted versions of the mother wavelet function φ which is similar to the sinusoidal element in the FFT but able to be adjusted into different wavelets by changing its scale and position characteristics. The mother wavelet is centred with centre frequency w_0 and band limited with bandwidth frequency Δw in the frequency domain and also in the time domain it can be defined at position t and with a duration of Δt[66]. For a mother wavelet at a fixed time, the different scales refer to different frequencies which are the stretched or the compressed version of the centre frequency and the position refers to the width of the bandwidth frequency. The relationship of the centre frequencies and the bandwidth frequencies can be explained by Figure 2.16.

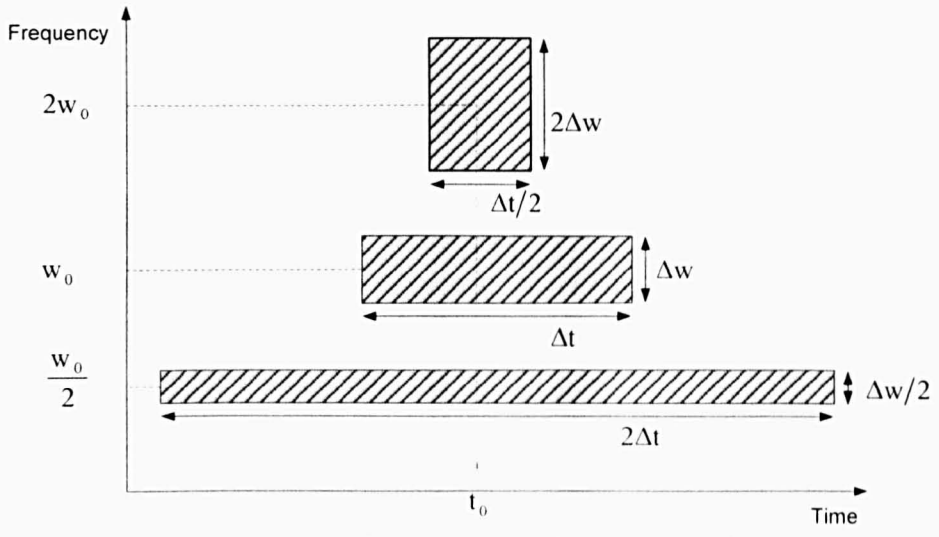

Figure 2.16 Time and frequency analysis of mother wavelet at different scales

As shown in Figure 2.16, the bandwidth is compressed at a lower centre frequency and stretched at the higher centre frequency for a fixed time [64][67]. The direct relationship between scale, centre frequency and the signal sampling frequency is [64]:

$$f_{ps} = \frac{f_c \cdot f_s}{a} \tag{2.17}$$

where f_c is the centre frequency in Hz, f_s is the sampling frequency in Hz and a is the scale. The f_{ps} is called the pseudo-frequency which is the CWT calculation frequency for the coefficient and also can be used for the time-frequency plot. This idea is to associate with a given wavelet a purely sinusoidal signal of frequency f_c.

When looking at the time domain and considering the absolute value of the mother wavelet, the CWT calculation can be explained using Figure 2.17

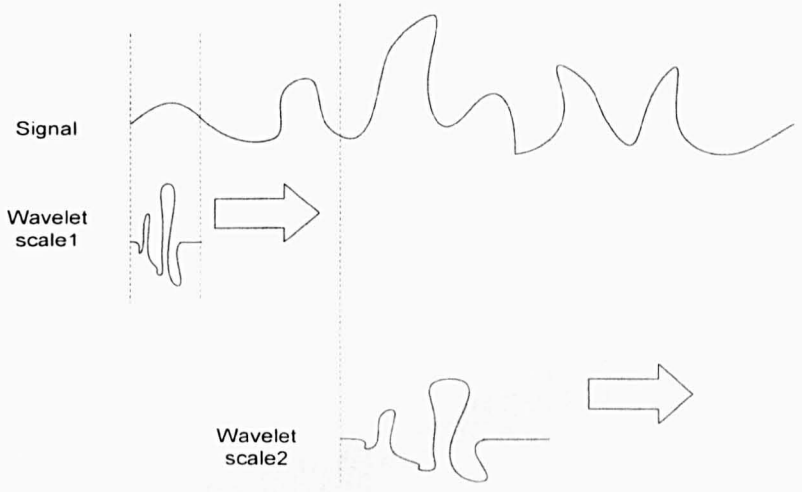

Figure 2.17 The time domain analysis of the CWT

As for a fixed scale of the mother wavelet, the CWT calculates the coefficient (c) which presents the relation between mother wavelet and the signal within the length of the scale. A higher value of c indicates higher similarity. The scaled mother wavelet is then shifted to cover the whole signal in the time domain. Then the scale is changed and the process repeated. So normally when the CWT is completed, for a certain frequency (certain scale), the results with highest absolute value through the time domain are the most accurate.

The complex Morlet wavelet [68] is chose here as mother wavelet for the impedance measurement test in order to calculate the both amplitude and phase information accurately in the frequency range below 5kHz. (Some wavelets, such as Haar wavelet, can not provide amplitude and phase information of the signal accurately)

$$\varphi(x) = \frac{1}{\sqrt{\pi f_b}} e^{i2\pi f_c x} e^{\frac{-x^2}{f_b}} \tag{2.17}$$

where the centre frequency f_c is 2Hz and the bandwidth f_b is 10Hz to emphasize the accuracy of estimated results in high frequency range.

As the CWT is able to produce a time-frequency coefficient result, it is helpful to check the influence of the edges of the measured signal waveforms to the impedance estimation. Figure 2.18 shows the abs value of the step current coefficient after a CWT without any window.

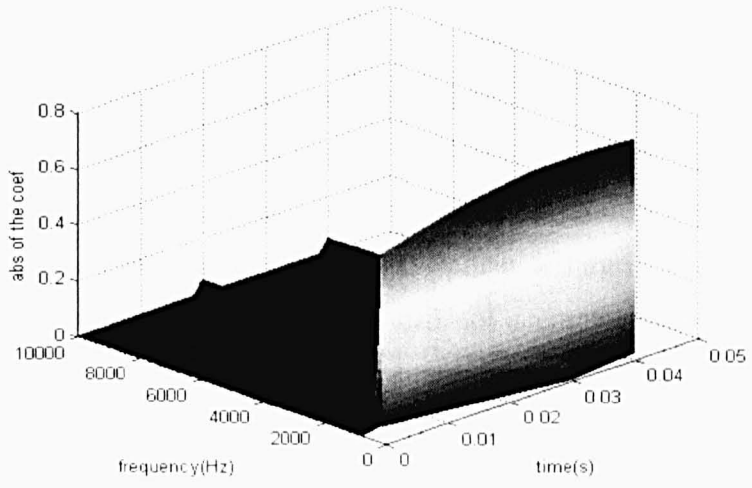

Figure 2.18 3D plot of the step current CWT results

As can be seen in Figure 2.18, except the low frequency inaccuracy, it is clear that the coefficient shows high SNR at both 0.02s and 0.04s in the time domain. The value at 0.02s is generated by the step transient and the value at 0.04s is due to the edges of the waveform.

Three particular frequencies of the CWT results of the voltage and the current without windowing are shown in Figure 2.19. The voltage results are more affected due to the bigger edges shown in Figure 2.9.

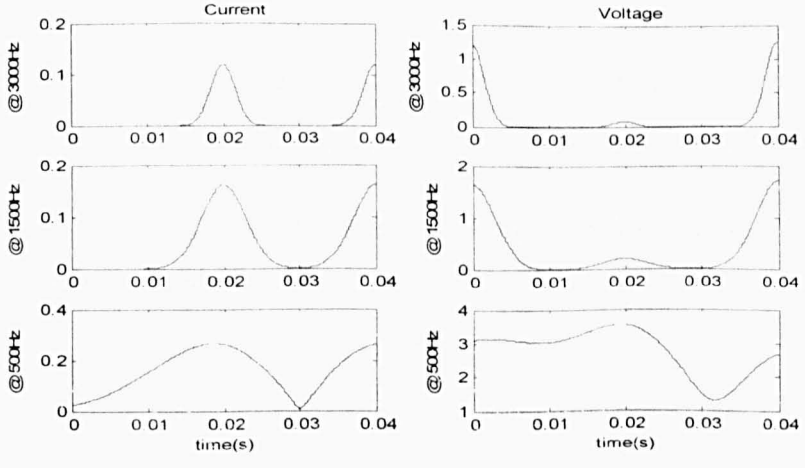

Figure 2.19 2D plot of the CWT results of current and voltage at 3 pscudo frequencies

For the FFT and the PSD calculations, the information generated by both transients and the edges is assembled into the same frequency and this will cause great inaccuracy in the estimated results. The current injection time is known (0.02s), for each frequency, it not necessary to select the coefficient with the largest absolute value for all the time domain and the area can be fixed to the time domain around the current injection (for example from 0.01s to 0.03s). However this is for very high frequency impedance estimation results (above 1kHz), the low frequency results which are produced by the mother wavelet with a narrow bandwidth which reflect a large scale in the time domain as described in Figure 2.16 are still not accurate as shown in Figure 2.20 where the actual value is the pre-set simulation impedance value.

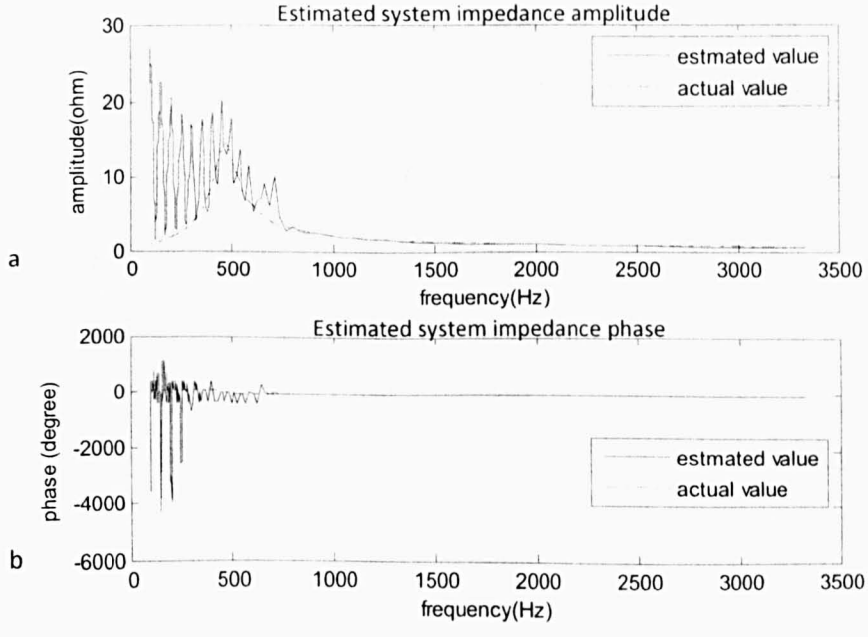

Figure 2.20 CWT impedance estimation results without the Blackman window

a) Amplitude of the system impedance b) Phase of the system impedance

The accuracy of the results can be greatly improved by adding a Blackman window as shown in the Figures 2.21 and 2.22:

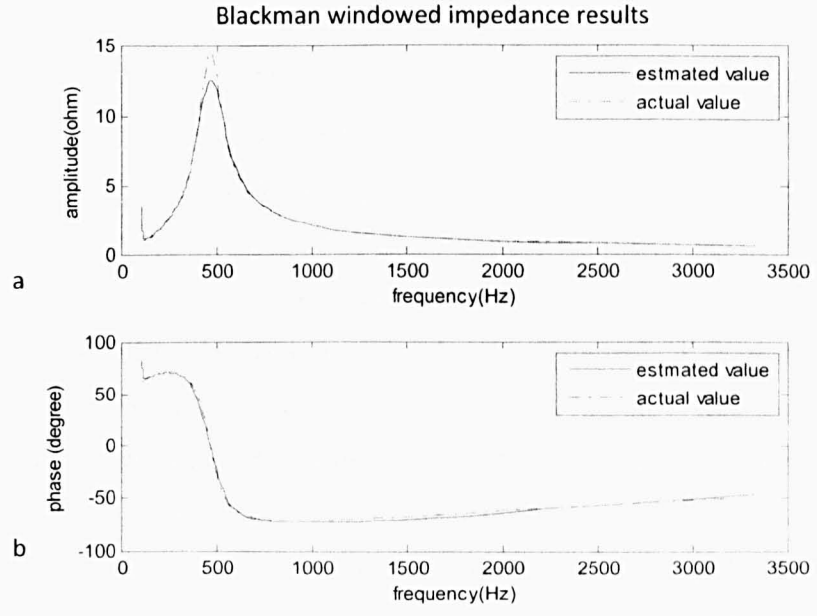

Figure 2.21 CWT impedance estimation results with a Blackman window

a) Amplitude of the system impedance b) Phase of the system impedance

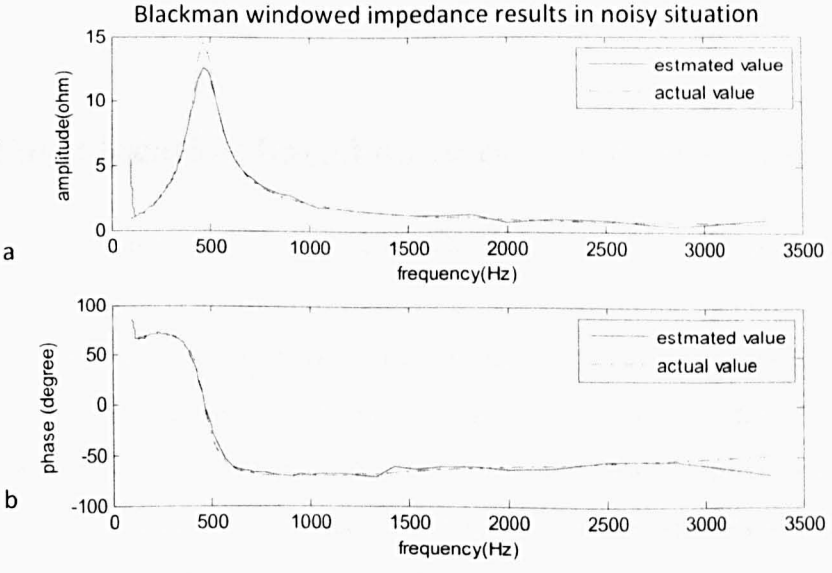

Figure 2.22 CWT impedance estimation results with Blackman window and noise

a) Amplitude of the system impedance b) Phase of the system impedance

Figure 2.21 and Figure 2.22 show the CWT impedance estimation results with a Blackman window when noise is not, and is added to the data. Similar to the FFT and PSD, CWT offers good accuracy with windowed data and in the non-noise situation, and the CWT provides better results than the FFT and the PSD when noise is added. The mother wavelets act as a band pass filter during the

CWT calculation. For each centre frequency, the pass-band equals the bandwidth frequency of the mother wavelet. As explained in Figure 2.16, in the higher frequency range the bandwidth of the mother wavelet is wider which means if it acts as a band-pass filter relatively less noise can be filtered out and this can explain why the high frequency results (2000Hz to 3500Hz) in Figure 2.22 are a little less accurate than the low frequency values (500Hz to 1000Hz). Directly comparing the three figures (Figure 2.21, 2.14 and 2.12), the CWT results are the best (provide smooth results in noisy situation). The CWT which has a band-pass filtering function for impedance estimation at each frequency gives a smoother result in the waveform even when it is not accurate. When noise is presented, the CWT results are impossible to be further modified by curve fittings. Due to the fact that the passing-band (bandwidth frequency) of the band-passing filtering function increases with frequency as presented in Figure 2.16, the high frequency results will be more influenced by the noise

2.4 Fault location based on impedance estimation

A rapid and precise fault location scheme plays an important role in the reliability of fault protection of modern power distribution systems. Ever since the first fault location by mean's of line inspection [77], methods to predict fault positions have been modified and improved to meet the fast development of electrical power networks. The two most common adopted fault location methods are based on impedance measurement and travelling waves [69]. The travelling wave method has been used in transmission line protection for many years because of its speed and accuracy but it is more suitable for long distance (several km) faults and not reliable enough for protection [70]-[73]. Travelling wave fault location has also been tried on distribution power systems but it requires high performance data acquisition equipment [74]-[76]. The fault location methods based on impedance measurement consists of passive methods [78]-[89] and active methods [90]-[96]

2.4.1 Passive method

The passive impedance based fault location schemes which do not require extra injection can be classified into single-ended and double-ended with respect to the voltage and current acquisition unit.

The single-ended impedance fault location method was firstly developed for the protection of transmission lines due to the fact that it does not require a communication channel for phasors from the remote end. However, the fault location results are influenced by assumptions (supply and load side impedance has to be pure reactive; fault current and supply current should be in the same phase and current distribution factor has to be known) as described below and also in [78]-[80].

In 1981, Takagi presented a classic fault location algorithm based on Fourier analysis of a faulted network [78]. The pre-fault and post-fault voltage and current data from one terminal of the transmission line was recorded and the pure-fault data was derived by the difference between pre-fault and post-fault data. The superposition model is shown in Figure 2.23

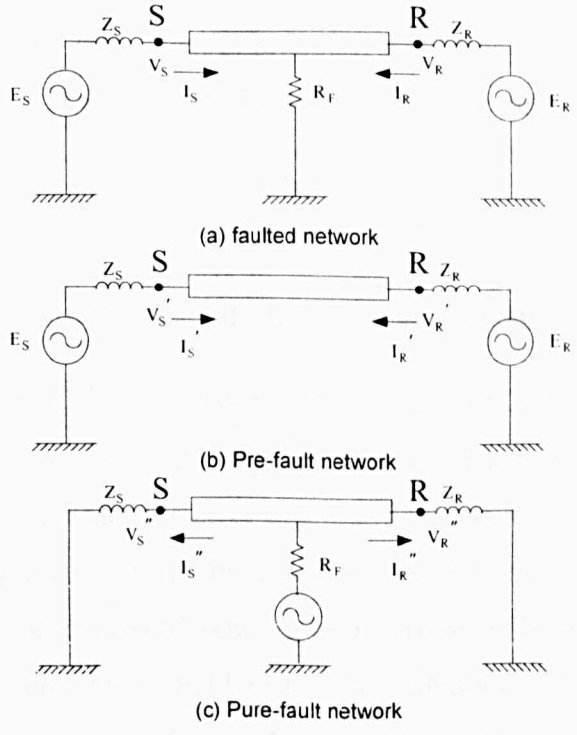

Figure 2.23 Superposition model of pure-fault network [78]

As shown in Figure 2.21, the phasors at the sending end of the superposition network (pure-fault network) are derived by using the measured faulted phasors minus the pre-fault phasors.

$$V_S'' = V_S - V_S' \tag{2.18}$$

$$I_S'' = I_S - I_S' \tag{2.19}$$

The author then developed (2.20) by using the pre-fault and pure-fault information at the supply point.

$$R_F[1 + K(x)] = V_f = -\frac{A(x)V_S - B(x)I_S}{C(x)V_S'' - D(x)I_S''} \tag{2.20}$$

where x is the distance between supply point to the fault point, $K(x) = I_R''/I_S''$, $A = D = cosh\gamma x, B = Z_c sinh\gamma x, C = sinh\gamma x/Z_c$ are the line propagation constant and Z_c is the characteristic line impedance.

Assuming the line impedance and the two source impedances are purely inductive, so that the imaginary part of equation (2.20) is zero. The fault distance x can be derived by solving the non-linear equation. However, the assumption will bring errors to the fault location and also this method is only suitable for the networks which have system parameters close to the assumption. One year later, Takagi proposed a modified single-ended method [79] which uses (2.21) to calculate the fault distance to the sending point:

$$x = \frac{Im(V_S \cdot I_S'')}{Im(z \cdot I_S \cdot I_S'')} \tag{2.21}$$

where z is the transmission line impedance per-unit length.

However, equation (2.21) is theoretically correct when I_S and I_S'' are in the same phase and this is only true in the situation that receiving end is open circuit or the fault resistance is zero. In 1985, Eriksson modified the method in [80] by involving a current distribution factor so that the fault current can be calculated using the measured sending end current without any assumption. This method has undergone field tests and evaluation. The accurate results derived from field tests confirmed the validity of the proposed idea, but in

order to calculate the current distribution factor, the supply impedances from both sending and receiving ends have to be known and this information can not be provided in some networks.

Double-ended fault locators normally provide more accuracy for the fault position results and require less system impedance information and assumptions than single-ended algorithms but need the current and voltage information from the remote end from a signal communication channel which was not easily implemented in the early years.

In 1990, A. T. Johns discussed a double-ended transmission line fault location method using the measured phasors from both ends of the transmission line [81]. The author used the post-fault voltage and current from both end of 400kV, 100km and 250km transmission line to form two equations to calculate the voltage along the transmission line from the view of both ends, as shown in Figure 2.24.

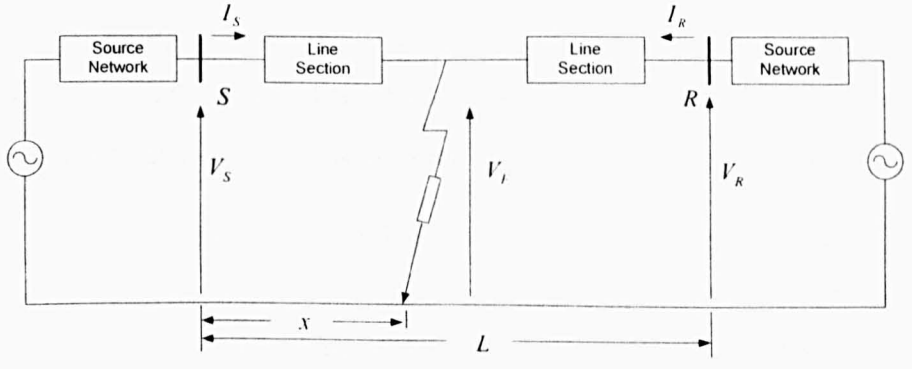

Figure 2.24 A typical transmission line faulted system[81]

$$V_F = \cosh(\gamma x)\, V_S - Z_0 \sinh(\gamma x)\, I_S \tag{2.20}$$

$$V_F = \cosh(\gamma (L - x))\, V_R - Z_0 \sinh(\gamma (L - x))\, I_R \tag{2.20}$$

where Z_0 is the surge (or characteristic) impedance and γ is the propagation constant.

The fault position where the voltages of the two equations are equal was given accurately and this procedure was shown in simulation results to have very small errors. The whole procedure requires no pre-fault phasors and due to the fact that the calculated line reactance of the system is a very small value, only

the line resistance was used. The good accuracy achieved by simulation is under the condition that the phasors measured from both ends are synchronized. Actually the synchronizing measurement is almost impossible without any time trigger reference and the synchronization is one of the main problems that the double-ended scheme suffers when employed into a real power system network by later researchers. Satellite Global Positioning System (GPS) equipment was use to provide a synchronized reference to the measured data. In [82], Kezunovic realized synchronous sampling with a GPS fault recorder. The fault detection and classification were achieved from the differential current from both ends the voltage differential was involved during fault location. However the synchronous measurement will only work when the satellite GPS is available. The other alternative methods calculated the phase difference between the measured phasors from both ends [83][84]. In [83] Damir used a similar post-fault equation as presented in [81] but involved the angle difference δ so that the equation contains two unknowns: the fault distance x and the δ. The equation was than separated into imaginary and real parts to cancel the x. Then the angle δ was calculated by an iterative Newton Raphson method while [84] chose not to use iteration but solve the trigonometric equations and the solution that is close to zero was used.

A. L. Dalcastagne [85]-[87] studied John's method [81] and proposed a new fault location method which calculates only the amplitude of the transmission line voltage using two voltage propagation equations mentioned in [81]. If solving the amplitude equations directly, the phasors difference from both ends will still cause errors. The John Horak and Basler decoupled the three phase model by symmetrical components [88] and only the positive sequence data was used and then a numerical technique was applied based on the assumption that the voltage magnitude calculated along the transmission line increases or decreases linearly with distance. Then instead of solving the real amplitude equations, the assumed linear equation was used and employed with an iteration process to reduce the error between assumed linear equations and the real amplitude equations at the point of the fault (cross point of the two assumed linear equations). However, assumptions of the proposed algorithm

will limit its utilization to certain transmission lines with an amplitude to distance characteristic close to linear.

The problem caused by asynchronous measurement can also be avoided by directly using the amplitude of the measured phasors from two ends [89]-[90]. In this case, no direct equations can be used, but a relationship exists between the amplitude of measured voltages and the system impedance for different fault distances. Zamora discussed the possibility of just using the amplitude of the measured voltages from both ends for fault location in the case when the high fault current may cause current transformer saturation [89]. This method involves superposition modelling and only focuses on the pure fault circuit. The author brought the idea of 'Distribution Factor' which was defined as the quotient of the two voltages of positive sequence resulting from the pure fault on both ends of the line. In fact, the Distribution Factor (DF) equals the amplitude ratio of the measured voltages of the pure fault circuit and is a value based on the system impedance calculation according to different fault positions. In order to locate the fault accurately, the DF has to be pre-known as a reference. When faults occur, by comparing the DF pre-known value with the measured value the fault position can be decided. However, the DF calculation may require a lot of off-line tests which may only be made for certain networks and also when considering the influence of the fault resistances the selection procedure could be more complicated.

2.4.2 Active method

Fault location based on active impedance measurement has been adopted in power distribution systems with the development of control and power electronic devices. The active method provides more flexible measurement, a shorter detection time (by using transient injection) and a better signal to noise ratio.

The most commonly used active fault location methods predict the fault position by comparing the system impedance difference in a fault situation with the healthy system impedance measured from the point of injection [91]-

[95]. An Active Shunt Filter (ASF) controlled current injection unit was designed and developed by M. Sumner et al [56][57] applied the active impedance estimation method on the fault location of the zonal marine power system. The current spike was injected after short circuit fault occurs and the post-fault system impedance was measured. By comparing the different system impedances, faults at different distance with varying fault impedances could be classified. A very short data segment was required for accurate impedance estimation in the high frequency as using the injected current transients and this will reduce the fault location time compared with methods which measured the steady state impedance at system supply frequency. This method was demonstrated in both AC and DC marine systems. The disadvantages of this idea is that off-line tests of system impedance for different fault situations are required as a reference for the fault location and also an active approach requires active equipment to be available and the current injection has to wait until the fault transient in the system has died out and the current created by a PWM converter adds noise to the system that affects the accuracy of fault location.

A similar active method can also be used as an islanding (loss of mains) detection for distributed generation systems [96] [97]. For a distribution network with embedded small generators, once islanding occurs, the system impedance measured from the point of injection increases and the sudden change of system impedance can be used for islanding detection. However the system impedance monitoring requires continuous injection which may cause current distortion.

2.5 Summary

This chapter has introduced previous work concerning on-line impedance estimation which includes passive (non-invasive) methods and active (invasive) methods. The non-invasive methods use disturbances generated by the existing system components whereas the invasive methods involve extra control and electronic devices but easily offer excitation with high signal to noise ratio (SNR).

Three commonly used data processing techniques: FFT, PSD and CWT have been demonstrated by calculating the impedance of a simple RLC circuit with a step current injection. In order to provide accurate impedance estimation, all of the three techniques require windowing to eliminate the edges of the captured data. CWT behaves better than the FFT and PSD for noisy signals due to the fact that the mother wavelets act as a band-pass filter. However, the bandwidths for different centre frequencies are different and this leads to different accuracy levels in the frequency range and also the smoothed curve does not respond to curve fitting.

Fault location methods based on impedance measurement have been discussed. The single-ended passive methods suffer from the assumptions which may not be true during application and double-ended methods require data communication and synchronization. Passive schemes measure the pre-fault or the post fault steady state impedance which slows down the fault location time. Active methods needs extra injecting unit and may cause distortion to the system but require shorter data segment and produce high SNR. It is clear that at present there is no single method which can be used to process accurate fault location for all situations and a new technique is required.

Chapter 3

Single-ended fault location

3.1 Introduction

This Chapter introduces a new single-ended fault location method based on high frequency components. It does not require the injection of pulses but uses the fault transient itself. The proposed algorithm can be employed in the more electric vehicle systems which have an integrated power system (IPS), such as the modern more electrical Marine vessels and aircrafts, to improve the system survivability and reliability. The high frequency information within fault transients is used to calculate the system supply impedance and the line impedance. The fault location is predicted accurately by comparing the calculated line reactance, from the measurement point to the fault point with the known line reactance value. Due to the fact that no injection unit is involved, the only required equipment is a voltage and current acquisition system located at the power supply end of the IPS. By exploiting the high frequency fault transient, the fault location time is also reduced to about 6ms after the fault occurs. It is found that fault location accuracy range within 1m

for a 21m cable distribution system can be achieved.

This chapter describes a novel single-ended fault location scheme and is divided into seven sections. After the introduction the basic theory is outlined in Section 2, system setup and cable impedance calibration are presented in Section 3 and Section 4 separately. The experimental results are given in Section 5, for comparison the performance of a traditional distance scheme is given in Section 6 and the overall summary is in Section 7.

3.2 Basic theory

3.2.1 Basic theory of single-ended scheme

The basis of this single-ended fault location method can be introduced by considering a single phase circuit as shown in Figure 3.1, where Z_s is the supply impedance and Z_{line} is the impedance of the line segment to be protected.

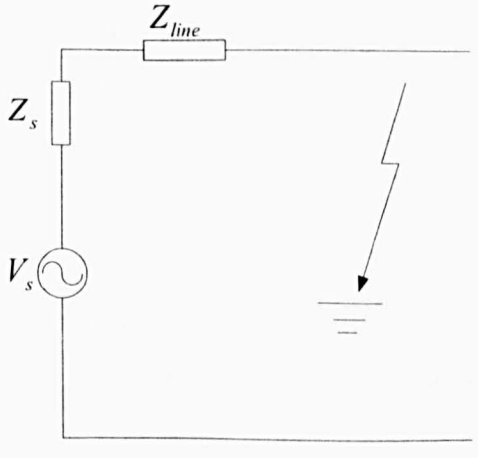

Figure 3.1 Single phase circuit with a phase to ground fault

The transient created by the sudden voltage collapse caused by faults can be considered to be due to a harmonic source (actually the information generated by fault transients contains a wide range frequencies, not just harmonic frequencies) at the fault location. The Thévenin equivalent circuit, at a non-fundamental frequency (frequencies which either higher or lower than the system supply frequencies), is a circuit with the supply voltage short-circuited.

The fault transients act as an excitation source in this circuit as shown in Figure 3.2

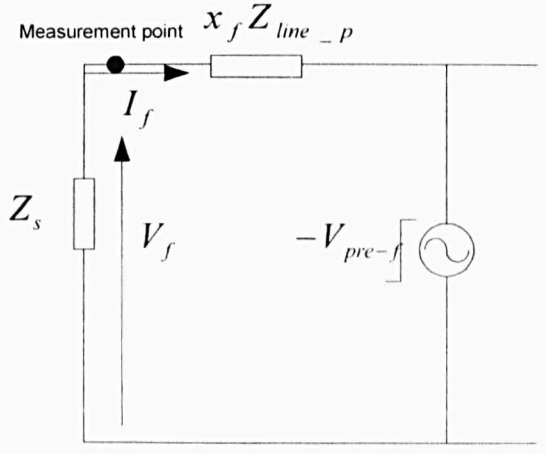

Figure 3.2 System at non-fundamental frequency during fault situation

The fault can be considered to create an equal and opposite voltage to the instantaneous pre-fault voltage $V_{pre\text{-}f}$ at the fault location causing the system voltage to collapse. From Figure 3.2, the impedance between the measurement point and the fault point can be calculated from (3.1)-(3.3). The source impedance can be found from the measured voltage and current transients (V_f and I_f) at the measurement point

$$Z_s = \frac{V_f}{I_f} \tag{3.1}$$

The total source and line impedance can then be found in terms of the pre-fault voltage at the fault location $V_{pre\text{-}f}$ and the measured transient current.

$$Z_s + Z_{line\_p} x_f = \frac{V_{pre-f}}{I_f} \tag{3.2}$$

where, Z_{line_p} is the per-unit length impedance of the line and x_f is the fault distance from the measurement point. Thus the line impedance between the measurement point and the fault location can be obtained from:

$$Z_{line\_p} x_f = \frac{V_{pre-f}}{I_f} - \frac{V_f}{I_f} \tag{3.3}$$

The pre-fault voltage can be considered to be a step waveform with the step value equal and opposite to $V_{fault\text{-}point}$ which is the healthy state voltage at the fault point at the time of the fault. In this fault location scheme, $V_{fault\text{-}point}$ is initially estimated to be the healthy state voltage at the measurement point at the time of initiation of the fault. In other word, $V_{pre\text{-}f}$ is voltage transient step and $V_{fault\text{-}point}$ is the pre-fault sinusoidal waveform right before the transient occurs. This is based upon the assumption that the voltage drop between the measurement point and the point at which the fault occurs is negligible. This will lead to an initial error in the fault distance estimation.

The error in the fault location measurement is due to the difference between the pre-fault voltage estimated at the measuring point ($V'_{fault\text{-}point}$) and the actual pre-fault voltage at the fault location ($V_{fault\text{-}point}$) as described in equation (3.4).

$$V_{fault-point} = V'_{fault-point} - I_{pre-f} Z_{line\_p} x_f \tag{3.4}$$

Initially the fault location and fault resistance will be unknown. However, an initial estimate can be formed from the imaginary part of equation (3.3) as it is independent of the fault resistance. The fault location is then estimated from:

$$x_f = \frac{imag(\frac{V_{pre-f}}{I_f} - \frac{V_f}{I_f})}{imag(Z_{line\_p})} \tag{3.5}$$

This estimate of the fault distance can be used in (3.4) to compensate the estimated pre-fault voltage. The fault location can then be re-estimated using (3.5) and an updated estimate of the pre-fault voltage. If necessary this iteration is repeated and the pre-fault voltage at the fault location can be re-compensated. This iteration procedure can be repeated until the solution converges to within a reasonable tolerance (For example $x_{k+1} - x_k < 0.2m$). Table 3.1 shows an example of this iteration procedure for a fault that occurred at the end of a 20m long distribution line.

iteration steps	estimated fault distance (m)
0	26
1	17
2	23
3	18.7
4	20.1

Table 3.1 Iteration procedure

As shown in table 3.1, when a 0.01Ω fault occurs at 20m of the line, the results of initial fault distance estimation is longer than 20m which is because the initial estimate of $V_{pre\text{-}f}$ is larger than the actual value. Then the new voltage estimated by equation (3.4) can be used in (3.5) as first step iteration. This procedure is repeated and is shown to converge quickly. The iteration procedure which reduces the line voltage difference between measurement point and the fault position is called line voltage iteration. The short circuit fault impedance is small and not considered here (not included in the diagrams). The situation which has a larger fault impedance (1Ω) will be discussed in Section 3.5.

3.2.2 Simulation studies

The single-ended fault location method proposed in Section 3.2.1 has been demonstrated using a Matlab/Simulink simulation of a three phase AC system, as shown in Figure 3.3

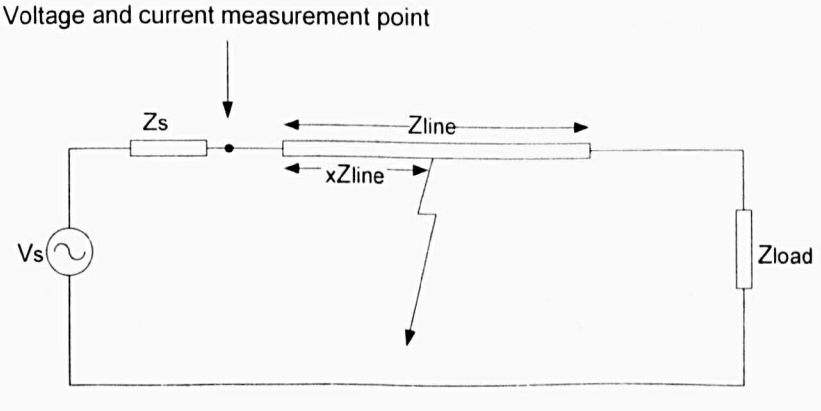

Figure 3.3 A three-phase system for demonstrating

The three phase system has a 440V (phase to phase rms) AC voltage source, a supply impedance Z_s= (0.0011+j0.0096)Ω, a 20m transmission line with line impedance per-meter resistance R_{per}=30μΩ and inductance L_{per}=0.24μH (the line capacitance is neglected because its value is very small in normal IPS and has little influence on the line impedance.). The load is a 438kW linear load with a power factor of 0.9. A phase to phase short circuit fault with 0.01Ω fault impedance was imposed on the transmission line at three separate positions: the start (0m), middle (10m) and end (20m). The voltage and current which contains fault transients are measured at the start point (right after the system supply impedance) of the transmission line. The per-unit length line impedance information is assumed to be known and used to estimate the distance between measurement point and the fault position. No other system information has to be fixed or pre-known before the procedure of the fault locating calculation.

The measured transients (at the measurement point) in the voltage and current in both time domain and frequency domain are shown in Figure 3.4 for the situation of a short circuit fault at the end of the power distribution line.

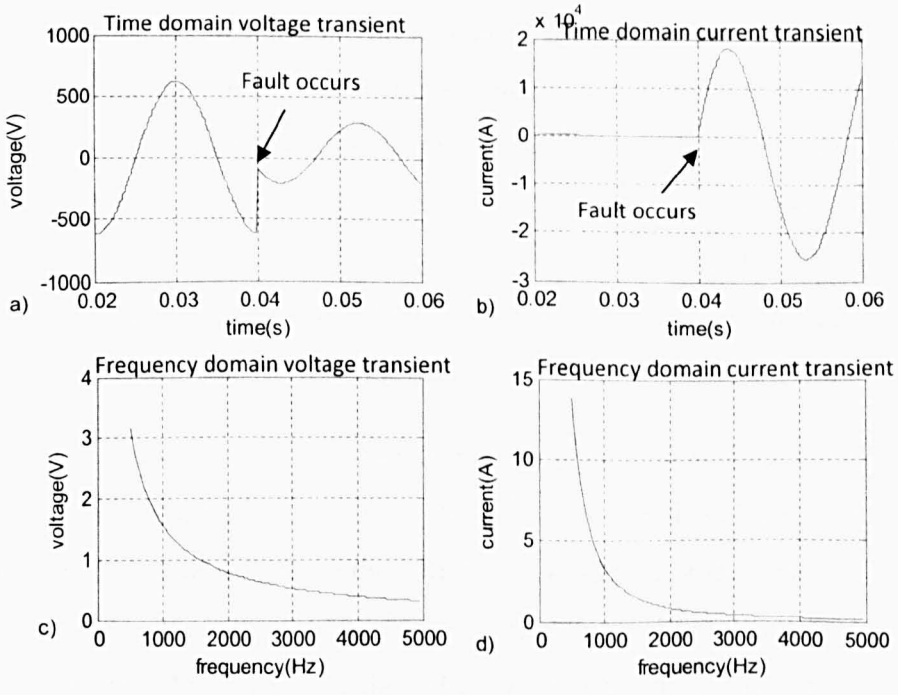

Figure 3.4 Measured voltage and current (include both transients and steady state)

a) Voltage transient in time domain b) Current transient in time domain
c) Voltage in frequency domain d) Current in frequency domain

In order to give a clear view of both the fault transients and the steady state system information, the data shown in time domain is about 2 cycles in length and has fault transients in the middle (fault occurs at 0.04s). Actually, only a 4ms length window (fault transients are captured within middle of the window) is needed to provide accurate calculation results within the high frequency range of interest. As discussed in chapter 2, a Blackman window is used on the 4ms data in time domain to eliminate the influence caused by the edges of the finite data segments. The frequency domain data in Figure 3.4 c) and d) is the results of the FFT of 4ms transient data. In Figure 3.4 a) and 3.4 b), the bigger transient in the current waveform has a larger signal to noise ratio than the voltage and this leads to fact that after FFT, in frequency domain, the current contains more energy than the voltage transient at the same frequency.

In the protection scheme, the voltage and current is continuously monitored by a 4ms length window. When a fault occurs, the measured current suddenly increases to a value which is larger than the pre-set threshold so that the fault phases can be detected and at this time a trigger signal is sent to capture the fault transient over the 4ms window after a 2ms delay (to keep the transients in the middle of the window). The trigger is located in the middle in the time domain of the captured measurement window so that the pre-fault information can easily be found. Not considering the data processing time (FFT and calculation time), the fault location can be detected 2ms after the fault occurs which makes the fault location time at least 10 times shorter than the normal impedance measurement fault location methods that involve using pre-fault or post-fault steady state system information.

The results of estimated line impedance are presented in Figure 3.5. In a), the line reactance (solid line) results which are calculated with (3.3)-(3.5) and by using the transient data from the simulation is shown in the frequency domain. The dashed is the actual value used in simulation. Due to the short processed data segment (4ms in total), the estimated reactance is more accurate in the high frequency range (3kHz-5kHz) than the value in the low frequency range (100Hz-1500Hz). Only high frequency results between 3kHz and 5kHz are used to determine the fault location. By using the high frequency estimated results, the errors are kept within 1m for the fault at 20m shown in Figure 3.5 b.

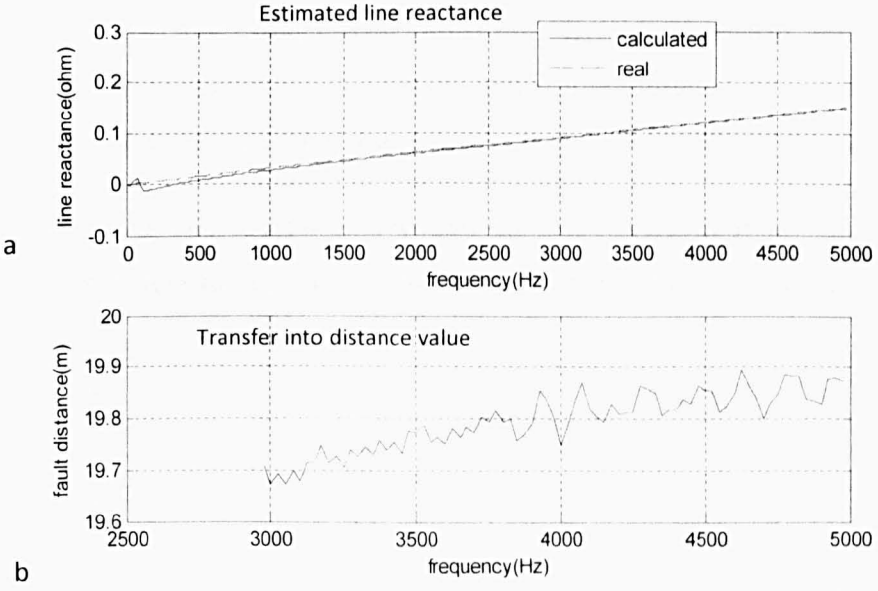

Figure 3.5 Calculated line reactance when fault occur at the end of line

a) Line reactance b) Line reactance divided by per meter value

Results shown in Figure 3.5 are the final estimation value after the voltage iteration process which involves using equation (3.3)-(3.5). The iteration procedure over the full frequency range is depicted in Figure 3.6

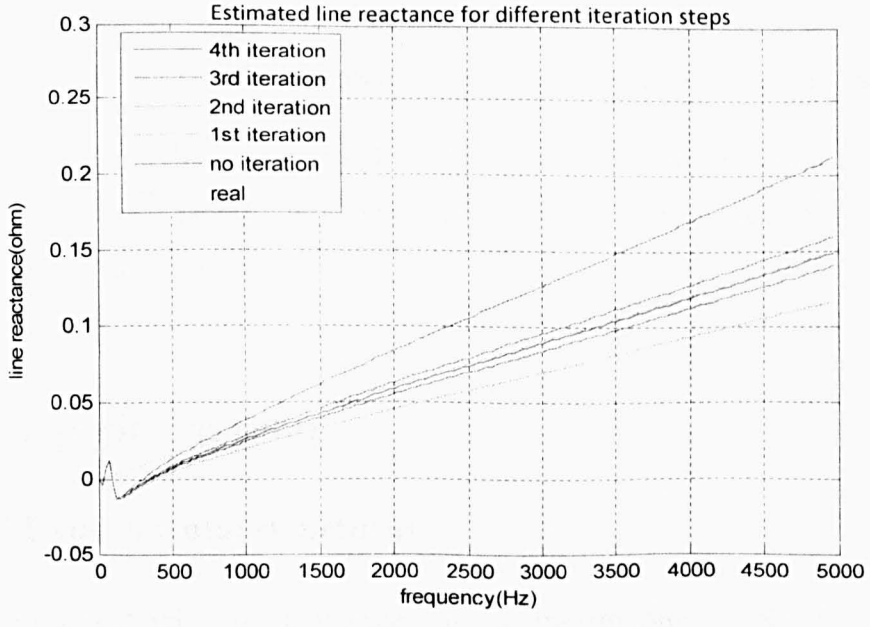

Figure 3.6 Iteration procedures for line reactance estimation

For the example in Table 3.1, the calculated line reactance converges to the actual value as shown in Figure 3.6. Even for a fault at the end of the line, which produces the largest error, only four steps of iteration are needed to reduce the errors to the required low values. For faults which are imposed at the other two positions of the transmission line, good accuracy is also achieved.

The calculated line reactance between the measurement point and the fault point for different fault positions are shown by the solid line in Figure 3.7.

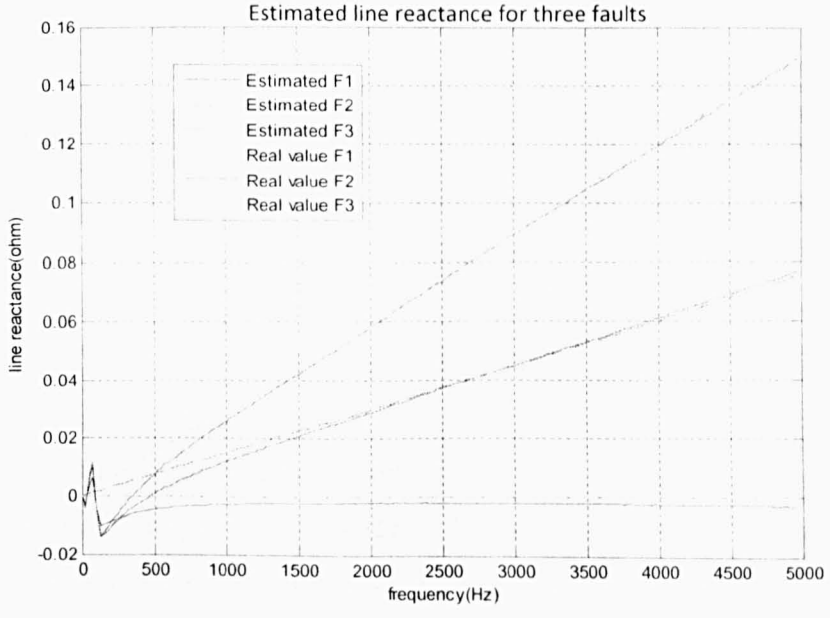

Figure 3.7 Estimated values compared with actual ones for different fault locations

Compared with the values used in the simulation model (dash line), the estimated values (solid line) only have a small error which is within the requirement of accuracy.

3.3 Experiment setup

3.3.1 Experimental structural

The experimental circuit consists of a transmission cable which was represented by 6mm^2 5 core SY cable (a type of the control flex cables which includes SY (galvanised steel wire braid screen), CY (Tinned copper wire

braid screen) and YY (no screen)) a resistive load and a programmable AC voltage supply (Chroma) as depicted in Figure 3.8.

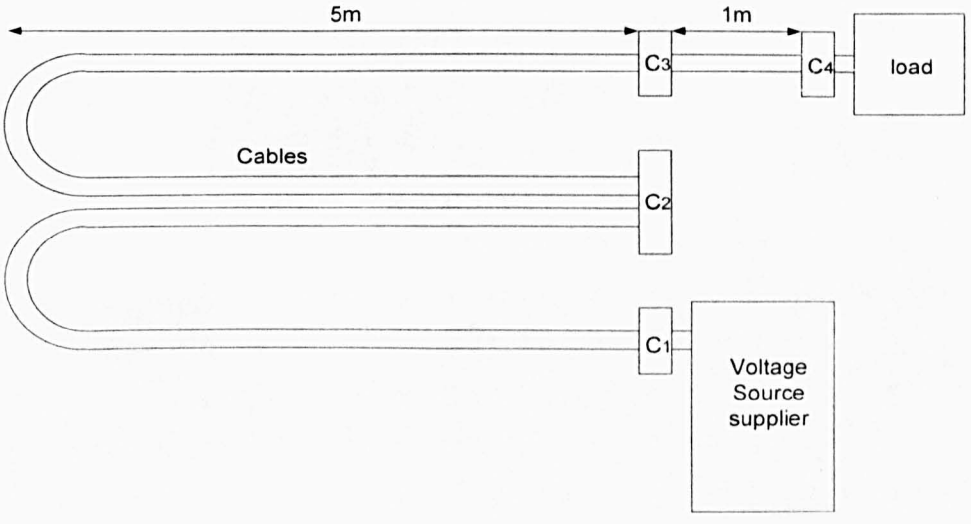

Figure 3.8 The configuration of experimental system

The three phase system model was built as shown in Figure 3.8 with a 50Hz AC voltage source of amplitude 50V (peak to peak line voltage value) which keeps the fault current within the limit (25A peak, AC) of the Chroma supply when the fault is imposed with a 1Ω fault resistance. The DC 60/50 H model voltage source is for the separate DC test. The distribution cables connected by connectors (C_1, C_2, C_3, C_4) are two 10m and one 1m SY type cable which have impedance similar to the impedance range of power transmission cables used in aircraft. The system also has a star connected resistance load (6.8Ω per phase) located at the end of the distribution line. Phase to phase and phase to neutral short circuit faults are imposed separately at the position of the four connectors to create different distance fault situations. The voltage and currents are measured at C_1 which is at the start of the SY cables. The experiment setup is shown in Figure 3.9

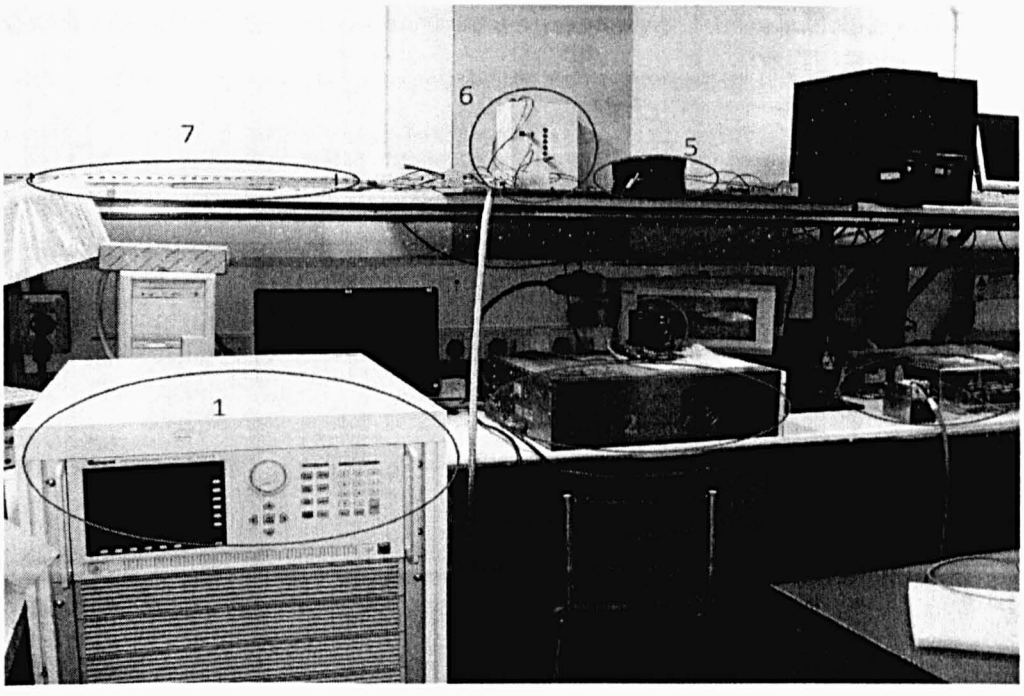

Figure 3.9 The components of experimental system

1) Chroma voltage source. 2) H series DC voltage source. 3) FPGA. 4) Non-linear load. 5) Resistor load. 6) Fault unit. 7) Cable trays

The Chroma voltage source is used as a steady state AC voltage supply. A DC voltage source with high output current limit (40A) is used for testing faults in a DC system. The FPGA unit is a central controller which is used to send the enable signal for the fault and also data acquisition. The Three-phase rectifier with a resistor and cooling fan is used to produce a non-linear load when required. A three - phase resistor with a heat sink acts as the system load. The fault unit creates faults with the fault resistance. The Cables are located on the cable tray, as shown in Figure 3.10 and act as lengths of system distribution lines.

3.3.2 The SY cable

The SY cable [100] is cut into two 10m and one 1m sections. The three different lengths of sections have connectors. Faults are imposed on the cable at the positions of connectors to demonstrate faults at different distances. The 1m cable acts as a reference to examine whether the estimated fault location can meet the minimum requirement.

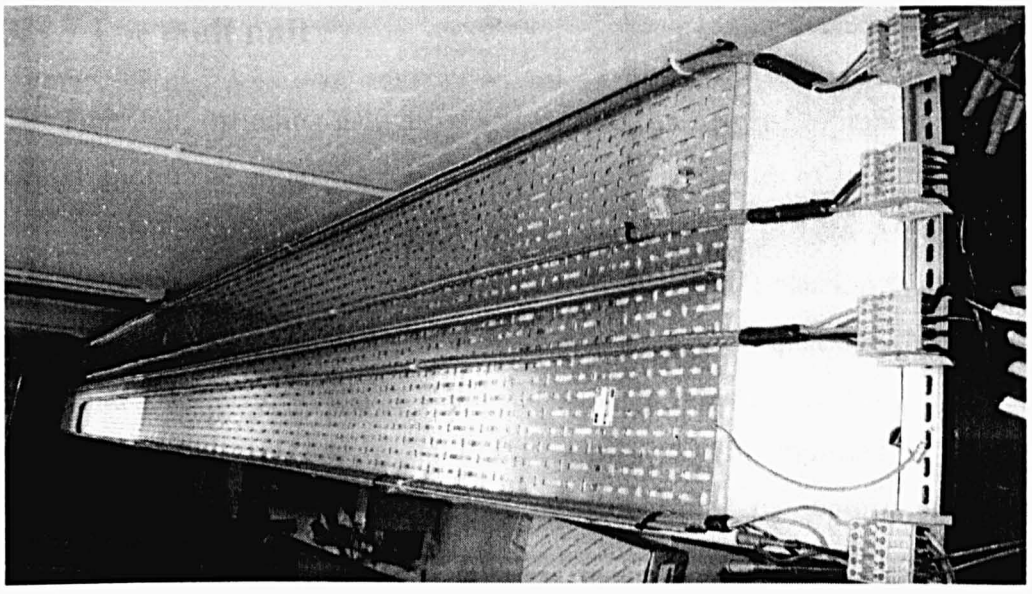

Figure 3.10 Experimental cables on the cable tray

This 5 core (A, B, C, neutral and earth), 6mm^2 armoured SY cable has a voltage rating of 300V phase to neutral, 500V phase to phase and a current rating of 40A. The cross section of the cable is depicted in Figure 3.11. The phases A, B, C, neutral and earth are classified by brown, black, gray, blue and earth (yellow and blue).

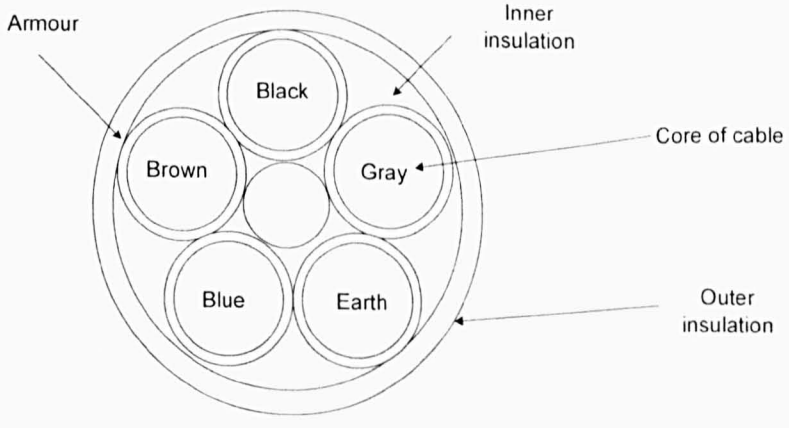

Figure 3.11 The cut section of the SY cable

This type of cable (12kW per-phase) can be used as interconnecting cable for measurement and control. It is suitable for both outdoor and indoor utilization. The steel wire braided screen (armour) offers protection of against mechanical damage and also acts as an electromagnetic shield [100]. The impedance of the cable is presented in the Section 3.4

3.3.3 The fault unit

The fault unit, including gate drive and switch, can be used to impose a short circuit fault on the transmission cable with different values of fault resistance (0Ω-5Ω in increment of 1Ω). The unit is able to work in both AC and DC conditions and is able to provide both a hard fault and a bouncing fault. For a system with a DC supply the hard short circuit faults are imposed in the system with a fault resistance using an IGBT as shown in Figure 3.12. The controlled signal (3.3V pulse) is sent by the FPGA board and then amplified by a NPN transistor to reach the input current requirement of the optocoupler. An HCNW3120 optocoupler is used in order protect the FPGA board. The optocoupler also acts as a gate drive to provide a suitable voltage to switch on and off the IGBT to impose and remove a fault from the system when required.

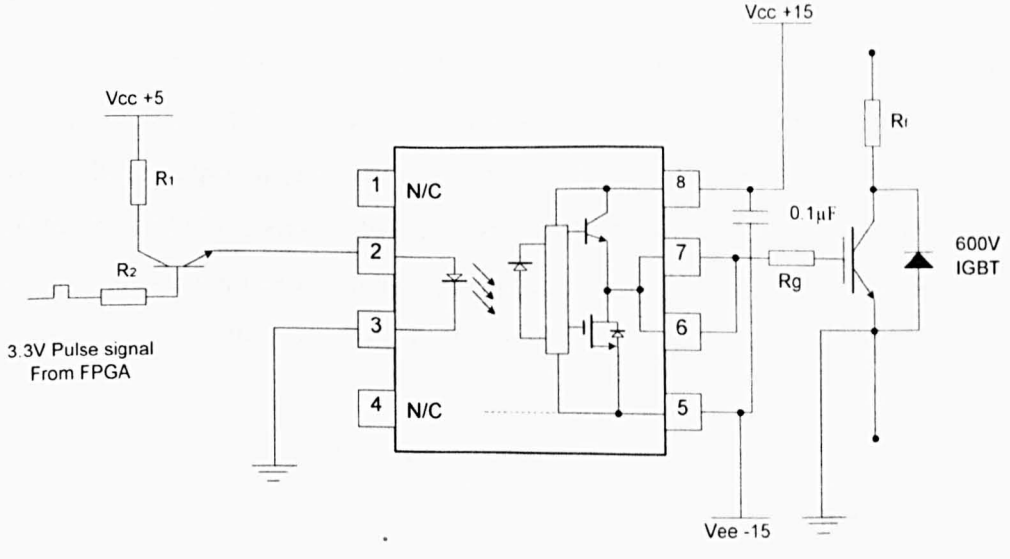

Figure 3.12 Circuit of controlled fault unit

The current flow into the optocoupler is recommended to be with in the range of 8mA to 16mA. Two resistors are connected to the collector and base of the transistor and are chosen to be 0.5kΩ and 1kΩ separately according to equation (3.6) [143].

$$8mA \leq \frac{V_{cc}-V_{ce}}{R_1} + \frac{V_{FPGA}-0.7}{R_2} \leq 16mA \tag{3.6}$$

where $R_1 = 0.5k\Omega,\ R_2 = 1k\Omega$

The supply voltage connected to the collector of the transistor is 5V as in Figure 3.12 and V_{CE} is less than 0.6V. So according to equation (3.6), the input current of the optocoupler is roughly 11.4mA. As recommended by the datasheet of the optocoupler [101], a 0.1μF capacitor is used between the collector and emitter to keep a steady output voltage. A 15V positive voltage is imposed on the gate of the IGBT to switch it on. In order to firmly switch it off (Vg<0.5V), the voltage across gate the emitter set to -5V. As shown in Figure 3.12, the low level output current of the optocoupler has to be smaller than 2.5A. R_g can be calculated by equation (3.7) and (3.8)

$$R_g \geq \frac{(V_{CC}-V_{OL})}{I_{peak}} \tag{3.7}$$

Assuming V_{OL} =2V, so that

$$R_g \geq 5.2 \tag{3.8}$$

R_g was chosen to be 10Ω according to (3.8). The gate drive circuit test output signal when the IGBT is switched on is shown in Figure 3.13 where the IGBT is connected to a 10V DC voltage supply with a 2Ω resistance. The waveforms of the three output signals are depicted in Figure 3.13. the switch on operation of the IGBT lasts about 150ns (red line in the Figure 3.13) and the time delay of the optocoupler output signal (green line) from -5V to +15V, compared with its input signal (FPGA output), is about 300ns.

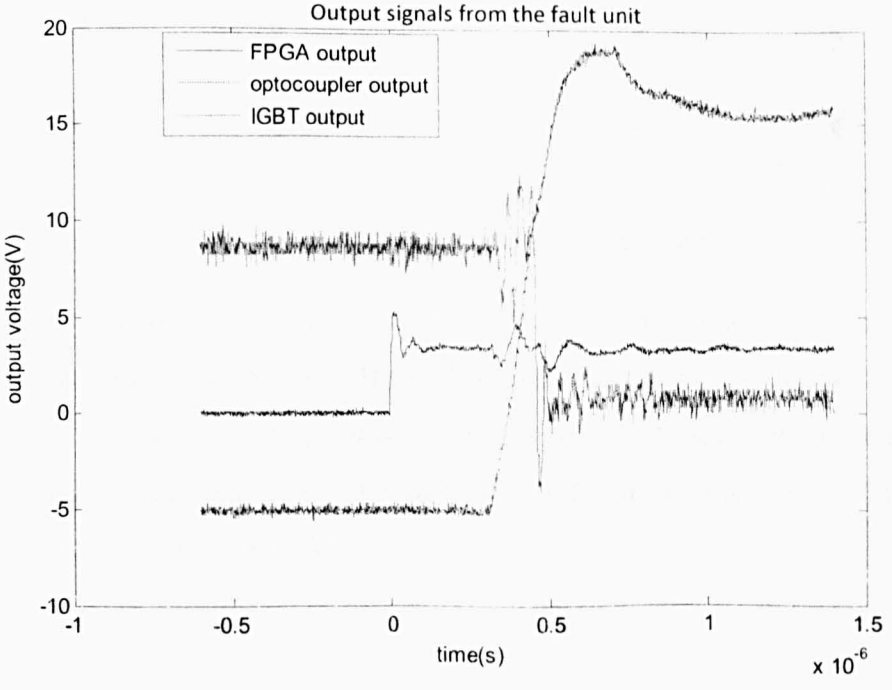

Figure 3.13 The output signal measured from the IGBT gate drive

Both of the time delays are with in the range of normal operation as suggested by the datasheets. These delays have little affect on the fault location as proved by later experiments. After receiving the impulse signal from the FPGA (blue line in the Figure), it takes about 500ns to impose or remove a fault from the system.

For an AC system, the switch must include two IGBT and reverse diode as shown in Figure 3.14. to work in a bidirectional mode.

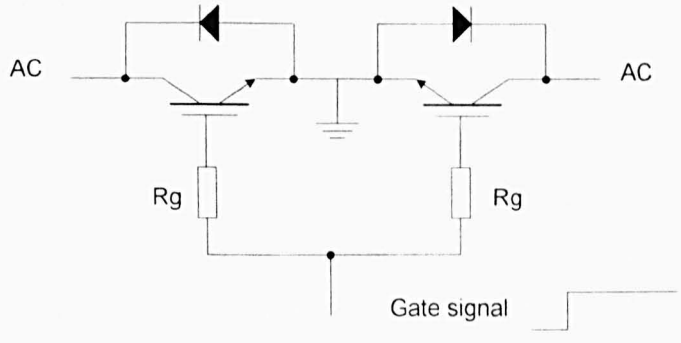

Figure 3.14 The IGBT switch used in AC system

Once the switch on gate signal is sent to the reverse blocked IGBT, current will only flow through one IGBT and one diode during each half cycle of the AC voltage waveform. In other words, the 'on' state IGBT works as a diode when the bypass voltage is negative as shown in Figure 3.15

Figure 3.15 Current flow in switch on situation

Figure 3.15 shows the fault current flow through the switching components during each half cycle of the voltage. The fault current should be much higher than the steady state working current and less than 25A peak (the limitation of the voltage source). Therefore, the diode and IGBT have been carefully chosen to withstand a current of 30A.

3.3.4 The FPGA board

The Field Programmable Gate Array (FPGA) board which is used to controlling the fault and data acquisition was designed by the University of Nottingham. The layout and testing of the main FPGA board was done by Dr. Hoang Nyguen [102] and Dr. Yiquan Zhu [103] was responsible for the layout of the ADC and USB board. Dr. David Coggins was responsible for the design and implementation of the software running on the Microblaze processor and the software on the PC for controlling and data acquisition [104].

The mother board shown in Figure 3.16 consists of an FPGA device [104], two Quad Data Rate (QDR) memories [104], a Programmable Read Only Memory (PROM), 6 Analog to Digital Converters (ADC), a Joint Test Action Group (JTAG) interface, a Digital to Analog (DAC) output trigger, a RS232 communication port and a USB communication device. The real board is shown in Figure 3.17

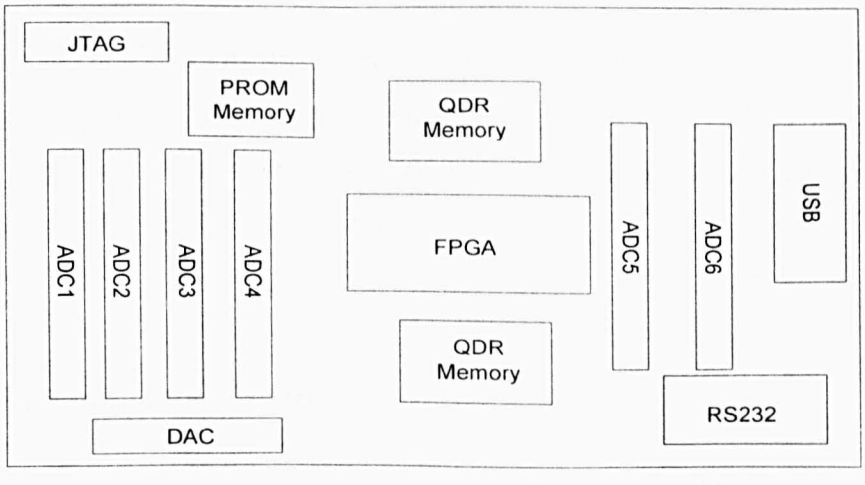

Figure 3.16 Structure of FPGA board

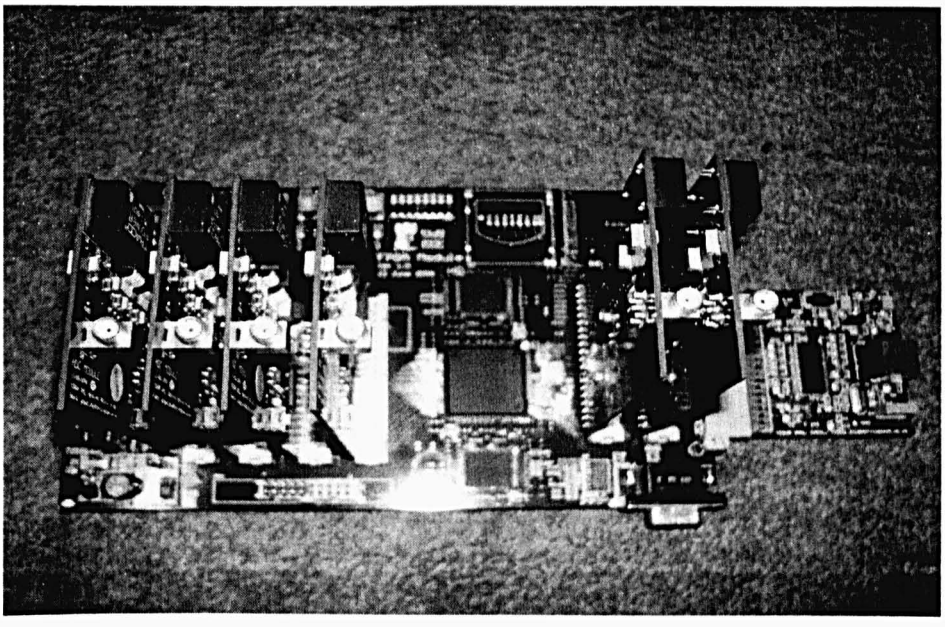

Figure 3.17 FPGA unit

The FPGA provides high speed logic I/O. The configuration data for the FPGA is located in PROM (Programmable Read Only Memory). When the board is powered up, the FPGA reads the data from the PROM for configuration automatically. This data can be reprogrammed using a JTAG interface.

QDR (Quad Data Rate) memories read and write data by using the falling edge and rising edge of the clock signal controlled by the FPGA. A 3.3V and -3.3V control signal which lasts for about 100ms is sent out from the DAC and this signal is used by the gate drive of the fault unit.

3.3.5 The non-linear load

Integrate Power System (IPS) within modern More Electric Marine (MEV) use electrical power devices on board in place of the mechanical, hydraulic and pneumatic power to drive the system [105]. Increasing use of electric power in a MEV optimizes the system performance, reduces the weight of system equipment and at the same time brings power electronic loads. The non-linear behaviours of power electronic equipment (drives of the loads) cause distortion to the system current and voltage.

In order to simulate this situation, the experimental test involves checking the single-ended scheme in a system with both a resistance load and a nonlinear load which is a resistor supplied by a diode rectifier. The non-linear load unit is number 4 in Figure 3.9 and is depicted in Figure 3.18

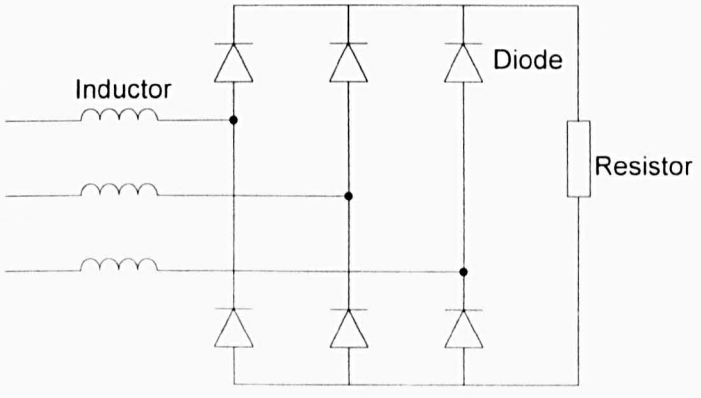

Figure 3.18 The layout of non-linear load

Figure 3.18 shows the resistance load which is made of four 48Ω resistors in a parallel connection (in order to reduce the current flow to each resistor) connected to the diode rectifier. A cooling fan, which is powered by the AC voltage, was added in order to keep the resistor working at required temperature. According to the high power quality requirement in the real IPS, the 12Ω resistor load is filtered by a three phase 1.3mH inductor filter to smooth the system current and make it continuous.

3.4 Cable impedance calibration

The calibrated impedance value of the transmission line impedance plays an important part as a reference in this method of system fault location. As described, the fault distance is detected by comparing the calculated line reactance between measurement point and the point at which faults occur with the calibrated per-unit length line impedance. The line impedance data has to be known and this could be achieved through calibration or from the data sheets. The cable impedance has been calculated both by current injection and impedance estimating equipment the Impedance Analysis Interface (IAI).

3.4.1 Calibration with injected current

The cable impedance is first calibrated by injecting current. The same cable as used as in the experiment system (in Figure 3.10) is cut into different lengths of 1.2m, 2m, 5m and 10m. The cables are short circuited at one of the ends between two phases and current is injected at the other end. The calibration procedure is described in Figure 3.19

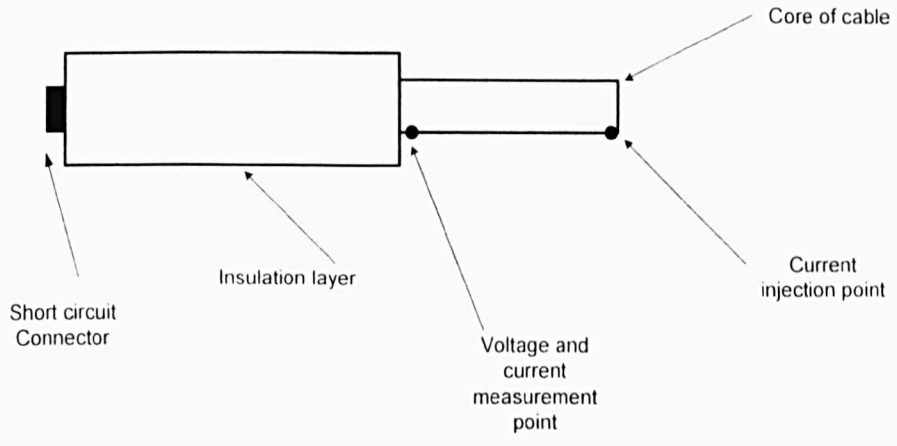

Figure 3.19 Cable impedance calibration by injecting current

As depicted the current injection point is set to be different from the voltage and current measurement point in order to reduce the errors caused by contact resistance. The short circuit connector's impedance is pre-calculated and removed from the final calculation results. A 6A and 8A Currents are injected to the cable separately in order to test the impedance behaviour under different current value. The current is injected into the cable at both 1kHz and 1.5kHz to investigate the impedance behaviour at high frequency. The calibrator consists of a Datron 4705 multifunction calibrator header [146] (for frequency control and voltage output) and a Ballantine transconductance amplifier [147] (for current output). The calibrated currents (6A and 8A) at 1kHz and 1.5kHz are injected into the cable separately for cable impedance measurement.

The impedance information is calculated from the measured current and voltage using equation (3.9)

$$Z = \frac{FFT(V)}{FFT(I)} \tag{3.9}$$

As in (3.9), the lengths used for the data segment of the voltage and current processed by the FFT were 20 cycles and 50 cycles for each injected frequency.

The results show little difference under the different calibration situations (different current, frequency, and measurement window) described above. For example, the impedance of 1.2 m cable, between phase blue to phase brown, as shown in Figure 3.11 under different current injection situation is presented in Table 3.2

1.2m Brown-Blue					
		1000 Hz	1500Hz	20 cycles	50cycles
4A	Resistance(mΩ)	8.73	8.69	8.71	8.71
	Inductance(μH)	0.77	0.77	0.77	0.76
8A	Resistance(mΩ)	8.66	8.71	8.71	8.68
	Inductance(μH)	0.76	0.76	0.77	0.76

Table 3.2 Impedance of the same cable derived by different current injection

The measured impedance in different test situations has very similar results. The small error (within 1%) is due to the voltage and current measurements and the initial contact resistance of the cable.

In the IPS cable system, the length of the cable with in each section is normally less than 100m, and the distance between phase to phase and phase to earth is very short. Compared with the inductance, the capacitance between phases contributes a small part of the measured reactance within the frequency of interest (0Hz to 3kHz as in the results of fault location).

During this experiment the influence of capacitance within the cable is ignored. The final results from the injecting current to different lengths of cables are presented in Table 3.3

Injection						
1.2m						
	Black-Gray	Black-Brown	Brown-Gray	Gray - Blue	Black -Blue	Brown - Blue
Resistance(mΩ)	8.65	8.62	8.63	8.67	8.61	8.69
Reactance(μH)	0.79	0.76	1.021	1.031	0.75	1.027
2m						
	Black-Gray	Black-Brown	Brown-Gray	Gray-Blue	Black-Blue	Brown-Blue
Resistance(mΩ)	14.15	14.13	14.31	14.31	14.18	14.24
Reactance(μH)	1.23	1.25	1.74	1.68	1.22	1.68
5m						
	Black-Gray	Black-Brown	Brown - Gray	Gray-Blue	Black-Blue	Brown-Blue
Resistance(mΩ)	34.93	34.97	34.95	35.92	34.91	34.93
Reactance(μH)	3.21	3.21	4.37	4.31	3.32	4.24
10m						
	Black-Gray	Black-Brown	Brown - Gray	Gray-Blue	Black-Blue	Brown-Blue
Resistance(mΩ)	69.81	69.76	70.12	70.15	69.91	69.92
Reactance(μH)	6.23	6.35	8.37	8.41	6.18	8.44

Table 3.3 Cable impedance results derived using different calibration tests

As shown in Table 3.3, the inductance between two different phases changes with the distance. The bigger the distance consistently the higher the inductance is. In the view of the cut section of cable described in Figure 3.11, the distance between two phases which are widely separated (brown and gray or black and blue etc) is larger than two phases which are close together (brown and blue or black and gray etc). Even for the same length of cable, the inductance between two close phases and two separate phases is different. For example, for a 1.2m length of cable, the inductance between the Black and Brown phases is 0.76μH while the inductance between the Brown and Gray phases is 1.02 μH as given in Table 3.3. The tested cable offers good linear behaviour between measured impedance and length. Dividing results in Table 3.3 by each length, the per-meter values of cables (1.2m, 2m, 5m and 10m) are very similar.

Impedance per meter				
	1.2m	2m	5m	10m
Resistance(mΩ)	7.20	7.19	7.12	7.09
Inductance(μH) (close)	0.64	0.62	0.65	0.63
Inductance(μH) (separate)	0.86	0.85	0.86	0.84

Table 3.4 The results of calibration in per meter value

In order to avoid contact resistance errors several special procedures as described before are considered, but the contact resistance is not totally

reduced. Thus for the per-meter value of resistance of the different length cable in Table 3.4, the shortest cable is affected the most. For the cable of 10m, after dividing by 10, the contact resistance value per-meter is small and the overall result is accurate. Even influenced by contact impedance, the errors in the data in Table 3.4 is within 2% which shows very good linearity against length. During fault location estimation, as long as the impedance to fault point is calculated accurately, the fault position can be predicted precisely.

3.4.2 Calibration with IAI

The cable impedance was also calibrated by using IAI impedance measurement equipment as a reference and compared with the results by using current injection. This method used a N4L impedance analyser with an LCR measurement capability [106]. The equipment is shown in Figure 3.20

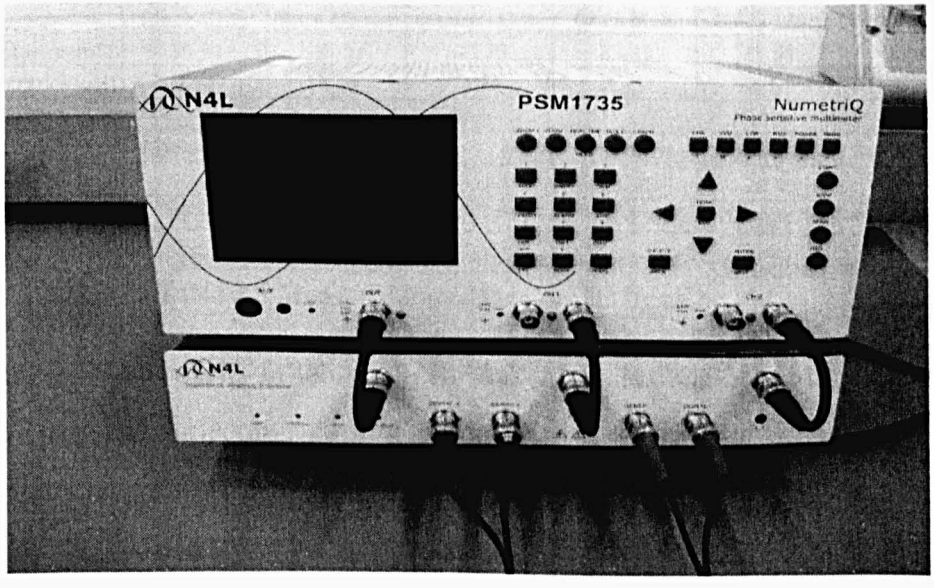

Figure 3.20 IAI unit for impedance calibration

Depicted in Figure 3.20, the IAI provides all of the functionality which includes a wider frequency and impedance measurement range plus higher nominal frequency. This is achieved by a more sophisticated design that includes an additional internal shunt range, a current amplifier to increase low impedance signal levels and calibration with PSM 1735 [106]. The IAI impedance measurement is accurate and with short and open circuit calibration

function it is less affected by the contact resistance. The only drawback of this equipment is that the injected current is not controllable and reduces with frequency. For example, for small impedance measured at high frequency, the result is less accurate than that measured at lower frequency because of low SNR in the high frequency range. By testing using a known inductance of several μH, it was found that inductances with a value in this range are best measured at 1000Hz. The results for the same cable configuration is shown in Table 3.5

IAI						
1.2m						
	Black-Gray	Black-Brown	Brown-Gray	Gray - Blue	Black -Blue	Brown - Blue
Resistance(mΩ)	8.73	8.66	8.62	8.71	8.75	8.6
Inductance(μH)	0.77	0.76	1.03	1.025	0.75	1.02
2m						
	Black-Gray	Black-Brown	Brown-Gray	Gray-Blue	Black-Blue	Brown-Blue
Resistance(mΩ)	14.13	14.25	14.21	14.3	14.15	14.21
Inductance(μH)	1.21	1.25	1.71	1.69	1.19	1.68
5m						
	Black-Gray	Black-Brown	Brown - Gray	Gray-Blue	Black-Blue	Brown-Blue
Resistance(mΩ)	35.94	35.91	35.79	35.29	35.91	35.93
Inductance(μH)	3.11	3.23	4.34	4.31	3.14	4.29
10m						
	Black-Gray	Black-Brown	Brown - Gray	Gray-Blue	Black-Blue	Brown-Blue
Resistance(mΩ)	70.61	70.89	70.84	71.31	70.75	70.94
Inductance(μH)	6.23	6.35	8.37	8.41	6.18	8.44

Table 3.5 Measured impedance results by using IAI

Compared with results in table 3.3, for the same sections of cable, the results from IAI and injecting current measurement offer high similarity (the difference is within 6%) which shows that the calibration results can be used for fault location.

3.5 Single-ended fault location using the experimental system

The experimental test was carried out in the system described in Section 3.3. Compared with the system in the simulation described in Section 3.22, the test system has a minimum fault resistance requirement of 1Ω to limit the current in the equipment to acceptable levels. A common short circuit fault normally

has a much smaller fault resistance than the load resistance. In this situation, the proposed voltage iteration using (3.4) and (3.5) is not enough to balance the error which in this case is mainly caused by the large fault resistance. The influence of a large fault resistance can be shown by Figure 3.20.

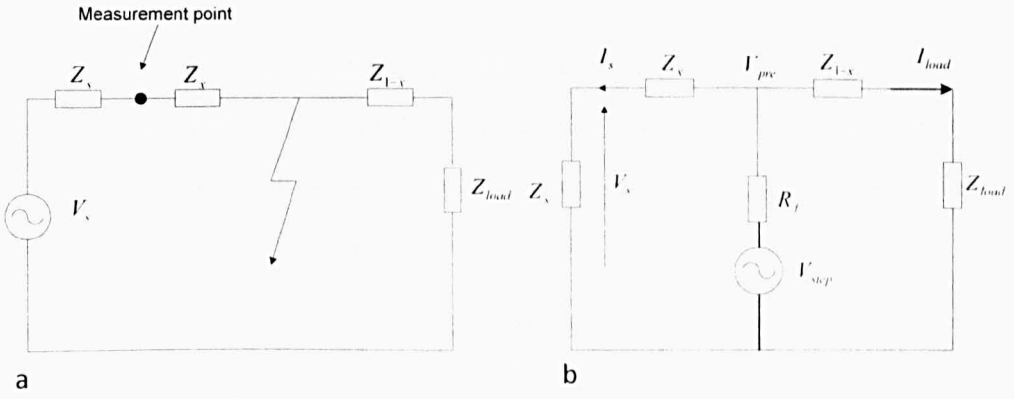

Figure 3.21 a) System model at power frequency

3.21 b) Thevien equivalent circuit for fault transient acts as voltage source

Figure 3.21 a) shows the pre-fault steady state of the test system where the cable is represented by a lumped impedance component (Z_x *and* Z_{1-x}). Figure 3.21 b) gives the situation of a fault at non-system frequencies where the Thevenin equivalent of the original voltage supply is a short circuit. Compared with Figure 3.2, when considering fault resistance, the system circuit is different. The equivalent circuit of the sytem shown in Figure 3.21 b) has a fault resistance that can not be ignored. Because the cable impedance is small compared with the fault resistance, the main reason for the error in the fault location is not the voltage drop from voltage measurement point to the point at which the fault occurs, but the big fault resistance (1Ω) compared with load impedance (6.8Ω). The results of this is that a signicant amount of current flows into the load can not be ignored. For this general system where the fault impedance is significant, equation (3.3) is modified:

$$Z_x = \frac{V_{pre}}{I_s} - R_f - \frac{V_s}{I_s} - \frac{I_{load}}{I_s} R_f \qquad (3.10)$$

In (3.10), V_s and I_s are measured and the step waveform V_{pre} is estimated using the pre-fault values of V_s as before. R_f and I_{load}/I_s in (3.10) can be calculated using:

$$R_f + R_x = real\left(\frac{V_{pre}}{I_s} - \frac{V_s}{I_s}\right) \tag{3.11}$$

Considering that $R_x \ll R_f$, (3.11) can be simplified to

$$R_f \approx real\left(\frac{V_{pre}}{I_s} - \frac{V_s}{I_s}\right) \tag{3.12}$$

As in (3.11), R_x is the real part of line impedance between the measurement point and the fault point and it is much smaller than the fault impedance R_f. During the estimation, (3.12) is used instead of (3.11). The other unknown part I_{load}/I_s can be calculated by using (3.13)

$$\left.\begin{aligned} \frac{I_{load}}{I_s} &= \frac{Z_s + Z_x}{Z_{load} + Z_{line} - Z_x} \\ Z_S &= \frac{V_S}{I_s} \end{aligned}\right\} \tag{3.13}$$

In (3.13), Z_{line} is the total line impedance and for an unknown load impedance Z_{load} the Z_s+Z_{load} can be calculated by using steady state voltage and current at the measurement point before the fault occurs. As Z_x is initially set to be zero, as it is not known at the beginning, an iteration process is used with (3.10) and (3.13) (similar to the voltage iteration process by using (3.4) and (3.5)). The final fault location after being modified such that, when the measured fault resistance R_f>0.4Ω, an impedance iteration is used, otherwise the voltage iteration will be used. In the experimental testing, in order to protect the equipment, R_f is1Ω and results with smaller value of R_f will be demonstated by simulation in chapter 5.

In this analysis, the fault inductance is ignored. It is expected that the fault inductance will be comparable to the stray inductance of the physical faults in the experiment or proportional to the fault arc length which will be small compared to the line length if an arc fault is considered. Any errors due to fault inductance will therefore be of the order of the fault arc length.

3.5.1 Fault location on a three phase AC system

The first test is performed using a three phase AC voltage supply with a resistive load. Short circuit faults were imposed on the cable at four different locations: 0m, 10m, 20m and 21m to the measurement point located next to the voltage supply as depicted within Figure 3.22. A Chroma 61500 power supply unit was used [144], to supply a voltage of 25V (peak phase to phase) at 50Hz

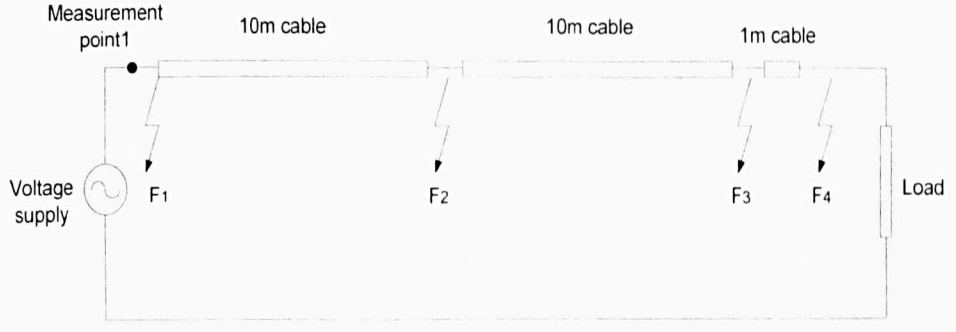

Figure 3.22 Simplified circuit for testing system

As shown in Figure 3.22, four different distance short circuit faults with fault resistance of 1Ω are added into the system using the fault unit described in Section 3.3.3. The 1m distance between fault 3 (F3) and fault 4 (F4) is set to distinguish the 1m fault and for each fault location the accuracy will be provided. Fault 1 (F1), which is close to the measurement point, is set to demonstrate faults close to generator and also to see if the proposed fault estimation method is able to calculate a negligible line impedance between the measuring point and the fault position.

The longest recording window at the measurement point is about 50ms so that a clear view of the fault transients and the steady state situation before and after the fault can be presented. As an example, the measured voltage and current waveform with the fault transient when F2 occurs is shown in Figure 3.23

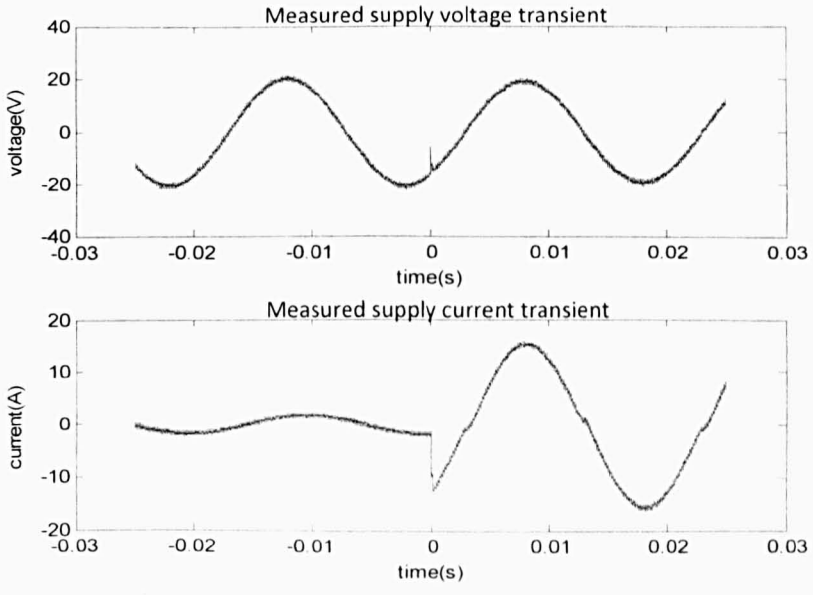

Figure 3.23 Measured voltage and current with fault transient

The data was recorded with a sampling frequency of 1MHz. The phase current and phase to phase voltage presented in Figure 3.23 has noise in the waveform. The noise consists of system noise and the measurement noise. The system noise is mainly from the voltage source and electromagnetic interference caused by other electrical equipments. The current and voltage are measured by oscilloscope and probes with 8bit (up to 12bit in high resolution mode) Analog to Digital Converter (ADC) [149]. The measurement noise due to the 8bit (ADC) results in an error of 0.78% which has little influence on the final results after curve fitting (proved in the experimental results in this chapter and the simulation results in Chapter 5). High frequency noise can be filtered using a analog low pass filter (transfer function $\frac{b}{as+1}$) with cut-off frequency higher than the frequency range of interest as shown in Figure 3.24.

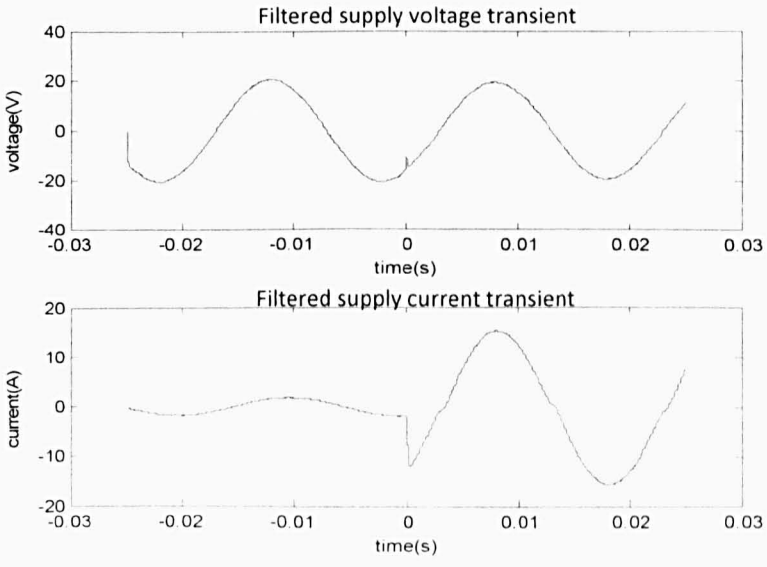

Figure 3.24 Voltage and current after being filtered by an analogue low-pass filter

The waveforms depicted in Figure 3.24 have less high frequency noise after being filtered by a low-pass filter with a cut-off frequency of 4kHz. In a balanced three phase AC system with a resistive load, the phase to phase voltage has 30° phase difference with the phase current in steady state as shown in Figure 3.23 before zero-time point of the x axis when the fault occurs. Short circuit faults between phases or between a phases and earth create a transient between the two phases (or phase to earth). The transient will not appear in the other healthy phases and this simplifies the calculation of the impedance information in this three phase system. Unlike other fault location schemes involving calculating the three phase system impedance, once the fault phases are detected by an over-current device, only the singe phase problem needs to be solved.

The voltage and current data required for accurately predicted fault location is captured for 6ms after the fault, a much shorter period than that presented in Figure 3.24. The cable does not have an ideal frequency response as in the simulation, and considering there is more noise existing in the test system than the simulation, the information above 3kHz is too noisy to be used so that in order to achieve more accuracy at low frequency (below 3kHz) a larger data segment is used compared with the 2ms after fault used in the simulation section. The created step voltage and fault voltage which are subsequently processed by an FFT are shown in Figure 3.25

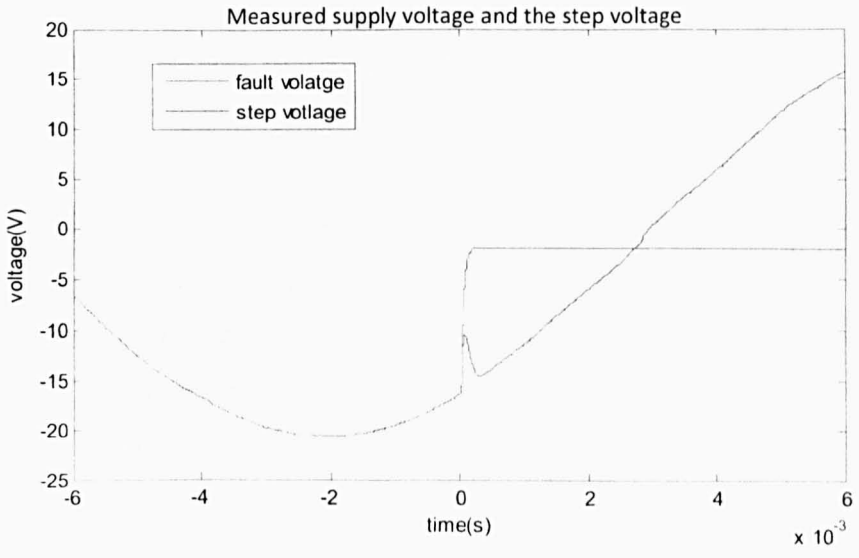

Figure 3.25 Measured fault voltage and the crested step voltage

In frequency domain, the rms value of measured voltage and current and the step voltage are shown in Figure 3.26. The captured data is filtered with a low-pass filter with a cut off frequency of 4kHz then a Blackman window is added to smooth the influence of the edges (discussed in Chapter 2). Zero-padding is utilized with the windowed data to increase the frequency resolution. This data processing technique is Blackman windowed FFT which is the same as the one discussed in the Chapter 2 to improve the estimation accuracy.

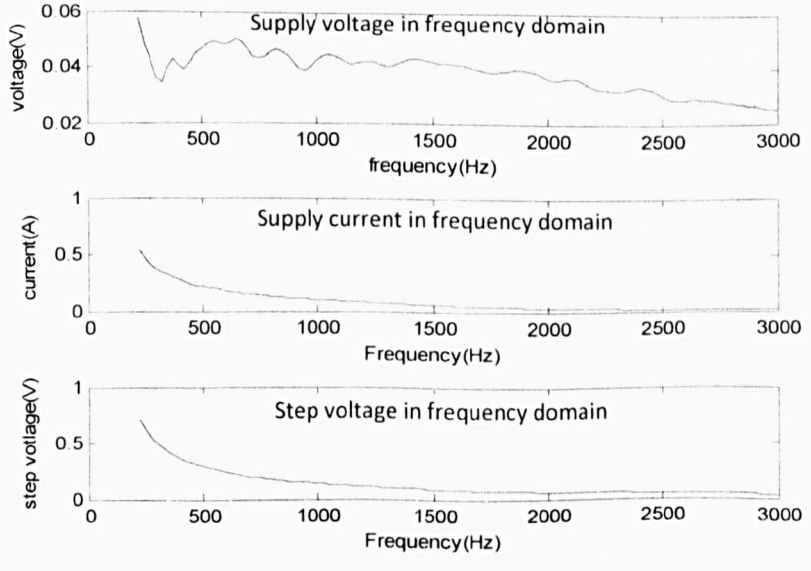

Figure 3.26 Measured voltage, current and step voltage data transformed into frequency domain.

Figure 3.26 shows that the measured voltage has lower SNR than the measured current and the created step voltage in frequency domain. The step voltage is created to simulate the fault voltage at fault point. As shown in Figure 3.25 and 3.24, the transient in the current and step voltage is larger than in the measured voltage. This transient in the measured voltage which is influenced by the supply impedance has almost 10 times less energy than the other measured signals in the frequency domain as shown by the rms scale values in Figure 3.26. 'Noise' in the measured voltage in the lower frequency range (below 1kHz) is stronger than in the high frequency range (1kHz-3kHz). The low frequency oscillation is not only caused by the system noise and measurement equipment (such as ADC errors) but also due to the small discontinuity waveform at the 'zero-crossing' caused by the nonlinear behaviour of the IGBT.

Large transients in the measured voltage are common in a real IPS or other distribution power systems with a short circuit fault. Firstly because the short circuit resistance of a fault is normally much smaller than the load impedance. Secondly, and most importantly, the system voltage level in a real system is much higher than the system tested here so that even with a relative high fault resistance, the transients in the measured voltage would still be enough to create a good SNR in the frequency domain.

By using (3.10)-(3.13), the line reactance between the measurement points and the fault (F2) can be estimated. Compared with the calibrated value, the estimated result offers good accuracy, as shown in Figure 3.27.

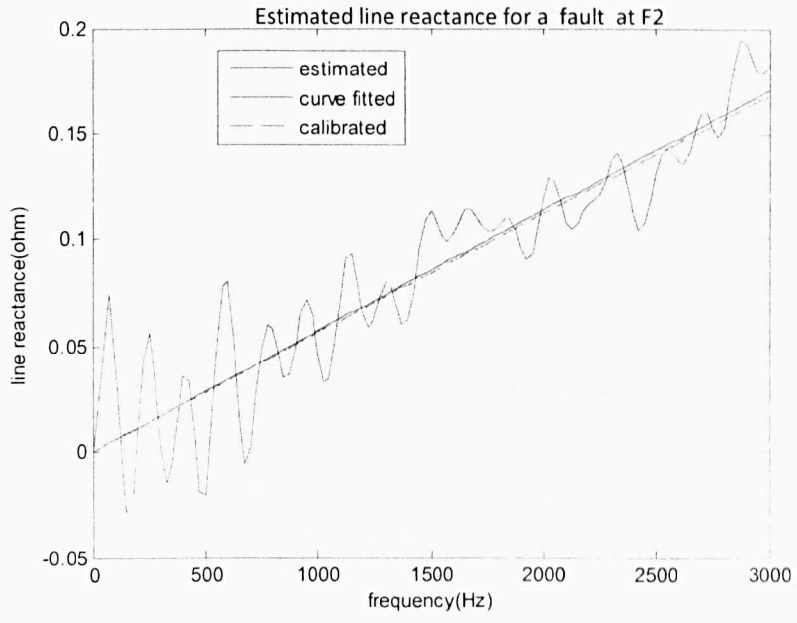

Figure 3.27 Estimated line reactance and the calibrated value for a fault at F2.

The original estimated values of line reactance are the solid line shown with oscillations. The solid straight line is the curve fitted with linear least squares curve fitting. The dashed line is the calibrated value. The estimated value (6.58μH) after being curve fitted matches with the calibrated value (6.25μH) accurately. (3.10) and (3.13) provide accurate line impedance calculation using fault resistance iteration. The low frequency data (below 400Hz) is removed before curve fitting because higher frequency data offers better accuracy with the short data segment. The original calculated results have a large error compared with the calibrated value due to the influence of the fault resistance. The iteration process reduces this error in each calculation steps and when the iteration variation is smaller than 0.5m in distance the iteration stops. Results for each of the iterations are shown in Figure 3.28.

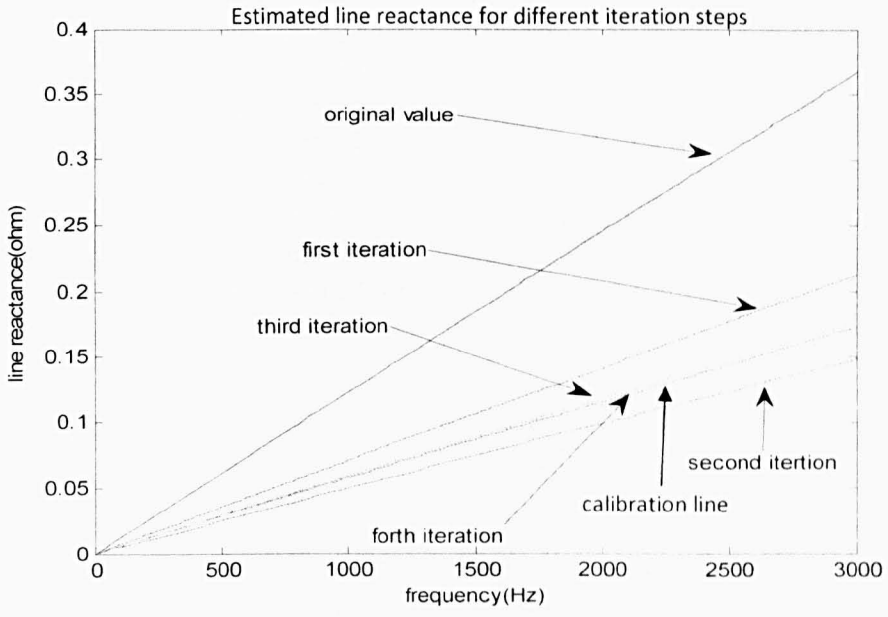

Figure 3.28 Iteration procedures of impedance estimation for a fault at F2

The estimated results (solid line) in Figure 3.28 are derived from a least squares curve fit. Compared with the dashed calibration results, the errors within original calculation can be reduced to within the requirement with only four steps of iteration.

Figure 3.29 shows estimated line reactance results in comparison with their calibrated values when a 1Ω fault occurs at different fault positions as described in Figure 3.22. Although with error, it is still possible to distinguish the 1m distance between F4 and F3.

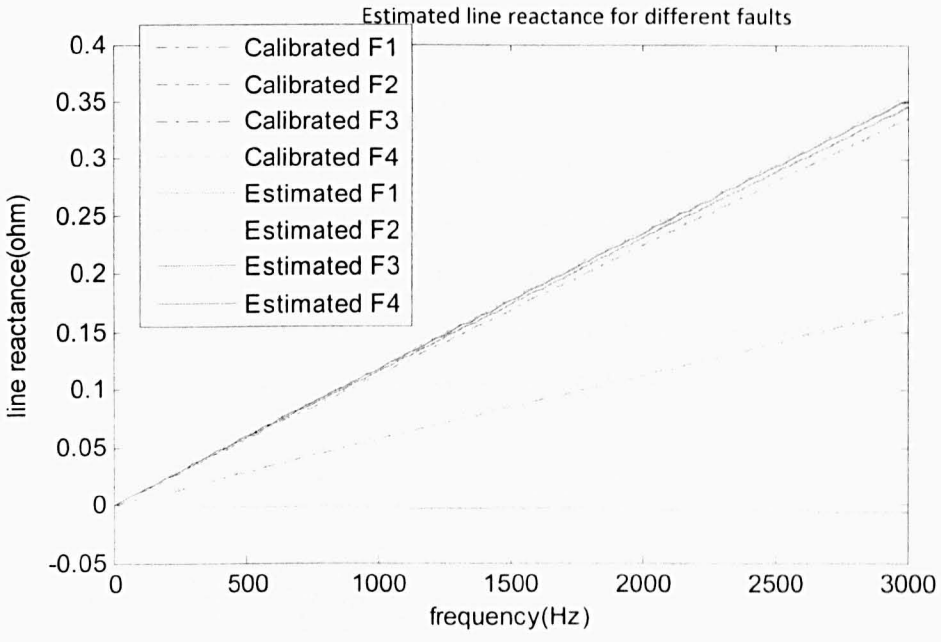

Figure 3.29 Estimated results achieved for different fault positions

As shown in Figure 3.29 the error is small for each fault location and is not increasing with distance. The gap between the calibrated line reactance (dashed lines), when fault occurs at F3 and F4, represents 1metre in distance and the estimated value (solid lines) of F3 and F4 can be distinguished. Errors for impedance estimation are shown in Table 3.6.

	F1	F2	F3	F4
Estimated results (μH)	-0.17	8.71	17.25	17.02
Calibrated results (μH)	0	8.43	16.92	17.16
error%	0.99	1.63	1.92	0.81

Table 3.6 Estimated line inductance value and errors for AC single-ended test

The largest estimation error is within 2% for all the four fault location calculation. The small negative impedance result for a zero distance fault is caused by a curve fitting which fits the original estimated results (for example, the green line in Figure 3.27) to a value close to the calibrated results and reduces the absolute error. This fitting procedure can not promise the results always larger than the calibrated value.

3.5.2 Fault location in DC system

Experimental tests on a DC system were carried out by using the same cable system but with a 40V DC voltage supply [145] for larger transients and better SNR After a short circuit fault at location 4 (F4) was imposed on the cable with a 1Ω fault impedance, the time domain measured current and voltage with the fault transient before and after low-pass filtering (with a cut-off frequency of 4kHz) were recorded, as presented in Figure 3.30

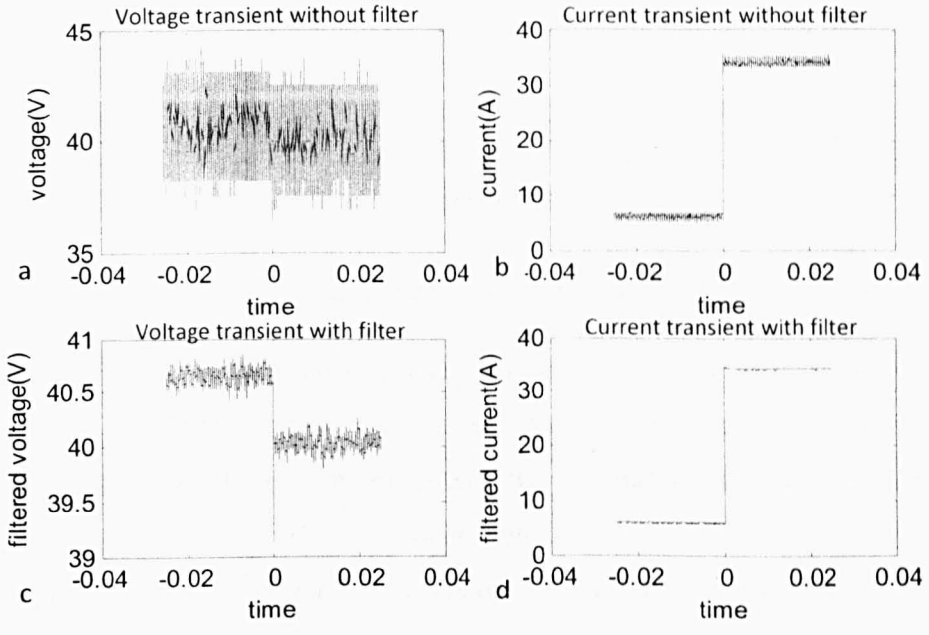

Figure 3.30 Measured DC voltage and current before and after filter

a) Measured voltage b) Measured current c) Filtered voltage d) Filtered current

The DC voltage source has a current limit of 40 A [145] and in this case high supply voltage (40V DC) can be used in this test. Figure 3.29 c) and d) show clear step transients in the measured waveform after processed with filtering.

Similar to the calculation in the AC system, the filtered data which is transformed by the FFT is 12ms in length in the time domain with the fault transient located in the middle of the data. Using only 6ms after the fault transient, the positions of the faults can be estimated. The estimated line reactance results before and after curve fitting is compared with the calibrated value in Figure 3.31 when a 1Ω short circuit fault is imposed at the end of the cable (F4).

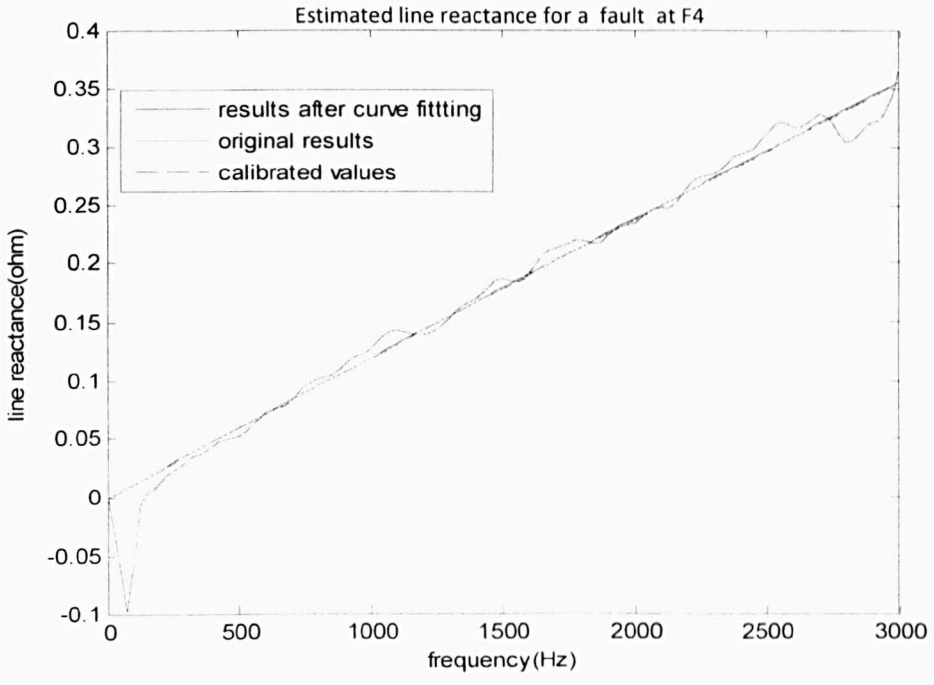

Figure 3.31 The estimated line reactance with fault at F4 in DC system

Compared with the original estimated line reactance (line with oscillations in Figure 3.26) which is produced in a AC system with a lower system voltage level (about 25V phase to phase peak), the oscillations in the estimated line reactance in the 40 V DC system are greatly attenuated. A higher system voltage level leads to larger fault transients in which case offer better SNR and a more accurate impedance calculation.

For the DC system, the single-ended algorithm gives more accurate line reactance estimations for different fault positions, as shown in Figure 3.32 and Table 3.7, than the AC system results (in Figure 3.29) due to the fact that; firstly a larger transient is generated by fault in a system with higher supply voltage and secondly faults within a DC system are more likely to have a larger transient than in an AC system even with the same supply voltage levels due to the different fault inception angles, the fault transients are different in the an AC system (this factor will be explain in detail in chapter 5).

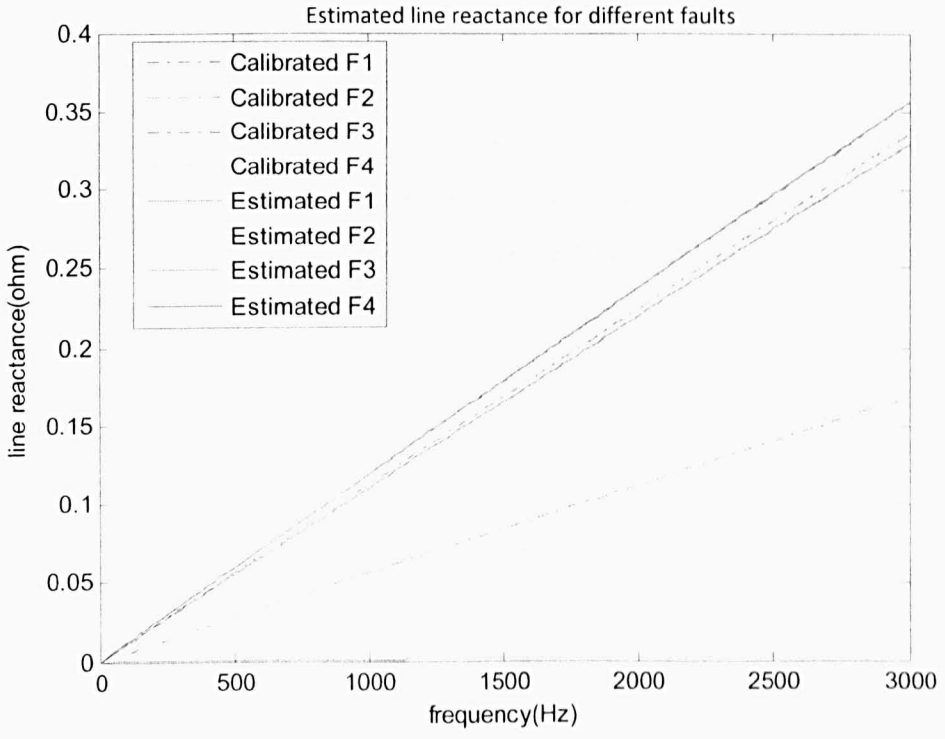

Figure 3.32 Line impedance calculation of different fault positions in the DC system

	F1	F2	F3	F4
Estimated results (μH)	0.08	8.57	16.75	17.13
Calibrated results (μH)	0	8.43	16.92	17.16
error%	0.46	0.81	0.99	0.17

Table 3.7 Estimated line inductance value and errors for DC single-ended test

Clearly, the fault location accuracy is improved by comparing Figure 3.32 with Figure 3.29. The author knows in a distribution system with larger voltage or smaller fault impedance, the accuracy can be further demonstrated in chapter 5.

3.5.3 Fault location in a system with a non-linear load

The application of power electronic devices has increased greatly in modern power systems. During the switching operation, the power electronic equipment can cause system disturbances which are mostly reflected in the harmonic system current. Switching frequency harmonics generated by converters with high frequency IGBT switches can be eliminated by adding a low pass filter. The distortion created diodes bridge rectifier, may cause a

problem for this single-ended fault location method which involves using the fault transient as a harmonic source.

In this experimental test, a non-linear load is added using a diode rectifier with a 12Ω resistive load in parallel with the original 6.8Ω resistive load at the end of transmission line. The distorted voltage and current waveforms, measured and filtered, are shown in Figure 3.33.

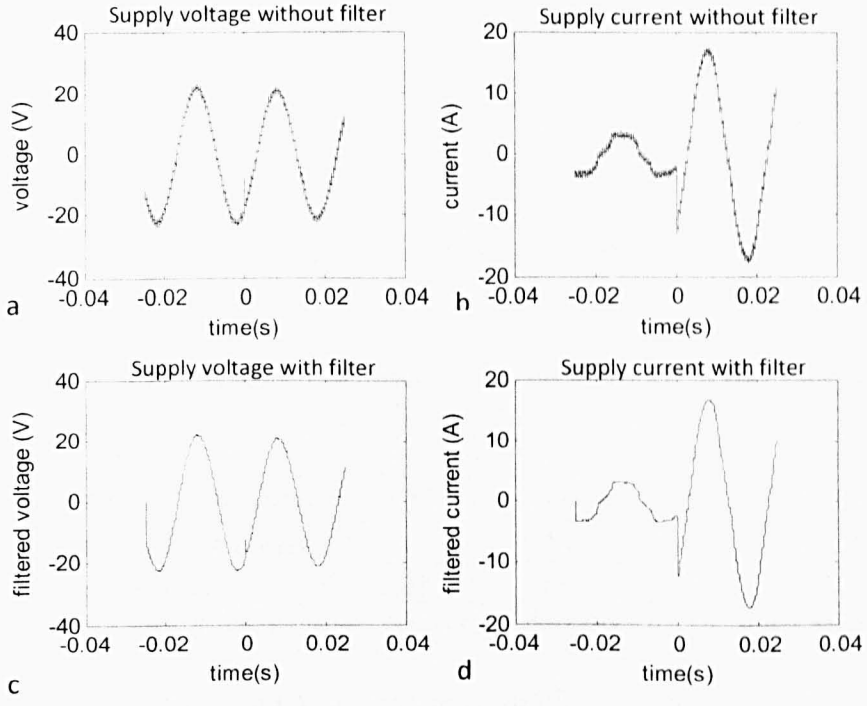

Figure 3.33 Voltage and current before and after low-pass filter, with nonlinear load

a) Measured voltage b) Measured current c) Filtered voltage d) Filtered current

The harmonics in the current caused by diode rectifier still exists in the transient after it is processed with a low-pass filter (with a 4kHz cut off frequency). However, the fault current increases to a value much greater than the steady state pre-fault current and brings a high SNR to the fault transient compared with system harmonics. Also because of a short measurement window (12ms) is used (less distortion is captured compared methods requires longer data segments), the distortion caused in steady state does not have very much influence on the accuracy of the estimated results, as shown in Figure 3.34 and Table 3.8

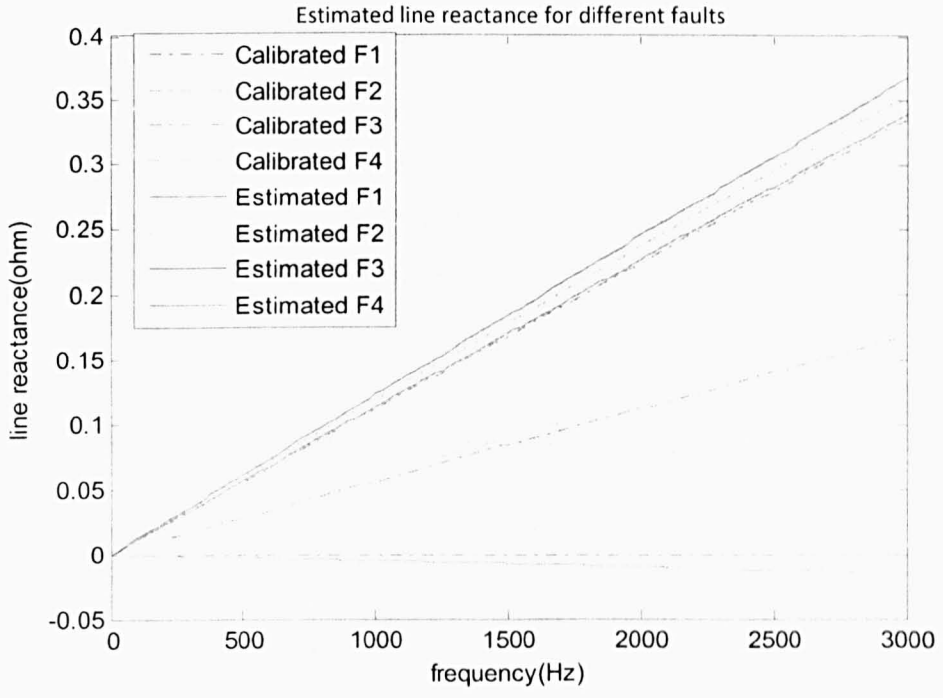

Figure 3.34 Line reactance of different fault positions with a non-linear load

	F1	F2	F3	F4
Estimated results (μH)	-0.35	8.71	16.99	17.38
Calibrated results (μH)	0	8.43	16.92	17.16
error%	2.03	1.63	0.40	1.28

Table 3.8 Estimated line inductance value and the errors for DC single-ended test

Compared with the estimated reactance results for the linear load system shown in Figure 3.29, the calculation errors increase for a non-linear load system as shown by the results in Figure 3.34 and Table 3.8, especially when the fault position is close to the measurement point and the fault transients in the measured voltage is smaller. The small negative impedance result for a zero distance fault is caused by a curve fitting which fits the original estimated results (for example, the green line in Figure 3.27) to a value close to the calibrated results and reduces the absolute error. This fitting procedure can not promise the results always larger than the calibrated value. Although the errors of estimation are enlarged by the existence of system distortion (beside the fault transients), it is possible to maintain a high accuracy (2%) and distinguish the faults with 1m as shown in the values of Table 3.8.

The single-ended method discussed works under the assumption that the fault transient is a step reflected in the system voltage at the fault point. For an arc fault or faults with oscillations (bouncing fault), the single-ended algorithm produces much larger errors than the 1m limitation of the accuracy requirement. This situation will be shown in the next chapter "double-ended fault location" in which the bouncing fault is studied.

3.6 Comparison with other single-ended methods

Single-ended fault location algorithms based on impedance measurement suffers from the unknown value of fault impedance and source impedance. Also the fault detection time is normally over 20ms because of the use of the power frequency voltage and current information.

The commonly used distribution network model represented by an impedance and voltage source is presented in Figure 3.35

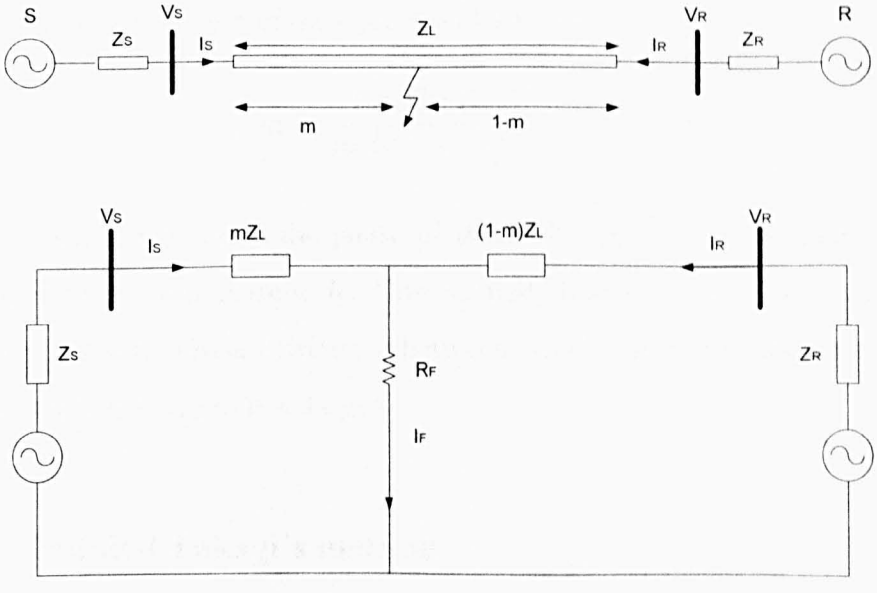

Figure 3.35 Circuit diagram of a distribution system with a short circuit fault

The distribution power system has a supply side and a receiver side. The supply side impedance (Z_S) and the receiver side impedance (Z_R) are the

connected by transmission line impedance. A short circuit fault with fault resistance (R_F) occurs on the transmission line.

3.6.1 Takagi's method

Paper [78] and [79] present a single-ended impedance fault location method by using the pre-fault and post-fault data to calculate the superposition fault current.

$$V_S = m \cdot Z_L \cdot I_S + R_F \cdot I_F \tag{3.14}$$

The superposition current I_{sup} can be derived by using the post-fault current I minus the pre-fault current I_{pre}.

$$I_{sup} = I - I_{pre} \tag{3.15}$$

The fault location (m) can be achieved by multiplying both side of the equation (3.14) by conjugate of I_{sup} (I^*_{pre}) .

$$V_S \cdot I^*_{pre} = m \cdot Z_L \cdot I_S \cdot I^*_{pre} + R_F \cdot I_F \cdot I^*_{pre} \tag{3.15}$$

Using the imaginary part of the equation (3.15), gives:

$$m = \frac{Im(V_S \cdot I^*_{pre})}{Im(Z_L \cdot I_S \cdot I^*_{pre})} \tag{3.16}$$

This method requires that the phase of the fault current I_F is the same as the measured supply side current I_S. This normally happens when fault resistance R_F is zero. As the phase difference between $I_F$and $I_S$increases, the calculation error of fault distance m is enlarged.

3.6.2 Modified Takagi's method

As a modificaiton of Takagi's method the discussed method in Eriksson's paper [80] involves using current distribution factor (D) and zero-sequence current from supply side I_{0s} to calculate the fault distance of a phase to earth fault.

Equation (3.14) is modified as:

$$V_S = m \cdot Z_L \cdot I_S + R_F \cdot \frac{I_{sup} - I_{0s}}{D} \cdot \frac{3}{2} \tag{3.17}$$

$$D = \frac{(1-m)Z_L + Z_R}{Z_S + Z_L + Z_R} \tag{3.18}$$

The unknowns m and R_F can be derived by solving the equation's real and imaginary parts of (3.17)

Another modified method described in paper [110] solves the phase difference between I_F and I_S by using zero-sequence current and without using the superposition current.

The equation (3.16) is changed to:

$$m = \frac{Im(V_S \cdot (3I_{0s})^* \cdot e^{-jT})}{Im(Z_L \cdot I_s \cdot (3I_{0s})^* \cdot e^{-jT})} \tag{3.19}$$

The angle T can be calculated by using the zero-sequence circuit in Figure 3.36

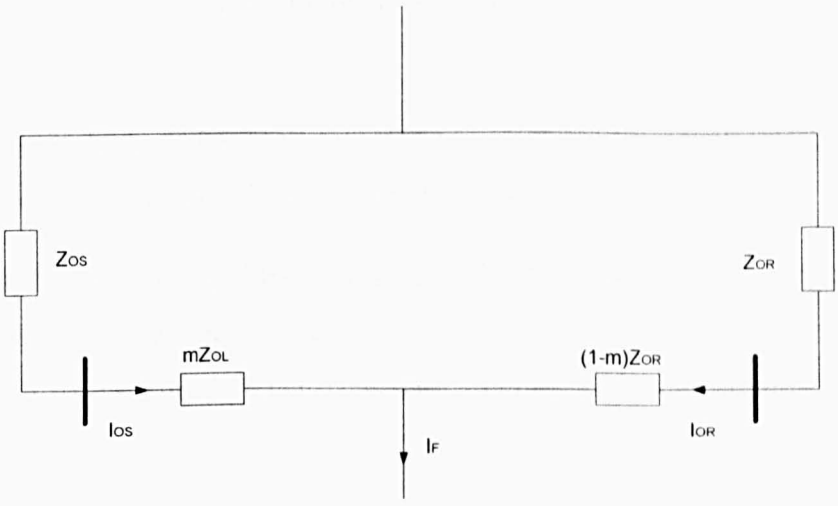

Figure 3.36 Zero-sequence circuit

T is the phase angle between current I_{0s} and I_F:

$$T = angle\left(\frac{Z_{0S} + Z_{0L} + Z_{0R}}{(1-m) \cdot Z_{oL} + Z_{0R}}\right) \tag{3.20}$$

The modified methods described above limit the fault type because of the required zero-sequence current and both of the methods need to know the source impedance of both sides of the protected transmission line. The source impedance may be the generator supply impedance alone or a combination of supply impedance, cable impedance and load impedance. Without special measurement, it is difficult to know the source impedance.

3.6.3 Simple reactance measurement method

Most single-ended impedance fault location methods and the three methods discussed in Section 3.62 can be seen as being based on the reactance measurement which uses the equation (3.21) to estimated fault distance:

$$m = \frac{Im(\frac{V_S}{I_S})}{Im(Z_{per-meter})} \tag{3.21}$$

where $Z_{per-meter}$is the per-meter length line impedance and the V_S and I_S are the measured voltage and current at the start of the distribution line at the system frequency (50Hz).

This requires I_S=I_F or the fault resistance to be zero or the fault resistance has too be much smaller than the load impedance: $R_F << Z_R$.

By using this method in the test system, the simulation results in Figure 3.37 show the estimated line resistance and reactance when a short circuit fault occurs at F3 (in Figure 3.22) at 0.06s with a fault impedance variation from 0Ω to 1Ω.

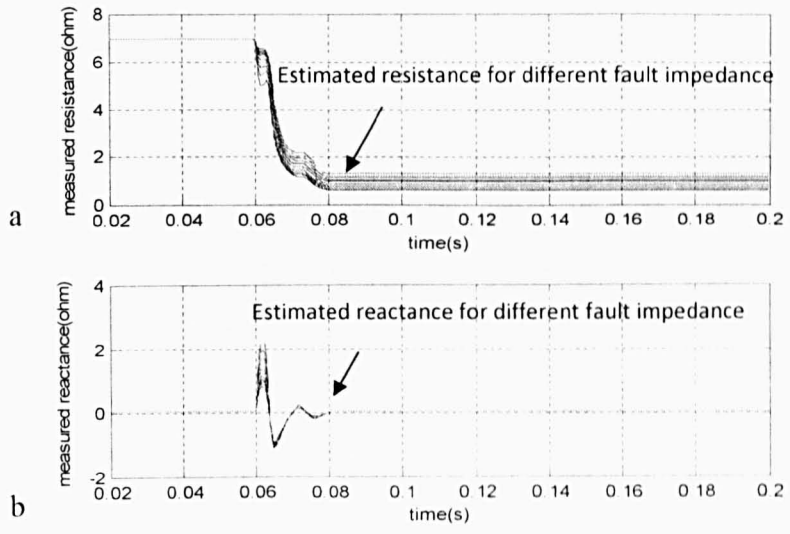

Figure3. 37 Measured impedance when fault occurs at F3

a) Resistance results b) Reactance results

At a time delay of 20ms after the fault is imposed (at 0.06s), the new steady state impedance is obtained. The resistance is measured to be from 0.61Ω to 1.35Ω and the variation of the reactance is from 0.0061Ω to 0.0182Ω. Figure 3.38 shows that the results when fault at F2 is imposed

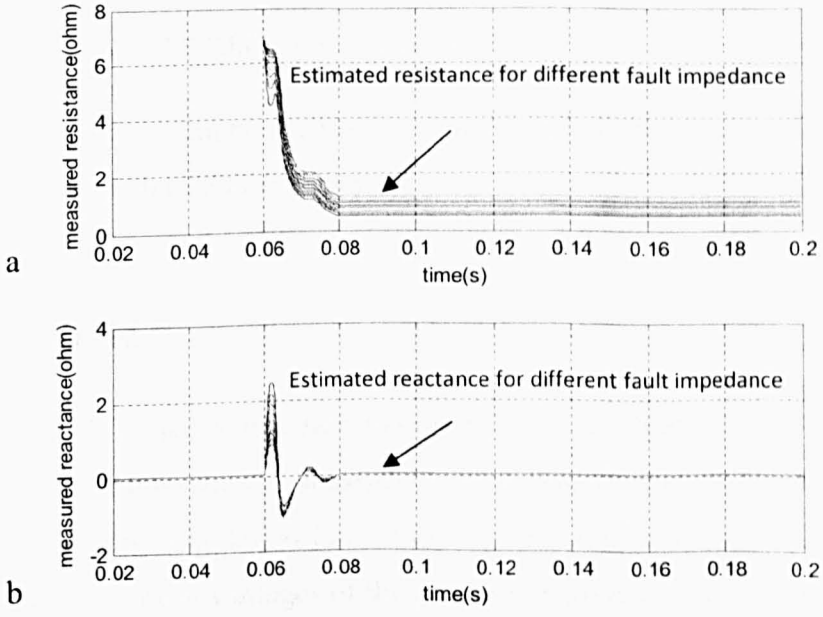

Figure 3.38 Measured impedance when fault occurs at F2

a) Resistance results b) Reactance results

The estimated resistance in Figure 3.38 is from 0.54Ω to 1.23Ω and the estimated reactance is from0.0044Ω to 0.0084Ω. By comparing the results of Figures 3.37 with Figure 3.38, it can be concluded that it is impossible to classify the fault location for a variable fault resistance by using estimated resistance or reactance at the system frequency in such a system. Besides even using the Takagi's or Eriksson's method the value of reactance is too small, at the system frequency, to classify the fault position.

The traditional methods are used in Extreme High Voltage (EHV) transmission lines where the distance is over 20Km. Utilized in a small distribution system, the calculated reactance at system frequency is too small to be used for fault location. The resistance value is normally influenced by the fault resistance can not be used for fault location either. Therefore, the traditional methods do not work in a small distribution system.

As a comparison to the discussed sing-ended fault location methods the algorithm proposed by the author has the following advantages:

a) Very short fault location time (only 6ms after fault) is needed.

b) Source impedance is not required.

c) Less influenced by the fault resistance.

d) High X/R ratio can be derived by using high frequency data which provides more accuracy during fault location.

3.7 Summary

A new single-ended impedance measurement based fault location method that uses the fault transients is discussed in this chapter. The proposed method is demonstrated by simulation in a simple system and tested by experiment in a cable system. The advantages of the proposed algorithm are then demonstrated by comparing with other single-ended fault location methods which use the power frequency system voltage and current information.

The algorithm which was demonstrated both using a laboratory experimental system and through simulation work on a small cable Integrated Power System (IPS). However, the method should be extendable to any type of distribution system and for over-head lines.

Chapter 4

Double-ended fault location

4.1 Introduction

This chapter introduces a new double-ended fault location scheme for IPS which uses the transients generated by faults. Although a data communication channel is required, this method has a simple and straight forward algorithm which is easy to realize in a practical distribution system and does not require GPS synchronization [82] as other methods introduced in Chapter 2. By using the high frequency (as high as 3kHz) information derived from the transients, the fault location time is reduced to as little as 4ms after the fault occurs and also it can provide an accuracy of 1m.

The single-ended fault location algorithm discussed in the previous chapter was used to locate the hard short circuit fault with a 1Ω fault resistance. Based on the same cable power system a double-ended fault location method is shown to conquer the disadvantages of the single-ended method as it can locate both hard faults and bouncing faults with the same or even higher fault resistance.

After the introduction and basic theory in Section 1 and Section 2, the experimental estimation results are presented in Section 3 for both hard faults and bouncing faults and a non-linear load is considered as well. The proposed double-ended method is then compared with an established double-ended scheme to demonstrate its benefits.

4.2 Basic theory

4.2.1 Basic theory of double-ended scheme

A double-ended fault location algorithm based on impedance measurement will be discussed and demonstrated in a power distribution power system. The basis of this method can be introduced by considering a single phase circuit with a short circuit fault on the distribution line as shown in Figure 4.1. Z_s can be the supply impedance alone or a combination of supply impedance, cable impedance and load impedance. Z_{load} the is equivalent load impedance. Assuming that the total transmission line impedance between the supply and load is Z_l, where Z_x is the part of line impedance between supply and the position of fault and Z_{l-x} is the remaining part of the line impedance.

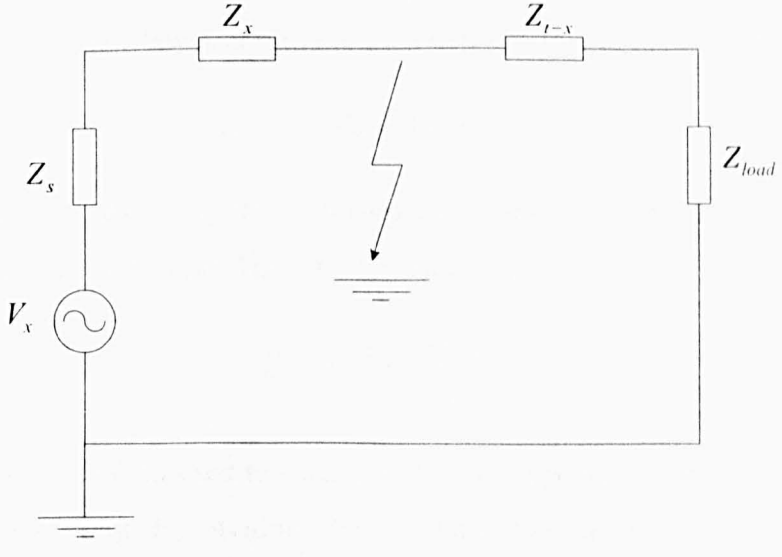

Figure 4.1 Single phase circuit with a phase to ground fault

The fault is considered to be a voltage source which creates voltage and current fault transients and contains information over a wide frequency range. The Thevenin equivalent circuit at a non-fundamental frequency has the supply voltage short-circuited and the fault as the transient source as shown in Figure 4.2.

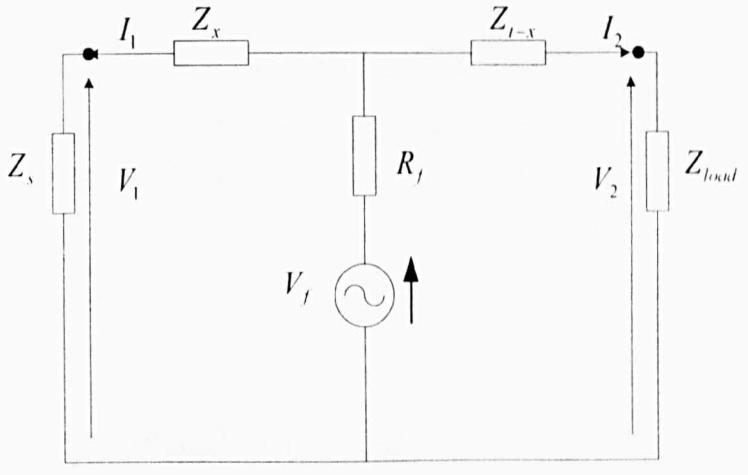

Figure 4.2 System at non-fundamental frequency during fault situation

As shown in Figure 4.2, the fault transient V_f act as voltage source that provides voltage transients at non-fundamental frequencies and R_f is the fault resistance. There are two measurement points located at the supply end and the load end of the power distribution line. The voltage and current are measured at both measurement points during the fault. Equation (4.1) is derived by using Kirchhoff's voltage law according to the circuit shown in Figure 4.2.

$$V_1 + I_1 \cdot Z_x = V_2 + I_2 \cdot Z_{1-x} \tag{4.1}$$

where the V_1, I_1 and V_2, I_2 are the measured current and voltage information from both ends of the line. The total line impedance $Z_1 = Z_x + Z_{1-x}$, thus:

$$Z_x = \frac{V_2 - V_1 + I_2 \cdot Z_1}{I_1 + I_2} \tag{4.2}$$

Equation (4.2) is then used to estimate the line impedance between the supply and the fault point. By dividing the estimated line impedance by the known per-unit length impedance of the line, the fault location can be found. It follows that this double-ended scheme does not require information concerning fault resistance and the waveform of the fault transients or knowledge of the

load and supply impedances and the calculation is also simple to implement. Similar to the single-ended method, the calculation is done in the frequency domain and a Blackman window is applied to the finite measured data segment to smooth the edges.

In an integrated power system (IPS), the synchronization of information from the two ends of the cable is realized by a trigger signal sent in a communication channel (after receive this signal, the FPGA starts to record the measured information from both ends at the same time). In other distribution power systems, a Newton-Raphson iteration method is used to solve the non-linear equations and cancel the unsynchronized errors and this is discussed in Chapter 5.

4.2.2 Evaluation through simulation

In order to evaluate the proposed double-ended scheme, a simple three phase system was built and simulated using Matlab/Simulink. The testing system is shown in Figure 4.3

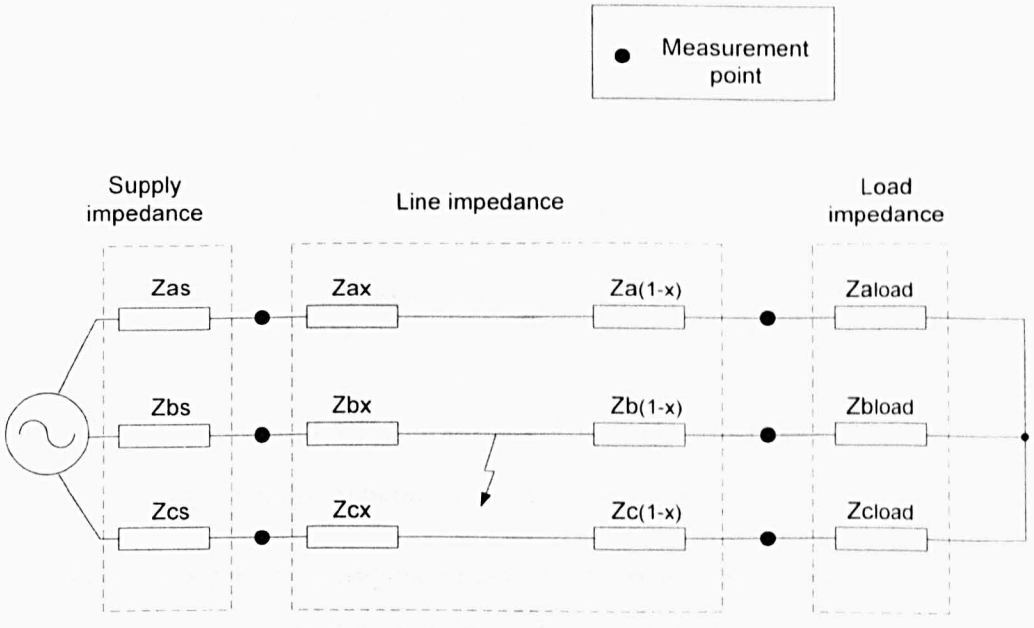

Figure 4.3 System configuration of simulation demonstration system

As shown in Figure 4.3, the three phase system has a 440V, 50Hz (phase to phase rms) AC voltage source. The supply impedance per phase is

Z_s=(0.001+j0.00942)Ω. The three phase star connected load is 90kW with a power factor of 0.9. The line impedance is represented by lumped RLC components with per phase value $Z_x=Z_{(1-x)}$=(0.0003+j0.00075)Ω. For a fault between phase B and phase C (fault impedance=0.1Ω), the three phase measured voltage and current in time domain at both supply and load ends are presented in Figure 4.4.

Figure 4.4 shows the measured V_{supply}, I_{supply} and V_{load} and I_{load} at the two terminals of the transmission line. V_{A-B} is the red line, V_{B-C} is the blue line and V_{C-A} is the green line. I_A is the red line, I_B is the blue line and I_C is the green line.

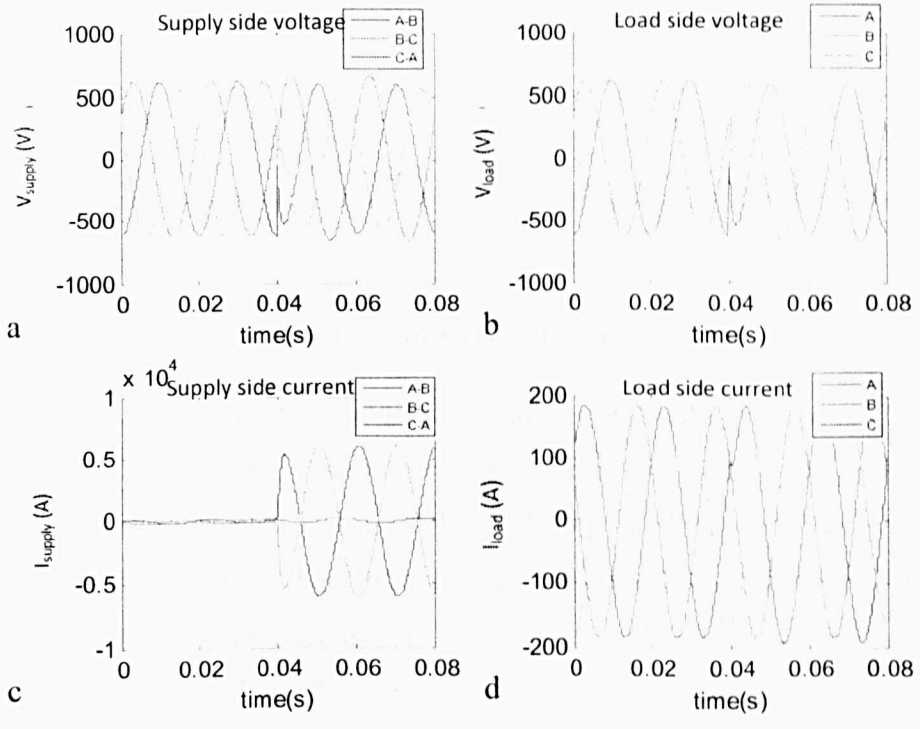

Figure 4.4 The measured voltage and current data

a) Supply voltage b) Supply current c) Load voltage d) Load current

The short circuit fault is imposed between the phase B and phase C at 0.04s. For a phase to phase fault in this three phase system, if the fault is considered as a voltage source, then there is no transient in the current of the healthy phases for a balanced system.

The cable impedance calculation for a fault occurring in the middle of the distribution cable is shown in Figure 4.5.

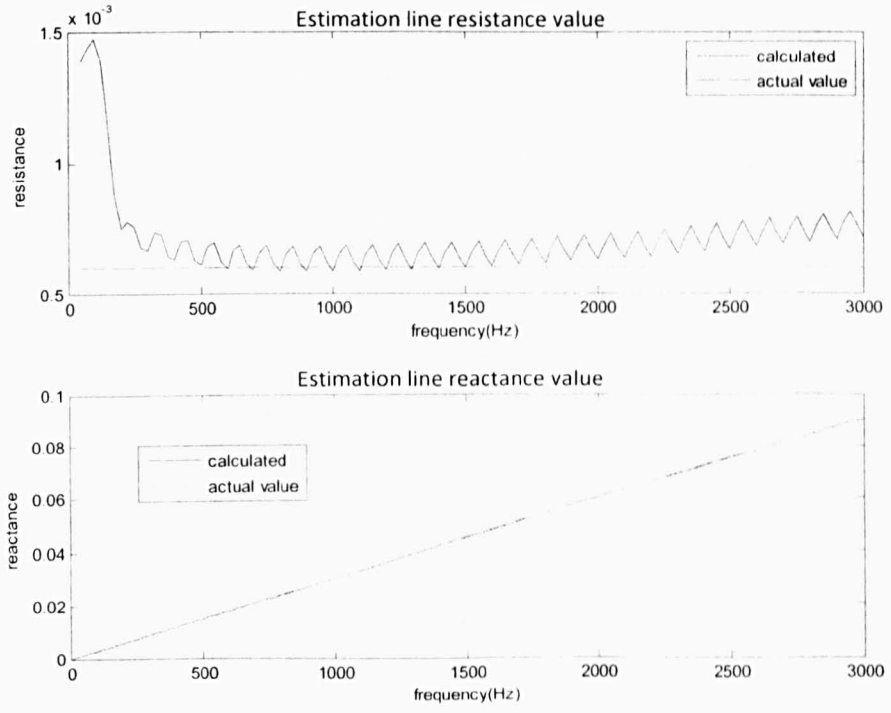

Figure 4.5 Impedance estimation results

Figure 4.5 shows the estimated line resistance and reactance between the fault position and the supply measurement points against frequency using the 8ms length of data presented in Figure 4.4 with the fault transient located in the middle of the window. The time domain data is windowed by a Blackman window (removing the edge influence) and transformed into frequency domain by FFT. The solid lines show estimated line impedance results between the supply point and fault position and the dashed lines indicate the actual values used in the simulation. Compared with the actual value, the calculated line reactance shows good accuracy against frequency (the dash line of reactance matches the solid line very well). The estimated line resistance results are not as accurate as the reactance, especially in the high frequency range (1500Hz to 3000Hz). The impedance is calculated using (4.2) and then it is separated into real part and imaginary parts. In Figure 4.5, the line resistance is much smaller than the line reactance in the high frequency range. If there are small errors with the total impedance calculation or the phase calculation, the errors are

magnified from the view of the calculated resistance. As frequency increases, the value of the imaginary part becomes much bigger than the real part and that leads to errors which increase in the estimated values of resistance. These impedance values are typical of cable parameters so that in the experiment and future simulation only the line reactance is used to locate the fault position.

The double-ended algorithm offers good accuracy (the largest error is within 0.3% of its actual value in simulation results) for the calculated line reactance when a fault occurs at either the supply end or the load end.

Figure 4.6 and Table 4.1 show the estimated line reactance results from supply measurement points to the fault for three different fault locations: F_1 at the source, F_2 in the middle of distribution cable and F_3 at the load side compare with the real value.

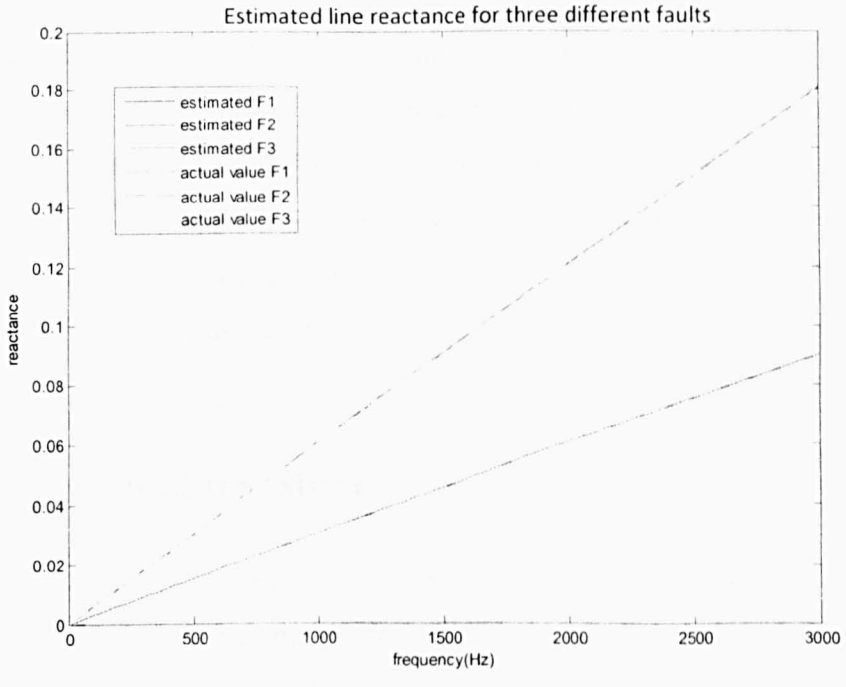

Figure 4.6 The estimated line reactance for different fault locations (simulation)

	F1	F2	F3
Estimated results (μH)	0.002	2.402	4.802
Calibrated results (μH)	0	2.4	4.8
error%	0.04	0.04	0.04

Table 4.1 Estimated line inductance value and errors for double-ended simulation

For the three different fault positions, the solid line (calculated line reactance) matches the dashed line (simulation value) with little error (within 0.3% of its actual value) in Figure 4.6. This gives the confidence that this double-ended fault location algorithm could be used in a protection scheme to detect the fault position.

In this fault location scheme, the voltage and current from both supply and load ends are continuously monitored by an 8ms length window. When a short circuit fault occurs and causes system current to suddenly rise, the difference between the measured currents from both ends suddenly increases to a value which is larger than the pre-set threshold so that the fault phases can be detected and at this time a trigger signal is sent to capture the fault transient over the 8ms window. A 4ms delay is used, to keeps the transients within the middle of the window. The trigger is located in the middle of the in time domain captured measurement window so that when the Blackman window edge filter is applied in the time domain, the energy of transient, which is located in the middle of the data segment, is less attenuated by the windowing function. The fault location can be detected 4ms after the fault occurs, which makes the fault location time much shorter than other double-ended impedance measurement fault location methods which use post fault system frequency voltage and current information.

4.3 Experimental system

The exerimental system for the examination of double-ended fault location algorithm is same as for the single-ended method. The only two different factors are that another current and voltage measurement unit is added at the load point (C4 of Figure 3.8) and the fault unit is modified to be able to provide not only a step fault but also a bouncing switch (mechanical switch) fault.

In order to create a fault with an oscillating fault voltage the fault unit described in Figure 3.12 was modified as shown in Figure 4.7

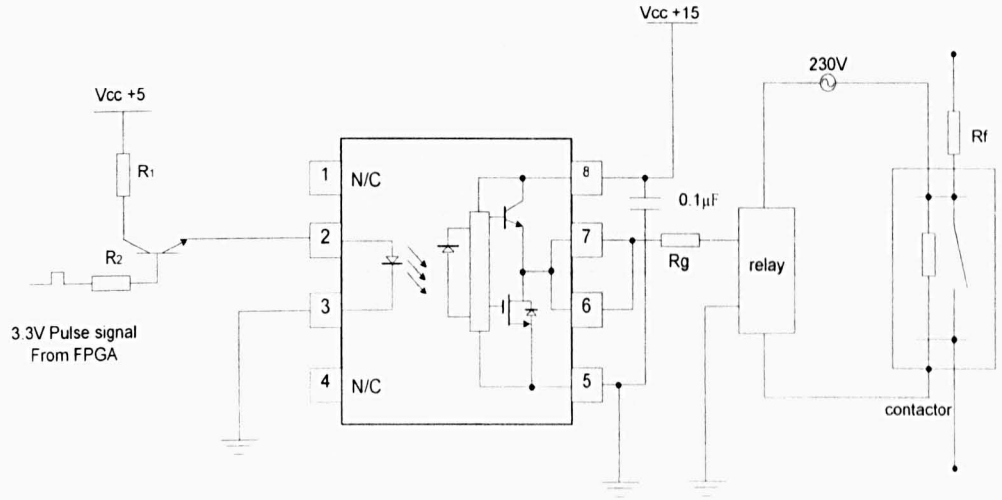

Figure 4.7 Fault unit for the oscillation fault transient

Compared with the fault unit of Figure 3.12, the fault is imposed in the system by a standard contactor (a mechanical switch) [111] which is driven by a 230V AC voltage. A relay [112] is used to separate the low voltage part from the high voltage part. The high output of the gate drive voltage (15V) is used to switch on the relay and the low voltage (-5) is used to switch off the relay. This contactor acts as a mechanical switch which is able to work in both AC and DC systems. Unlike the IGBT switch which creates a fault step in the voltage waveform, the mechnical contactor once supplied with 230AC voltage normally does not close itself instantaneously (the copper contactor vibrates when switched on and off). Its closing action, in the time domain, has several close, open and reclose actions as the contactor bounces.

The output voltage of the fault unit, the voltage across the relay and the trigger votlage are shown in Figure 4.8 for a test on an AC system which is imposed a short circuit fault with 2Ω fault resistance (in order keep the fault current low) to the system which has a supply voltage of 20V rms using the bouncing fault unit.

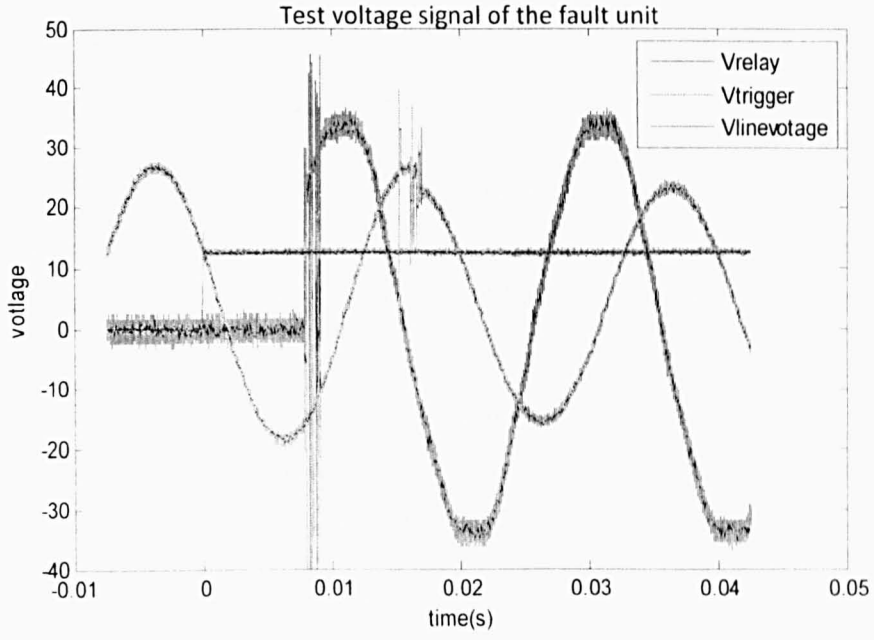

Figure 4.8 The voltage output of different component of the fault unit

As shown in Figure 4.8, the green line is the trigger signal (output voltage of the drive) which triggers at 0s in the time domain. The blue line is the voltage across the relay (230V AC rms) devided by 10 (in order to keep it in the same scale range with the other measured voltage data). The red trace is the output voltage of the fault unit (votage across the fault resistance R_f). Compared with waveforms in Figure 3.13 of chapter 3, it is clear that the mechinical switch has a much longer reaction time than the IGBT. About 9ms after 15V is supply to the relay circuit, the relay turns on and creates high frequency transients at about 0.01s in the votlage (shown in blue). The relay itself is an mechanical switch and switch action reflected in the voltage waveform is not a step. 8ms later, the contactor closed in a oscillating way as shown by the red line. As expected, the system fault transient in the measured voltage waveform (red line) is an oscillating waveform rather than a step. The contact copper bar of the mechanical switch can not be closed without boncing and leads to a bouncing waveform in the voltage.

4.4 Fault location results

4.4.1 Results for a bouncing fault

Short circuit faults within the power system are commonly hard faults which create a step change in the system line voltage at the fault point. However other different fault transients may exist. The exact nature of the fault can not be predicted. In this chapter, a type of arc fault (or bouncing fault) is imposed on the cable by the operation of a mechanical switch is considered because ideally the proposed double-ended algorithm does not require any detailed knowledge of the fault transient as long as a suitable transient exists.

The first test is carried out with a 25V (phase to phase peak) AC voltage supply and a 6.8Ω resistive load as described in chapter 3. Faults with different fault resistances were imposed on the cable at four different locations: F1 (fault 1, at the start of the cable), F2 (fault 2, at 10m from the start of the cable), F3 (fault 3, at 1m from the end of the cable) and F4 (fault 4, at the end of the cable) as in shown Figure 4.9. Voltage and current are measured at both the supply and the load side of the system.

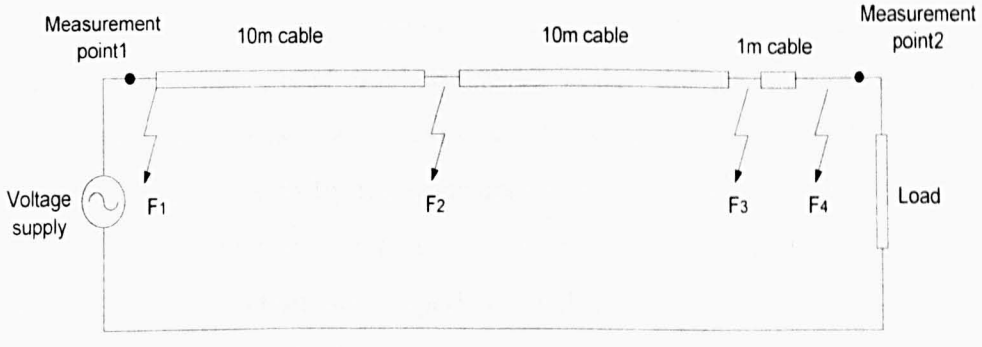

Figure 4.9 Four different locations in the experiment system

For a fault situation, with a 1Ω fault resistance (in order to limit the fault current within the safe operation range of the supply), the measured voltages and currents from both measurement points are presented in Figure 4.10

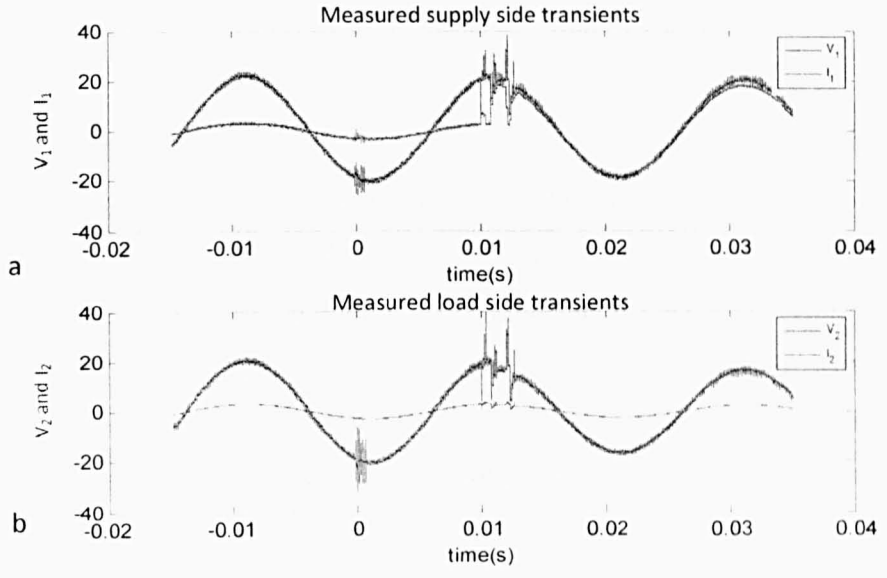

Figure 4.10 Measured waveforms for a bouncing fault transient fault transient created by a mechanical switch

a) Voltage and current at supply side b) Voltage and current at load side

In Figure 4.10, the relay is closed at 0s which creates a high frequency bouncing waveform. After about 12ms the mechanical switch is closed and the bouncing transient waveform appears. For the single-ended method discussed in chapter 3, the line reactance between the fault and the supply measurement point can be estimated by using the data in Figure 4.10 a). However, the single-ended method works under the assumption that the voltage fault transient is a step waveform. As in equation (3.10), the created step voltage V_{pre} divided by the measured bouncing current I_s will create a very large error which can not be reduced by iteration and the large error compared with the actual line impedance value leads to an non-converging iteration. One example is that when the bouncing fault occurs at 20m the iteration results in Table 4.2

iteration steps	estimated fault distance (m)
0	47
1	52
2	64
3	79
4	92

Table 4.2 The failure iteration using single-ended method to locate bouncing fault

When the program detects that the first iteration error is larger than the second one, it will report a failure which means the single-ended algorithm may not work under this situation.

The proposed double-ended algorithm works under this bouncing fault situation because it has no detailed requirement for the fault transient signal as long as the SNR is high enough to produce accurate results. The measured data length is two cycles (40ms) of the supply frequency. However, after being pre-processed by a low-pass filter (cut-off frequency of 4000Hz), a Blackman window and zero padding, the data length needed to produce an accurate result is very short and is only 6ms after the fault occurs. The FFT processed current and voltage magnitudes in the frequency domain are shown in Figure 4.11.

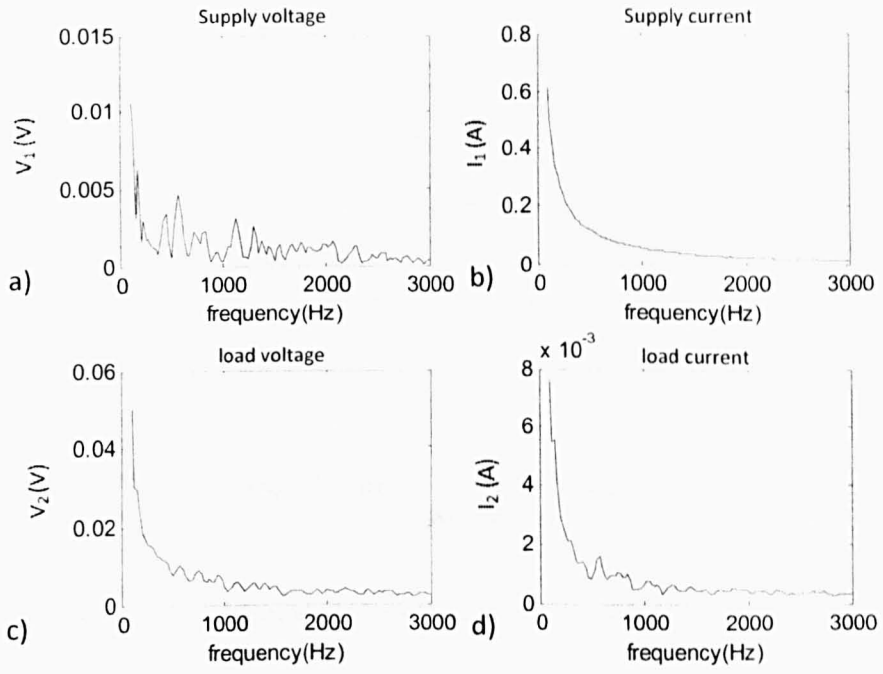

Figure 4.11 Voltage and current magnitudes in frequency domain

a)Supply voltage b)Supply current c)Load voltage d)Load current

Compared with the time domain information shown in Figure 4.10, the transients in frequency domain for the voltage measured at supply point (V_1) is more affected by noise than the other measured quantities. Due to the very low supply impedance, the voltage drop during the fault produces less energy

than the current, which has a bigger transient in the time domain. In Figure 4.11, the fault transient in current I_1 has a good frequency domain content.

Using equation (4.2) with the measured voltage and current data, the line impedance between measurement point1 and the fault position can be calculated. As discussed in Section 2, in the high frequency range the measured resistance has less accurate than the reactance. This double-ended scheme therefore uses reactance to locate fault positions on the cables.

For example, when a 1Ω short circuit between two phases (phase brown and phase blue) occurs at F_4, the estimated line reactance compared with calibrated reactance from chapter 3 is shown in Figure 4. 12.

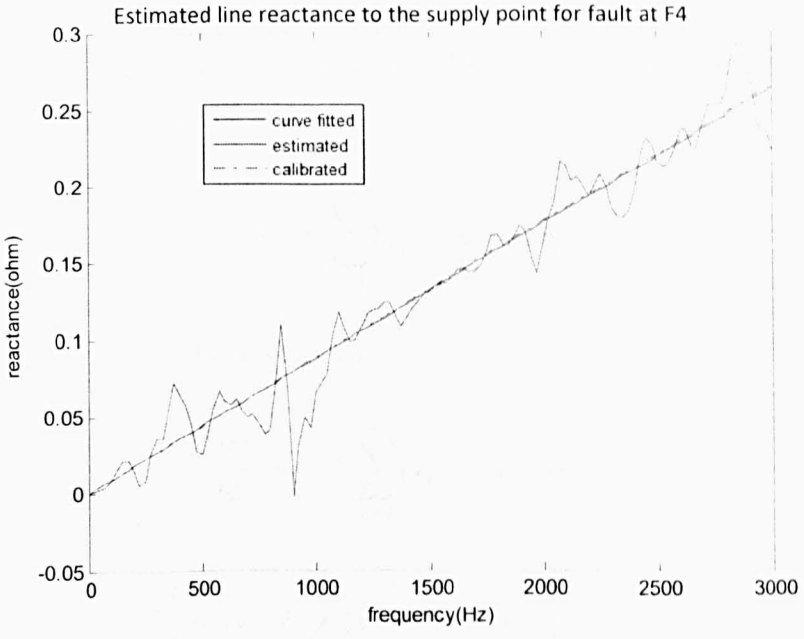

Figure 4.12 Estimated line reactance compared with calibrated value

In Figure 4.12, the solid line (green), which has oscillation and increases with frequency is the estimated result using the double-ended method. The dashed line (red) is the value derived from calibration (described in chapter 3). The solid stranght line (blue) is the estimated value after being processed by a first order least squares curve fitting. The curved fit line matches very well with the calibrated results.

The linear least squares (first order) is one of the most commonly used linear regression method uised to find the best fit curve to a given set of points by

minimizing the sum of the squares of the offset. The first order least squares fit provides a fitted straight line to a given set of points. The functional relationship between the two fit quantities is known as muliply [113][114]. As shown in Figure 4.12, the y axis reactance value increases proportionally with frequency ($X = 2 \cdot pi \cdot f$), which means it is suitable for the linear least squares curve fitting. In order t o achieve accurate linear curve fit results in a x-y domain, the original behaviour of the y axis values against the x axis values must be linear. The calibrated cable impedance in the experimental test has a linear behaviour. However, for the calculation of the system impedances which may consist of parallel connected inductors, both the reactance and the resistance do not change linearly in the frequency domain, so the first order curve fit does not work accurately.

Unilizing a linear least squares curve fitting to a n point data, the vertical offset R^2 of the data is defined as:

$$R^2 = \sum_{i=1}^{n} [y_i - (a + bx_i)]^2 \tag{4.3}$$

In order to minimize the deviations:

$$\frac{\partial(R^2)}{\partial a} = -2 \sum_{i=1}^{n} [y_i - (a + bx_i)] = 0 \tag{4.4}$$

$$\frac{\partial(R^2)}{\partial b} = -2 \sum_{i=1}^{n} [y_i - (a + bx_i)] x_i = 0 \tag{4.5}$$

(4.6) and (4.7) are derived from equation (4.4) and (4.5)

$$na + b \sum_{i=1}^{n} x_i = \sum_{i=1}^{n} y_i \tag{4.6}$$

$$a \sum_{i=1}^{n} x_i + b \sum_{i=1}^{n} x_i^2 = \sum_{i=1}^{n} x_i y_i \tag{4.7}$$

and written into matrix form

$$\begin{bmatrix} n & \sum_{i=1}^{n} x_i \\ \sum_{i=1}^{n} x_i & \sum_{i=1}^{n} x_i^2 \end{bmatrix} \begin{bmatrix} a \\ b \end{bmatrix} = \begin{bmatrix} \sum_{i=1}^{n} y_i \\ \sum_{i=1}^{n} x_i y_i \end{bmatrix} \tag{4.8}$$

Thus:

$$\begin{bmatrix} a \\ b \end{bmatrix} = \begin{bmatrix} n & \sum_{i=1}^{n} x_i \\ \sum_{i=1}^{n} x_i & \sum_{i=1}^{n} x_i^2 \end{bmatrix}^{-1} \begin{bmatrix} \sum_{i=1}^{n} y_i \\ \sum_{i=1}^{n} x_i y_i \end{bmatrix} \tag{4.9}$$

The unknown variables 'a' and 'b' can be calculated by using (4.9), as the relationship between frequency and reactance is not just linear but also starts from zero. The variable a is set to zero which simplifies the fitting calculation procedure.

The ocillation in the original estimated results (green line in Figure 4.13) are due to the low signal to noise ratio (SNR) of the measured data (especially the voltage data measured at the supply end). The supply voltage of the system is 25V phase to phase peak as presented in Figure 4.10. In a real IPS, with a much higher supply votlage level, larger transients are generated by faults and the SNR will be higher as well, the oscillation in the reactance results will be greatly reduced so that more accurate results can be achieved as proved by the later DC tests in Section 4.4.1.

The estimated results for different fault locations and fault resistances between two phase are presented in Figure 4.13 :

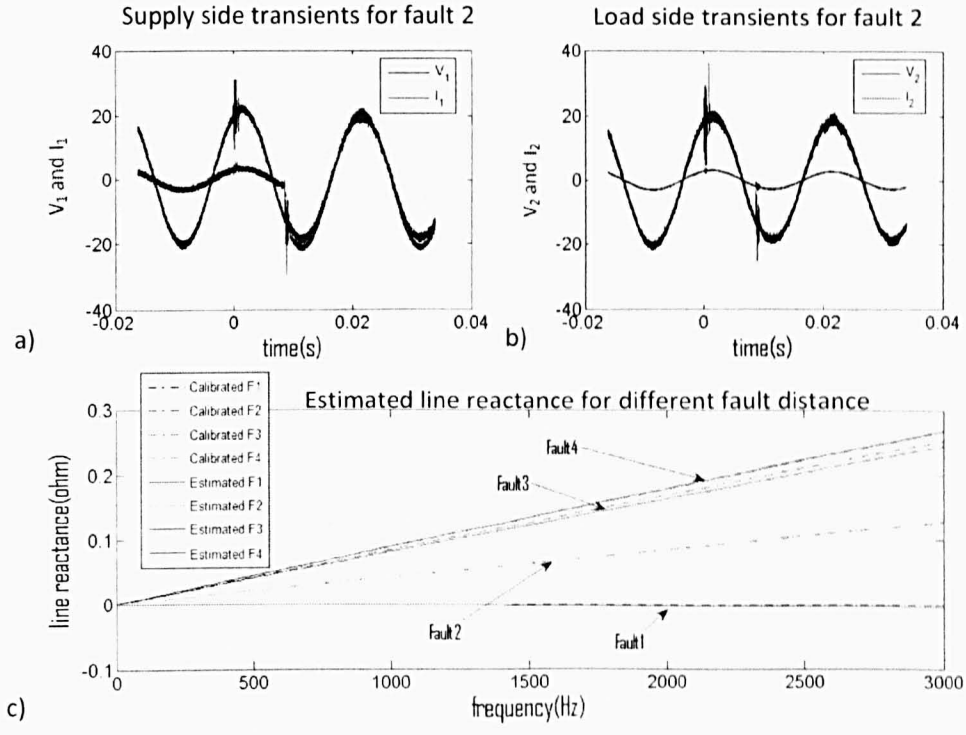

Figure 4.13 Estimated results for a 1Ω fault resistance between phase and neutral using double-ended method

a) Supply side transients b) Load side transients c) Fault location results

	F1	F2	F3	F4
Estimated results (μH)	-0.01	6.32	12.61	13.34
Calibrated results (μH)	0	6.29	12.72	13.36
error%	0.07	0.22	0.82	0.15

Table 4.2 Estimation errors for 1 Ω faults

Figure 4.13 a and b show the typical fault transients (measured voltages and currents at the two ends (V_1, I_1, V_2, I_2)) for fault 2 and the estimated line reactance (solid line) for the different fault locations when a 1Ω phase to neutral fault occurs. The actual values used are shown as dashed lines. As expected the estimated line reactance value increases with fault distance to the supply measurement point (Figure 4.13c). Compared with the calibrated value, the estimated value shows good accuracy (in Table 4.2) which can easily be used to locate faults within distances of 1m (the distance between Fault 3 and Fault 4). The fault transients are attenuated as the fault resistance increases, this situation brings more errors to the estimated results compared with faults

of low fault resistance. The estimated results for a higher impedance fault are shown in Figure 4.14.

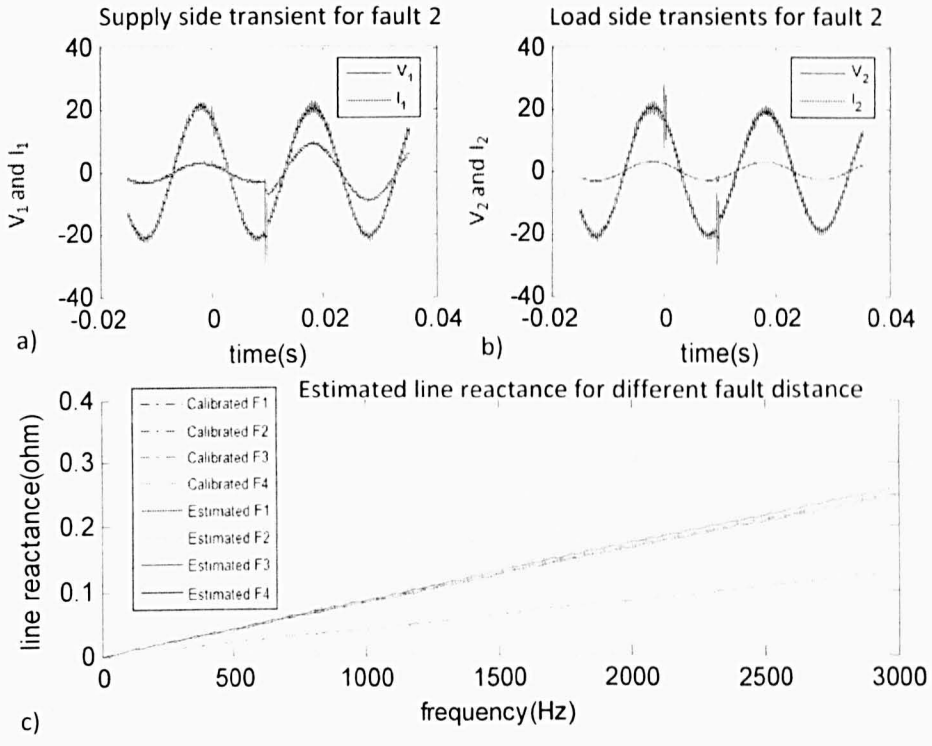

Figure 4.14 Estimated results for a 3Ω fault resistance between phase and neutral using double-ended method

a) Supply side transients b) Load side transients c) Fault location results

	F1	F2	F3	F4
Estimated results (μH)	0.02	6.12	12.61	13.22
Calibrated results (μH)	0	6.29	12.72	13.36
error%	0.15	1.27	0.82	1.05

Table 4.3 Estimation errors for 3 Ω faults

In Figure 4.14, the results show that with a 3Ω fault resistance the typical fault transients in the measured voltages and currents are smaller than same situation with a 1Ω fault (in Figure 4.13). This gives a smaller SNR and the results after curve fitting are less accurate (as shown in Table 4.3). However, the errors in fault location are still within 1m.

As discussed in chapter 3, cores in the cable with different distances from each other have a different phase to phase reactance. This difference within line

reactance has no influence on the accuracy of fault location once the per-unit length of line reactance between different phases is known. In Figure 4.15, the results show that phase to phase (Brown and Gray) faults with different fault resistances (1Ω and 3Ω) still provide signals allowing good accuracy (the largest error is 2.9% in Table 4.5) in the location information.

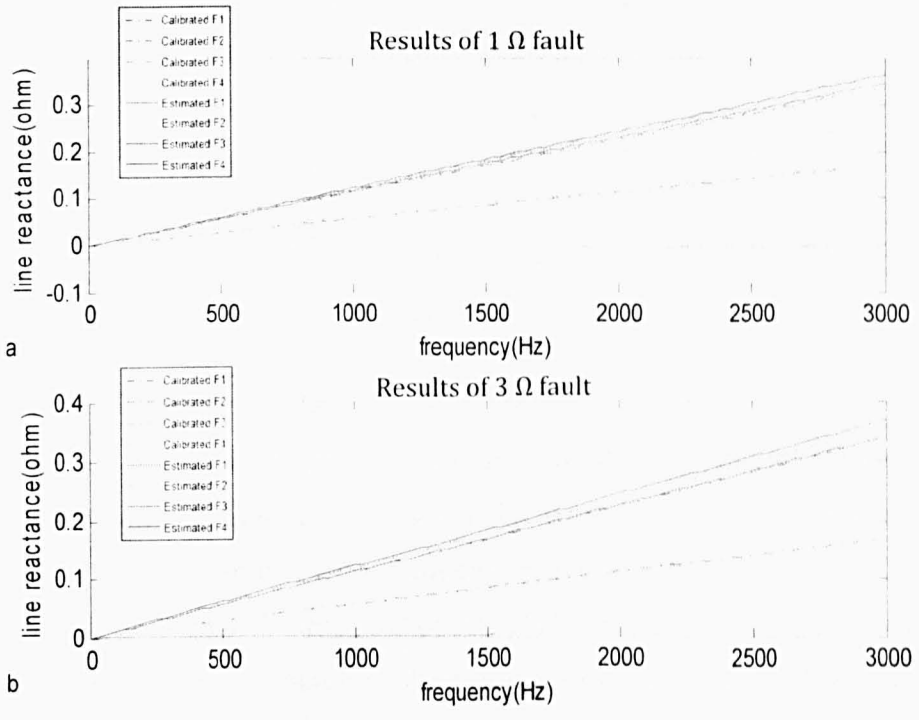

Figure 4.15 Estimated line reactance compared with calibrated one

a) Phase to phase fault with 1Ω R_f b) Phase to phase fault with 3Ω R_f

Similar to the results in Figure 4.13 and Figure 4.14, compared with the calibrated line reactance, the errors of calculated results increase with fault resistance as shown in Figure 4.15. In order to maintain 1 meter accuracy as required, the short circuit fault resistance limitation for this experimental test is 5Ω, which is a very high resistance fault compared with 6.8Ω load resistance. This high impedance fault situation is not common in an IPS cable system. Figure 4.16 shows that the main difference, compared with the previous fault location results for short circuit fault between close phases (Brown-Blue as phase to neutral), is that the estimated line reactance values are bigger for a fault between phases for the same fault resistance at the same fault distance and that is due to larger mutual inductance caused by bigger

distance between phases. For all the line reactance estimations, the errors are shown in Table 4.4 and 4.5

	F1	F2	F3	F4
Estimated results (μH)	-0.03	8.57	16.95	17.35
Calibrated results (μH)	0	8.43	16.92	17.16
error%	0.17	0.82	0.17	1.11

Table 4.4 Estimation errors for 1 Ω faults

	F1	F2	F3	F4
Estimated results (μH)	0.02	8.28	16.99	17.66
Calibrated results (μH)	0	8.43	16.92	17.16
error%	0.12	0.87	0.41	2.91

Table 4.5 Estimation errors for 3 Ω faults

This new double-ended fault location method can provide accurate fault position by using fault transients in either AC or DC supplies. During the fault situation, the fault transients can be considered as a voltage source which has information in a large frequency range (ideally 0Hz to several kHz), at non-system frequency state (DC or AC 50Hz or other system power supply frequency), the supply source is short circuited as in Figure 4.2 and has no influence for the fault location estimation.

The fault transients from measured voltages and currents and fault location results for a DC system with 10V voltage source are presented as in Figure 4.16.

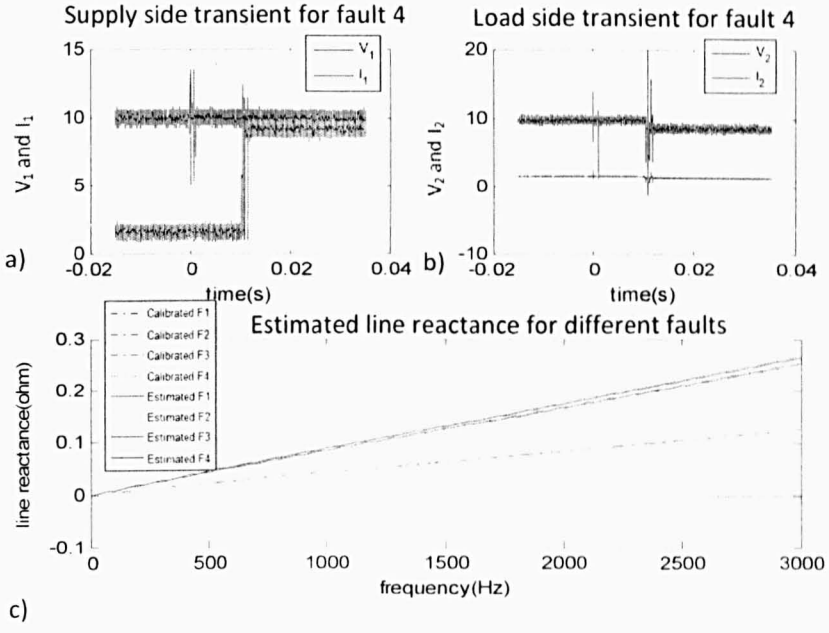

Figure 4.16 Estimated fault locations in DC

a) Supply side transients b) Load side transients c) Fault location results

A 1Ω fault resistance is imposed phase to phase (Brown and Black) and 10V DC voltage is supplied by Chroma (to limit the fault current within 10A DC when the 1Ω fault is added), the estimated results (solid line) matches the calibrated value (dashed line) within the 1m distance error (between F_3 and F_4). The errors for each fault location are shown in Table 4.6.

	F1	F2	F3	F4
Estimated results (μH)	0.01	6.25	12.69	13.39
Calibrated results (μH)	0	6.29	12.72	13.36
error%	0.07	0.30	0.22	0.22

Table 4.6 Estimation errors for 1 Ω faults

Results in DC system have fixed errors for each fault and better accuracy than in the same situation in an AC system. This is because in DC system the voltage is constant while in an AC system the fault may occur when voltage is close to the zero crossing point and creates a smaller high frequency fault transient. The faults are imposed in the system randomly so that the errors in the results of the AC system are not so stable for each fault (but the results are able to meet the accuracy requirement), the details of this influence will be discussed in chapter 5.

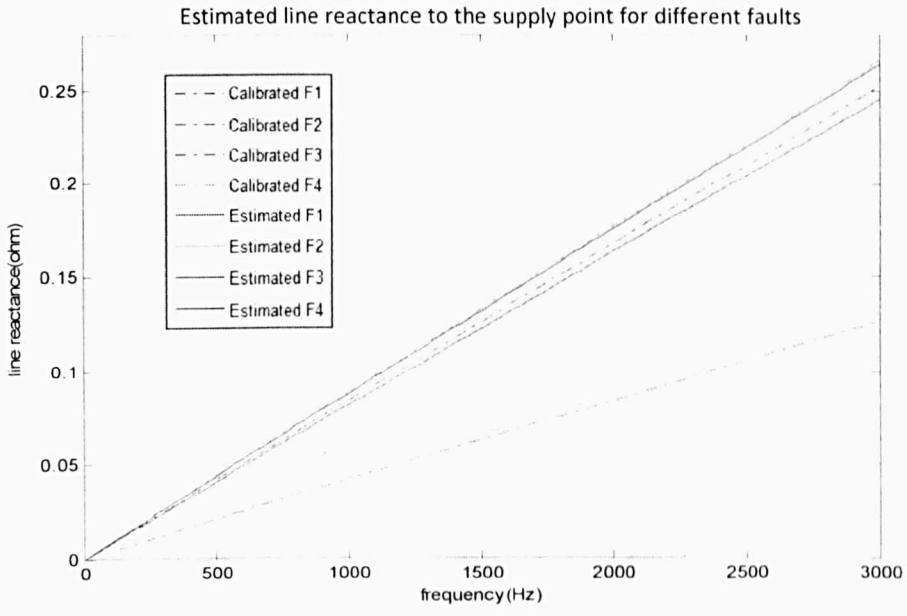

Figure 4.17 Fault location results for faults with 3Ω fault resistance

As shown in Figure 4.17, in DC, errors in the estimated results increase when a 3Ω short circuit fault is added into the system. Although there are larger errors compared with the results in Figure 4.16 due to a larger fault resistance, it is still possible to distinguish the 1m distance in faults and the errors are small for all fault locations (in table 4.7).

	F1	F2	F3	F4
Estimated results (μH)	0.03	6.45	12.63	13.32
Calibrated results (μH)	0	6.29	12.72	13.36
error%	0.22	1.20	0.67	0.30

Table 4.7 Estimation errors for 3 Ω faults

4.3.2 Step fault results

The proposed double-ended algorithm has been shown to be more robust than the single-ended method with regard to bouncing faults and higher fault resistances. The proposed modified method will work in a step fault situation as well.

By applying the same fault unit with the IGBT switch used in chapter 3, for a short circuit fault with 1Ω fault resistance, the measured fault voltages and currents from both ends are as shown in Figure 4.18.

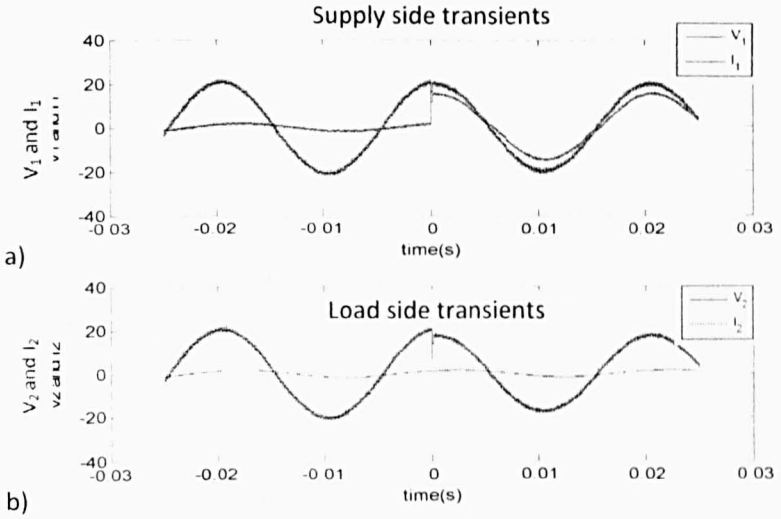

Figure 4.18 Measured voltage and current step transient at both ends

a) Supply side voltage and current b) Load side voltage and current

Compared with results derived from the bouncing fault transient, the fault transients created by an IGBT switch is just a step waveform as shown in Figure 4.18. This hard fault transient can also create useful information up to 3kHz. The estimated fault location of 4 different fault positions with 1Ω and 3Ω fault resistances are presented in Figure 4.19.

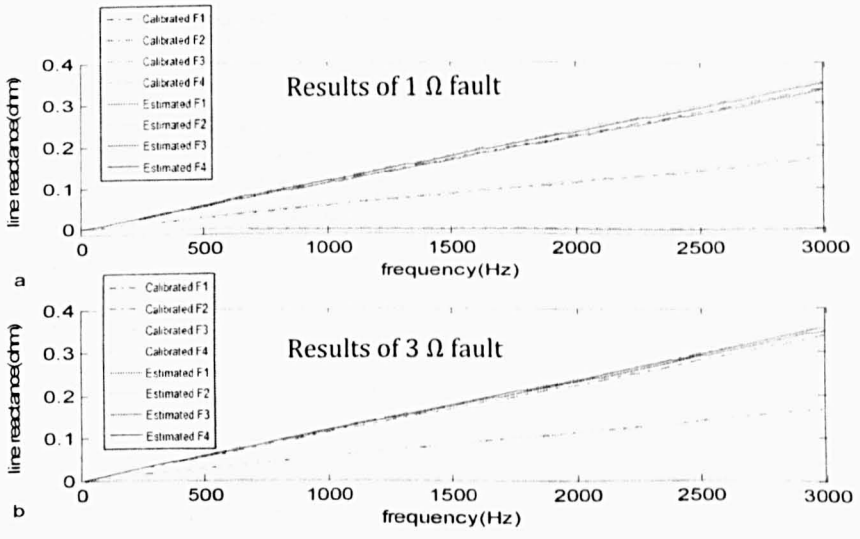

Figure 4.19 Estimated results of step faults

b) The results of 1Ω fault b) The result of 3Ω fault

As expected, the fault location results in Figure 4.19 are accurate and the estimation errors increase with fault resistance as well (in Table 4.8 and 4.9).

	F1	F2	F3	F4
Estimated results (μH)	-0.21	8.59	16.82	17.02
Calibrated results (μH)	0	8.43	16.92	17.16
error%	1.22	0.93	0.58	0.82

Table 4.8 Estimation errors for 1 Ω faults

	F1	F2	F3	F4
Estimated results (μH)	0.04	8.28	17.12	17.66
Calibrated results (μH)	0	8.43	16.92	17.16
error%	0.23	0.87	1.17	2.91

Table 4.9 Estimation errors for 3 Ω faults

The discussed double-ended algorithm also works with a step fault in the DC state. This time the supply voltage is replace by stand alone DC voltage (the 60/50 H series DC voltage supply introduced in Section 3.31) which has a higher current limitation to create a larger fault transient. The supply voltage is increased to 39V DC and the data being processed by FFT is also of a 4ms length in time domain. When Fault 4 (as in Figure 4.10) occurs, the results of the calculated line reactance compared with the calibrated value are shown in Figure 4.20

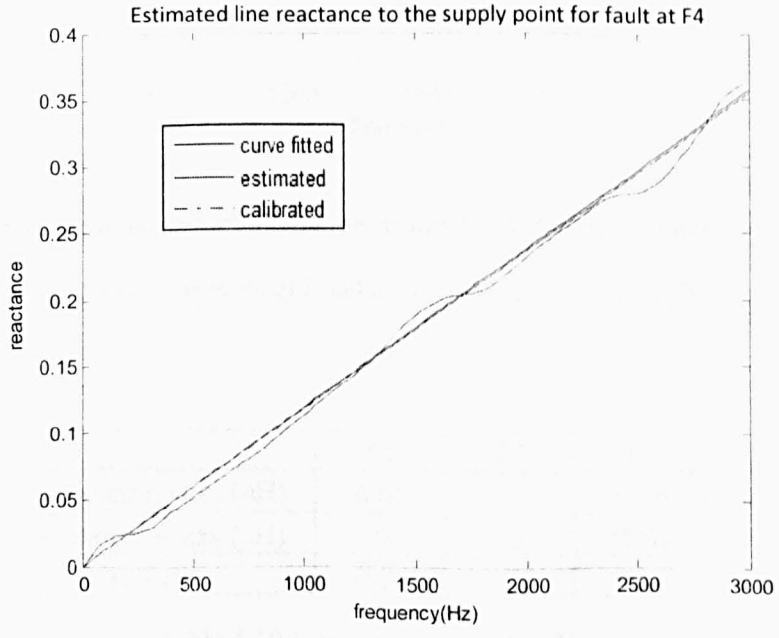

Figure 4.20 Fault location results with high DC voltage supply

Compared with results in Figure 4.13, it is clear that the original calculated results (green line) have much less oscillation than results produced by low voltage level transient. This is the same tend as seen for the single-end algorithm, the double-end method is expected to provide a better fault location results when utilized in a real distribution system with high system voltage level.

The results of measured current and voltage and line reactance of four different fault locations with high DC voltage supply are shown in Figure 4.21 and Table 4.10.

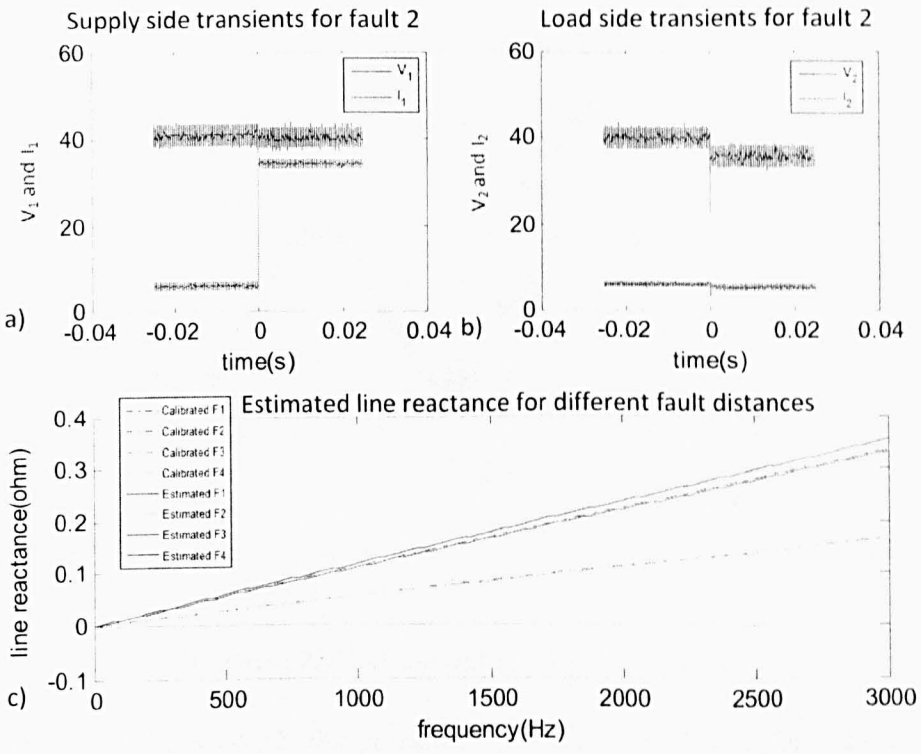

Figure 4.21 Line reactance calculation results for different fault position in 40V DC

a) Supply side transients b) Load side transients c) Fault location results

	F1	F2	F3	F4
Estimated results (μH)	0.01	8.39	17.01	17.21
Calibrated results (μH)	0	8.43	16.92	17.16
error%	0.06	0.23	0.52	0.29

Table 4.10 Estimation errors for DC faults

Higher voltage offers higher SNR to provide the better results shown in Figure 4.21, and compared with results achieved by using lower level voltage supply shown in Figure 4.14.

4.3.3 Results with non-linear load

Considering the application of a real IPS which may have loads with power electronic converters, tests are carried out with a non-liner load added to the system. The distorted fault current waveforms, including transients, measured at both measurement points are shown in Figure 4.22

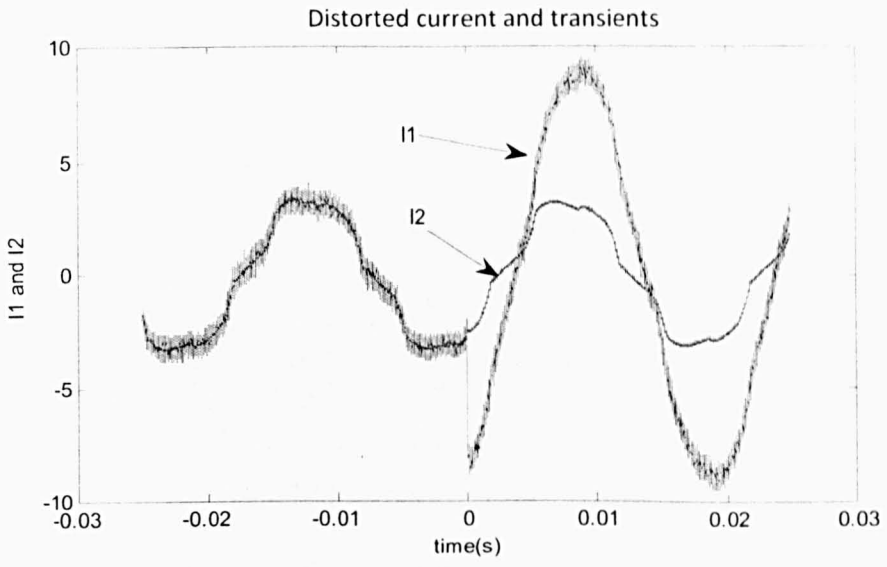

Figure 4.22 Fault current measured at both ends

As shown in Figure 4.22, the current distortion is much smaller than the fault transient for the data measured. The errors within the estimated results (in table 4.11) are larger than errors derived from linear load test. Fault within 1m distance can still be distinguished. The data can be pre-processed by a low-pass filter and with a short data segment (4m after fault which contain less distorted current waveforms), the results are shown in Figure 4.23 and Table 4.11.

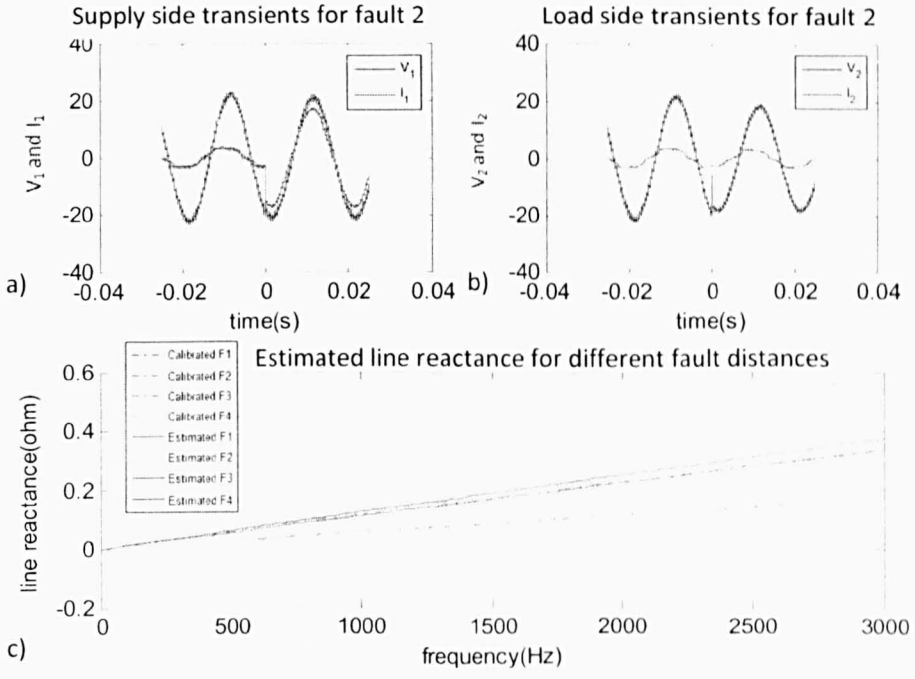

Figure 4.23 Fault location results for non-linear load

a) Supply side transients b) Load side transients c) Fault location results

	F1	F2	F3	F4
Estimated results (μH)	0.09	8.34	17.01	17.20
Calibrated results (μH)	0	8.43	16.92	17.16
error%	0.52	0.52	0.52	0.23

Table 4.11 Estimation errors for step faults

Compared with Figure 4.14 and the demonstrated difference with the single-ended estimated results between linear and non-linear load, the results in Figure 4.23 achieved by the double–ended method are less influenced by the current distortion created by the non-linear load. This will be further proved in the simulation part in chapter 5.

4.4 Comparison with tradition double-ended scheme

The traditional double-ended fault location scheme as described in [84] which uses synchronised post fault voltage and current information is simulated using Matlab/Simulink. The test system has the same parameters as the calibrated experimental system.

This algorithm uses post fault synchronized double-ended voltages and currents as V_1, I_1, V_2, I_2 in Figure 4.24 measured at system frequency (50Hz).

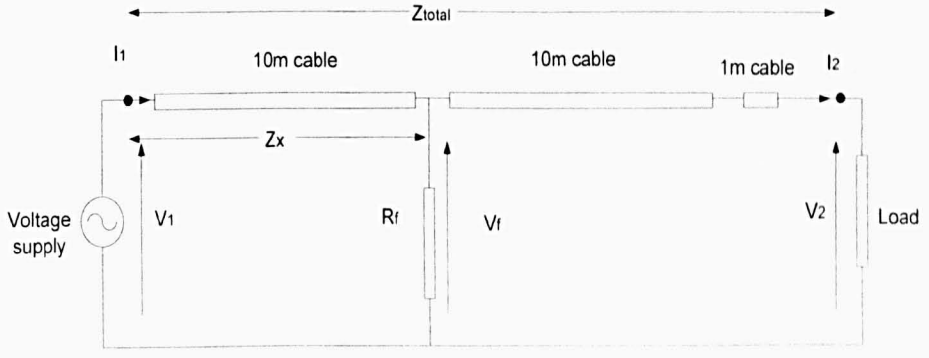

Figure 4.24 The circuit for post-fault system demonstration

The fault location can be estimated by calculating the line impedance between measuring point and fault point (Z_x) divide by value of impedance per m.

$$V_f = V_1 - Z_x I_1 \tag{4.10}$$

$$V_f = V_2 + I_2(Z_{total} - Z_x) \tag{4.11}$$

The value of Z_x can be derived by substituting (4.13) and (4.1)

$$Z_x = \frac{V_1 - V_2 - I_2 Z_{total}}{I_1 - I_2} \tag{4.12}$$

The calculated resistance (Rx) and reactance (Xx) for four different fault positions as shown in Figure 4.10 are shown in Figure 4.25

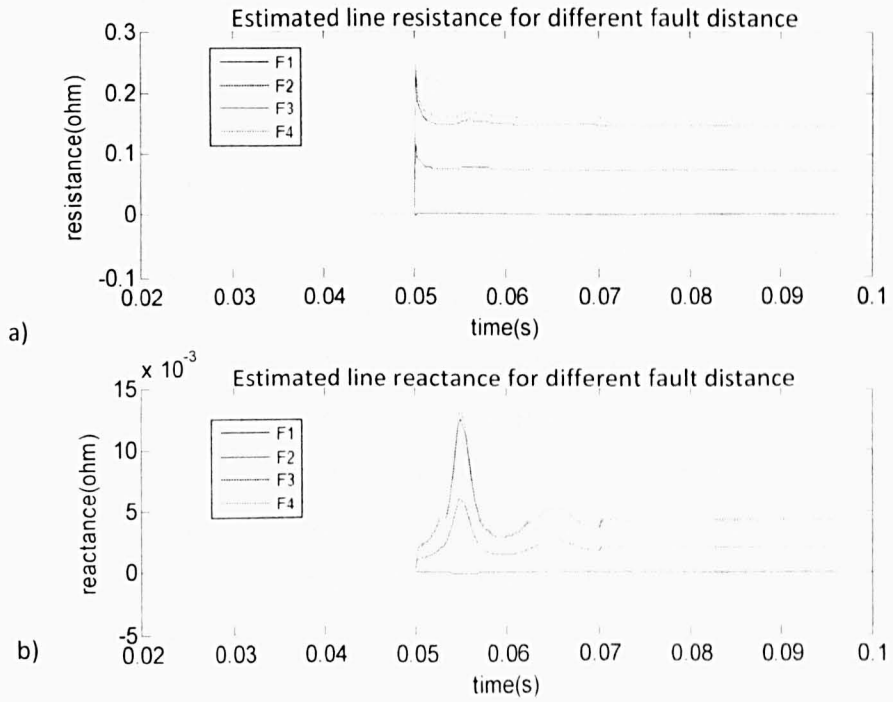

Figure 4.25 Results of traditional double-ended fault location

a) The resistance results b) The reactance results

In Figure 4.25, the fault occurs at 0.05s and the pre-fault data was set to zero because during healthy state both the numerator and denominator are zero in equation (4.12). The value of the reactance can not be used to distinguish fault location, because it is too small at 50Hz, for a very short distribution line (20m). This method is normally used in transmission system where the line inductance is significant compared with distribution system. Only the resistance results are able to provide the fault locations after 1 cycle (20ms) of fault transient using the FFT. The time data used is 5 times more than the proposed double-ended method presented in this chapter. The simulated double-end fault location scheme requires synchronization of the information measured at both ends. This is commonly realized by GPS in a distribution network which results in more investment. For an IPS system which may have a small synchronization error caused by delay of signal transmission or the errors of the current and voltage transducer, the synchronization angle can be calculated and involved in the final line reactance estimation. This data will be introduced in the simulations in chapter 5.

4.5 Summary

A new double-ended fault algorithm for fault location in IPS is presented in this chapter. This method can be easily applied to fault location using an on-line analysis because of its short computational time, straight forward algorithm and robustness to different fault situations. This chapter focused on validating of the method using an experimental system. The experimental tests involve both AC and DC state situations and the faults imposed on the distribution cable are classified by step faults (hard faults) and oscillation faults (bouncing faults). During the test, in order to simulate a situation more similar to a real IPS system a non-linear load is added and a common synchronized double-ended fault location method is introduced as a contrast to the presented scheme.

The approach has been demonstrated on a small cable based IPS system. However, it is totally general and could be applied to overhead lines and transmission systems. The accuracy and range of the validity on a transmission system will form part of future work.

Chapter 5

Simulation verification

5.1 Introduction

In Chapter 3 and Chapter 4 the single-ended and the double-ended fault location method were demonstrated by using a simple cable based laboratory model. This chapter investigates the presented algorithms using computer simulations with the same system parameters as the calibrated experimental system.

The simulations for both algorithms explore the fault situations that can not be experimentally implemented due to the limitation of the laboratory equipment, such as very high current faults (low fault impedance), faults with a high supply voltage and faults with a small high frequency transient (faults which occur at or close to the voltage zero-crossing point). The possibilities of un-synchronized measurement for the double-ended method and fault location using circuit breaker reclosing transients are also investigated.

5.2 Simulation of the experimental system

5.2.1 Simulation of the single-ended method

The cable system has been simulated with lumped resistors and inductors, as shown in Figure 5.1, using the Matlab/simulink. Each segment of the cable (including the neutral cable section which is used as the return path) is represented with the same parameters calibrated from the experimental system, shown in Chapter 3. Phase to phase and phase to earth faults are imposed on the cable at four separate locations (0m, 10m, 20m and 21m to the voltage source).

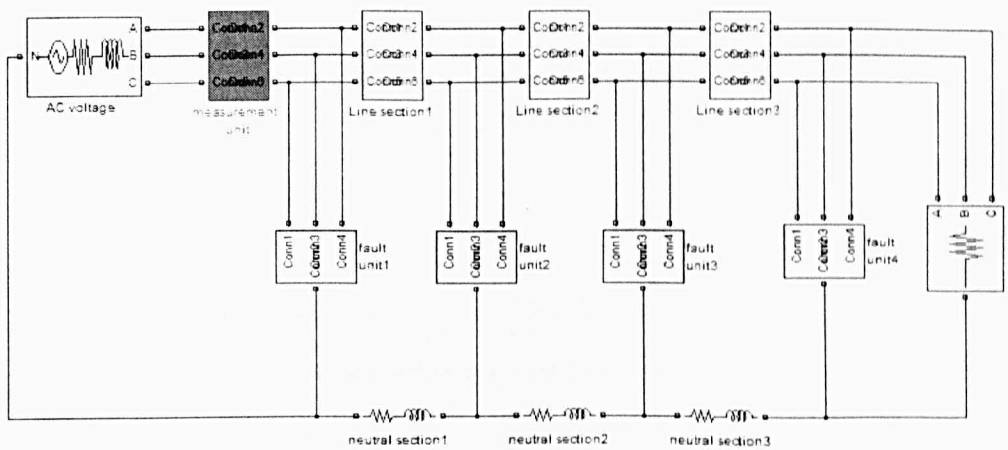

Figure 5.1 Simulation demonstration system for single-end fault location

The measured voltage and current data during experimental testing should be the same as for the results simulated when the two systems have the same parameters. Even the phase and amplitude of fault transients in simulation should match the experimental results once the phase angle of the supply voltage is matched. Figure 5.2 shows the measured voltage and current for both the experimental and simulated systems when a phase to phase 1Ω fault is imposed at the end of line section1. The data is sampled (for processing) with the same sampling frequency (1MHz) and the 8bit analogue to digital converter (ADC) of the experimental system was represented using a quantization block.

a)

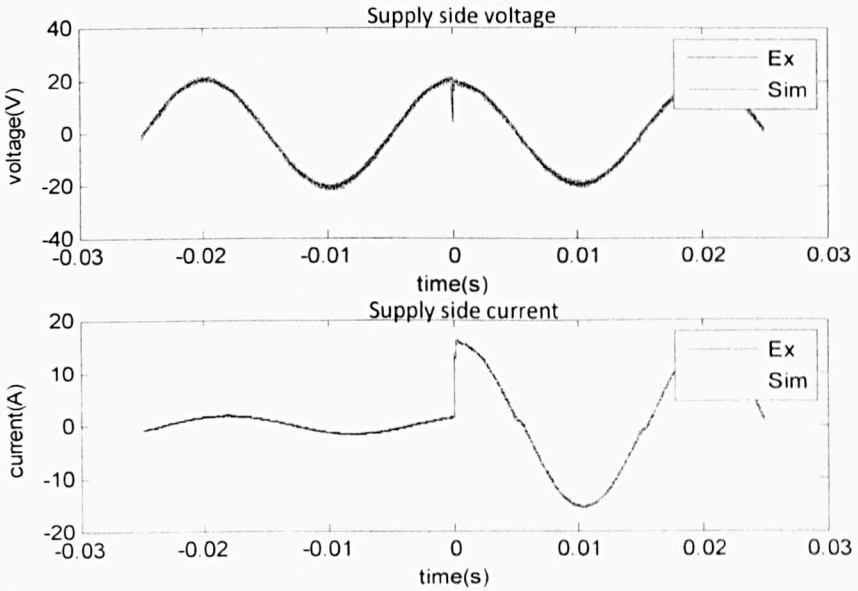

b)

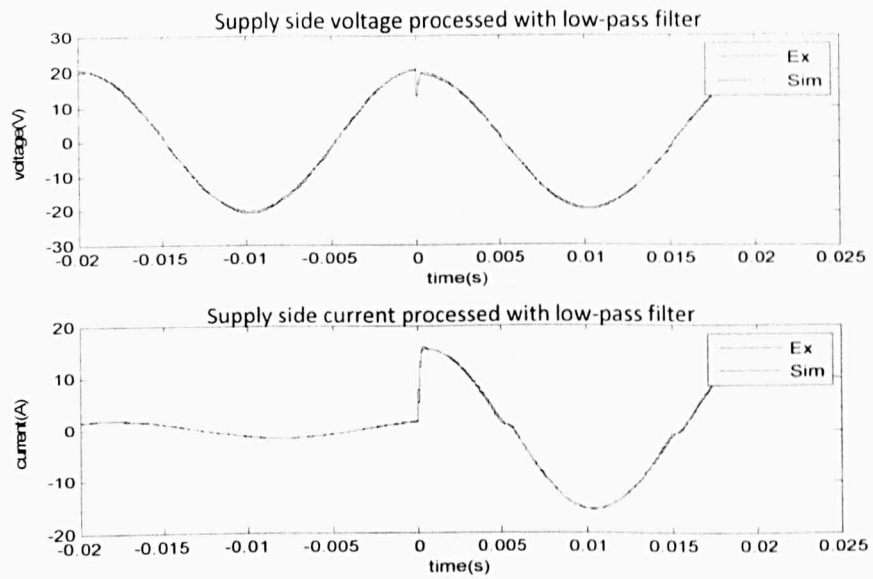

Figure 5.2 Voltage and current measured from simulation and experiment

a) Data without filtering b) Data with a low-pass filter

In Figure 5.2 a) and b) the data is shown before and after being processed with a low-pass filter with a cut-off frequency of 4kHz. The simulated voltage and current match the experimental test results for both the steady state and the fault transient situation. The time axis is derived from the experimental measurement in which faults were set at 0s as shown in the previous chapters. The chosen IGBT block from Matlab/Simulink acts as ideal switch with snubber resistance and capacitance. The turnoff characteristic of the IGBT

model is approximated by two segments. When the gate signal falls to 0, the collector current decreases from Imax to 0.1 Imax during the fall time (T_f), and then from 0.1 Imax to 0 during the tail time (T_t)[151]. T_f and T_t are used according to the data sheet [152] IGBT adopted in the experiment, the simulation voltage and current waveforms have the same discontinuity at the zero-crossing area as the results from the experimental system.

For the single-ended fault location method, the line reactance between the measurement point and the fault position is calculated using (3.10)-(3.12) with the same length of measured data segment employed in the experimental system. Figure 5.3 shows the measured voltage and current transients, the created step voltage and the estimated line reactance for a 1Ω fault imposed at the end of section 1 as shown in Figure 5.1.

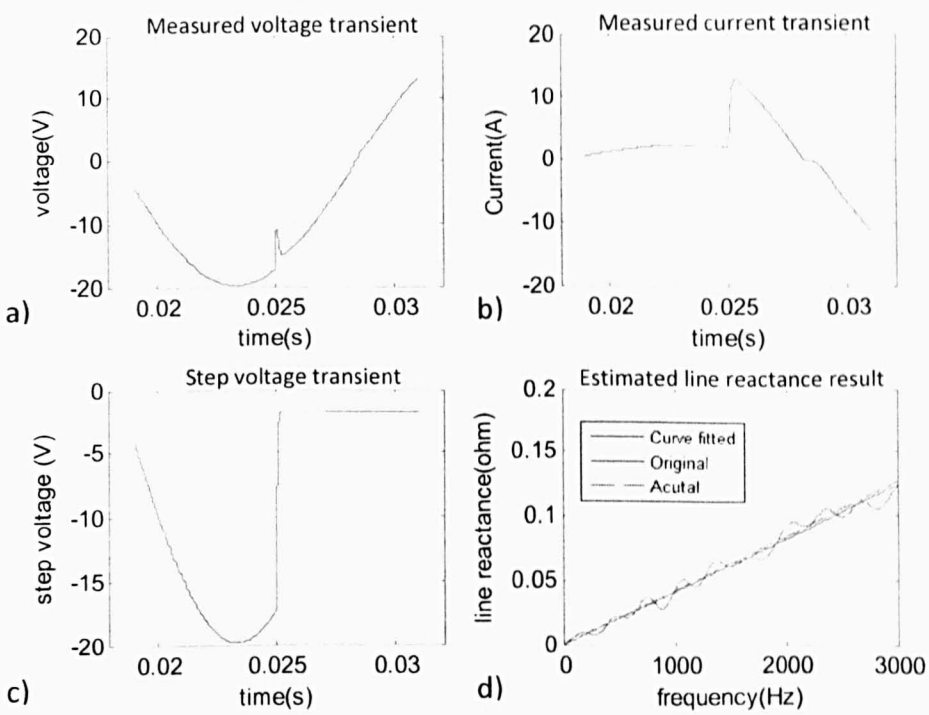

Figure 5.3 Processed data and the estimated results

a) Processed voltage b) Processed current c) Step voltage d) Estimated line reactance

As shown in a), b) and c) of Figure 5.3, the total length of data being processed, from the simulation is 12ms which is 6ms of post fault data. In d) of Figure 5.3, after a linear least squares curve fitting (solid blue line), the oscillation in the

original estimated result (solid green line) is reduced (solid blue line) and matches with the actual simulation value (dashed red line) with only 4% error. In the simulated system with ideal system components the only distortion which has influence on the fault transients is due to the post-fault voltage and current discontinuity at the zero-crossing point caused by the IGBT switch (as shown at 0.027s in the a) and b) of the Figure 5.3). The influence of the discontinuity caused by the IGBT can be demonstrated by setting the segment of the measured current in simulation such that if does not contain a post fault zero-crossing time for the same fault location as in Figure 5.3. This is realized by changing the phase angle of the supply voltage to a pre-determined value when the fault is imposed at the fixed time as shown in Figure 5.4. (or changing the fault inception angle which is same as changing the time of fault).

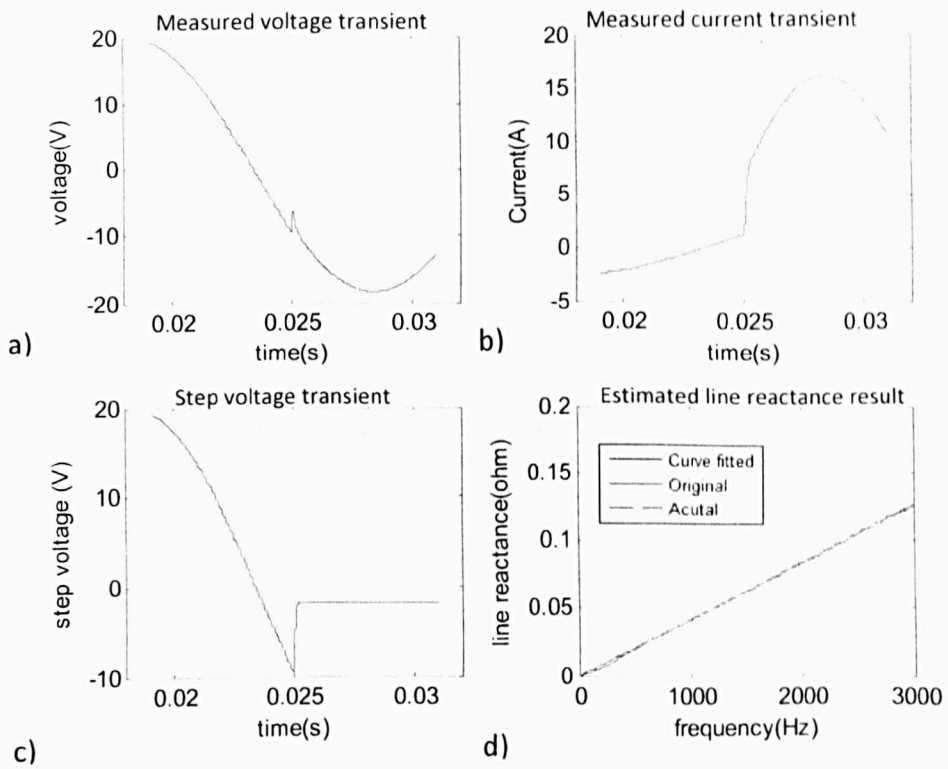

Figure 5.4 Results for no post-fault zero-crossing in the current

a) Processed voltage b) Processed current c) Step voltage d) Estimated line reactance

In Figure 5.4, for the same fault location and fault resistance as shown in Figure 5.3, when there is no distortion in the estimated data because there is no current zero-crossing waveforms in the measured information as presented in a)

and b). The original estimated reactance in d) has a smaller oscillating error compared with the results from Figure 5.3 for the same fault location. The result after being processed with curve fitting has little difference to the original estimated value which means that the original value without any curve fitting provides a good fault position. Curve fitting is needed due to the fact that distortion within the system is unavoidable and the fault inception angle is random for the real-time application. The fault transients generated in the situation of common short circuit fault with low fault resistance and high supply voltage in a real system offers higher SNR which also leads to a smoother original estimated waveform (less error after curve fitting). These situations will be discussed later in this chapter.

Figure 5.5 shows the simulated estimated line reactance results of phase to phase and phase to ground faults which are imposed at 4 different positions on the distribution line (shown in Figure 5.1) with a 1Ω fault resistance

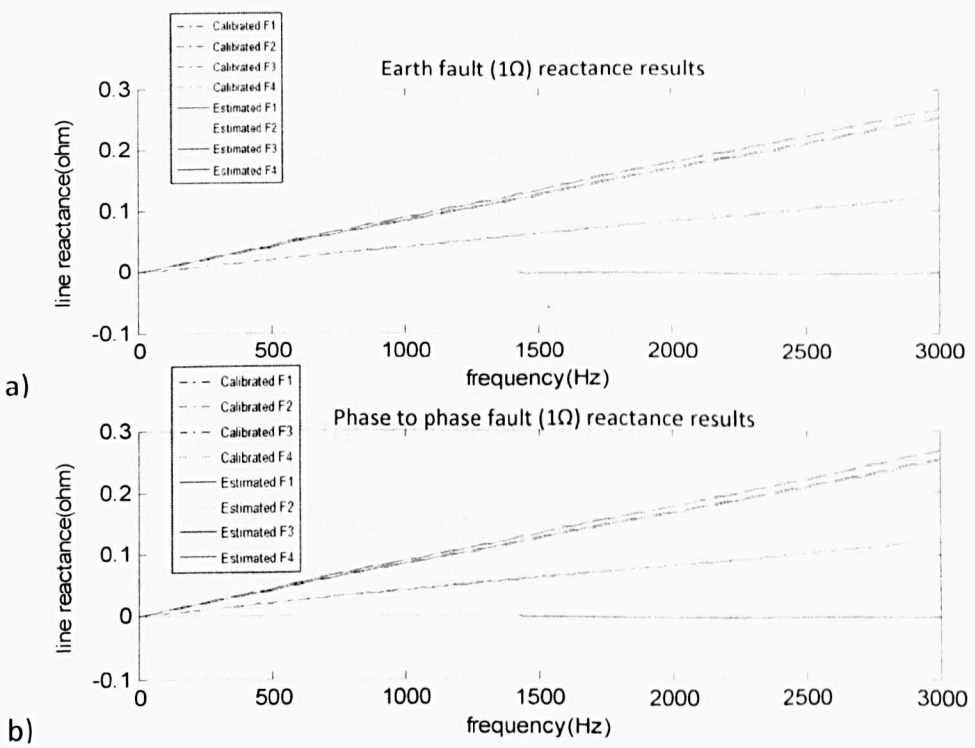

Figure 5.5 Line reactance results of different fault locations

a) Ground fault results b) Phase to phase fault results

	F1	F2	F3	F4
Estimated results (μH)	0.03	6.25	12.63	13.32
Calibrated results (μH)	0	6.29	12.72	13.36
error%	0.22	0.30	0.67	0.30

Table 5.1 Estimation errors for step switching ground faults

	F1	F2	F3	F4
Estimated results (μH)	0.03	6.25	12.63	13.32
Calibrated results (μH)	0	6.29	12.72	13.36
error%	0.22	0.30	0.67	0.30

Table 5.2 Estimation errors for step switching phase faults

Because of the reduced influence of noise from voltage source, data acquisition units and environmental electromagnetic interference (EMI), for the same fault situations, the simulation results offer more accuracy than the experimental test results which were presented in chapter 3. In simulation results the largest error for all the fault locations is 0.3 m (0.67% as shown in Table 5.1 and Table 5.2) in distance. In simulation, the two set of test has exact the same line impedance between fault and the measurement point and the fault impedance. The only difference is that the fault inception angle slightly varies. This small variation does not influence the estimated results when the fault inception angle is not close to zero.

5.2.2 Simulation of the double-ended method

The double-ended fault location simulation system requires another set of measurements at the load side as shown in Figure 5.6.

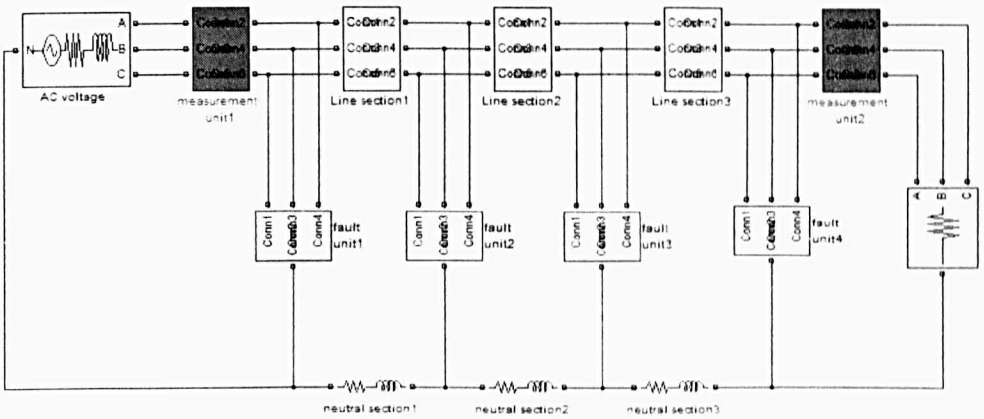

Figure 5.6 Double-ended fault location simulation system

Faults are applied with the same fault inception angle as in the experimental system. The measured simulation data at both ends matches with the experimental data (filtered with a low-pass filter) as shown in Figure 5.7.

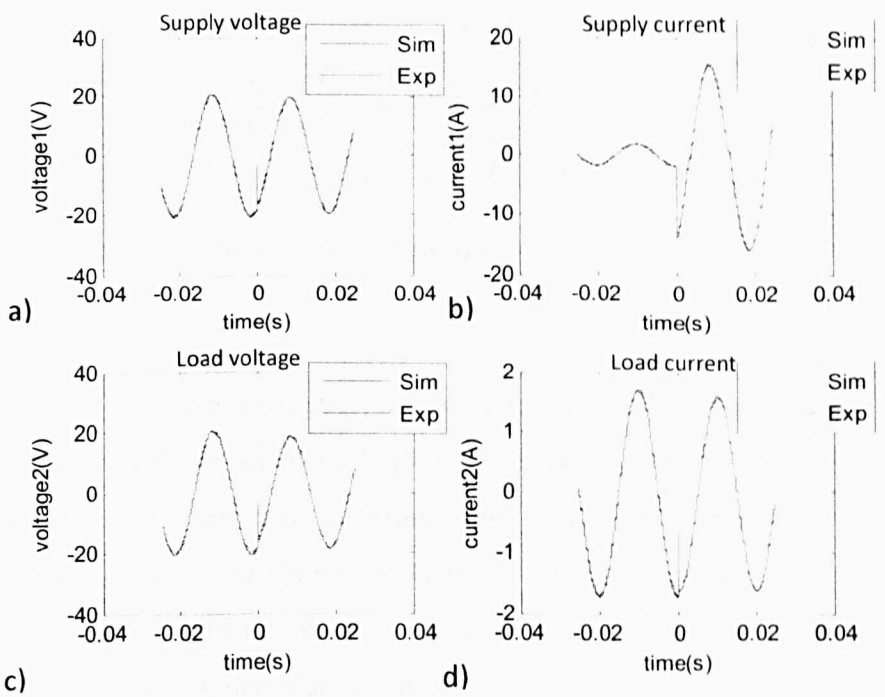

Figure 5.7 Measured simulation data compared with the experimental data

a) Supply voltage b) Supply current c) Load voltage d) Load current

Figure 5.8 shows the estimated line reactance compared with the actual value used for different fault positions, using a 1Ω fault resistance. The double-end

scheme offers good accuracy (as shown in Table 5.3) for the fault location results using the 12ms data set (6ms after fault) shown in Figure 5.7.

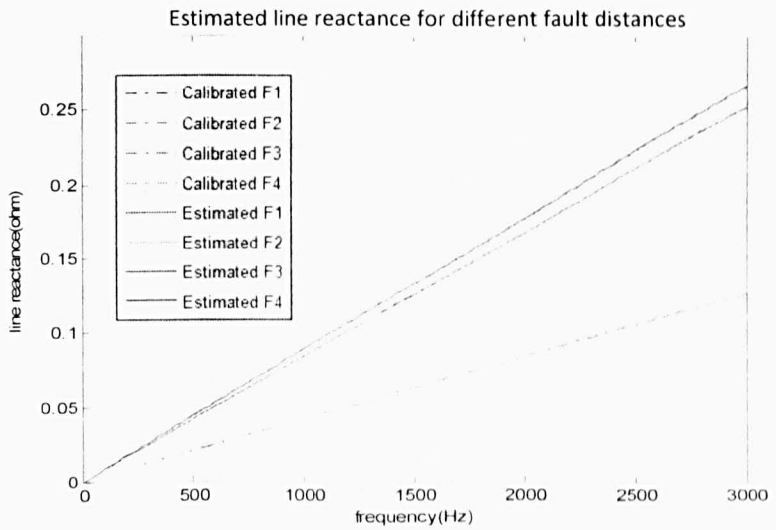

Figure 5.8 Double-ended simulation fault location results

	F1	F2	F3	F4
Estimated results (μH)	0.02	6.27	12.70	13.34
Calibrated results (μH)	0	6.29	12.72	13.36
error%	0.15	0.15	0.15	0.15

Table 5.3 Estimation errors for the double-ended fault location scheme

Figure 5.9 shows the simulation results with different fault resistance. Similar to the test with the experimental system, the accuracy of the simulation results is influenced by the fault resistance and becomes worse when the fault resistance increases (as shown in Table 5.4 and 5.5). Also, because there is little noise in the simulation, the simulation results offer similar results as the experimental test but better accuracy.

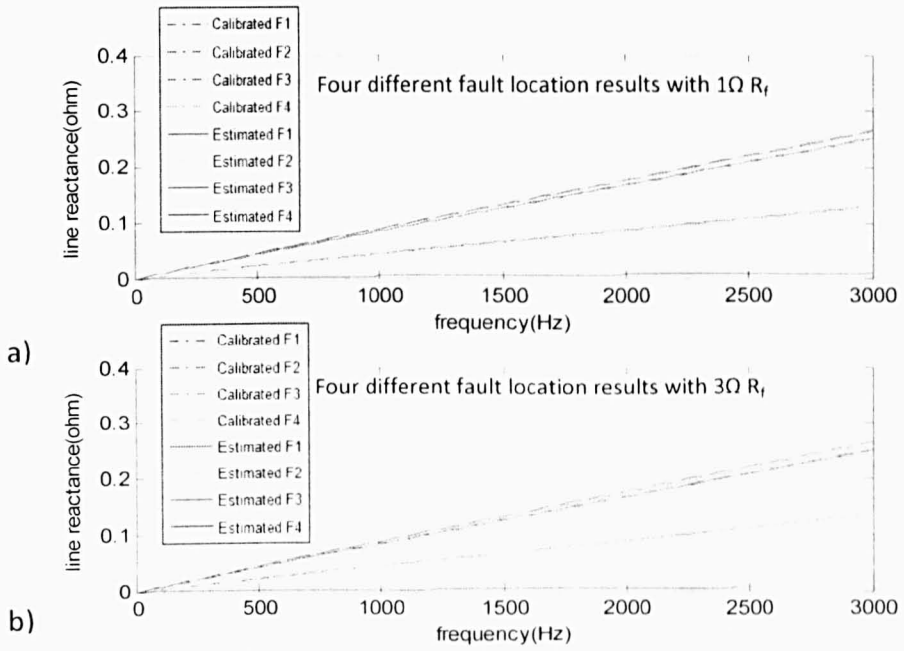

Figure 5.9 Estimated line reactance for different fault positions with different fault resistance (R_f)

a) Results when R_f=3Ω b) Results when R_f=5Ω

	F1	F2	F3	F4
Estimated results (μH)	0.02	6.25	12.63	13.32
Calibrated results (μH)	0	6.29	12.72	13.36
error%	0.15	0.30	0.67	0.30

Table 5.4 Estimation errors for double-ended scheme 3Ω fault

	F1	F2	F3	F4
Estimated results (μH)	0.03	6.21	12.63	13.30
Calibrated results (μH)	0	6.29	12.72	13.36
error%	0.22	0.60	0.67	0.45

Table 5.5 Estimation errors for double-ended scheme 5Ω fault

5.3 Extension of simulation work

The simulation work involves using the experimental parameters not only confirms the results of the experimental test but more importantly demonstrates that the difference between real time test results and the simulation results in the frequency range of interest (below 3kHz) is small. The

simulation has a slightly better accuracy because the noise caused by voltage source, data measurements and EMI is not included in the simulation. With the confidence that only a predictable small difference exists between the two situations, further simulations can expand the rage of scenarios to evaluate the situations that are not possible to test on the experimental system.

5.3.1 Low fault resistance

Normally during a short circuit fault situation, the system voltage collapses and the system current increases abruptly to a value that is far more than system components can tolerate. The fault current produces considerable thermal and mechanical stresses in electrical distribution equipment. Faults are seldom solid and involve varying amounts of resistance. In the studies of faults and protection relaying, the connection between phases or ground involves a very low and in general negligible impedance [115].

The smallest fault resistance used in the experimental test, limited by the equipment current level, was 1Ω. Compared with the 6.8Ω load resistance, the fault situation created is more like a load being added than a typical short circuit fault. The following simulation results presents faults with resistance varying from 0Ω to 1Ω for both proposed fault location methods.

5.3.1.1 Single-ended fault locations

As mentioned before for equation (3.3)-(3.5) of Chapter 3, the single-ended fault location scheme uses a voltage iteration algorithm to eliminate the error caused by the voltage drop between the pre-fault voltage at the measurement point and the pre-fault voltage at the fault position. In the later experimental test part of chapter 3, the estimated results are influenced by the large fault resistance, so that, as presented in equation (3.10)-(3.12), a resistance iteration is adopted to eradicate the calculation error. Overall, the single-ended scheme uses six equations. Equation (3.11) is used to estimated the value of fault

resistance and determine whether a resistance iteration or a voltage iteration is going to be used for the fault location process. If the fault resistance is comparable to the load impedance value the resistance iteration is employed otherwise the voltage iteration is used.

For example, when phase to phase short circuited faults which have fault resistance varying from 0Ω to1Ω are imposed at the end of the cable, the largest errors appear when R_f=0.4Ω which is the critical value at which voltage iteration is replaced by resistance iteration as shown in Figure 5.10

a)

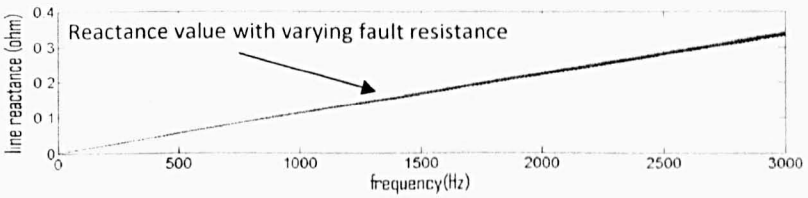

b)

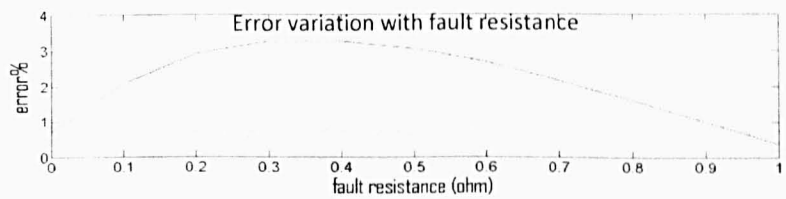

Figure 5.10 Single-ended results for different fault resistances

a) Values for reactance of various fault resistance b) Errors for each fault resistance

Figure 5.10 a) shows the calculated reactance values against frequency as it changes with the fault resistance. Figure 5.10 b) shows the error in percentage according to the actual value used. The resistance iteration starts when R_f=0.4Ω where the estimation results have the largest error. According to the load level, fault resistance level and the accuracy requirement, the resistance iteration starts at different R_f values for different systems and this has to be studied. Normally the fault impedance is much smaller than the load impedance in an IPS, so that only the voltage iteration is required. (such as the single-end method for the protection of a marine power system which will be discussed in chapter 6). The resistance iteration is investigated mainly due to the limitation of the experimental components. The estimated fault distance result for each fault resistance is shown in Table 5.6.

Fault resistance(Ω)	0	0.1	0.2	0.3	0.4	0.5	0.6	0.7	0.8	0.9	1
Estimated(m)	21.18	21.464	21.596	21.641	21.645	21.617	21.573	21.452	21.328	21.254	21.088
Errors%	0.85	2.21	2.84	3.05	3.07	2.94	2.73	2.15	1.56	1.21	0.42

Table 5.6 The detail estimation results for each fault resistance

5.3.1.2 Double-ended fault location

The double-ended scheme has a simple algorithm which involves only equation (4.2) if not considering the equations which are used for calculating the synchronization angle between the measured data from two ends (in case of un-synchronized measurements). Values of fault resistance do not need to be considered in the double-ended method, as long as there are fault transients. The results when faults are added at the end of line section 1 with the same range of fault resistance as in single-ended situation are presented in Figure 5.11

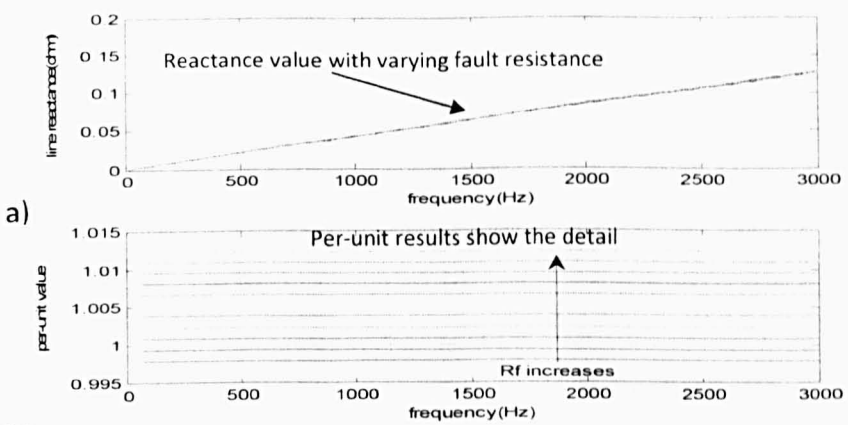

Figure 5.11 Double-ended results with different fault resistance

a) Result of reactance b) Per-unit value of each estimation

Figure 5.11 a) shows almost the same reactance results against frequency for different fault resistances. In Figure 5.11b), the values are nomalized by dividing each estimating result with the actual value used. The precision of the estimated results decreases a little bit when R_f rises due to the smaller SNR for the high fault impedance transients. However, the errors are very small and fixed compared with the results from the single-ended method.

5.3.2 Simulations with a high voltage level

The proposed methods both involve using fault transients for fault location. For a certain fault resistance and certain fault distance, a system with higher voltage level is more likely to produce larger fault transients during short-circuit fault situations. As mentioned in Figure 5.3, with a phase to phase 20V (peak) voltage supply, the current discontinuity at a zero-crossing time caused by the characteristics of the IGBT results in oscillations in the estimated line reactance value. Although, after processing with linear least squares curve fitting, this influence is minimised, it still leads to an error in the fault distance calculated. However, in a system with a higher voltage supply level (550V phase to phase peak) the results without curve fitting are good enough to predict the fault positions as shown in Figure 5.12

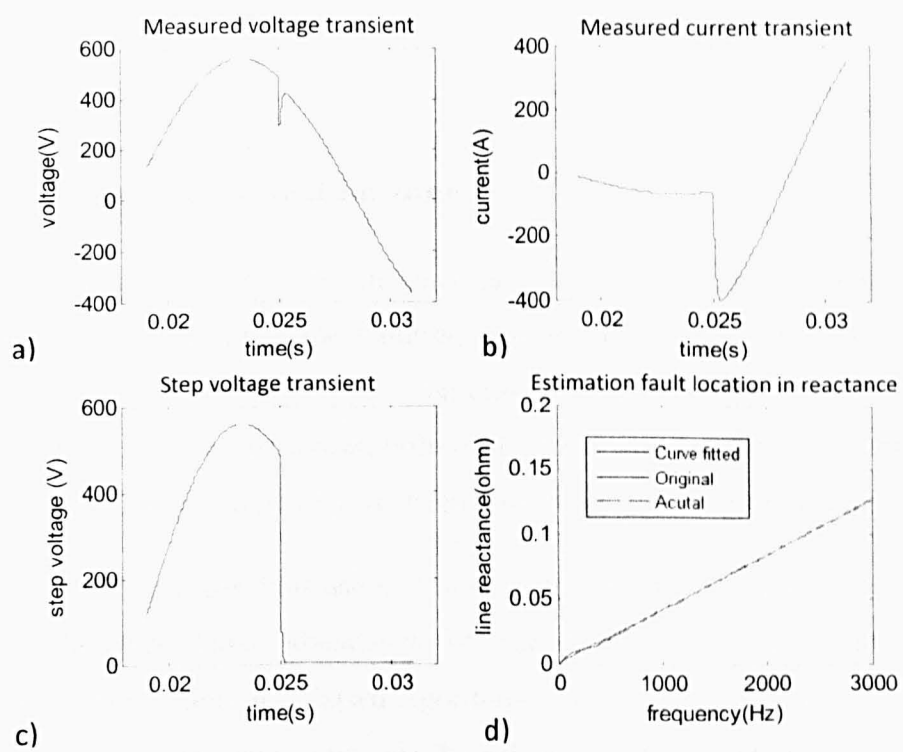

Figure 5.12 Results with high supply voltage

a) Processed voltage b) Processed current c) Step voltage d) Estimated line reactance

The voltage level for a normal terrestrial distribution system ranges from several kV to around 100kV. For More Electric Marines (MEMs) with an Integrated Power System (IPS), for example, in a common aircraft system the

voltage level is about 115V AC at 400 Hz [2] and in marine system it is between several hundred volts to several kV[1][2]. Short circuit faults within these systems normally create large transients which contain enough information in the frequency domain to offer an accurate fault location. As shown in a) and b) of Figure 5.12, in the measured voltage and current waveforms for the single-ended method, the discontinuity at zero-crossing area is negligible compared with the bigger fault transients. In d), the difference between the original and the fitted results is small and that means the original results have a good accuracy and can be directly used to predict the fault locations.

The estimation accuracy is also improved for fault location using the double-ended scheme in the system with a high supply voltage because the double-ended algorithm offers better results than the single-ended method for the same fault situation.

5.3.3 The "non-Location zone"

Fault location methods for distance protection schemes have been modified and improved to meet the requirements of the rapidly developing electrical industry. Such methods as based on impedance calculation, travelling wave or intelligent systems have been utilized in power systems for many years. Their reliability and practicability has been proved for real time application.

The proposed algorithms use fault transients to estimate the fault positions and the therefore have advantages of speed and accuracy compared with conventional impedance based algorithms. However, for a fault without a fault transient, the presented methods do not work. This situation is not common and only exists in an AC power system when a fault occurs at the system voltage zero-crossing time (fault inception angle equal to or very close to zero). The condition in which the fault location estimation is not accurate due to the fault transient occurring with a very low SNR is called the non-location zone here. In the experimental system, faults are imposed on the cable randomly, so that it is almost impossible to find a fault with no transient. In other words,

although the non-location zone transient exists, its probability is very small. This non-location zone is therefore demonstrated by simulation results.

For the single-ended fault location scheme, the non-location zone can be examined by imposed a short circuit fault at fixed position of the cable, for example at the end of line section 2 in Figure 5.1, at a fixed time, and varying the phase angle (θ) of the supply voltage from 0° to 180° (this is the same as changing the fault inception angle). Estimated results of line reactance against frequency for each θ are given in Figure 5.13.

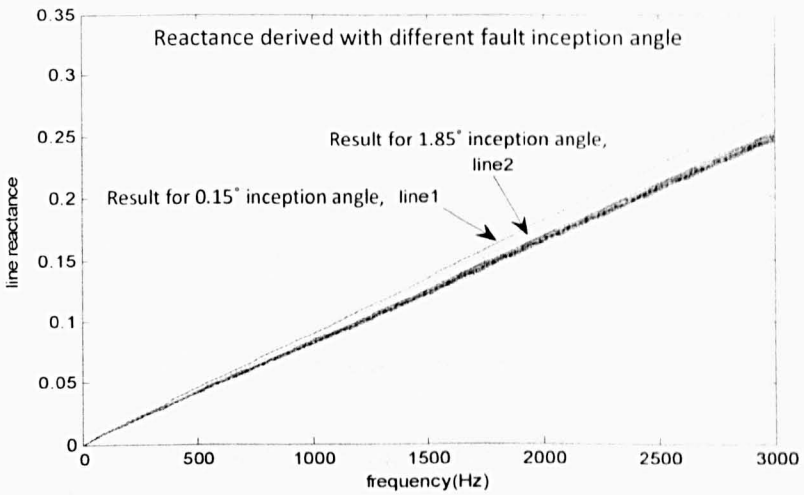

Figure 5.13 Results of short circuit fault at different fault inception angle

The tests were carried out using the simulation model with the same parameters derived from the experimental test system. The two lines: line1 and line2 in figure 5.13 depict the estimated line reactance results when faults are imposed on the cable at a fault inception angle of 0.15° and 1.85° to the zero-crossing angle (0°) of the system voltage waveform separately (fault inception angle equal to 0.15° and 1.85°). These results are derived from tests that increase the fault inception angle by 0.05° each time. When the fault inception angle is smaller than this two value, the high frequency fault transients is too weak to provide accurate impedance estimation. Compared with the actual reactance value between fault point and the measurement point (dashed line), the error of value presented in line1 and line 2 are over the 1m accuracy requirement (the errors in distance are 1.13m for line2 and 2.75m for line1). A fault occurring at a fault inception angle very close to 0° will provide worse

accuracy as the results given in line 1 have larger errors than line2. For the single-ended method, the non-location zone, referring to the fault inception angle, is ±2° (faults within this fault inception angle range produce errors larger than 1m due to very small SNR) to the voltage zero-crossing point as shown by the area between two dash lines in Figure 5.14.

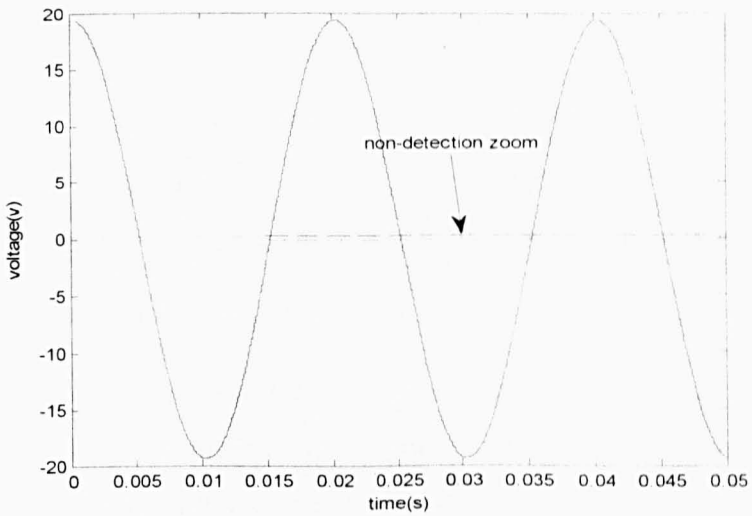

Figure 5.14 Non-location zone of single-ended method refer to system voltage

A fault in the non-location zone shown in Figure 5.14 occurs very rarely. However, it is more likely that the high voltages have a greater probability of inducing insulation failure and causing a fault which would lead to an even lower probability of the non-location zone occurs. The single-end algorithm has a bigger non-detection zone than the double-ended scheme. Because when a poor SNR occurs (i.e. a very small fault transient, and noise from the 8bit ADC), a method that involves iteration is more likely to produce errors in the results. For the same fault situation, the double-ended method offers a smaller non-location zone according to different fault inception angles as shown in Figure 5.15. The detail results within a inception angle of $\pm 5^{\circ}$ is shown in Table 5.6.

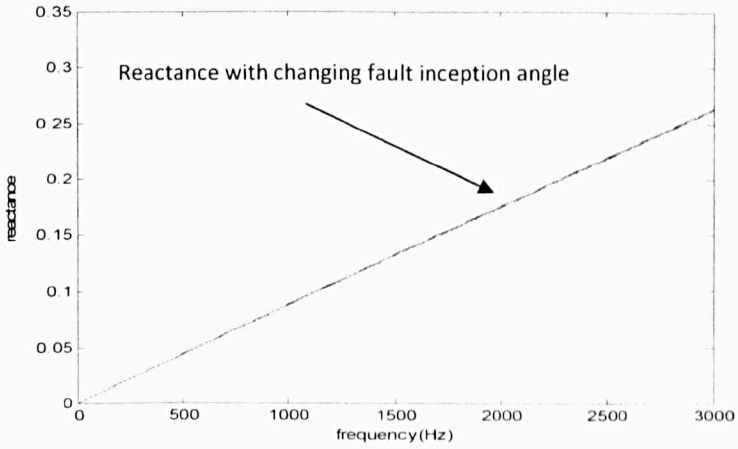

Figure 5.15 Double-ended results for a fault at different fault inception angle

inception angle (°)	-0.5	-0.4	-0.3	-0.2	-0.1	0	0.1	0.2	0.3	0.4	0.5
errors %	0.021	0.023	0.027	0.04	0.1	1	0.1	0.04	0.027	0.023	0.021

Table 5.7 Estimation errors for double-ended scheme 5Ω fault

In Figure 5.15 the results for each inception angle match and this is true even for the ones that have a small fault inception angles. The non-location zone for the double-ended algorithm in a system with a linear load is too small to be considered as shown in Table 5.7.

5.3.4 Influence of non-Linear load

As shown in chapter 3 and chapter 4, the non-linear load has little influence on the fault location accuracy because only a small segment of measured data and curve fitting are used in the calculation procedure. However, the existence of a non-linear load in the proposed system will influence the non-location zone for both proposed methods. The non-linear load which distorts the system voltage and current waveforms makes the transient for the same fault inception angle have a lower SNR, and this is especially true when the transients themselves are weak. When noise is present, the non-location zone for both proposed methods will be enlarged.

By using the same diode rectifier load as explored in the experimental system in chapter 3 and chapter 4, the non-location zone for the double-ended method in a noisy system with a non-linear load is discussed as follows:

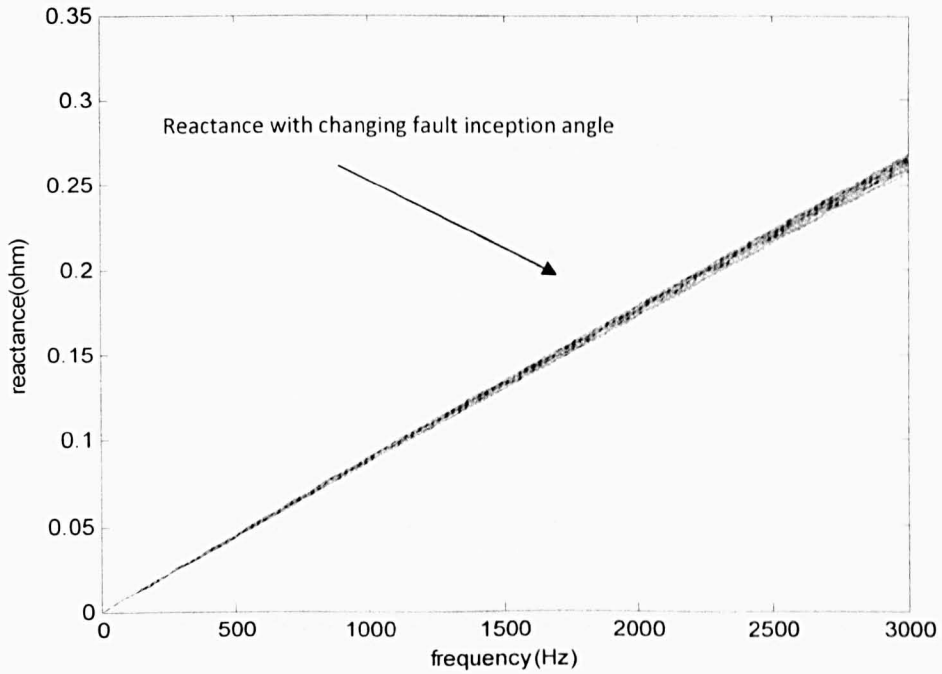

Figure 5.16 Results of double-ended scheme with non-linear load

For the double-ended fault location scheme, in a system with a non-linear load, the non-detection zone can not be neglected. Compared with Figure 5.15, the errors within the estimated results for a fault with fault inception angle close to zero in Figure 5.16 are more obvious. Referring to the voltage zero-crossing point, faults occurring at an inception angle of 0.95° have the largest error (5.1% and 1.075m in distance) as shown in Table 5.8.

Inception angle(°)	20	10	5	1	0.95	-0.95	-1	-5	-10	-20
errors%	0.021	0.025	0.85	4.7	5.1	5.1	4.7	0.85	0.025	0.021

Table 5.8 Estimation errors for double-ended scheme used in non-linear load system

Table 5.8 shows the detail part of the non-location zone according to the fault inception angle. The non-location zone (±0.95° of fault inception angle) for the double-ended algorithm in the presences of non-linear loads is smaller than the single-ended scheme can provide in a system with only resistance load (±2° for the fault inception angle in Figure 5.14 and within this fault inception angle

range the estimated results have errors larger than 1m) in the proposed system. The single–ended method has an even larger non-location zone (±4.5° for the fault inception angle) when the system is added with the same non-linear load and faults as shown in Figure 5.17.

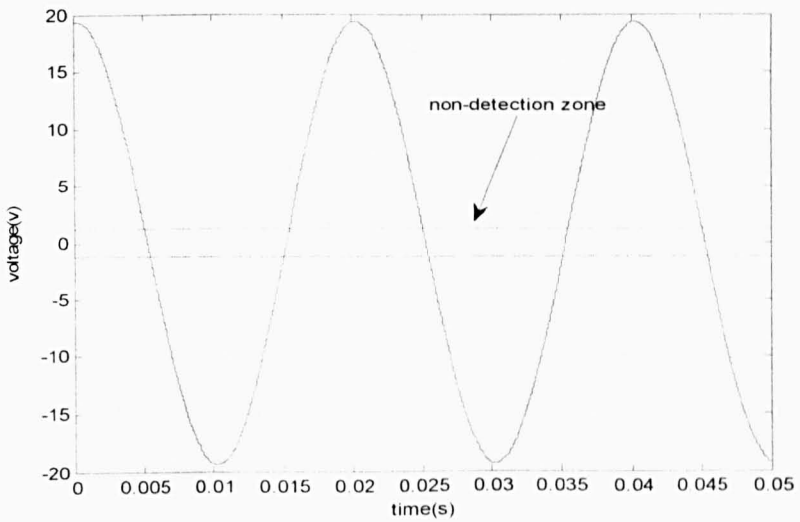

Figure 5.17 Non-detection zone of single-ended method for a non-linear load

The single-ended method offers a larger non-location zone than the double-ended method for both linear and non-linear load situation. This is the reliability factor that needs to be considered when utilizing the method in an AC system.

5.4 Influence of non-synchronized measurement

For the double-ended fault location scheme that was examined in the Chapter 4, the synchronization of the the measured data signal from both measurement points was realized using a trigger signal from the FPGA unit. This approach is suitable for small power distribution system such as an IPS. For utilization of this double-ended fault location scheme on a larger terrestrial distribution sytem, the problem of non-synchronization may cause inaccurate fault location estimation. In a larger distribution system, the non-synchronized measurements may be caused by the voltage and current transducer and also the synchronization trigger signal sent in the

communication channel may have a delay or for some situations it is not possible to provide such a synchronization signal.

The synchronization angle can be calculated as a compensation for the double-ended fault location method which uses non-synchronized measurements [84][83]. In Izykowski's method [84], the synchronization angle was calculated by solving the trigonometic equations (such as (5.2) and (5.3)) and the solution that was close to zero was chosen. Since the angle difference for the measurements in distribution systems is normaly small, the unsynchronized errors can also be cancelled by using a Newton Raphson iteration method modified from [83].

The synchronization angle between the two sets of measured information (V_1,I_1 and V_2, I_2) is defined as δ, so that equation (4.1) in Chapter 4 can be rewriten as equation (5.1)

$$V_1 e^{j\delta} + I_1 e^{j\delta} \cdot Z_x = V_2 + I_2 \cdot (Z_T - Z_x) \tag{5.1}$$

Putting $Z_x = xZ_T$ (x is distance of fault and line impedance value has a linearity against distance) in equation (5.1), then the new equation can be separated into real and imaginary parts as in (5.2) and (5.3).

$$-Re(V_1)\sin\delta - Im(V_1)\cos\delta + Im(V_2) + C_4 = x(C_1\sin\delta + C_2\cos\delta + C_4) \tag{5.2}$$

$$-Re(V_1)\cos\delta + Im(V_1)\sin\delta + Re(V_2) + C_3 = x(C_1\cos\delta - C_2\sin\delta + C_3) \tag{5.3}$$

C_1, C_2, C_3 and C_4 within (5.2) and (5.3) are defined as:

$$C_1 = Re(Z_T)\cdot Re(I_1) - Im(Z_T)\cdot Im(I_1) \tag{5.4}$$

$$C_2 = Re(Z_T)\cdot Im(I_1) + Im(Z_T)\cdot Re(I_1) \tag{5.5}$$

$$C_3 = Re(Z_T)\cdot Re(I_2) - Im(Z_T)\cdot Im(I_2) \tag{5.6}$$

$$C_4 = Re(Z_T)\cdot Im(I_2) + Im(Z_T)\cdot Re(I_2) \tag{5.7}$$

Eliminating x in (5.2) and (5.3) by dividing, the new equation (5.8) has only one unknown factor, δ.

$$F(\delta) = a \cdot \sin\delta + b \cdot \cos\delta + c = 0 \tag{5.8}$$

The following equations defines the a, b and c in the equation (5.9)

$$a = C_3 Re(V_1) + C_4 Im(V_1) + C_1 Re(V_2) + C_2 Im(V_2) + C_1 \cdot C_3 + C_2 \cdot C_4 \tag{5.9}$$

$$b = -C_4 Re(V_1) + C_3 Im(V_1) + C_2 Re(V_2) - C_1 Im(V_2) + C_2 \cdot C_3 - C_1 C_4 \tag{5.10}$$

$$c = -C_2 Re(V_1) + C_1 Im(V_1) + C_4 Re(V_2) - C_3 Im(V_r) \tag{5.11}$$

Equation (5.8) which involves only one unknown δ can be solved by using a Newton-Raphson iteration:

$$\delta_{k+1} = \delta_k - \frac{F(\delta_k)}{F'(\delta_k)} \qquad k = 1,2,3,4 \ldots\ldots \tag{5.12}$$

$$F(\delta_k) = b \cdot \cos\delta_k + a \cdot \sin\delta_k + c \tag{5.13}$$

$$F'(\delta_k) = a \cdot \cos\delta_k - b \cdot \sin\delta_k \tag{5.14}$$

The value of δ is small and close to zero in most situations with non-synchronized measurements and in the first guess for the iteration the $\delta_k = 0$. The iteration process stops when δ meets the requirement to produce accurate result in the fault location estimation. For example the minimum requirement for this simulation is $\Delta\delta = \delta_{k+1} - \delta_k < 10^{-3}$. In the frequency range used, for each frequency there is a calculated δ. When the measured phase has synchronizing errors, the calculate $\Delta\delta$ will increase with frequency as in equation (5.15).

$$\delta = \Delta t \cdot 2 \cdot pi \cdot f \tag{5.15}$$

Δt is the time delay caused by phase difference.

In the simulation system as used previously, when a fault occurs at the end of line section 2, a 1° phase angle difference between measured V_1, I_1 and V_2, I_2 was set deliberately during processing. The calculated results of the line reactance compared with calibrated ones are presented in Figure 5.18.

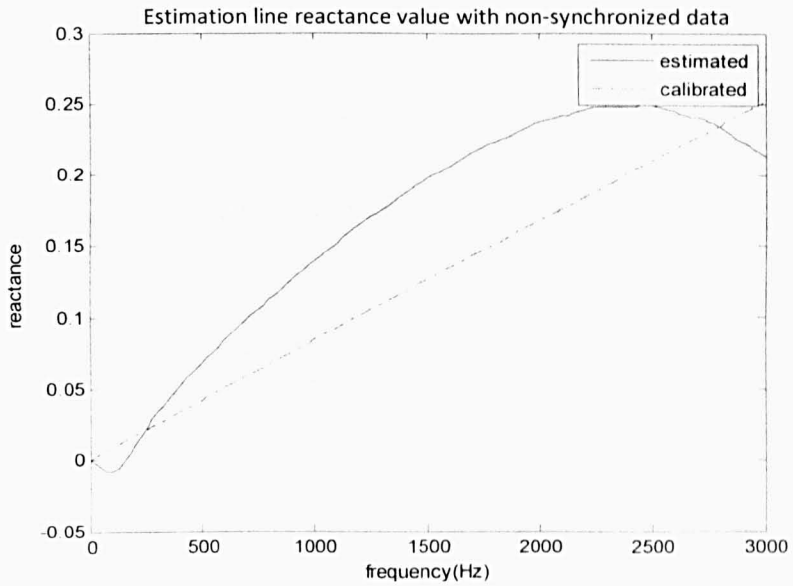

Figure 5.18 Results with non-synchronized measurements

In Figure 5.18, the estimated value (solid line) has a large error compared with the calibrated value because of a phase difference caused by non-sychronized measurements. With the same non-synchronized phases and by using the Newton Raphson iteration method described above in (5.12)-(5.14) δ can be estimated. Figure 5.19 shows the line reactance calculation results by using (5.1) which involves δ calculated from each step of the Newton Raphson iteration discribed above.

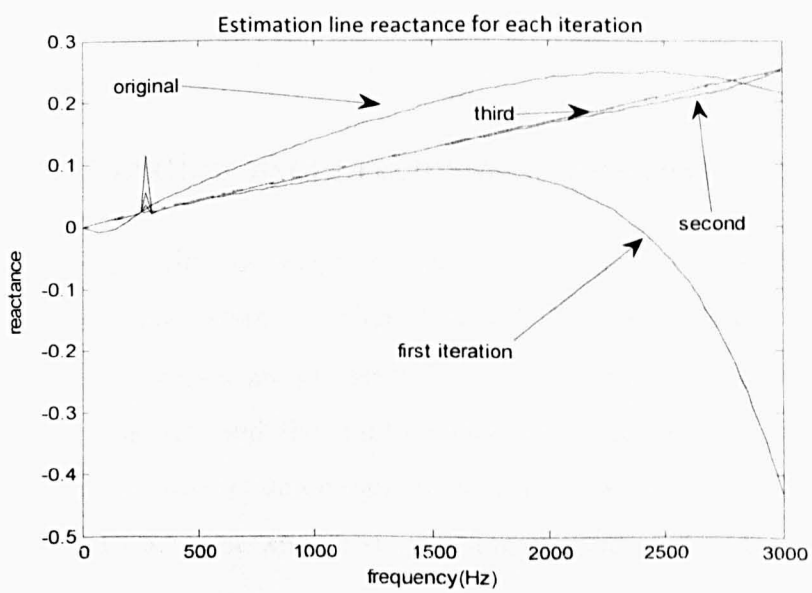

Figure 5.19 Proceeding results for each iteration

As shown in Figure 5.19, for a 1° phase difference only four steps of iteration are required to produce accurate results. The calculated synchronization angle against frequency is given in Figure 5.20.

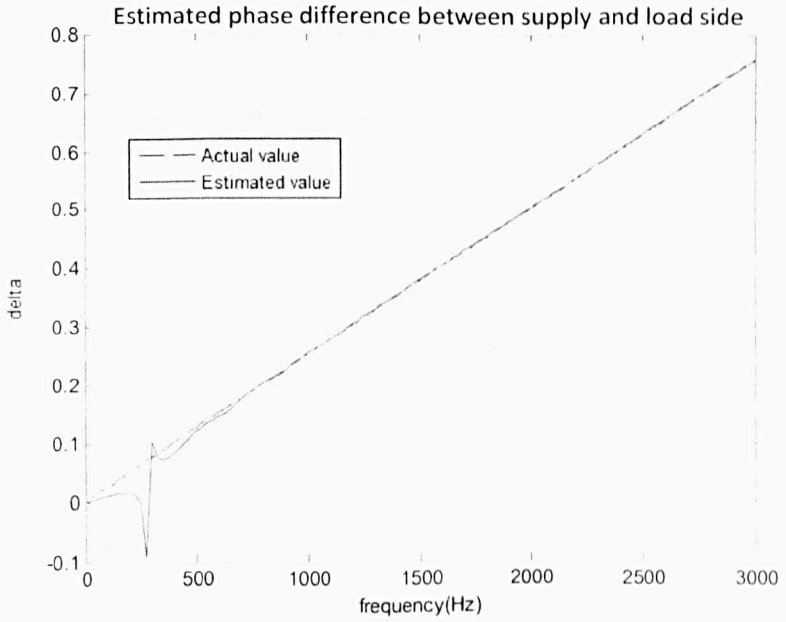

Figure 5.20 The calculated phase difference angle in frequency range

In figure 5.20, the dashed line is the δ result calculated by equation (5.15) with a set time difference for both measurement. The solid line is the δ calculated for each frequency in the final step of the Newton Raphson iterations.

5.5 Fault location using reclosing transients

Automatic line reclosing relays are commonly employed in High voltage power transmission system in which close to 77% [150] of faults are transient (temporary faults) that result primarily from flashover of the insulators induced by lighting transients and the miss-contact flashover from trees [115]. The service can be restored by de-energizing the line for a certain length of time for the fault arc to deionise and then reclosing the circuit breaker. In case of transient faults, the system outage time can then be significantly reduced to provide a better power supply quality. According to Rosen's paper [148], in

1989, 30% of the faults in an 11kV distribution system are due to lighting in UK.

The reclosing procedure can be one single attempt (one-shot) or multiple-shot with various time intervals. The first attempt, not considering the circuit breaker operation time, should have a time delay of Δt which is able to allow the fault arc to deionise. The equation mentioned by Blackman [115] defining Δt is:

$$\Delta t = \frac{kV}{34.5} + 10.5\ cycles \tag{5.21}$$

Considering the typical operation of the circuit breaker, the typical closing operation time is about 20-30 cycles [115] (which is larger than the Δt in equation (5.21)), the trip signal and reclosing signal are sent together. If a distribution line protection unit is equipped with an automatic reclosing function, the transients in both voltage and current caused by circuit breaker reclosing can also be used to predict the fault location. If necessary, this reclosing fault position estimation procedure can be applied as a compensation for the previously discussed fault location methods.

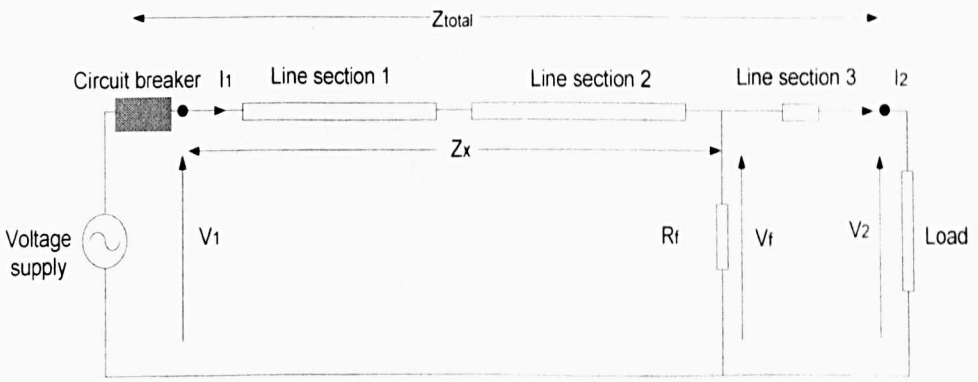

Figure 5.21 System for fault location using reclosing transient

In a similar way to the double-ended fault location algorithm, fault location which uses transients caused by auto reclosing relay requires two sets of voltage and current transducers equipped at the start and the end of the protected distribution line in Figure 5.21. If during the first time of reclosing attempt, the fault it still in the system (a permanent fault), the transient data is

captured. The recorded data has to be synchronized or if not the previously introduced Newton Raphson iteration method has to be employed.

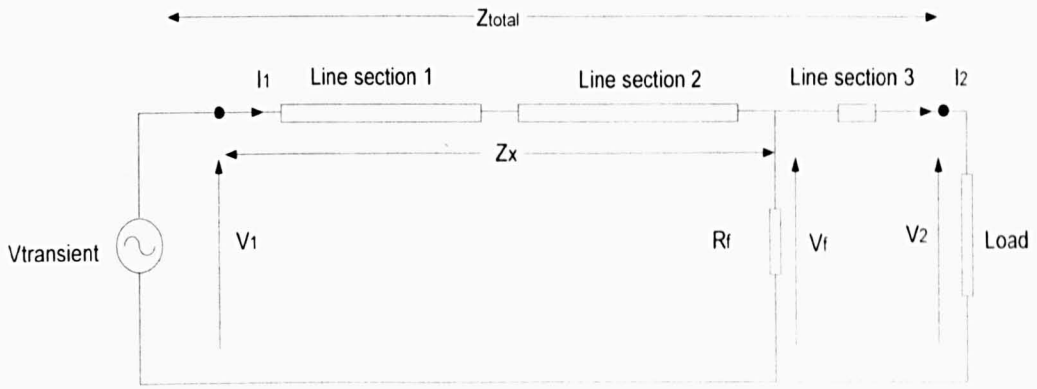

Figure 5.22 System model considering transient as voltage source

As described in Figure 5.22, considering the transients generated by circuit reclosing as a voltage source, the original voltage source is short circuited and the line impedance $Z_x$can be calculated by (5.22):

$$V_1 - I_1 \cdot Z_x = V_2 + I_2 \cdot (Z_{total} - Z_x) \tag{5.22}$$

In which Z_{total} is the line impedance of the total length of the protected line and the impedance between measurement point 1 (where V_1 and I_1 was measured) and the fault position $Z_x$can be calculated by (5.23):

$$Z_x = \frac{(V_1 - V_2 - I_2 \cdot Z_{total})}{I_1 - I_2} \tag{5.23}$$

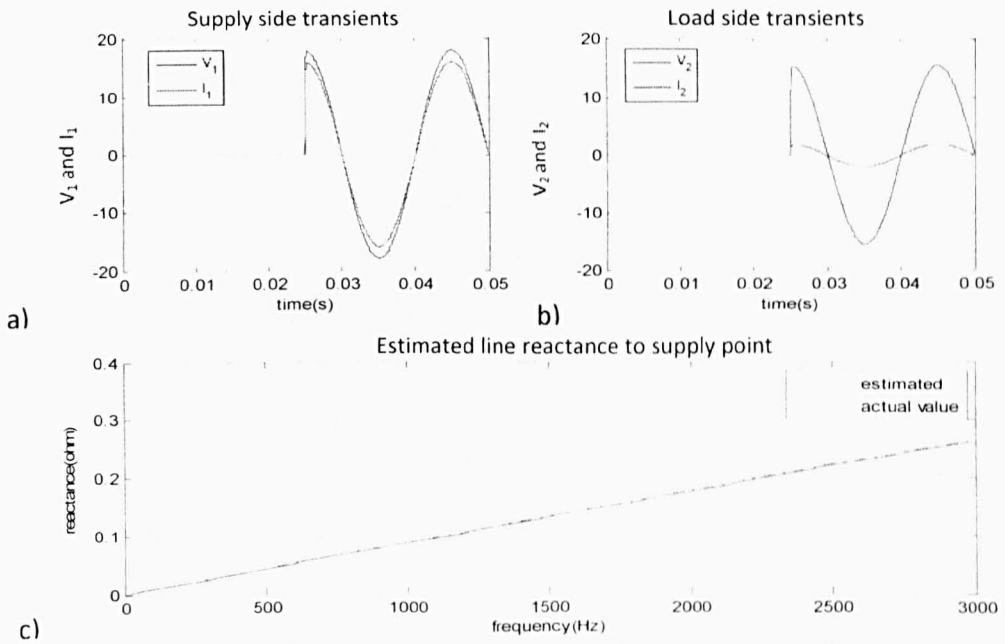

Figure 5.23 Reclosing transient and the estimated results

a) – b) Measured voltage and current c) Estimated reactance

Figure 5.23 shows the fault location results using the transients caused by the single phase reclosing process. The measured phase voltage and current from both measurement points as shown in a) and b) contain reclosing transients and then transferred into frequency domain by FFT. For locating a fault with reclosing transients, the single-ended algorithm which requires the knowledge of the pre-fault voltage information can not be applied. The estimated reactance values are used to predict the fault position. Compared with the actual line reactance value to the fault point, the estimated results show good accuracy and the same procedure can be employed to a three phase reclosing relay as well.

5.6 Summary

This chapter described computer simulation results which enhanced the investigation of the previous two chapters. To validate by simulation, models were built with the same parameters as the experimental system and gave similar results to the experimental rig (only less noisy). This gives confidence that the previous test results are correct and also by simulation, the proposed

fault location methods can be re-examined in the conditions that are not possible in the experimental rig.

Both proposed methods works better in the system with a high voltage where a larger fault transient can be generated. The small non-location zone in both methods, according to the fault inception angle, is explored in both the linear and nonlinear load situations. The single-ended algorithm has a slightly larger non-location zone than the double-ended method for both load conditions. A synchronization method which calculates the different phase angle between the two sets of data acquisition units at both ends is demonstrated by using Newton Raphson iteration algorithm to improve the accuracy of double-ended scheme in case of un-synchronized measurement. In the system equipped with automatic reclosing relays, the posibility of fault location using transietns created by system reclosing is demonstrated.

Chapter 6

Application to a marine system

6.1 Introduction

Modern large ships have moved towards using electric propulsion systems and many other subsystems are looking to employ electrical power instead of hydraulic or pneumatic systems. The electrical distribution systems can now be rated as high as 40MW and the ship is totally reliant on its correct behaviour [116]. New architectures, such as zonal distribution [120], have been proposed and DC system is considered an attractive proposition compared to AC system which feeds the main distribution bus directly with the generator output and a step transformer [94].

This chapter discusses the application of the two proposed fault location methods in a zonal marine distribution system with an Integrated Power System (IPS) configuration. Faults in each zone can be detected and located by monitoring the voltage and current within the protected zone. Faults outside the protected zone are detected and classified according to the line impedance estimation results. The basic structure of modern ships will be

introduced in Section 6.2. Sections 6.3 and 6.4 will focus on the fault location on a ship system for a phase to phase fault and phase to earth fault. Only short circuit faults are considered in this chapter because the open circuit faults interrupt the load power supply but do not harm the system equipment. The conclusion and summary will be made in Section 6.5. The open circuit fault on buses can be easily detected by monitoring the bus current. If it occurs at the load side, the fault can be detected using active impedance estimation methods.

6.2 Zonal marine power system structure

6.2.1 IPS within ship power system

The IPS utilized in ships is a revolution [2]. The traditional Segregated Power System (SPS) supplies the mechanical propulsion power and electrical power from separate prime mover systems as shown in Figure 6.1. However, the IPS uses electrical and electronic equipments to meet the different loads such as propulsion, ship service loads and combat systems (for naval ships) as shown in Figure 6.2.

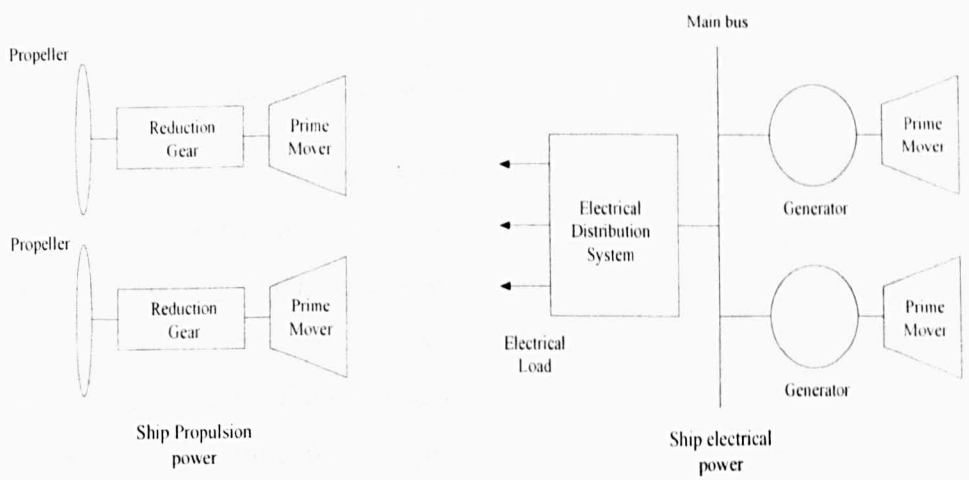

Figure 6.1 Segregated ship power system [2]

In a traditional segregate ship power system mechanical loads and electrical loads are supplied by different prime movers. This simplifies the electrical system design but the separate prime mover supply system increases the

system layout complexity and at the same brings more difficulty to system maintenance and expansion.

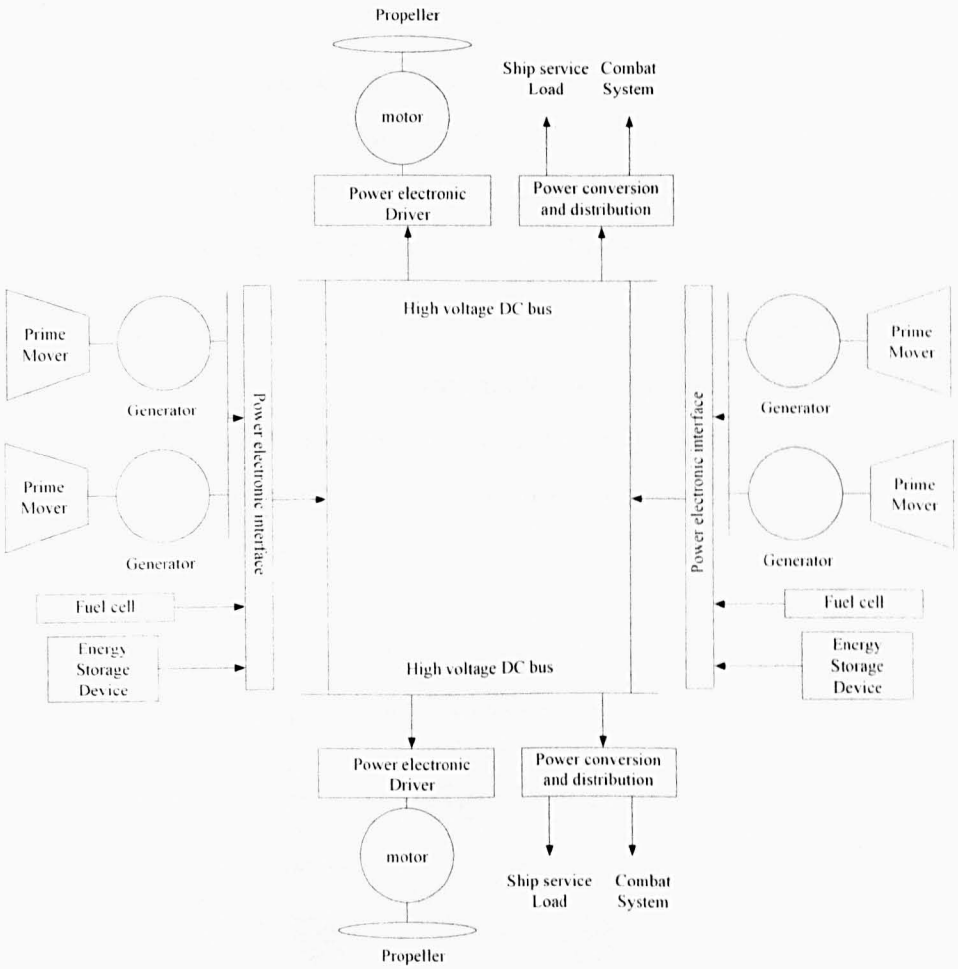

Figure 6.2 Integrated DC ship power system [2]

Utilizing IPS in a ship power system, as shown in Figure 6.2, improves the power supply efficiency by using integrated power generation and accompanied power electronic devices to supply different loads. Without large mechanical components such as gear boxes, the weigh of the system is reduced leaving more space for the other loads and passengers. The system layout and expansion are also more flexible in an IPS. Loads accompanied with a drive unit can be added in or removed out from the system as easy as a "plug in and plug out" process. The environment is less noisy and using controlled electronic drives, the system load response can be faster than in a traditional ship system with SPS. Fuel consumption is also reduced, as the prime mover can be operated in its most economical mode for a given ship speed.

6.2.2 Zonal ship power system

In a ship with an IPS all the loads (such as propulsion, navigation, communication and other ship service loads) rely on the electric power. The power distribution is vitally important to maintain reliable operation of the More Electric Ship (MES). Due to the high demand for electric power the efficiency and configuration of the distribution system is one of the main considerations when designing and building a MES.

In order to maintain power to all the loads (especially the vital loads such as propulsion, control centre and communication systems) and enhance the continuity of electric service for the vessel, the traditional configuration of the shipboard power distribution system is a 'ring' structure in which the loads can be supplied by any generator.

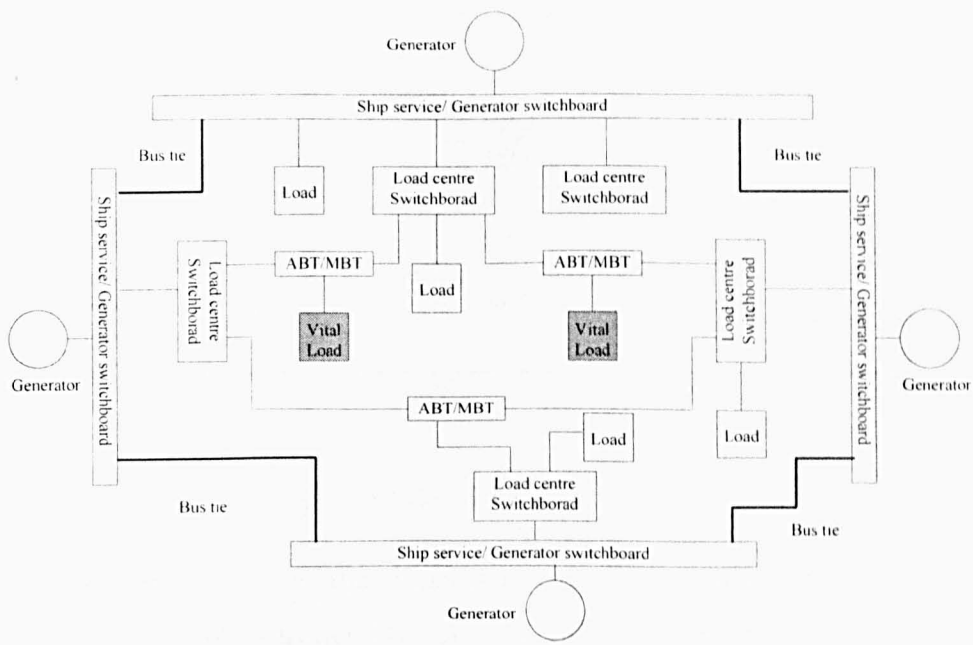

Figure 6.3 Ring configuration of marine power distribution system

This ring feature is of great importance in order to ensure power supply to vital loads in case of failure of a generator. For a naval ship system, for instance, interruptions of 70-100ms of electric power can cause the entire combat system to shut down, with a long recovery time [117]. The generator switchboard and the load switchboard contain circuit breakers, controls and protection devices to supply the power to the loads. The bus ties connecting the generator

switchboards allow power transfer from one board to another. Normally, the vital individual loads are connected via the bus transfer system [118] which can be an Automatic Bus Transfer (ABT) or a Manual Bus Transfer (MBT) to realize a multiple power supply in case the failure of the power supply from one of the generators .

Zonal marine power distribution systems are more efficient and economical compared with conventional ring configurations due to the cost of cables and switchboard feeders [119]. A zonal ship system is the solution being considered for future marine system design [120]-[123]

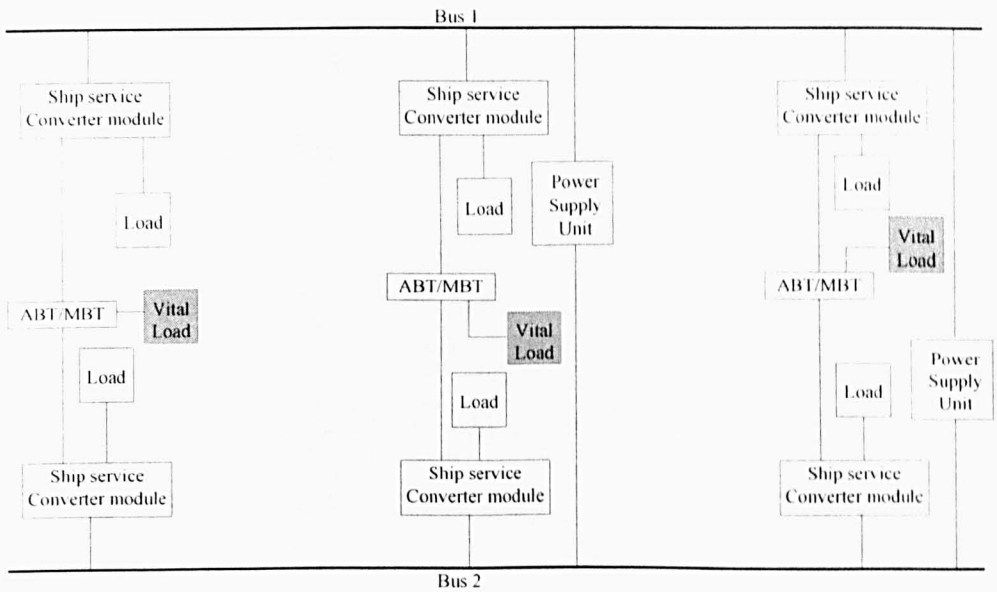

Figure 6.4 Zonal distribution system

The zonal architecture of the shipboard system, as shown in Figure 6.4, is a proper design can considerably enhance the re-configurability of the ship system under faults and battle damage [120]. The power supply unit transfers power through two buses to the ship service converter module which could be a Buck converter or inverters in a DC zonal system. The two buses are port side bus and starboard bus. Normally the port side bus acts as the main power supply bus and the starboard bus is the alternative bus. The starboard bus is operated by bus interface unit (bus transfer unit) during the situation that faults are detected in the main power supply system. Note that the two buses may not physically be located on the port and starboard side, for security, one may be

located in the keel. Vital loads can be supplied by both buses so that even in a fault situation in which the main supply is switched off the vital loads can still work from the alternative bus. Buses are usually powered by two or more power supply units (including generators, converters or transformers) to prevent power discontinuity caused by a single generator fault.

Figure 6.5 [123] clearly shows the advance of the zonal configuration compared with conventional design.

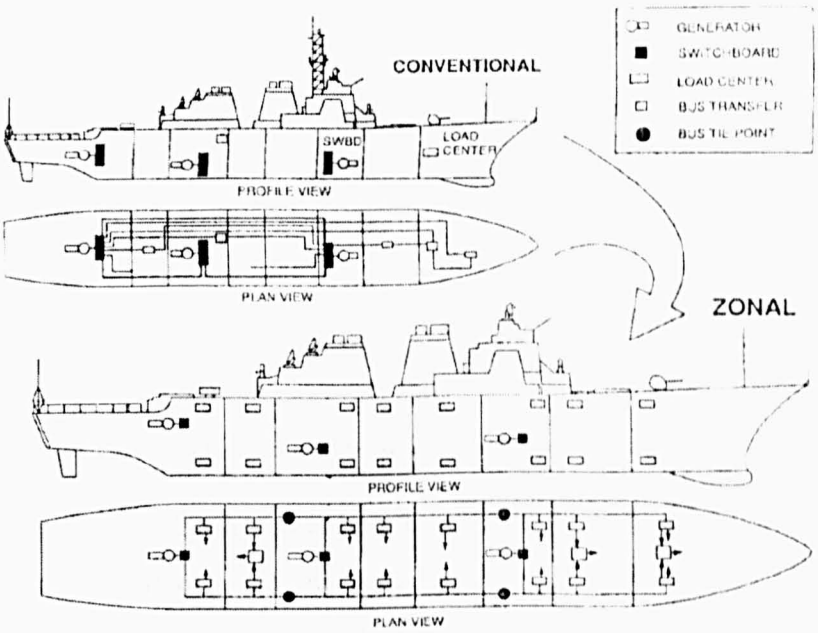

Figure 6.5 Comparison between zonal and conventional configuration [123]

The electric power supply system layout is more compact in a zonal system and it improves the system survivability considering the casualty of individual equipment or widespread damage due to battle damage. With respect to the power transfer efficiency and economy factors, the zonal configuration will be the main considerate for future marine power system designs.

6.2.3 The proposed zonal distribution system

The proposed low voltage AC zonal distribution system is depicted in Figure 6.6. The 6-zone, two generators' configuration is used to demonstrate an

actual ship power system which would have five and eight zones and three to five generator sets [121].

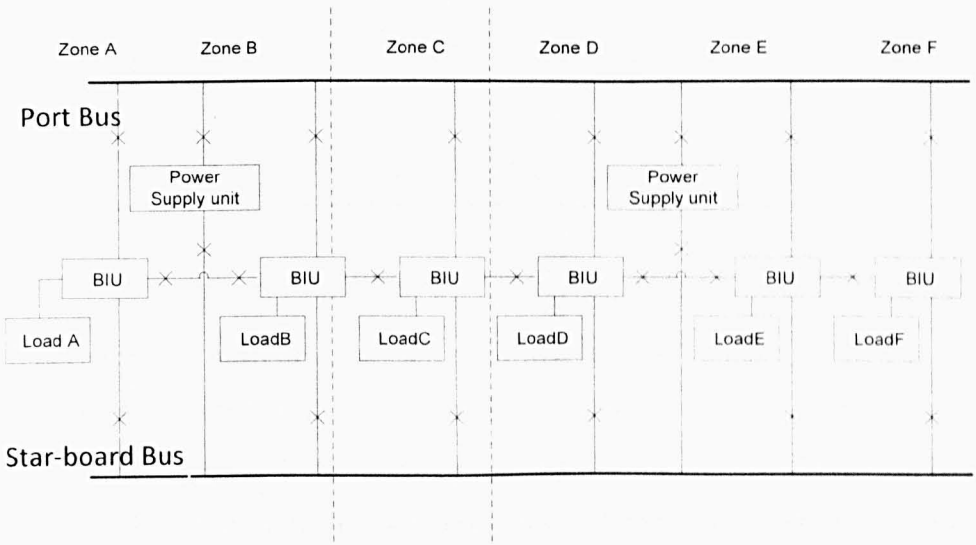

Figure 6.6 Proposed 6-zone marine power system

The configuration in Figure 6.6 is based on a circuit investigated [116]. Each zone works independently and the loads within it are viewed as a black-box with only a known power consumption rating. The detail of the load is not considered for this work. The two power supply units which contain generators and transformers will not work at the same time. One acts as a backup power supply for the maintenance or break down of the other. Both generators are earth connected with a high resistance to provide low phase to ground fault current and limit the potential transient over-voltages. Loads within each zone can be connected to the two main buses within each zone and the buses of adjacent zones.

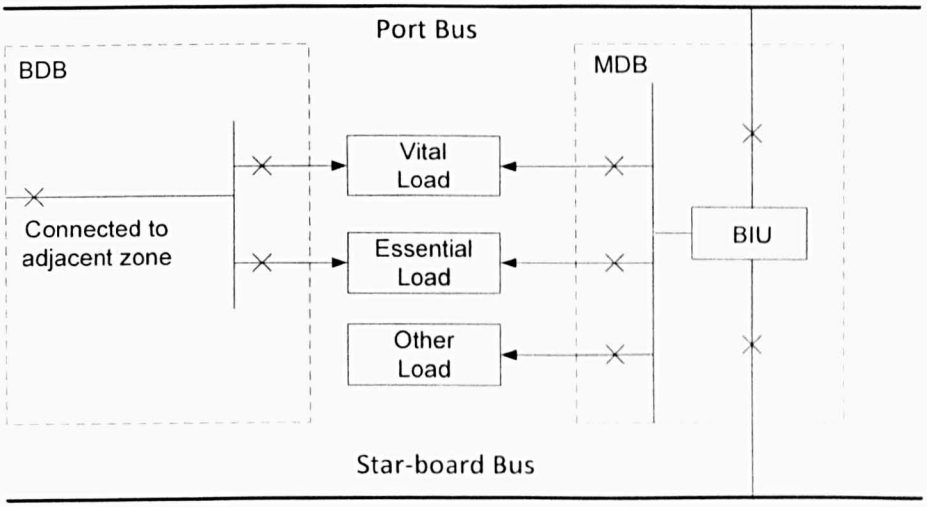

Figure 6.7 The Bus interface unit

A Bus Interface Unit (BIU) is used to switch the vital loads and the essential loads from the faulty bus to the healthy buses within the zone or adjacent zones while providing power from its energy storage during the switching operation. Both of the two main low voltage buses can feed the Main Distribution Board (MDB) which supplies the load in each zone [124], with connection and bus changeover facilitated by the BIU which is incorporated with power electronic converters and energy storage[124][116]. A Backup Distribution Board (BDB) is also provided in each zone to supply these vital and essential loads from the MDB of the adjacent zone.

6.2.4 System impedance representation

The proposed system was modelled in Matlab/Sim-Power System with lumped impedance components and a three-phase voltage source as shown in Figure 6.8 [116] with the assumption that only the generator in zone A is connected to the system.

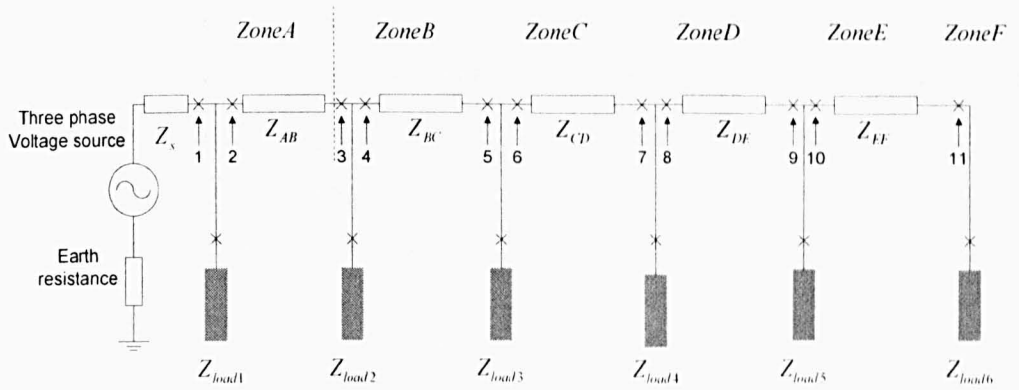

Figure 6.8 AC zonal distribution system model

The generator is represented by 60Hz 440V three phase voltage sources located in zone A and zone E (disconnected) as shown in Figure 6.6. The source impedance (R_s=3.12mΩ, L_s=7.65μH) is derived from the transformer parameters: 5% leakage and 98% efficiency. The lumped linear loads within each zone are simulated with star connected and non-earthed resistors and inductors (phase to phase load). The impedance value is decided by the active power rating of each star connected load (un-earthed) and the required 0.9 power factor as given in Table 6.1. The load active power is given but not necessarily fixed which means the given information of loads can not be used as pre-known during fault location estimation. The system generator is earth connected through a large earth resistance which is about 260Ω so that the fault current caused by an earth fault is very small compared with the normal operating current.

system loads regulation						
	Zone A	Zone B	Zone C	Zone D	Zone E	Zone F
P(kw)	126	438	906	372	1085	94
Q(kvar)	61	212	438	108	525	45.5
R(Ω)	1.24	0.36	0.17	0.42	0.14	1.67
X(Ω)	0.603	0.17	0.08	0.204	0.07	0.81
L(mH)	1.92	0.55	0.27	0.65	0.22	2.57

Table 6.1 Load power rating and impedance

The low voltage bus which represents the length of the 6-zone ship, is one hundred meters in length. Divided into five sections equally, twenty metres of cable is used within each section. The twenty meters of cable is then divided

equally into 10 small sections for the simulation of faults locations. Since the bus is essentially limited by the length of the ship, transmission line dynamics do not play a significant role [119]. Therefore the bus is considered to be a three cable system with lumped parameters and since the distance is short, the cable capacitance is ignored here.

Z_{cable}	R_{cable}	0.03mΩ/m
	X_{cable}	0.24μH/m

Table 6.2 Parameter of cable impedance

The current rating of the impedance described in Table 6.2 is 1kA. However, considering the different load rating in each section in Table 6.1, the bus current of some sections may exceed the bus rating current and the highest can be up to 4kA. Therefore, for some sections with large loads, additional cables are connected in parallel to meet safe current rating and this is calculated by equation (6.1)

$$I_{peak} = \frac{\sqrt{2} \times P}{0.9 \times 440 \times \sqrt{3}} \tag{6.1}$$

where P is the load power rating and I_{peak} is the peak current that may appear in each bus section. According to equation (6.1), the maximum current within each bus section with respect to its load rating is calculated and shown in Table 6.3

	I_{max} (A)	Cable No.	Z_{cable} (mΩ) of 20m
Zone A-B	258	1	0.6+j1.8
Zone B-C	1096	2	0.3+j0.9
Zone C-D	3262	4	0.15+j0.45
Zone D-E	2496	3	0.2+j0.6
Zone E-F	193	1	0.6+j1.8

Table 6.3 Current rating and cable impedance

As shown in Table 6.3, for the zone with largest load, 4 cables are required in parallel. For zones with different maximum current levels the bus cable impedance is different. So that during the fault locating process, the variation

of per-meter value of cable impedance in different zones has to be considered for accurate fault position estimation.

6.3 Single-ended bus fault location in marine system

6.3.1 Fault location strategy

The single-ended bus fault detection and location method which does not require communication channels is utilized in each zone. The current and voltage transducers within the circuit breaker at location 2, 4, 6, 8 and 10, shown in Figure 6.8, monitor the system voltage and current information. The detection of faults within each zone is achieved by measuring the fault current transient. The tripping signal of the circuit breaker is sent with the logic cooperation of fault detection and fault location estimation. For example, consider the cable section Z_{CD} as shown in Figure 6.9.

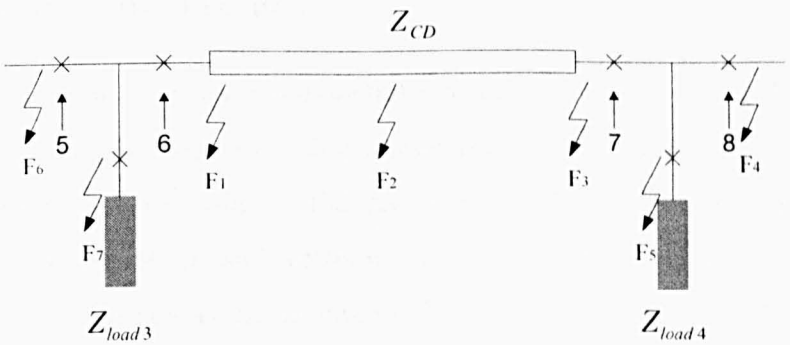

Figure 6.9 Demonstration of single-ended bus fault location

Only phase to phase short circuit faults are considered in this section because a phase to ground fault will not do harm to the system immediately. A phase to ground fault will not cause a large fault current in a system as the generator is connected to earth by a large (260Ω) earth resistance (in fact, for this single-ended fault location calculation, the earth is considered to be floating at the generator side). However if a second fault appears, without the clearance of the first one, a large fault current may be created in the fault circuit loop. A method for eliminating the potential danger of a second earth fault is discussed in section 6.5.

All the faults (F_1-F_7) in Figure 6.9 can be detected by measuring the over-current caused by the faults. The distance of the fault can be calculated by using the proposed fault location method. The distance of faults F_1, F_2, F_3 and F_5 can be estimated. If the accuracy is within 1m, then this technique will be able to distinguish the difference between F_4 and F_3. The 1m accuracy is decided by the position of circuit breaker instalment which here is 1metre to the start or the end of the cables within each section. However, faults at F_3 and F_5 will be treated as the same location using this method. For faults occurring behind the protected section, F_6 and F_7, the calculated results will be negative. When the fault location is decided, it will be clear if the fault is within the protected zone or not and the circuit breaker can be operated if required. If the estimated faults are shown to be behind the protected section or 1m after it, the circuit breaker will not be operated. A similar protection strategy can be used in the other zones.

6.3.2 Fault location results

The fault location results are demonstrated within two zones (Zone A and zone D) which have different bus cable impedances, in the rest of the zones the same algorithm works due to the fact that all the zones have the similar electrical configuration and different loads (the load variation does not influence the accuracy as mentioned in Chapter 3 and Chapter 4.) Figure 6.10 shows the typical fault transient within the measured voltage and current waveforms when a 0.01Ω phase to phase short-circuit fault in imposed at the end of the zoneA.

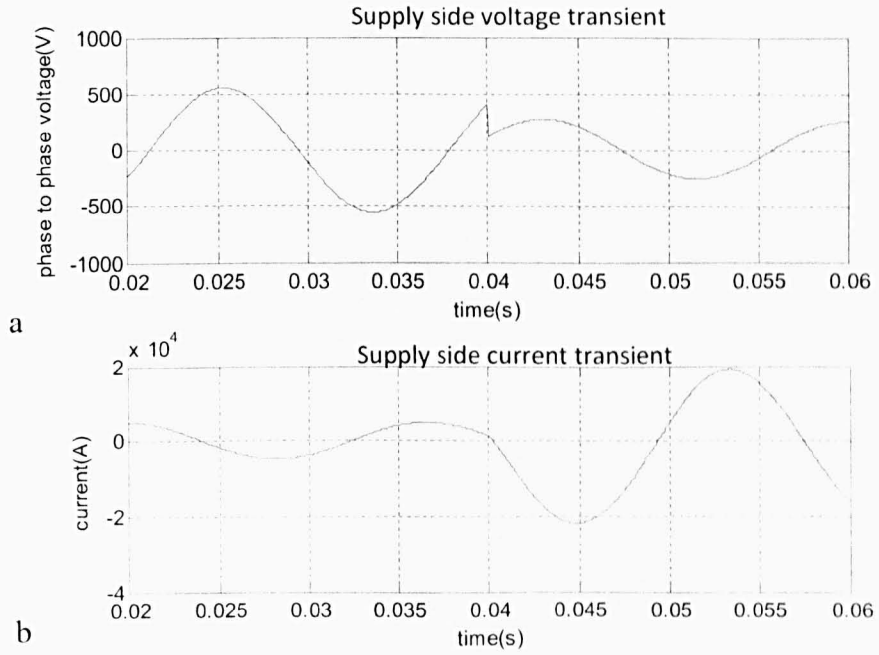

Figure 6.10 Measured fault voltage and current in zone A

a) Voltage transient b) Current transient

The voltage and current which contains both transient and steady state information measured at circuit breaker 2 in Figure 6.8 is shown in Figure 6.10. The Fault occurs at 0.04s of the 40ms data length which starts at 0.02s. Figure 6.10 gives the system voltage and current at the pre-fault, fault and post fault stages, but the actual fault location process does not require all the data. The data being processed with the FFT is only 12ms in length, with the fault transients in the middle. In other words, the fault location calculation process can be completed 6ms after the fault occurs, without considering the calculation time, once the fault is detected by an over current strategy. The captured data is Blackman windowed and zero-padded before being processed with a FFT to realize smooth results with high frequency results. In the marine system, most short circuit faults on cables are caused by insulation failure or external force damage and have small fault impedances so that when utilizing the single-ended fault location algorithm, the line voltage iteration processes is enough to make an accurate estimation. The results of the fault location estimation for all the fault scenarios are shown in Figure 6.11.

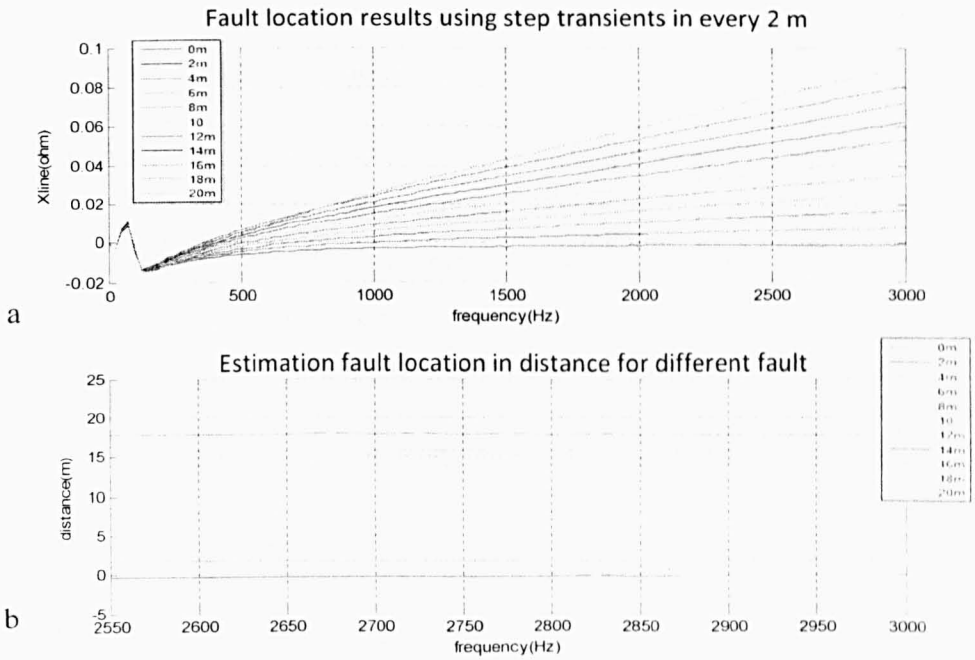

Figure 6.11 Fault location results of different fault distance in Z_{AB}

a) The measured line reactance b) Fault distance

Actual distance (m)	0	2	4	6	8	10	12	14	16	18	20
Estimated distance(m)	-0.1	1.95	4.28	6.15	7.91	9.85	11.93	13.95	16.01	18.07	20.11
errors%	0.5	0.25	1.4	0.75	0.45	0.75	0.35	0.25	0.05	0.35	0.55

Table 6.4 Errors within each fault location in ZoneA

In Figure 6.11a) the reactance between circuit breaker 2 and the fault point calculated for different fault positions is presented. The estimated reactance value (the slope of the curves) increases with the fault distance (by 2m each time). Figure 6.11 b) shows the distance values after dividing the reactance values by the known per-meter length line reactance parameter in the high frequency range (2550Hz to 3000Hz). Due to the fact that a short data segment (12ms) is used for data processing, the results show better accuracy at high frequencies. For all of the estimated fault positions, the largest error in the high frequency range is about 0.3m (1.4%) in distance as shown in Table 6.4.

The low frequency distortion in Figure 6.11 a) (below 500Hz) is caused by the time domain steady state information, the Blackman windowing affect and the short data segment. This low frequency distortion is more obvious when an even shorter data window is used. In order to maintain a good accuracy, only

the average value of the high frequency results presented in Figure 6.11 are used to predict the fault locations.

When faults occur beyond the protection zone, for example, in the middle of the bus cable Z_{BC} or inside the generator, the over-current strategy will detect the fault but the fault location algorithm will decide that the fault is outside the protected zone. Figure 6.12 shows the estimated reactance results when fault occurs at the end of the protection zone and in the middle of the next zone.

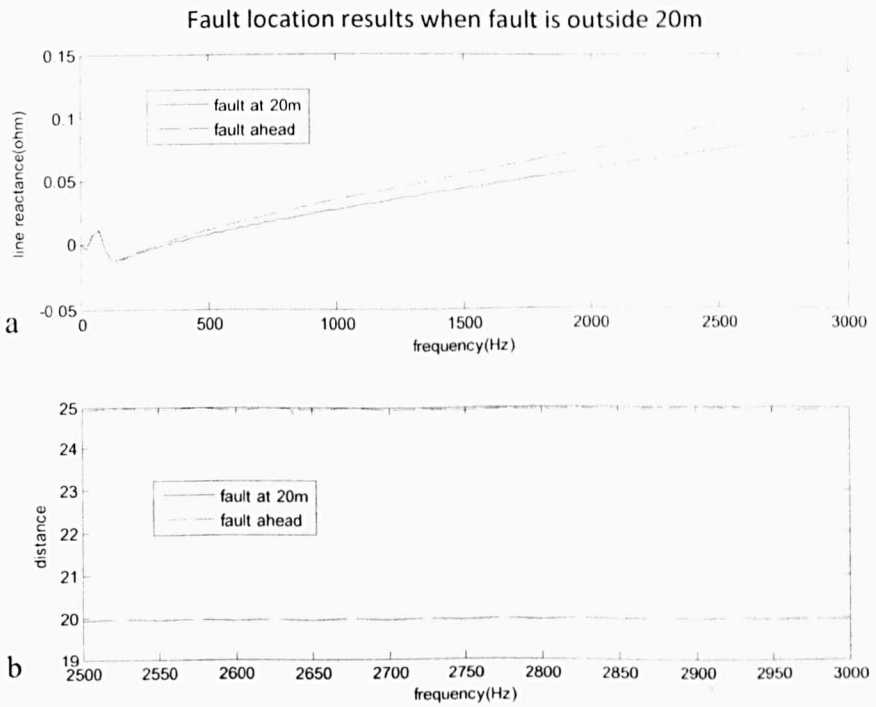

Figure 6.12 Fault occurs outside the protection zone

a) The measured line reactance b) Fault distance

As shown in Figure 6.12, the dash line is the estimated result when a fault occurs in the middle of bus Z_{BC} while the solid line which shows the results of a fault at the end of bus Z_{AB} (20m) acts as a comparison. The calculated line reactance is larger than the total line reactance of the protected zone in a) which indicates a fault beyond the section. In b), the distance results show that the fault is at 25m (actually it should be at 30m which is the middle of the next section) because the line reactance results are divided by the per-meter value of line Z_{AB} which is twice of the per-meter value of the cable in Z_{BC} (Z_{BC} has a double line due to the current rating). This problem can be solved by adding a

simple logic to the algorithm. Once the line reactance X_{AB} is estimated, the distance D can be calculated as:

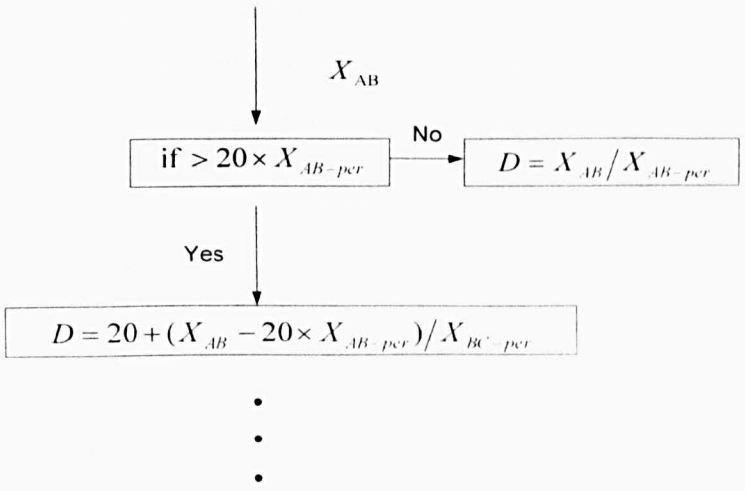

Figure 6.13 Logic distance calculation for outside protection zone fault

The actual fault distance can be estimated using the logic described in Figure 6.13. However errors in the estimated fault distance results may be over 1m when the fault is beyond the protection zone due to the fact that the fault transient flows into the load before reaching the voltage and current transducer located in CB2 (e.g. faults on cable Z_{CD}). The error for a fault in the middle of Z_{BC} is 0.8m and for a fault at the end of Z_{BC} is 1.2m and if faults are in Z_{CD}, the fault location error, by using voltage and current measured at CB2, is even larger. This outside protection zone error varies with the load variation and can not be predicted when load information is not known. One single-ended fault location scheme is only able to cover one zone in the zonal marine system.

A fault ahead of the protected zone can be distinguished, as can a fault behind it (generator fault). Faults behind CB 2 can be detected by monitoring the fault current but the location estimation results will be negative. The scheme does not have to wait for the final reactance iteration results. Once the result of the measured voltage divided by the measured current is negative, the fault is behind the CB and the iteration process stops.

For the protection scheme in CB2, both short circuit faults in the generator in load Z_{load1} and beyond cable Z_{AB} are considered as outside protection zone and

no circuit breaking operation signal will be sent to CB2 in the present of these faults.

The same fault protection scheme can be employed to cover the bus section Z_{DE} while the only difference is that in section Z_{DE}, the line reactance is smaller because four cables are connected in parallel in this zone.

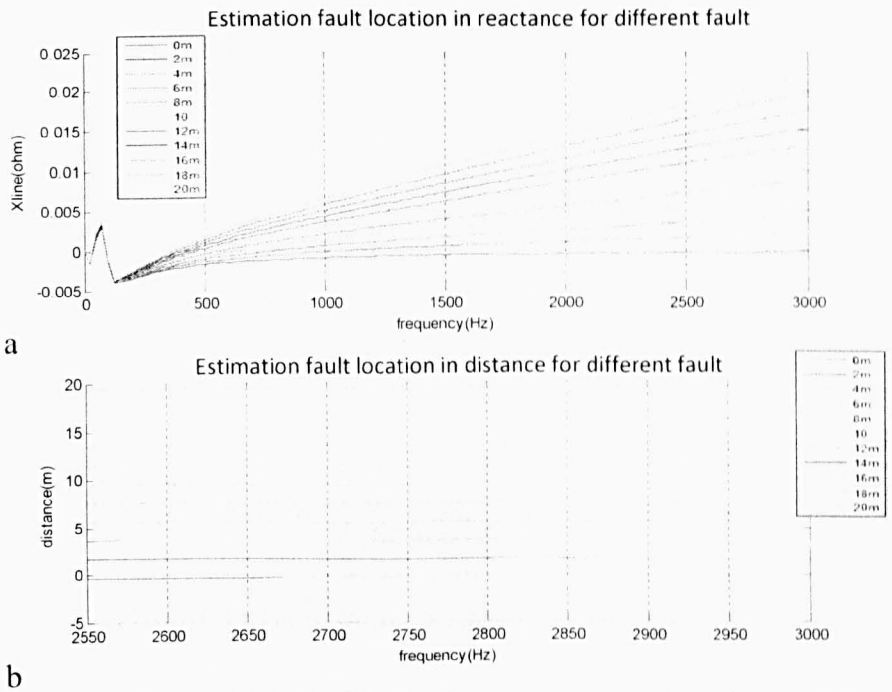

Figure 6.14 Fault location results of different fault distance in Z_{DE}

a) The measured line reactance b) Fault distance

Actual distance (m)	0	2	4	6	8	10	12	14	16	18	20
Estimated distance(m)	-0.13	2.15	4.21	6.45	8.12	10.33	12.14	13.95	16.01	18.07	19.83
errors%	0.65	0.75	1.05	2.25	0.6	1.65	0.7	0.25	0.05	0.35	0.85

Table 6.5 Errors within each fault location in ZoneD

Short circuit faults with 0.01Ω fault resistance are added at every 2m along cable section Z_{DE} and the fault location results (both line reactance and fault distance values) are shown in Figure 6.14. The low frequency inaccuracy is caused by the same reasons as described in the protection of Z_{AB}. For a section with smaller cable impedance, the fault location errors increase to a maximum value of 2.25% (as shown in Table 6.5) for all the different fault location results. The faults outside the protected section Z_{DE} can be distinguished using the same method as demonstrated in section Z_{AB}.

Within each protection zone, the estimated fault distance results are influenced by the fault resistance. This is demonstrated by increasing the fault resistance from 0.1Ω to 0.5Ω when a fault occurs in the middle of this section (Z_{DE}). The results are shown in Figure 6.15

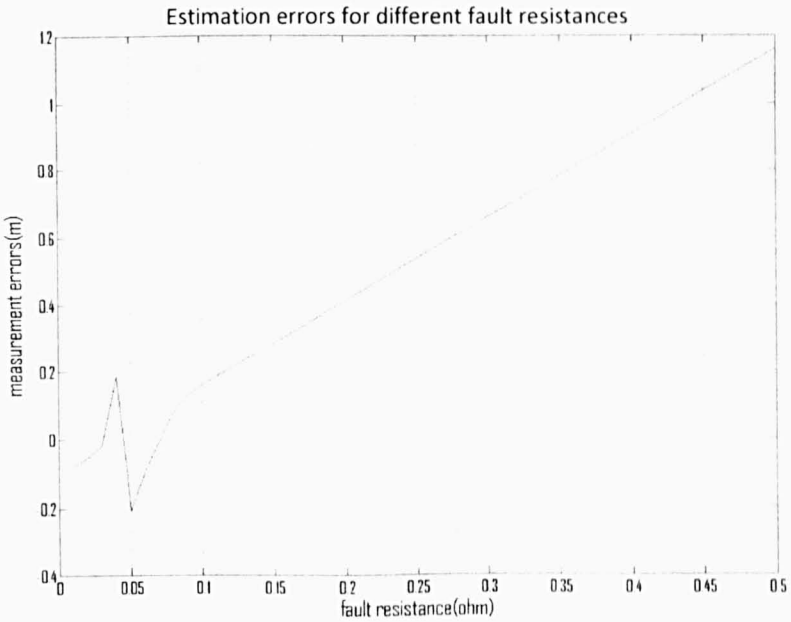

Figure 6.15 Fault resistances against estimation errors

For the required 1m accuracy in this marine electrical system demonstrator, the fault resistance can be as high as 0.45Ω which is comparable to the load impedance presented in the Table 6.1. This fault impedance (0.45Ω) can be seen as a high impedance fault. Faults with higher impedance, over 0.45Ω, are not considered here.

6.3.3 Influence of the generator location

The proposed marine distribution system has two generators: one is the main generator and the other is the backup generator for maintenance or in case the failure of one generator, as shown in Figure 6.6. The results in Section 6.3.2 shows the situation when the generator at the beginning of the ZoneA is considered as the main power supply. When the generator located in ZoneD acts as main power supply, using this single-end protection scheme, the voltage and current transducer locations have to be changed as well to realize

accurate fault position calculations. This is due to the fact that the supply impedance (at approximately the same value level as the line impedance) in this marine electric system is much smaller compared with the load impedance. For a short circuit fault, most of the fault transient information flows in the supply side. The proposed single-ended method uses transients to locate the fault. The transducer is preferred to be in the side that most transient flowing to for a higher signal to noise ration and better accuracy. For each section, the transducers have to be located close to the generator side to receive better transient information

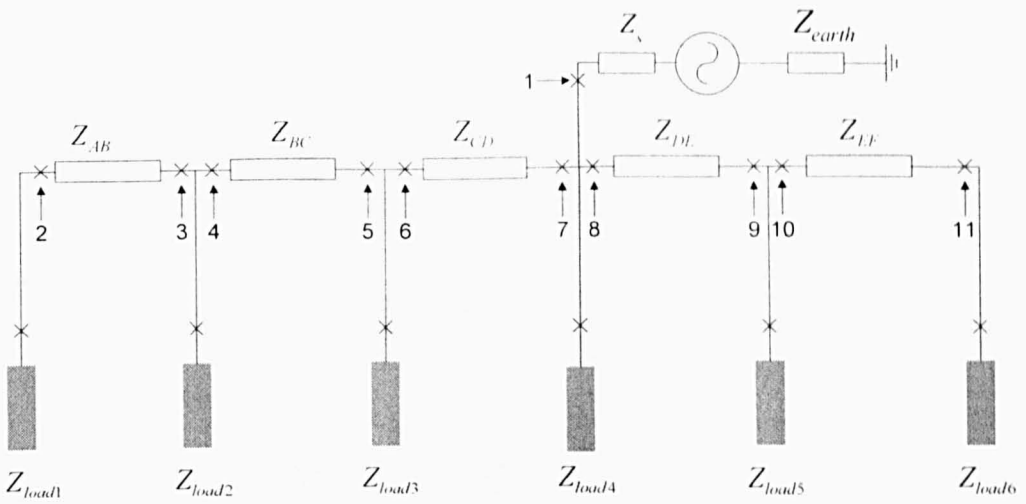

Figure 6.16 Configuration of system with the generator at a different location

In the configuration as shown in Figure 6.16, the main generator is located at the end of section Z_{CD}, the transducers for each section are equipped in the circuit breakers: 3, 5, 7, 8 and 10. The fault location algorithm is the same as discussed before.

6.4 Double-ended protection in marine system

Unlike the single-ended algorithm which works alone and does not require any communication channel, the double-ended fault location method needs transducer information from the remote end to achieve accurate fault position estimation. However this two-end measurement method provides robust and

precise fault location results for different fault types (bouncing fault and step fault) and is able to operate at higher fault resistances.

Short circuit faults can be detected by comparing the difference in the current measured from both ends and accompanied with the double-ended algorithm the fault position can be located. In the discussed marine electrical system, the double-ended method can cover bus cables from two zones (40m) with the estimation results meeting the 1m accuracy requirement regardless of the influences caused by the load impedance in the middle.

For example, in order to protect the cable Z_{AB} and Z_{BC} in Figure 6.8, there has to be current and voltage transducers installed in CB2, CB5 and a load side current transducer in the load circuit breaker of Z_{load2} (CBL2) shown in Figure 6.17.

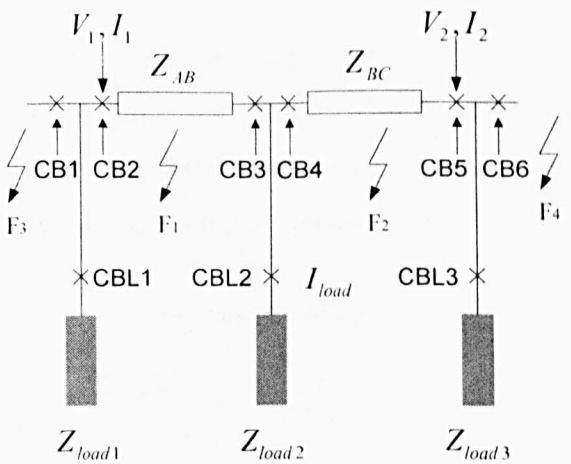

Figure 6.17 Example of protection of two zones

A short circuit fault can be detected by comparing the current I_1, I_2, and I_{load} measured from CB2, CB5 and load CB of Z_{load2}. When the result of $\Delta I = I_1 - I_2 - I_{load}$ is larger than the pre-set threshold value (fault detection), the measured voltage and current data (V_1, I_1 and V_2, I_2) from both ends is used to predict the fault position. Faults outside the protected zone will give the negative results, fault positions can be calculated when the results are positive and inside the protection area. Faults within the load Z_{load2} and faults at CB3 are considered to be in the same position for this protection scheme. The measured transients and the fault location results are shown in Figure 6.18 and Figure 6.19.

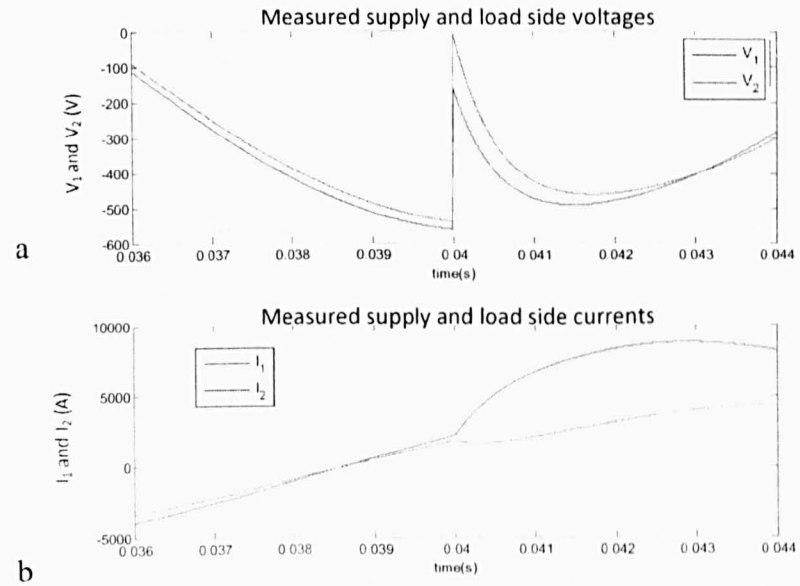

a

b

Figure 6.18 Measured waveforms including both steady and transient information

a) Measured voltages b) Measured currents

Short circuit faults with 0.1Ω fault resistance were imposed in the system at 5m intervals at 0.04s. An 8ms data length with the fault transients located in the middle needs to be processed with a FFT. Similar to the single-ended method, the data is windowed and zero-padded before being processed.

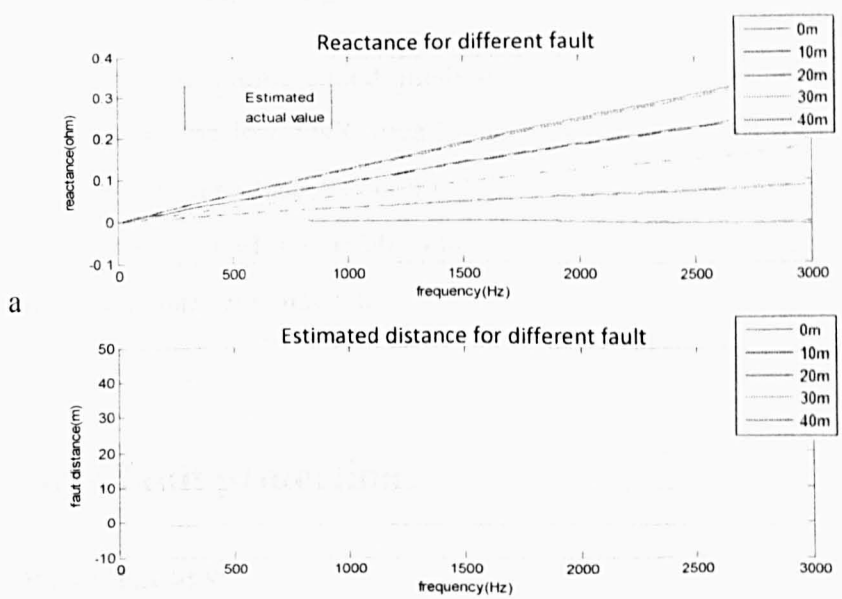

a

b

Figure 6.19 Double-end fault location results in marine system

a) The measured line reactance b) Fault distance results

In Figure 6.19 a), faults within the protection zone (40m) are located after being detected. Although a small amount of the transient current flows into the load in the middle of the protection zone, this does not have much influence on the accuracy of the estimated results. The cable impedance in different zones varies, but as long as the per-meter value of the cable impedance and the cable numbers that each zone has is known, by using a similar logic as that used in the single-ended protection method, the fault distance to CB2 can be derived as shown in Figure 6.19 b).

For other zones, the location scheme is used in the same manner as discussed in this Section. Unlike the single-ended method, the fault transients are measured from both ends so that the position and number of the generators do not affect the required location of transducers when applying the double-ended algorithm.

The fault resistance is not considered during the line impedance calculation. A fault with an extremely high fault resistance (10Ω) will not be detected as a fault because its fault resistance value is almost 4 times the largest load impedance for all the zones. However, this double-ended algorithm can still locate the fault position accurately.

Compared with the single-ended method, the double-ended method offers better accuracy in the low SNR situation (transients generated by faults have fault inception angles close to zeros). However, it requires the information from the remote end of the cable and this means more transducers and a communication channel is needed.

6.5 Earth fault protection

6.5.1 Basic theory

For a system with unearthed loads and a generator connected to earth through large impedance, the first earth fault should not cause any large short circuit current to damage the system equipment. However, if the first ground fault is

not removed immediately, second earth fault may create a short circuit loop with the first fault and may produce a high current.

Earth fault protection in a high impedance earthed system is not commonly considered. Because system operation is not interrupted, it is difficult to detect an earth fault in such a system by monitoring the line voltage and current information. Since there are no obvious fault transients, the two proposed passive fault location methods do not work here. In order to eliminate the potential over current danger, an active way of fault location method which creates little change or disturbance to the existing system will be discussed.

In an example system, as shown in Figure 6.20, the three-phase AC voltage source is connected to earth through the earth impedance Z_{Earth}. The earth impedance is much larger than the other system impedances including the three phase supply impedances right after the voltage source, the two sections of line impedances for each phase and the load impedances.

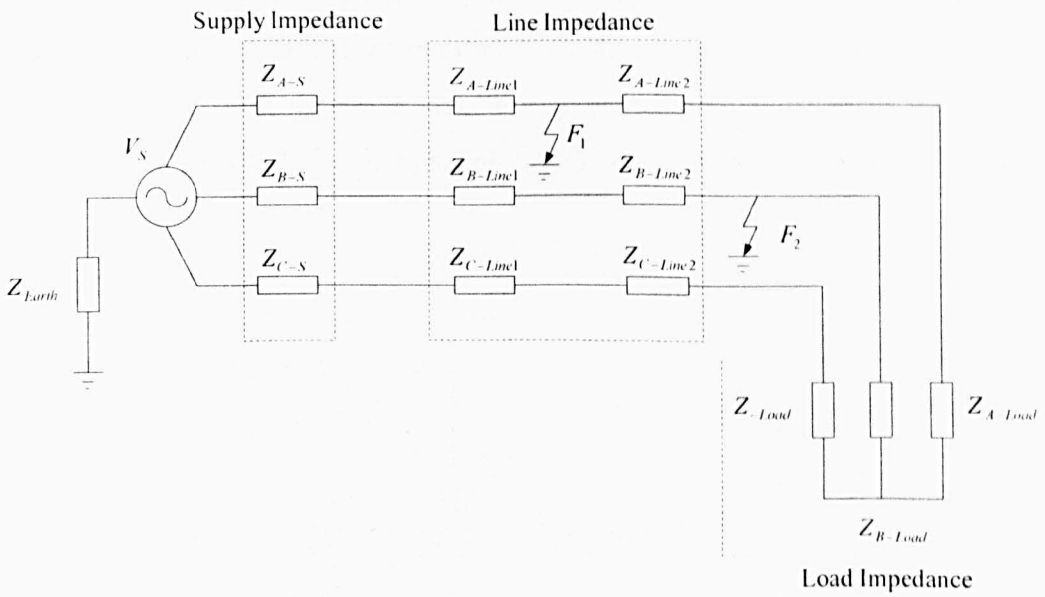

Figure 6.20 The model of three power system with large earth impedance

When the first ground fault (F_1) occurs, the fault current is small because of the earth impedance. If there is a second ground fault (F_2) imposed on the transmission line in the same phase with the first fault, the fault current within the new fault loop which contain both ground faults is small because the voltage drop along the distribution line is small and this newly generated fault

current does not harm the rest of the system. If the second fault exists in any of the other two phases, for example the fault on the phase B (F_3), the fault current will be large and could do harm to the system. The key point of the protection scheme is to detect and locate the first ground fault when it occurs so that it can be removed quickly to stop the high ground fault current damaging the system when another ground fault occurs. The detection of the first fault does not trip the circuit breaker and this keeps the load supply continuous without requiring the load changing operation.

The first ground fault (F_1) can be detected by continuously monitoring the earth current at the generator side. During the healthy state, this current is zero in a balance three phase system. When a ground fault occurs on the distribution line, a small current value can be detected and the faulted phase can be selected by monitoring the phase voltage (voltage sag detection).

Once the current flowing into the earth of the generator side is detected, after 2ms (to let the small transient of the first ground fault die out) another resistance R_{switch} which is in parallel with the Z_{Earth} is switched on to the ground line of the generator to create a larger current transient in the short circuited loop in which the first ground fault is included as in Figure 6.21.

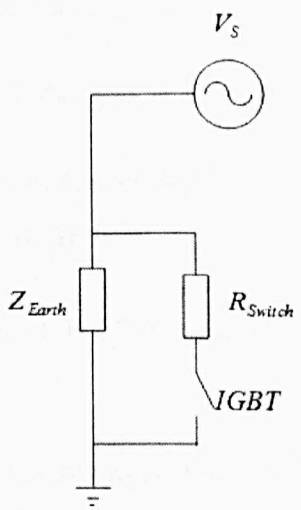

Figure 6.21 Switch on R_{switch} after earth fault occurs

The current transient (I_{Switch}) which contains high frequency information in the frequency domain is generated by the switching of R_{switch} and it then acts as a current source in the faulted loop which can be used for fault location

calculation. In order to switch on R_{switch} and also at the same time create as small disturbance as possible to the system, R_{switch} is selected carefully to make sure that the peak value of I_{Switch} is smaller than the healthy state system current and lasts less than 8ms. Considering the non-system power frequency range, in the power system model described in Figure 1, during the operation of the switching, the system generator is short circuited and I_{Switch} is a current source for the circuit as depicted in Figure 6.22.

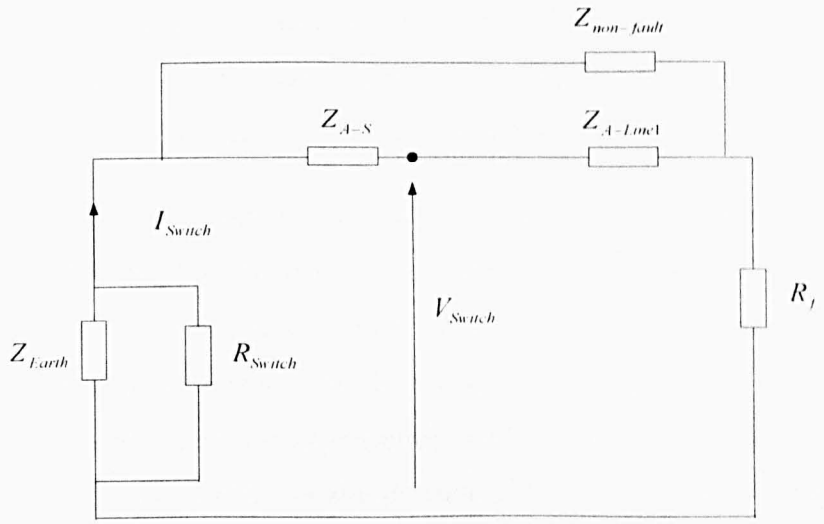

Figure 6.22 Consider the I_{Switch} as current source at non-system frequency

For the circuit in Figure 6.22, the $Z_{non-fault}$ is described by equation (6.2)

$$Z_{non-fault} = Z_T + Z_{A-Load} + Z_{A-Line2} \tag{6.2}$$

where Z_T is the paralleled impedances from the un-faulted phases during the first fault (F_1) as in equation (6.3)

$$Z_T = (Z_{B-S} + Z_{B-Line1} + Z_{B-Line2} + Z_{B-Load})//(Z_{C-S} + Z_{C-Line1} + Z_{C-Line2} + Z_{C-Load}) \tag{6.3}$$

Considering $Z_{non-fault}$ is much larger than $(Z_{A-line1} + Z_{A-S})$, the current flowing into it is neglected. The distance between the phase voltage measurement point (V_{Switch}) and the fault position can be calculated as

$$x = \frac{Imag(\frac{V_{Switch}}{I_{Switch}})}{X_{per-meter}} \tag{6.4}$$

where $X_{per-meter}$ is the per-meter value of the line reactance.

6.5.2 Demonstration in a single zone marine system

The proposed earth fault Location method is proved by the demonstration in one zone (zoneA) of the marine system with the generator located at the start of the zone distribution bus. The generator is modelled by a three phase voltage source which is connected to earth by a 260Ω resistor. The R_{switch} is switched on by an IGBT. The system supply impedances, cable impedances and the load impedances are the same as described in previous sections.

The system healthy working state current is about 400A (peak). During an earth fault situation, the monitored earth current at the generator side is about 1.5A peak and this value has a small variation for different fault resistances (from 0Ω to 10Ω) at different positions because of the larger earth resistor (260Ω). The fault detection current threshold is set to be 1.2A positive. After 2ms, the IGBT switch receives the positive gate signal for switching on, the voltage across it is positive. By doing this, it is able to avoid the situation that the IGBT is switched on at the zero-crossing of the fault current (in this case the transient is small or zero, the SNR may not high enough to provide accurate results).

When the phase to ground fault occurs at 10m on the distribution line with a 0.5Ω fault resistance, a 30Ω R_{switch} is switched (using IGBT) in parallel with the 260Ω earth resistor. The IGBT switching takes place 2ms after the detection of the ground fault. The measured current I_{Switch} and voltage V_{Switch} in time domain are presented in Figure 6.23.

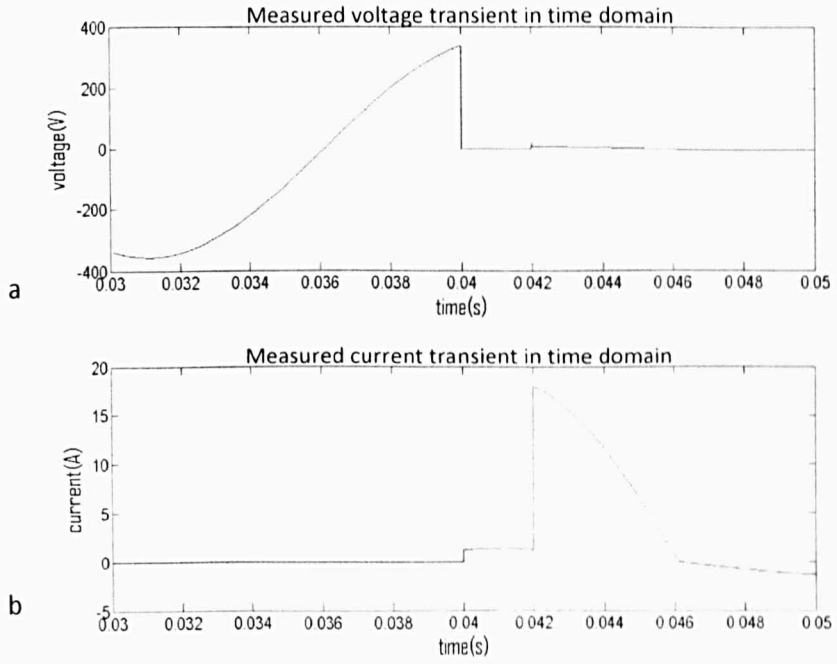

Figure 6.23 The measured V_{Switch} and I_{Switch}

a) Voltage transient in time domain b) Current transient in time domain

As shown in Figure 6.23, a short circuit ground fault is imposed on the transmission line at 0.04s and 2ms later the IGBT is switched on and the positive gate signal lasts 6ms. The data acquisition units start working 1ms after the detection of the fault (at 0.041s) and last 9ms. The 9ms data of the current transient and voltage transient caused by the IGBT switch are Blackman windowed and zero-padded and transformed into the frequency domain using an FFT giving the results shown in Figure 6.24.

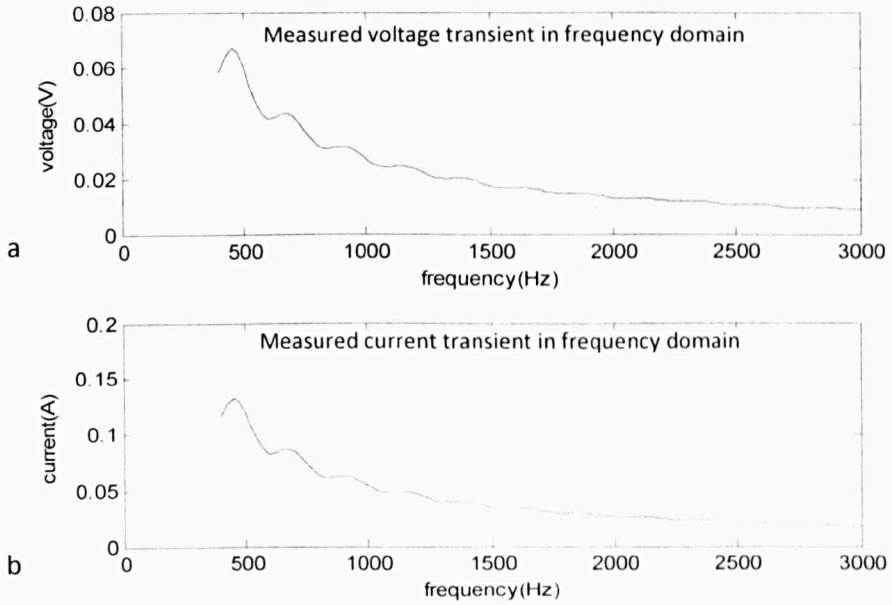

Figure 6.24 The rms value of transients presented in frequency domain

a) Voltage transient in frequency domain b) Current transient in frequency domain

As expected, in Figure 6.24, the voltage and current transients in the frequency domain which are created by the switching of the IGBT (0.042s in time domain) are influenced by the smaller transient caused by switching off the IGBT (0.046s in time domain in Figure 6.23). This oscillation within the waveforms has little influence on the estimated reactance results after being processed with a linear least square curve fitting as shown in Figure 6.25.

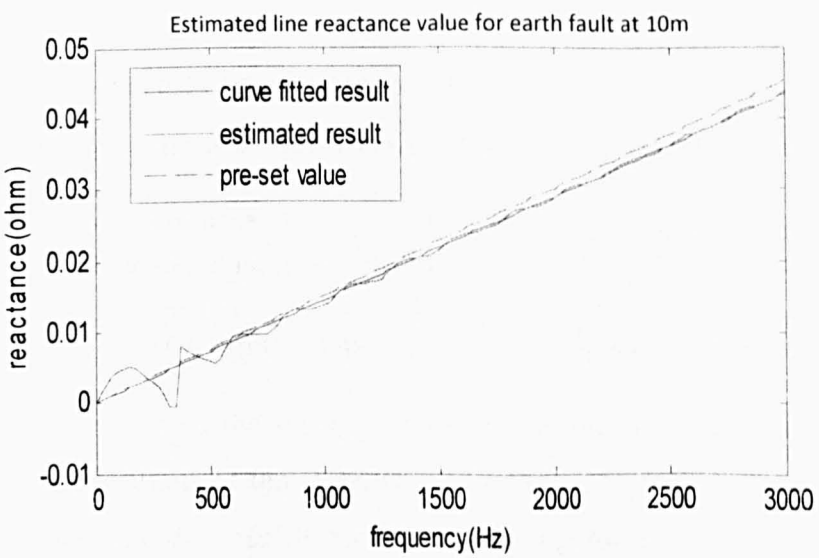

Figure 6.25 Estimated results and the pre-set value

The dashed line in Figure 6.25 is the pre-set value of line reactance between voltage measurement point and the fault position in the simulation. The solid line with oscillation is the one calculated by using equation (6.3) and the straight solid line is the results after linear least squares curve fitting. Compared with the pre-set value, the calculated line reactance has a small error which is caused by the system impedance $Z_{non-fault}$ as described in equation (6.2). The estimated distance from the voltage measurement point is 9.65m, and compared the real fault distance (10m) the error is small and within the accuracy requirement of 1m. As for the ground faults at other positions of the transmission line (0m and 20m), the estimated value compared with the actual value is shown in Figure 6.26.

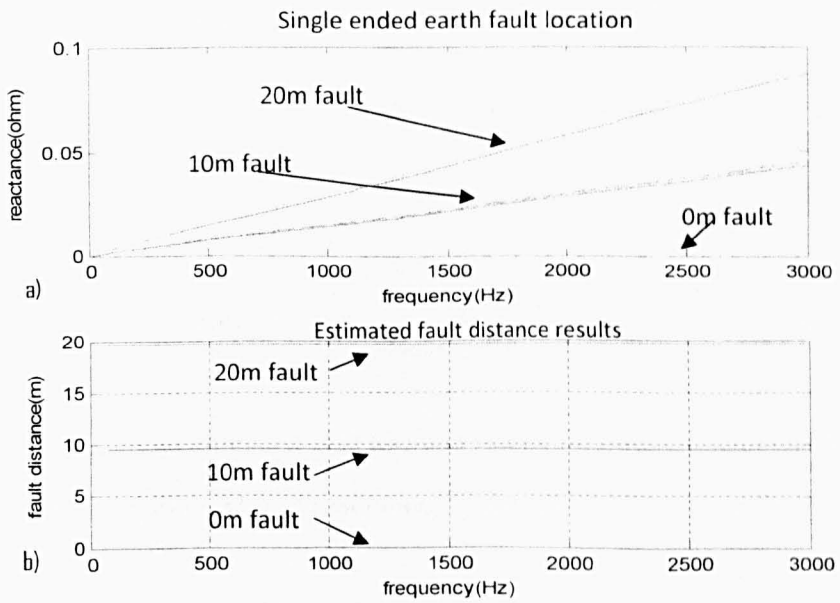

Figure 6.26 The estimated results of different fault position

a) Results of estimated line reactance b) Results of estimated fault distance

Actual distance (m)	0	10	20
Estimated distance(m)	0.12	9.65	19.43
errors%	0.6	1.75	2.85

Table 6.6 Errors within single-ended earth fault location

Figure 6.26 a) shows the change of estimated line reactance for different ground fault positions at 0m, 10m and 20m. The accuracy is good and after transfer it into the distance of each fault locating estimation by dividing the

values it with per-meter length cable reactance, the results are shown in Figure 6.26 b). The small error for each fault location is shown in Table 6.6.

The proposed fault location method is not influenced much by the variation of the fault resistance. Figure 8 shows the results when ground fault is imposed at 10m of the cable with fault resistance varying from 0Ω to 10Ω by 0.2Ω each step.

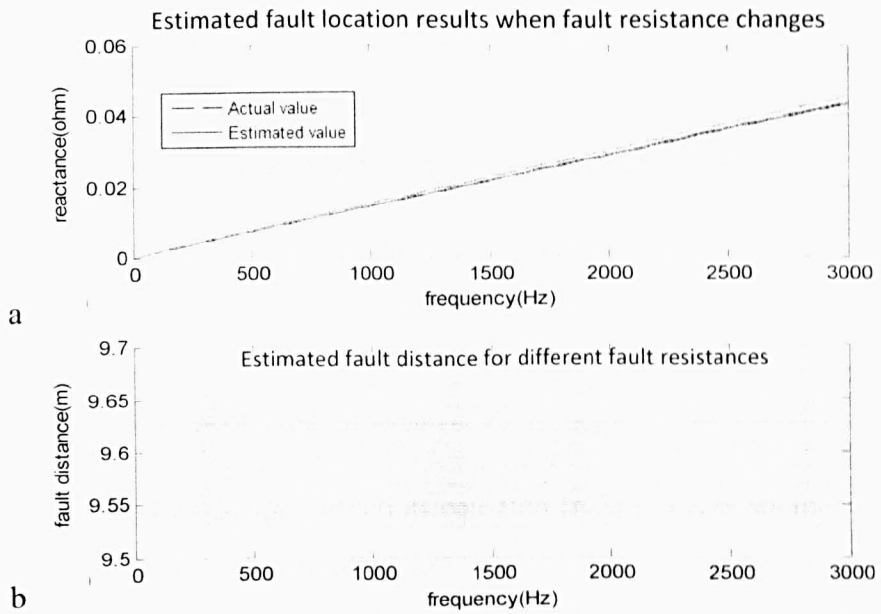

Figure 6.27 The estimated fault location results for different fault resistance

a) Results of estimated line reactance b) Results of estimated fault distance

As shown in Figure 6.27 b, the error of the estimated fault distance increases with the fault resistance because of the lower SNR and even with a 10Ω fault resistor, the accuracy of the estimated results still meets the requirement. R_{switch} is in the resistance range of 0.4Ω to 75Ω in this system to maintain the peak value of switched current transient lower than the system current and at the same time to offer a 1m accuracy when added with 0.1Ω fault resistance. Smaller R_{switch} will lead to higher SNR, but the resistor that has higher power rate increases cost of fault location. The R_{switch} has to be chosen by considering both the cost and the current distortion in the typical system.

The proposed method not only locates the fault position but also calculates the value of fault resistance which may be useful for the fault classification and system restoration. Once the fault distance (x) is known, using the real part of the equation (6.4), the fault resistance R_f can be estimated by equation (6.5).

$$R_f = Real\left(\frac{V_{Switch}}{I_{Switch}}\right) - x \cdot R_{per-meter} \tag{6.5}$$

where $R_{per-meter}$ is the cable resistance value in per-meter length.

6.5.3 Demonstration in the six-zone marine system

For a single zone of the marine system, the estimated results are accurate enough to locate the fault position. However, the proposed marine system has six zones, as shown in Figure 6.8. The line reactance estimation will be influenced by the neglected impedance $Z_{non-fault}$.

The impedance $Z_{non-fault}$ given in equation (6.2) is much smaller in the six-zone system than in the single zone situation when six loads are connected in parallel. This leads to a larger error in the fault distance estimation. The total length of the distribution line within the 6 zone system is 100m. When the ground fault is imposed at each 10m of the transmission line, the error caused by the six paralleled loads can be as high as 29% in Table 6.7.

Fault distance (m)	0	10	20	30	40	50	60	70	80	90	100
Estimated(m)	0	7.81	16.54	26.41	28.45	35.74	45.56	54.26	62.14	70.12	78.21
Errors%	0	21.9	17.3	11.967	28.875	28.52	24.067	22.486	22.325	22.089	21.79

Table 6.7 Fault location results for situation that all the six loads are working

The modification for this large error situation could be that when the ground fault is detected, within the next 10ms, the large loads are switched off (loads with small load impedance) to calculate the fault position and then switch on again. 10ms disconnection will not cause damage to the load and not all loads need to be switched off at the same time.

Actual distance (m)	0	10	20	30	40	50	60	70	80	90	100
Estimated distance(m)	0	9.86	19.76	29.69	39.65	49.6	59.6	69.57	79.52	89.49	99.49
errors%	0	0.14	0.24	0.31	0.35	0.4	0.4	0.43	0.48	0.51	0.51

Table 6.8 Fault location results for situation that load in zone1 is working

Actual distance (m)	0	10	20	30	40	50	60	70	80	90	100
Estimated distance(m)	0	9.78	19.52	29.48	39.17	49.1	59.01	68.85	78.76	88.38	98.13
errors%	0	0.22	0.48	0.52	0.83	0.9	0.99	1.15	1.24	1.62	1.87

Table 6.9 Fault location results for situation that loads in zone1 and zone6 are working

Table 6.8 and Table 6.9 show the estimated fault distances compared with the actual ones when different loads are connected. Only loads with small load impedances have to be disconnected for the 10ms fault location estimation time to meet the required one metre accuracy. Normally the loads with small impedances (large power rating) are the essential loads which should be switch to the other healthy bus or the energy storage unit by BIU once the earth fault is detected.

In order to utilize the proposed ground fault protection method in the discussed marine system or any other distribution system and also to achieve 1m accuracy for the whole protected cable, the ratio of the load impedance over cable impedance at the system frequency has to be larger than 83.24 (this value is derived by repeating the test of different ratios of load impedance over cable impedance under the condition of 1m fault location accuracy) so that the influence of the impedance $Z_{non-fault}$ can be ignored.

For the described zonal marine system with generator ground connected through a large resistor, the proposed ground fault protection method eliminates the potential harm to the system (damage caused by the second ground fault) by using the simple IGBT switch equipment which causes small disturbance to the system. This ground fault protection scheme offers advantages such as small time consumption (within 10ms), no non-detection zone, R_f estimation (helps during the later fault removing) and only one set of voltage transformer and current transformer is needed. The advantages

described above makes the fault protection method easy to be utilized in a real distribution system.

6.6 Summary

This chapter introduced the zonal marine power system with IPS and compared it with the conventional ship system. The possibility of utilizing the proposed single-ended and double-ended fault location methods for the protection of a zonal marine power system is discussed. The single-end method works independently in each zone without requiring any communication equipment. The double-ended method can cover two zones and provide more accurate results and is more robust to different fault situations. Both methods can be used to locate the fault and protect the system. They can be chosen according to different system protection requirements.

The active earth fault detection and location method is discussed as well to eliminate the potential danger that a double earth fault can cause to a high impedance ground system. When it came to the situation that the single ground fault has very small transients, the two proposed passive methods do not work. A simple IGBT switch is added to the supply earth impedance to generate transients as an excitation source for the impedance estimation. The method is demonstrated in a singe-zone system and the limitations of employing this method for a six-zone marine system are presented.

Chapter 7

Conclusions and future work

7.1 Research objectives

The research project mainly focused on developing fast and accurate impedance based fault location schemes which can be utilized in small distribution systems (vehicular IPS) for quick system repair and recovery in the event of short circuit faults. The main objectives of the thesis which are introduced in Chapter 1 are summarised as:

1. Develop a fast and accurate single-ended fault location method based on system impedance estimation using fault transients.

2. Develop a fast and accurate double-ended fault location method based on system impedance estimation using fault transients as an alternative option for applications according to different fault conditions.

3. Evaluate the proposed single-ended and double-ended algorithms according to different system conditions and fault conditions.

4. Apply the proposed fault location schemes into the protection of a zonal marine power system and also solve the earth fault location problem when the system generator is connected to earth through large impedance.

7.2 Conclusions

Passive impedance based fault location methods are commonly considered to have a smaller signal to noise ratio (SNR) than active methods. For a cable distribution system, the short circuit faults caused by insulation failure or damage from an outside force normally have small fault impedances and can create very large transients in both voltage and current waveforms. If the fault transients can be directly used as an excitation source for impedance measurement to predict the fault locations, then the low SNR problem for the passive methods could be solved.

7.2.1 Objective 1

An impedance based fault location method which directly uses the measured fault transients in the current and voltage waveforms from one end of the distribution cable was developed in chapter 3. The singled-ended algorithm assumes that the voltage fault transient is a step waveform during the fault situation and uses an iteration method to reduce the error between the assumed step voltage using measured pre-fault voltage and the actual fault step voltage at the fault point. The method was validated by experimental test and the results show very good accuracy (error within 1m for the 21m cable system) in both an AC and a DC system with both linear and non-linear loads. The fault location process can be completed within 6ms after faults occur and compared with the traditional schemes which use steady state measurements and normally require data of few cycles, it is much faster.

7.2.2 Objective 2

The assumption used for the single-ended method may not be true for a bouncing fault which may have oscillations in the fault transients and this will cause errors in the fault estimations results. An alternative passive method which uses the voltage and current transients from both ends of the distribution cable was developed in chapter 4. The double-ended algorithm which requires the remote end measurement information offers better fault location results for the same fault situations as investigated by the single-ended method but more importantly it gives good results in the situation of a bouncing fault and high impedance fault within the same fault location time (6ms after the fault occurs).

7.2.3 Objective 3

Influenced by the limitation of the experimental equipment the proposed two fault location methods were tested with a low voltage supply level and high impedance fault conditions in the experimental cable system. Software simulation in chapter 5 investigated the fault situations which are close to a real distribution system to get confidence that the simulation can provide more results than the experimental rig with the same parameters. Both methods work better in the high voltage and low fault impedance system where larger fault transients are generated. The two proposed fault location algorithms have a small 'non-location zone' (double-end method offers a smaller non-location zone for the same fault conditions) due to the very small or zero fault transients when the fault inception angle is close or equal to zero and the small possibility of a non-detection zone can be reduced by using the transients generated by circuit breaker reclosing. Without any assumptions (as used for the single-ended method), the un-synchronized measurement from both ends may introduce errors to the double-ended method and this problem can be solved by using a Newton Raphson iteration method as discussed in the chapter 5.

7.2.4 Objective 4

The two proposed fault location methods were used in the protection of a zonal marine power system in the case of phase to phase faults in chapter 6. The single-ended algorithm accompanied with an over-current strategy works well in each zone while the double-ended method equipped with a current-differential scheme can detect and locate faults fast and accurately within two zones. The phase to ground fault in the proposed marine system which has the generator connected to earth through a high value of earth impedance cannot be accurately located. An active algorithm which involves adding a switch to the earth impedance was suggest to eliminate the potential danger of larger current being induced by the second earth fault. The active method suggested can cover 6 zones with predictable small errors in the estimated fault location results.

7.3 Future work

The proposed double-end and single-ended fault location algorithms were validated by computer simulation and experimental test on a simplified distribution system. They now need to be investigated in more detail for specific applications. In particular, the effect of power system elements such as capacitors, filters, PWM power converters and other power electronic devices, as well as noise (data acquisition) need to be considered.

7.3.1 Future investigation in marine system

Further investigation will focus on employing the proposed fault location schemes in a marine power system with more PWM converters which not only causes voltage and current discontinuity but also introduces high frequency noise from their switching components. The electric ship system will be simulated in more detail to assess the evaluation of the fault location method from a more realistic point of view.

An experimental validation on a more realistic ship demonstrator which includes distribution parameters rather than lumped parameters is a good option. For example, the power supplied by a generator and DC inverter based source, transmitted by the type of cable used in a real marine system and distributed to loads with constant power controls should be investigated. A study on how to control and combine the proposed fault location algorithm with the already existing over-current [128] or current differential [129] algorithm and a Bus Interface Unit (BIU) into one integrated protection scheme needs to be carried out. The operation time of BIU, the average speed of fault detection and the accuracy of fault location of the new integrated protection need to be fully evaluated. The active method for earth fault location will be investigated in a new marine system demonstrator as well. The influence of distributed energy storage around the system should also be considered.

7.3.2 Application for arc fault

Arc faults appear in distribution systems. There are two possible kinds of arc faults. Parallel arc faults occur between two phases, or phase and ground, and are often a result of degrading insulation or contamination. Series arc faults may be a result of loosening screw rivet connections in a bus bar [130]. A high current level arc fault can be detected by an over-current relay and once the power supply is stopped by circuit breaker, the arc is extinguished. In distribution systems, especially in the cable IPS of MEVs, the arc fault has a low fault current which can be demonstrated using laboratory equipment [131][132]. Although it may not have a high fault current, the arc current can seriously damage cables, switchgear and components. Heat generated from the arc can completely destroy the metallic terminals of connectors as presented in [131]. Low arc fault current are distinguished and re-ignited at the current-zero point which gives a unique discontinuous gap in the current waveform and the fault normally can be detected by comparing the frequency characteristics of the fault current with the normal operating current[130] [133].

The proposed single-ended method was based on the assumption that the fault voltage waveform is a step. In the case of an arc fault, the waveform of the fault voltage transient is discontinuous or oscillating. The possibility of using the single-ended method for locating the arc fault, which may act as a high impedance fault, needs to be investigated in the future.

Parallel arc faults (arc between phases), once detected, can be located by using the double-ended method which uses the transient of the arc current and voltage waveforms similar to the bouncing short circuit fault with a high fault impedance. Due to the fact that the transients generated by arc faults are smaller, a longer data measurement window may be required to produce a good SNR. Although there are no official analyses available, it is widely assumed that the series arc faults (arc fault on a particular phase) occur more often than parallel arc faults [130]. However, the proposed double-ended algorithm can not work for locating the series arc faults by directly using the fault transients. The double-ended method has to be modified and future research work is required to locate the series arc fault.

7.3.3 Application in EHV transmission lines

Extra High Voltage (EHV) transmission lines are designed to transfer a large amount of electrical power from power generation sources to regional load areas or adjacent power systems over a long distance with high voltage levels (in order to reduce the energy losses due to the long distance transmission)[125]. The long exposed transmission lines are prone to short circuit faults.

The main challenge to apply the proposed fault location algorithm into EHV transmission line in future work is the line capacitance. Beside the line capacitance caused by the distance between line and the earth, series and shunt capacitor banks are frequency installed in the long power transmission lines to reduce the total line impedance and reactive power compensation, thereby reducing the system loss and increase the system stability[126][127]. The existence of large amount of capacitance in the system will result in a longer

time fault transient. Within the proposed fault location time, the fault transients may not be fully captured which may lead to inaccuracy in certain frequency ranges and also the changing of line impedance characteristic (in proposed vehicular IPS system line capacitance is neglected) may cause error in the line impedance calculation results.

The second challenge is that the EHV transmission line is connected to the power supplies and the loads through step-up and step-down transformers. The larger reactance may attenuate the transient information received from the measurement point. Also both the single-ended and double-ended scheme has a non-location zone which may be enlarged in an AC system with its voltage and current waveform distorted by non-linear loads. The non-location zones have to be considered according to the requirement of the protection reliability.

7.3.4 Application in off-shore wind farm distribution system

In UK, the government aims to increase the renewable energy sources up to 20% (40% in Scotland) of total energy production by 2020. It is projected that the increase in renewable energy share from the present 3% will be largely based on increase in wind energy generation, which is likely to become one of the main source of renewable energy in UK and in many other countries [134][135]. Because of the economy of scale and increasing energy demand, wind farms will have larger capacity in the future. As of November 2010, the Thanet Offshore Wind Project in United Kingdom is the largest offshore wind farm in the world at 300 MW, followed by Horns Rev II (209 MW) in Denmark[137]. At the start of 2011, the installed capacity of wind power in the United Kingdom was over 5.2 GW [138] and the UK is ranked as the world's eighth largest producer of wind power. Wind power is expected to continue growing in the UK for the foreseeable future and 'Renewable UK' estimates that more than 2 GW of capacity will be deployed per year for the next five years [139].

Due to the environmental and social aspects, the off shore wind farm rated at 100-500MW has a distance of 100-150km from the shore [136] and the

connection of the wind farm to the on shore grid is carried out by HVDC links (because of the capacitance of submarine cables, and the corresponding high reactive currents, the HVAC is avoided) [140]. The cost of removing and repairing faults on these submarine transmission lines could be very high without knowing the exact fault locations. A fast and accurate fault location algorithm is needed for the protection of submarine HVDC transmission lines.

The proposed methods have the advantage on an HVDC system that there will not be a non-location zone when the voltage is close to zero. However, for employing the proposed fault location method in the HVDC transmission line as future work, the challenges have to considered are: firstly, the large capacitance exists on transmission line. Normally capacitor filtering banks are installed at the two ends or in the middle of the transmission lines. Secondly, the behaviour of the power supply. Wind farms commonly use double fed induction generators with filter banks and the reaction of the capacitive supply according to faults has to be considered. Thirdly, the HVDC links have controlled converters such as the voltage source converters and the STATCOM for line voltage and frequency regulation. Voltage drops on the transmission line will be compensated. For the proposed methods which use fault transients a fast fault location which could be completed before the proceeding of the voltage correction is required.

Reference

[1] S. Onoda, S. M. Lukic A. Nasiri and A. Emadi, "A PSIM-vased modelling tool for conventional, electric, and hybird electric vehicles studies," *IEEE* 56th Vehicular Technology Conference, October, 2002.

[2] Ali Emadi, Mehrdad Ehsani, John M.Miller, *Vehicular electric power systems,* New York. Basel Publishers, ISBN 0-8247-4751-8, January,2004.

[3] C Christopoulos and A Wright, *Electrical power system protection,* Kluwer Academic Publishers, ISBN 0-412-81760-8, February, 1999.

[4] L. G. Andersson, Carl Ohlen, Wolfgang Wimmer, Ivan de Mesmaeker and T. Jones, "The intelligent protection, control and monitoring terminal," Fifth International Conference on Developments in Power System Protection, July, 1993.

[5] C.Booth, G.Dudgeon, J. R. McDonald, A. Kinson, and J. Hill, "Protection of modern marine power systems: challenges and solutions," Eighth *IEE* International Conference on Developments in Power System Protection, June, 2004.

[6] C. D. Booth, I. Elders, A. Mackay, J.D. Schuddebeurs and J. R. McDonald, "Power system protection of all electric marine systems", *IET* 9th International Conference on Developments in Power System Protection, April, 2008.

[7] J wang, P Kadanak, M Sumner, DWP Thomas and R DGeertsma, "Active fault protection for an AC zonal marine power system architecture," *IEEE* Industry Applications Society Annual Meeting, January, 2008.

[8] K. J. Payne, "Electrical characteristics and protection of aircraft power systems," Proceedings of the *IEE* - Part A: Power Engineering, December, 2008.

[9] A. Lucken, J. Brombach and D. Schulz, "Design and protection of a high voltage DC onboard grid with integrated fuel cell system on more electric

aircraft," Electrical Systems for Aircraft, Railway and Ship Propulsion (ESARS), January,2010

[10] D. Lzquierdo, A. Barrado, C. Raga, M. Sanz, P. Zumel and A. Lazaro, "Protection devices for aircraft electrical power distribution systems: a survey," 34th Annual Conference of *IEEE* industrial Electronics, January, 2008.

[11] Crook, J, "Electric propulsion for future carriers," *IEE* Power Engineer, November, 2003.

[12] F. Feudale, P. Bordignon, C. Ferrero and P. Castangia, "Tradition and innovation in ship electrical component and systems," SPRTS Ship Propulsion and Railway Traction Systems Conference, Bologna (Italy) October, 2005

[13] USN, N.H.D. and J.C.D USN, "Integrated power system for marine applications," Naval Engineers Journal, January, 1994.

[14] DADE, R.B., "Advanced electric propulsion, power generation and power distribution," Naval Engineers Journal, January, 1994.

[15] Giuseppe CalaBrese, "Performance of distance relays", *IEEE Transactions of the American Institute of Electrical Engineers*, Vol. 4, June, 2009.

[16] W. A. Lewis and L. S. Tippett, "fundamental basis for distance relaying on 3-phase systems", *IEEE Transactions of the American Institute of Electrical Engineers*, December, Vol. 2, 1947.

[17] D. W. P. Thomas, C. Christopoulos, Y. Tang, and P. Gale, "A single ended fault location scheme," *IEEE* Seventh International Conference on Developments in Power System Protection, Amsterdam, Netherlands, April, 2001.

[18] M. EL-Hami, L. L. Lai, D. J. Daruvala and A. T. Johns, "A new travelling-wave based scheme for fault detection on overhead power distribution feeders", *IEEE Transactions on Power Delivery*, Vol 7, July, 2001

[19] M. Aurangzeb, P. A. Crossley, and P. Gale, "Fault location using the high frequency travelling waves measured at a single location on a transmission

line," In Seventh *IEE* International Conference on Developments in Power System Protection, Amsterdam, Netherlands, November, 2001.

[20] P. F. Gale, J. Stokoe, and P. A. Crossley, "Practical experience with travelling wave fault locators on scottish power's 275 & 400 kv transmission system," In Sixth *IEE* International Conference on Developments in Power System Protection, March 1997.

[21] F. Eickhoff, E. Handshicn, and W. Hoffmann, "Knowledge based alarm handling and fault location in distribution networks," *IEEE Transactions on Power Systems*, Vol. 2, October, 1992.

[22] M. Kezunovic, "Intelligent systems in protection engineering," *IEEE* International conference on Power System Technology, PowerCon, Perth, Australia, April, 2000.

[23] S. S. Mohamed, E. F. El-Saadany, T. K. Abdel-Galil, and M. M. A. Salama, "ANN- Based technique for fault location estimation using TLS-ESPRIT," *IEEE Transactions on Power Delivery*, Vol. 7, October, 1992.

[24] K. R. Cho, Y. C. Kang, S. S. Kim, J. K. Park, S. H. Kang and K. H. Kim, "An ANN based approach to improve the speed of a differential equation based distance relaying algorithm," *IEEE Transactions on Power Delivery*, Vol. 14, April, 1999.

[25] K. M. EL-Naggar, "A genetic based fault location algorithm for transmission lines," *IEEE* 16th International Conference on Electricity Distribution, Amsterdam, Netherlands, June, 2001

[26] L.V. Bewley. *Traveling wave on transmission systems,* 2n Edition. Constable and Company, October, 1933.

[27] M. B. Hughes, R. W. Leonard and T. G. Martinich, "Measurement of power system subsynchronous driving point impedance and comparison with computer simulation," *IEEE Transactions on Power Delivery*, Vol. 3, No. 3, February, 1993.

[28] Daniel Crevier and Andre Mercier, "Estimation of higher frequency network equivalent impedances by harmonic analysis of natural waveforms," *IEEE Transactions on Power Delivery*, Vol.7, September, 1996.

[29] D. T. Rizy, E. W. Gunther and M. F. Mcgranaghan, "Transient and harmonic voltages associated with automated capacitor switching on distribution systems," *IEEE Transactions on Power Delivery*, Vol. 2, August, 1998.

[30] A. S. Morched and P. Kundur, "Identification and Modelling of Load Characteristics at High Frequencies," *IEEE Transactions on Power Delivery*, Vol. 2, July, 2001.

[31] Adly A. Girgis and R. Brent McManis, "Frequency domain techniques for modelling distribution or transmission networks using capacitor switching induced transients," *IEEE Transactions on Power Delivery*, Vol. 4, June, 2007.

[32] M. Nagpal, W. Xu and J. Sawada, "Harmonic impedance measurement using three-phase transients," *IEEE Transactions on Power Delivery*, Vol. 13, March, 1997.

[33] E. Ahmed, W. Xu and X. Liu, "Application of medal transformations for power system harmonic impedance measurement," *IEEE* international journal of Electrical power and Energy System, December, 2004.

[34] Wilson Xu, Emad E. Ahmed, Xiqin Zhang and Xian Liu, "Measurement of Network Harmonic Impedances: Practical Implementation Issues and Their Solutions," *IEEE Transactions on Power Delivery*, Vol. 17, January, 2001.

[35] Diana V, Sumner M, Zanchetta P and Marinelli M, "Non-invasive power system impedance monitoring for improved power quality," *IEEE* Second International Conference on Power Electronics, Machines and Drives (PEMD), October, 2004.

[36] E. W. Palmer and G. F. Ledwich, "Three phase harmonic modelling of power system loads," *IEE Processing-C*, Vol. 140, December, 1992.

[37] A. de Oliveira, J. C. de Oliveira, J. W. Resende and M. S. Miskulin, "Practical approaches for AC system harmonic impedance measurement," *IEEE Transactions on Power Delivery*, Vol. 6, October 1991.

[38] Yao Xiao, Maun, J.-C., Mahmoud, H.B., Detroz, T., Stephane Do "Harmonic impedance measurement using voltage and current increments from disturbing loads," *IEEE* Ninth International Conference on Harmonics and Quality of Power, April, 2000.

[39] Matthew B. Harris, Arthur W. Kelley, Jason P. Rhode and Mesut E. Baran, "Instrumentation for measurement of line impedance," *IEEE* Ninth Annual Applied Power Electronics Conference and Exposition, October, 1994.

[40] Jason P. Rhode, Arthur W. Kelley and Mesut E Baran, "Complete characterization of utilization-voltage power system impedance using wideband measurement," *IEEE* Industrial and Commercial Power Systems Technical Conference, March, 1996.

[41] Jason P. Rhode, Arthur W. Kelley and Mesut E. Baran, "Line impedance measurement: a nondisruptive wideband technique," Thirtieth *IAS* Annual Meeting on Industry Applications Conference, September, 1995.

[42] Lesaek S. Czarnecki and Zbigniew Staroszczyk, "On-line measurement of equivalent parameters of distribution system and its load for harmonic frequencies," Instrumentation and Measurement Technology Conference, October, 1995.

[43] Lesaek S. Czarnecki and Zbigniew Staroszczyk, "On-line Measurement of Equivalent parameters for harmonic frequencies of a power distribution system and load," *IEEE Transactions on Instrumentation and Measurement*, Vol. 45. June,1996

[44] M. Tsukamoto, S. Ogawa, Y. Natsuda, Y. Minowa and S. Nishimura, "Advanced technology to identify harmonics characteristics and results of measuring," *IEEE* Ninth International Conference on Harmonics and Quality of Power Proceedings, April, 2000.

[45] Lucian Asiminoaei, Remus Teodeorecu, Frede Blaabjerg and Uffe Borup, "A new method of on-line grid impedance estimation for PV inverter," *IEEE* Applied Power Electronics Conference and Exposition, October, 2004.

[46] Adrian Vasile Timbus, Remus Teodorescu, Frede Blaabjerg and Uffe Borup, "On-line grid measurement and ENS detection for PV inverter running on highly inductive grid," *IEEE Power Electronics Letters*, Vol. 2, March, 1993.

[47] Lucian Asiminoasei, Remus Teodorescu, Frede Blaabjerg and Uffe Borup, "A digital controlled PV-inverter with grid impedance estimation for ENS detection," *IEEE Transactions on Power Electronics*, Vol. 20, June, 1998.

[48] Lucian Asiminoaei, Remus Teodorescu, Frede Blaabjerg and Uffe Borup, "Implementation and test of an online embedded grid impedance estimation technique for PV inverters," *IEEE Transactions on Industrial Electronics*, Vol. 52, March, 2000.

[49] Y. L. Familiant, K. A. Corzine, J. Huang and M. Belkhayat, "AC impedance measurement techniques," *IEEE* International Conference on Electric Machines and Drives, March, 2005.

[50] B Palethorpe, M Sumner and D W P Thomas, "System impedance measurement for use with active filter control," *IEEE* Eighth International Conference on Power Electronics and Variable Speed Drives, October, 2000.

[51] M. C. Di Piazza, P. Zanchetta, M. Sumner and DW P Thomas, "Estimation of load impedance in a power system," *IEEE* Ninth International Conference on Harmonics and Quality of Power Proceedings, November, 2000.

[52] Mark Sumner, Ben Palethorpe, David Thomas, Pericle Zanhetta and Maria Carmela Di Piazza, "Estimation of power supply harmonic impedance using a controlled voltage disturbance," *IEEE* Power Electronics Specialists Conference, October, 2001.

[53] Mark Sumner, Ben Palethorpe, David W. P. Thomas, Pericle Zanchetta and Maria Carmela Di Piazza, "A technique for power supply harmonic

impedance estimation using a controlled voltage disturbance," *IEEE Transactions on Power Electronics*, Vol. 17, No. 2, July, 2005.

[54] Mark Sumner, Ben Palethorpe, David W. P. Thomas, "Impedance measurement for improved power quality-part 1: the measurement technique," *IEEE Transactions on Power Electronics*, Vol. 19, February, 2006.

[55] Mark Sumner, Ben Palethorpe, David W. P. Thomas, "Impedance measurement for improved power quality-part 2: A new technique for stand-alone active shunt filter control," *IEEE Transactions on Power Delivery*, Vol. 19, October, 2007.

[56] Mark Sumner, Abdullah Abusorrah, David Thomas and Pericle Zanchetta, "Improved power quality control and intelligent protection for grid connected power electronic converters, using real time Parameter estimation," 41st *IAS* Annual Meeting on Industry Applications Conference, June, 2006.

[57] Mark Sumner, David Thomas, Abdullah Abusorrah and Pericle Zanchetta, "Power system impedance estimation for improved active filter control, using continuous wavelet transforms," 41st *IAS* Annual Meeting Conference on Industry Applications Conference, December, 2006.

[58] Math Works, T, MATLAB Reference Guide. The Math Works Inc. October, 2002.

[59] S. M. Kay, "Spectrum analysis-a modern perspective," Pro. *IEEE*, Vol.69, January, 1981.

[60] Tadeusz Lobos and Jacek Rezmer, "Real-time determination of power system frequency," *IEEE Transactions on Industrial and Measurements*, Vol. 46, No. 4, October, 1997.

[61] Leslie Balmer, *Signals and systems an introduction*, second edition, Prentice Hall press. March, 1998.

[62] Gwnilym M. Jenkins and Donald G. Watts, *Spectral analysis and its applications*, San Francisco, January, 1968.

[63] Robert, A. et al, "Guide for assessing the network harmonic impedance," Electricity Distribution. Part 1: Contributions. CIRED. 14th International Conference and Exhibition , October, 2007.

[64] Gilbert Strang and Truong Nyuyen, *Wavelets and filter banks*. Wellesley-Cambridge Press, December, 1996.

[65] Mertins, A., Signal Analysis: *Wavelets, filter banks, time-frequency and application*. John Wiley & Sons, July, 1999.

[66] Qian, S. and D. Chen, *Time frequency analysis: methods and applications*. Prentice Hall, June, 1996.

[67] Mallat. S. G, *A wavelet tour of signal processing*, San Diego; London: Academic Press, February, 1999.

[68] Math Works, T., *Matlab Help*. 7.2.0.232(R2006a) ed. December, 2006.

[69] André Luís Dalcastagnê, Sidnei Noceti Filho, Hans Helmut Zürn, and Rui Seara, "An iterative two-terminal fault-location method based on unsynchronized phasors", *IEEE Transactions on Power Delivery*, VOL. 23, March, 2008.

[70] D. W. P Thomas and C Christopoulos, "Ultra-high speed protection of series compensated lines" *IEEE Transactions on Power Delivery*, Vol. 7, October, 1992.

[71] D. W. P Thomas, Ricardo J. 0. Carvalho and Elisete T. Pereira, "Single and double ended travelling-wave fault location on a MV system," *IEE* International Conference on Developments in Power System Protection, October, 2004.

[72] D W P Thomas, C Christopoulos, Y Tang, P Galen and J Stokoe, "Single ended travelling wave fault location scheme based on wavelet analysis," Eighth *IEE* International Conference on Developments in Power System Protection, June, 2004.

[73] D W P Thomas, C Christopoulos, Y Tang and P Gale, "Validation of a novel unit protection scheme based on superimposed fault currents," *IEEE*

Seventh International Conference on Developments in Power System Protection, October, 2001.

[74] D.W.P. Thomas, R.J.O Corvalho, E.L. Pereira, "Fault location in distribution systems based on travelling waves," *IEEE* Power Tech Conference Proceedings, September, 2003.

[75] David Coggins, David WP Thomas, Barrie R Hayes-Gill, Yiqun Zhu, "An FPGA based travelling wave fault locaton," *IEEE* International Conference on Field-Programmable Technology, April, 2007.

[76] D.P Coggins, D.W.P Thomas, B.R Hayes-Gill, Y. Zhu, E.T. Pereirat and S.H.L. Cabralt "A new high speed FPGA based travelling wave fault recorder for MV distribution system," *IET* 9th International Conference on Developments in Power System Protection, January, 2008.

[77] T. W. Stringfield, D. J. Marihart and R. F. Stevens, "Fault location methods for overhead lines," Power Apparatus and Systems, Part III. Transactions of the American Institute of Electrical Engineers, October, 1957.

[78] T. Takagi, Y. Yamakoshi, J. Baba, K. Uemura, T. Sakaguchi, " A new alogrithm of an accurate fault location for EHV/UHV transmission lines Part I – Fourier Transformation method," *IEEE Transactions on Power Delivery*, Vol. 1, March, 1981.

[79] T. Takagi, Y. Yamakoshi, M. Yamaura, R. Kondow, T.matsushima, "Development of a new type fault locator using the one-terminal voltage and current data," *IEEE Transactions on Power Delivery*, Vol. 1, October, 1982.

[80] Leif Eriksson, Murari Mohan Saha, G. D. Rockefeller, "An accurate fault locator with compensation for apparent reactance in the fault resistance resulting from remote-end infeed," *IEEE Transactions on Power Delivery*, Vol. PAS-104, February 1985.

[81] A. T. Johns, S. Jamali, "Accurate fault location technique for power transmission lines," *IEE Processing S*, Vol. 137, November 1990.

[82] M. Kezunovic and B. Perunicic, "Automated transmission line fault analysis using synchronized sampling at two ends," Power Industry Computer Application Conference, 1995. Conference Proceedings, January, 1995.

[83] Damir Novosel, David G. Hart, Eric Udren and Jim Garitty, "Unsynchronized two-terminal fault location estimation," *IEEE Transactions on Power Delivery*, Vol. 11, December, 1996.

[84] Jan Izykowski, Rafal Molag, Eugeniusz Rosolowski and Murari Mohan, "Accurate location of faults on power transmission lines with use oftwo-end unsynchronized measurements," *IEEE Transactions on Power Delivery*, Vol. 21, October, 2006.

[85] A. L. Dalcastagne and S. L. Zimath, "A study about the sources of error of impedance-based fault location methods," *IEEE/PES* Transmission and Distribution Conference and Exposition: Latin America, November, 2008.

[86] Andre Luis Dalcastagne, Sidnei Noceti Filho, Hans Helmut Zurn and Rui Seara, "A two-terminal fault location approach based on unsynchronized phasors," *IEEE* International Conference on Power System Technology, October, 2006.

[87] Andre Luis Dalcastagne, Sidnei Noceti Filho, Hans Helmut Zurn and Rui Seara, "An iterative two-terminal fault-location method based on unsynchronized phasor," *IEEE Transactions on Power Delivery*, Vol.23, June, 2008.

[88] John Horak and Basler Electric company, "A derivation of symmetrical component theory and symmetrical component networks," *IEEE* the 59th annual Georgia Tech Protective Relay Conference Atlanta, Georgia, July, 2005.

[89] I. Zamora, J. F. Minambres, A. J. Mazon, R. Alvarez-Isasi and J. Lazaro, "Fault location on two-terminal transmission lines based on voltages," *IEE Proceedings-Generation, Transmission and Distribution*. VOL.143. October, 1996.

[90] Przemyslaw Balcerek and Jan Izykowski. "Improved unsynchronized two-end algorithm for locating faults in power transmission lines," *IEEE* Bologna PowerTech Conference, December, 2003

[91] M. Sumner, D. Thomas A. Abusorrah, L. Yao, R. Parashar, M. Bazargan, "Intelligent protection for embedded generation using active impedance estimation," 2nd *IEEE* International Symposium on Power Electronics for Distributed Generation Systems (PEDG), March, 2010.

[92] J. Wang, M. Sumner, DWP. Thomas, and R.D. Geertsma, "Fast fault detection and location for a marine power system using system power converters and active impedance sstimation," *IET* 9th International Conference on Developments in Power System Protection, October, 2008.

[93] Edward Christopher, Mark Sumner, David Thomas and Frans de Wildt, "Fault location for a DC zonal electrical distribution systems using active impedance estimation," Electric Ship Technologies Symposium (ESTS), March, 2011.

[94] Edward Christopher, Mark Sumner, David Thomas, Xiaohui Wang and Frans de Wildt, "Fault location in a zonal DC marine power system using active impedance estimation," *IEEE* Energy Conversion Congress and Exposition (ECCE), June, 2010.

[95] J. Wang, DWP. Thomas, M. Sumner and R.D. Geertsmat, "Fast fault detection and location of a zonal marine power system: using active impedance estimation developments in power system protection," *IET* 9th International Conference on DPSP, October, 2008.

[96] P. D. Hopewell, N. Jenkins and A. D. Cross, "Loss of mains detection for small generators," *IEE Proc-Electr. Power appl.* Vol. 143, July, 1996.

[97] P. O'Kane, B. Fox, "loss of main detection for embedded generation by system impedance monitoring," *IEE* Developments in Power System Protection, May, 1997.

[98] Oppenheim, A.V., and R.W. Schafer. *Discrete-time signal processing.* Upper Saddle River, NJ: Prentice-Hall, January,1999.

[99] Mitram Danjit Kumar, *Digital signal processing: a computer based approach*, New York: McGraw-Hill. May, 2011.

[100] Eland Cable's Datasheet Electrical Cable, SY Control Flexible Cable to BS6500, Eland Product Group A5J, 2001.

[101] 2.0 amp output current IGBT gate drive optocoupler technical data. Agilent Technologies. Innovation the HP way,2002.

[102] Hoang Nyguen. *High speed FPGA board design*. Master's thesis, School of Electrical and Electronic Engineering, The University of Nottingham, August, 2006.

[103] Y. Zhu. *User's guide to the high-speed USB interface*, May, 2005.

[104] David Coggins. *Single-ended travelling wave fault location on radial distribution line*. PhD's thesis, School of Electrical and Electronic Engineering, The University of Nottingham, August, 2010.

[105] Elisabetta Lavopa. *A novel control technique for active shunt power filters for aircraft applications*. PhD's thesis, School of Electrical and Electronic Engineering, The University of Nottingham, May, 2010.

[106] LCR Active Head and Impedance Analysis Interface. Newtons4h Ltd. http://www.newtons4th.com/wp-content/uploads/2010/02/LCRActiveHead-IAI1.pdf.

[107] Edward Christopher, Mark Sumner, David Thomas, Xiaohui Wang and Frans de Wildt, "Fault location in a zonal DC marine power system using active impedance estimation," *IEEE* Energy Conversion congress and Exposition (ECCE), June, 2010.

[108] F. Barruel, N. Retiere, J. L. Schanen and A. Caisley, "Stability approach for vehicle DC power networks: application to aircraft," *IEEE power electronics specialists conference*, November, 2005.

[109] M. Sauteruil, N. Retiere, D Riu and O. SEname, "A generic method for robust performance analysis of aircraft DC power system," 34th annual conference *on* industrial Electronics, February, 2008.

[110] Karl Zimmerman and David Costello, "Impedance–based fault location experience," *IEEE* Rural Electric Power Conference, May, 2006.

[111] GC4040M5 contactor datasheet. http://uk.farnell.com/telemecanique/gc4040m5/contactor-4-p.

[112] MK-I / -S general purpose relay. Omron. http://www.ia.omron.com/product/family/1885/index_I_u.html.

[113] Steven J .Miller. The Method of Least Squares. Mathematics Department Brown University Providence, RI 02912.

[114] Least Squares Fitting. Wolfram Mathworld. http://mathworld.wolfram.com/LeastSquaresFitting.html

[115] J. Levis Blackbourn, Thomas J. Domin, *Protective Relaying principles and applications. Third edition.* CRC Press, Taylor & Francis Group, April, 2002.

[116] Jing Wang, *Marine power system protection using active impedance estimation.* PhD thesis, School of Electrical and Electronic Engineering. The University of Nottingham, May, 2010.

[117] Karen L. Butler, N.D.R. Sarma, Cliff Whitcomb, Hyder Do Carmo, Haibo Zhang, "Shipboard Systems Deploy Automated Protection," *IEEE Computer Applicatons in Power,* April,1998.

[118] Amit Raje, Anil Raje, Jack McCall, Arvind Chaudhary, "Bus Transfer Systems: Requirements Implementation and Experiences," *IEEE Transactions on Industry Aplications*, VOL. 39, January, 2003.

[119] CDR John V. Amy Jr, U.S. Navy, "Considerations in the design electric power system," *IEEE* Power Engineering Society Sumner Meeting, May, 2002.

[120] Baranm M.E. and N. Mahajan, "System reconfigureation on shipboard DC zonal electrical system," *IEEE* Electric Ship Technologies Symposium, March, 2005.

[121] Edwin L. Zivi, "Integrated shipboard power and automation control challenge problem," *IEEE* Power Engineering Society Sumner Meeting, June,2002.

[122] werdong Zhu, Steve Pekarek, Juri Jatskevich, Oleg Wasynczuk, Dana Delisle, " A model-in-the-loop interface to emulate source dynamics in a zonal DC distribution system," *IEEE Transactions on Power Electronics*, Vol.20, May, 2005.

[123] Norbert Doerry, "Shipboard distribution systems: present and future," CAPS 10th Anniversary Celebration & NGIPS Workshop. Florida State University, Tallahassee, Florida, October, 2010.

[124] Sumner, M., D. Thomas and P. Kadanik, "Novel marine power system fault protection study final report," University of Nottingham. March, 2007.

[125] Harjinder Singh Sidhu. *High speed digital protection of EHV transmission lines using travelling waves,* Thesis Submitted to the College of Graduate Studies and Research in Partial of the Requirement of the Degree of Masters of Science, December, 2004.

[126] Liu Qing and Wang Zengping, "Research on the influence of TCSC to EHV transmission line protection," *IEEE* Third International Conference on Electric Utility Deregulation and Restructuring and Power Technologies, 2008.

[127] Yufeng Hu, Xianggen Yin, Deshu Chen and Zhe Zhang, "The study of high voltage shunt reactor protection of series compensated line," *IEEE PES* Transmission and Distribution Conference and Exposition, May, 2003.

[128] Z Q Bo, J HHe, X Z Dong, B R J Caunce and A Klimek, "Overcurrent relay based integrated protection scheme for distribution systems," *IEE* International Conference on Power System Technology, February, 2006.

[129] P.A. Crossley, H.Y. Li and A.D. Parker, "Design and evaluation of a circulating current differential relay test system," *IEEE Transactions on Power Delivery,* Vol. 13, May, 1998.

[130] Peter Müller, Stefan Tenbohlen, Reinhard Maier and Michael Anheuser, "Characteristics of series and parallel low current arc faults in the time and frequency domain," Proceedings of the 56th *IEEE* Holm Conference on Electrical Contacts (HOLM), May, 2010.

[131] Malakondaiah Naidu, Thomas J. Schoepf and Suresh Gopalakrishnan "Arc fault detection scheme for 42-V automotive DC networks using current shunt," *IEEE Transactions on Power Electronics*, VOL. 21, 2006.

[132] Thomas J. Schoepf, Malakondaiah Naidu and Suresh Gopalakrishnan, "Mitigation and analysis of arc faults in automotive DC networks," *IEEE Transactions on Component and Packing Technology*, VOL. 28, January, 2005.

[133] Hongkun Zhang, Tao Chen and Wenjun Li, "Arc fault signatures detection on aircraft wiring system," *IEE* Proceedings of the 6th World Congress on Intelligent Control and Automation, March, 2006.

[134] D. Jovcic, "Interconnecting offshore wind farms using multi-terminal VSC-based HVDC," *IEEE* Power Engineering Society General Meeting, July, 2006.

[135] K. Bell, D. Cirio, A.M. Denis, L. He, C. C. Liu, G. Migliavacca, C. Moreira, and P. Panciatici, "Economic and technical criteria for designing future off-shore HVDC grids," *IEEE PES* Innovative Smart Grid Technologies Conference Europe (ISGT Europe), November, 2010.

[136] N. M. Kirby, Lie Xu, Martin Luckett and Werner Siepmann, "HVDC transmission for large offshore wind farms," Seventh International Conference on AC-DC Power Transmission, April, 2001.

[137] Wind farm in Wikipedia. http://en.wikipedia.org/wiki/Wind_farm.

[138] BWEA, "Statistical overview of wind farms today". http://www.bwea.com/statistics

[139] RenewableUK 23 September 2010 Press Release. http://www.bwea.com/media/news/articles/pr20100923-1.html

[140] R. Blasco-Gimenez, S. Ano-Villalba, J. Rodriguez, R. Pena, R. Cardenas, S. Bernall and F. Morant, "Fault analysis of uncontrolled rectifier HVDC links for the connection of off-shore wind farms," 35th Annual Conference of *IEEE* Industrial Electronics, May, 2009.

[141]S. M. Kay, "Spectrum analysis-a modern perspective," *Proceedings of the IEEE*, vol. 69, June, 1981.

[142]Ben Palethorpe, *A novel system impedance measurement for power system analysis and improvement in power quality* PhD thesis, University of Nottingham, December, 2002.

[143] E. J. Kennedy, *Operational Amplifier Circuits Theory and Applications.* Holt, Rinehart and Winston, Inc. The Dryden Press. Saunders College Publishing. USA April, 1988.

[144] Model 61500 series Programmable AC Source, Chroma turnkey test & automation solution provider: http://www.chromaate.com/product.

[145] Farnell H60/50 DC power supply. http://www.testequipmenthq.com/1.asp?x=FARNELL-H60/50

[146] WaveTek Datron 4705 AUTOCAL MULTIFUNCTION CALIBRATOR. http://www.testelectronics.com/used/wavetek4705.htm

[147] Data sheet of the Ballantine 1620A Transconductance Amplifiers http://www.testequipmentconnection.com/37461/Ballantine_1620A.php.

[148] P. R. Rosen, "The development of an integrated protection and reclosing relay for rural feeders," *IEE* Fourth International Conference on Developments in Power Protection, May, 1989.

[149] The data sheet of the analogue to digital converter. http://www.livingston-products.com/products/pdf/126466_1_en.pdf

[150] Sun, X. and Redfern, M. A., 2010. "Protection computers or protection relays," *IEEE* International Conference on Electricity Distribution, CICED May, 2010.

[151] Matlab/Help/IGBT.

[152] IGBT data sheet. http://www.infineon.com/